The oxidative nucleophilic substitution of Hydrogen (ONSH): A theoretical modelling of 2-phenylquinoxaline reacting with organolithium nucleophiles

by

Kamogelo Brian Mdhluli[a]

Supervisor: Professor Ignacy Cukrowski[b]

Department of Chemistry

University of Pretoria

Co-supervisor: Professor Winston Nxumalo[c]

Department of Chemistry

University of Limpopo

Submitted in partial fulfilment of the requirements for the degree

Master of Science in Chemistry

in the Faculty of Natural and Agricultural Sciences

University of Pretoria

Pretoria, South Africa

December, 2020

Emails: [a] u15106129@tuks.co.za

[b] ignacy.cukrowski@up.ac.za

[c] winston.nxumalo@ul.ac.za

i

Declaration

I, Kamogelo Brian Mdhluli, hereby declare that the work presented within this dissertation, which is being submitted for the degree Master of Science in Chemistry at the University of Pretoria, is my own. Moreover, I declare that this work has not been submitted for any formal assessment at any other institution.

_____

(*Signature of Candidate*)

Signed at the University of Pretoria on the ____ day of _____ 20___.

Outputs from this work

Brian K. Mdhluli, Ignacy Cukrowski and Winston Nxumalo. Understanding reaction mechanisms from fundamental properties of molecular systems: A DFT study of the preferred electrophilic site for nucleophilic substitution of 2-phenylquinoxaline – *European Journal of Organic Chemistry* (Submitted for publication, December 2020)

Brian K. Mdhluli and Ignacy Cukrowski. Understanding reaction mechanisms from fundamental properties of molecular systems: a DFT study of the nucleophilic substitution of 2-phenylqunoxaline, *Proceedings of the South African Chemical Institute Young Chemists Symposium*, University of Venda, October 2019.

iii

Abstract

The recently implemented REP-FAMSEC method was used to explain each step along the reaction energy profile computed for the assumed Oxidative Nucleophilic Substitution of Hydrogen (ONSH) reaction between 2-phenylquinoxaline (**1**) and two organolithium reagents, namely lithium phenylacetylide (**2**) and 1-octynyllithium (**10**). Intermolecular and intramolecular interaction energies and their changes between consecutive steps of ONSH were quantified for selected molecular fragments. This revealed that the two reactants have a strong affinity for each other, driven by the strong attractive interactions between the Li- and two N-atoms, leading to four possible reaction pathways (RP-C2, RP-C3, RP-C5 and RP-C10).

Therefore, a theoretical study for the preferred electrophilic site when **1** reacts with **2** is presented in Chapter 3. From this study, four comparable in energy and stabilizing molecular system adducts were formed, each well prepared for the subsequent formation of a C–C bond at either one of the four identified sites. However, as the reaction proceeded through the TS to form the so called σ^H-adducts, very high energy barriers were observed for RP-C5 and RP-C10. Supported by REP-FAMSEC data, these RPs were eliminated. Although RP-C3 appeared more favourable than RP-C2, their energy barriers were very comparable, indicating that they can both proceed to the formation of the respective σ^H-adducts. A similar study but with **10** is presented in Chapter 4. From these studies, it was observed that the phenyl substituent at C2 of **1** guides the incoming nucleophile towards C2 and C3, suggesting that the preferred RP and relatively low yields cannot be attributed to steric hindrance caused by this substituent.

Upon the introduction of H_2O to the system, both RP-C2 and RP-C3 were nearly spontaneous towards their respective hydrolysis products. The results suggest that RP-C2 competes with RP-C3 which may lead to a possible mixture of their respective products. A secondary RP along RP-C2 was investigated and found a much more stable hydrolysis product, indicating yet another possible waste that may influence the yield of the desired product. Of the three reported hydrolysis products, only that of RP-C3 can proceed to the final oxidation stage of the ONSH reaction mechanism to give the desired product. Moreover, it was observed that since hydrolysis and oxidation occur once the reaction is exposed to the atmosphere, they can be seen as concurrent reactions. Modified experimental protocol is suggested to increase the yield of the desired product.

In Chapter 5, we present a theoretical study of the oxidation of the σ^H-adducts with halogens, namely bromine and chlorine. The computed data shows that this reaction should proceed

smoothly to the desired aromatic compound. Because the use of halogens to oxidize the σ^H-adducts requires no moisture which is important for RP-C2, this route can be seen as a way to eliminate RP-C2 and to maximize yields.

Acknowledgements

First and foremost, I would like to thank the Lord all mighty for his mercy and grace that saw me throughout this project. My deepest gratitude goes out to my family, who made sure I remain within the boundaries of my mental health. I would also like to acknowledge my colleagues within the computational chemistry research group as well as my friends in the Department of Chemistry at the University of Pretoria for the words of encouragement throughout.

Lastly, my deepest gratitude, appreciation and respect goes out to my supervisor Prof. Ignacy Cukrowski for his guidance, moral support, dedication, understanding, financial supports as well as his faith in me as a member of his research group. My co-supervisor, Dr. Winston Nxumalo, thank you for your guidance and clarification on how the reactions reported in this work were conducted in the laboratory.

Table of contents

List of Figures

CHAPTER 4

CHAPTER 5

Appendix A

Appendix B

List of Schemes

List of Tables

CHAPTER 5

Appendix A

Appendix B

Appendix C

List of Abbreviations

ONSH: Oxidative Nucleophilic Substitution of Hydrogen

RP: Reaction path

REP: Reaction Energy Profile

PES: Potential Energy Surface

REP-FAMSEC: Reaction Energy Profile and Fragment Attributed Molecular System Energy Change

QTAIM: Quantum Theory of Atoms in Molecules

IQA: Interacting Quantum Atoms

QM: Quantum Mechanics

HF: Hartree Fork

DFT: Density Functional Theory

TS: Transition State

IRC: Intrinsic Reaction Coordinates

PCM: Polarizable Continuum Model

QHO: Quantum Harmonic Oscillator

QCT: Quantum Chemical Topology

AIL: Atomic Interaction Line

SI: Supplementary Information

CHAPTER 1: INTRODUCTION

INTRODUCTION

Background on Quinoxaline and Synthetic Methods of Quinoxaline Derivatives

Quinoxaline is a chemical compound made up of benzene and pyrazine rings fused together. Quinoxaline is also called benzopyrazine and is characterized as a bioisostere of naphthalene, quinoline and benzothiophene.[1] The atomic numbering of quinoxaline is shown in Figure 1.1. In recent years, these heterocyclic compounds have attracted a lot of attention in medicinal chemistry as they have been identified as pharmacologically important compounds due to their distinct biological properties. Quinoxaline derivatives are active against bacteria, fungi, leishmania, tuberculosis, malaria, depression, cancer and neurological activities, among others.[2] These compounds are also of great interest due to their potential in fighting pathophysiological conditions such as Alzheimer's diseases and epilepsy.[3] Therefore, quinoxaline derivatives are regarded as an important class of *N*-heterocyclic compounds in organic synthesis and drug discovery. Quinoxaline is not only important in medicine but this substructure serves as a skeleton for the design of many heterocyclic compounds that are important in fluorescent dyeing agents, electroluminescent materials, chemical switches and semiconductors.[4-9] In contrast to their vast medicinal and other applications, there are no reports on computational modelling of the reactions to synthesize quinoxaline derivatives.
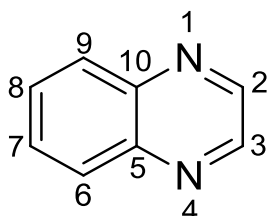
Figure 1.1. Numbered structure of Quinoxaline.

Quinoxaline is a commercially available and an inexpensive water soluble white crystalline powder, at standard conditions, with a low melting point of 29-30 ℃ and a boiling point of 226-230 ℃. Quinoxaline has a molecular formula of $C_8H_6N_2$ with a molecular weight of 130.15 g mol^{-1}. A dipole moment of 0.51 Debye for this compound was measured. Furthermore, using photon electron spectroscopy, the first and second ionization potentials for quinoxaline were measured to be 8.99 and 10.72 eV, respectively.[10] However, naturally occurring derivatives of quinoxalines are very rare, hence most of them are synthetic.[11] Therefore, many methods for the preparation of quinoxaline derivatives have been reported and published in a wide range of scientific journals over the years. The most common procedure for synthesizing quinoxaline

derivatives is the condensation of *o*-disubstituted benzene with a two-carbon synthon. Scheme 1.1 shows the condensation of *o*-phenylenediamine with an α-dicarbonyl compound resulting in the formation of a quinoxaline derivative.[10] This procedure requires high temperatures and long reaction times. Moreover, the use of pre-defined starting materials in this procedure limits the number of substituents that can be added.
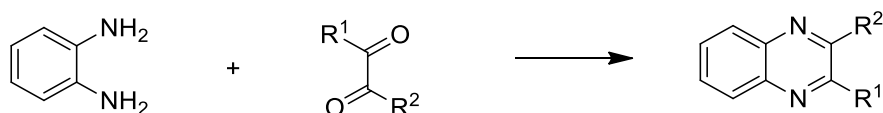
Scheme 1.1. Synthesis of quinoxaline derivatives via the condensation of *o*-phenylenediamine with an α-dicarbonyl compound.

Other methods such as the cyclization of a terminal alkyne and *o*-phenylenediamine catalysed by Cu(II) in the presence of a base[12] and the direct oxidative condensation of *o*-phenylenediamine with acetaldehyde in the presence of an inorganic base (K_2CO_3), but in the absence of a catalyst,[13] have been reported and are said to proceed smoothly to give products in modest yields. The general reaction schemes of these methods are shown in Scheme 1.2.
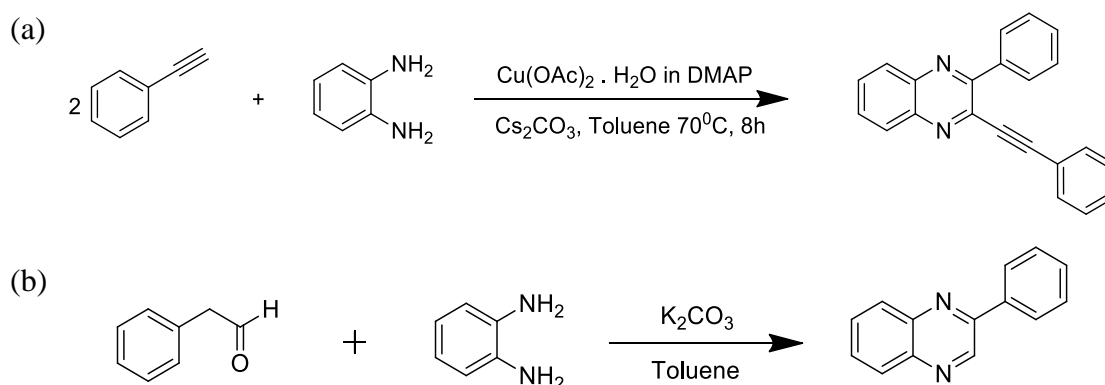
Scheme 1.2. (a) Cyclization of terminal alkyne and *o*-phenylenediamine catalysed by Cu(II) in the presence of a base and (b) the direct oxidative condensation of *o*-phenylenediamine with acetaldehyde in the absence of a catalyst.

A facile synthetic route of quinoxalines from ethyl gallate by green chemistry protocol was recently reported for the first time by Rafaely Lima and André Porto.[14] This efficient synthesis was found when they attempted to find an effective method for synthesizing amides through aminolysis reactions between ethyl gallate and ethylenediamine, diethylenetriamine and aminoethylethanolamine (Scheme 1.3). These reactions were carried out under a maintained temperature of 65 ºC for 30 minutes under magnetic stirring. Ethanol was employed as a green solvent for these reactions. Upon characterization using GC-MS, FTIR and NMR spectroscopy,

3

properties such as the molecular weights of the obtained products were not consistent with those of the expected amides. Instead, these compounds were characterized as quinoxaline derivatives, namely ethyl 8-hydroxy-1,2,3,4-tetrahydroquinoxaline-6-carboxylate, ethyl 2,3,6,7- tetrahydro-1H,5H-pyrazino[1,2,3-de]quinoxaline-9-carboxylate and ethyl 8-hydroxy-4-(2-hydroxyethyl)-1,2,3,4-tetrahydroquinoxaline-6-carboxylate. These were obtained with 97, 92 and 95% yield, respectively.
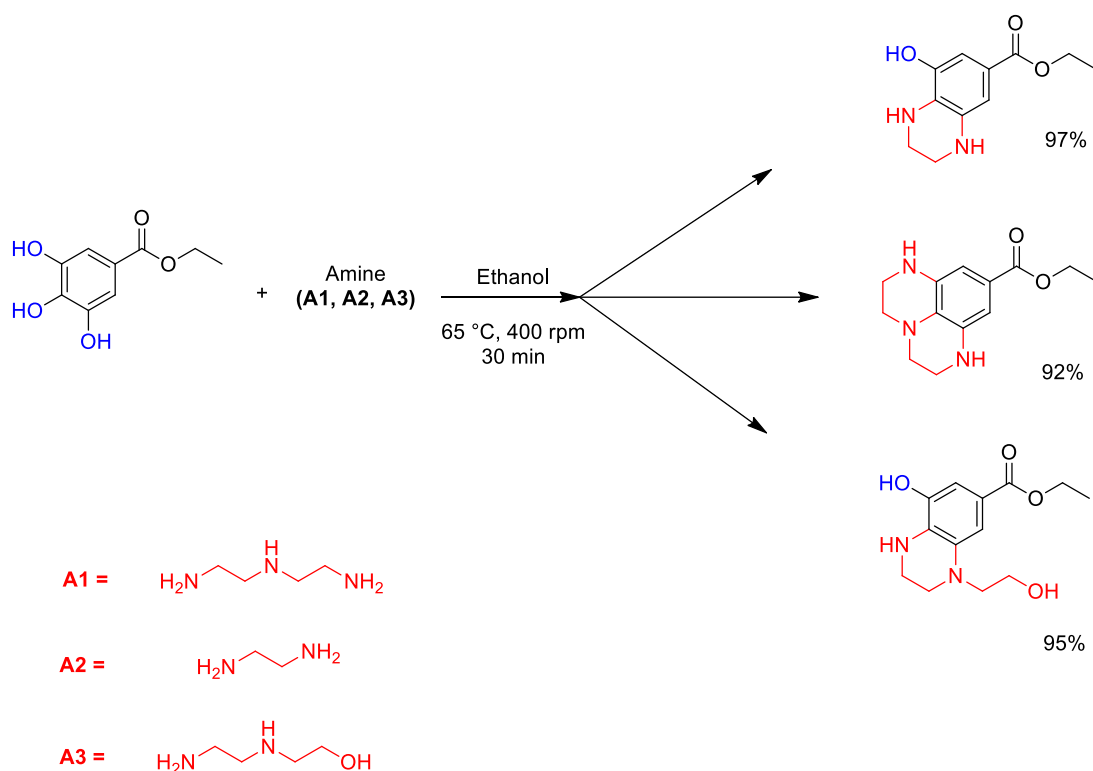
Scheme 1.3. Synthesis of quinoxaline from ethyl gallate and amines A1-A3.

Other methods including the intramolecular cyclization of *N*-substituted aromatic ortho-diamines,[15] ring transformation of benzofurans[16] and the condensation of benzofuran-1-oxide to form quinoxaline-*N*-oxides[17] have also been reported as methods of preparing quinoxaline derivatives. The oxidative coupling of epoxides and diaminoaryl compounds has also been reported as a strategy for synthesizing quinoxaline derivatives in moderate yields. This reaction is catalysed by bismuth powder, Bi(0), and proceeds by oxidative ring opening in DMSO under molecular oxygen.

A more convenient method for the synthesis of quinoxaline derivatives is the Oxidative Nucleophilic Substitution of Hydrogen (ONSH) using carbon-based nucleophiles. This is an addition-elimination mechanism that is characterized by three steps, namely *nucleophilic addition*, *hydrolysis,* and *oxidation*.[18,19] Examples of reactions following the ONSH

4

mechanism includes that of an organolithium compound (*n*-BuLi) reacting with pyridine to form a lithium derivative (σ^H-adduct) through the addition of an alkyl (Bu^n) to position 2 of pyridine – see Scheme 1.4 (a).[20,21] The σ^H-adduct then undergoes hydrolysis by interacting with the moisture (H_2O) in the air resulting in a dihydro compound which then undergoes oxidative elimination of H_2 in atmospheric O_2 to give a 2-substituted pyridine. The addition of organolithium compounds to quinolines and isoquinolines via a lithium derivative intermediate are also examples of reactions following the ONSH reaction mechanism (Scheme 1.4 (b)).[22,23] However, unlike in the ONSH in pyridine, here the substituted aromatic compound is obtained through oxidation under drastic conditions.
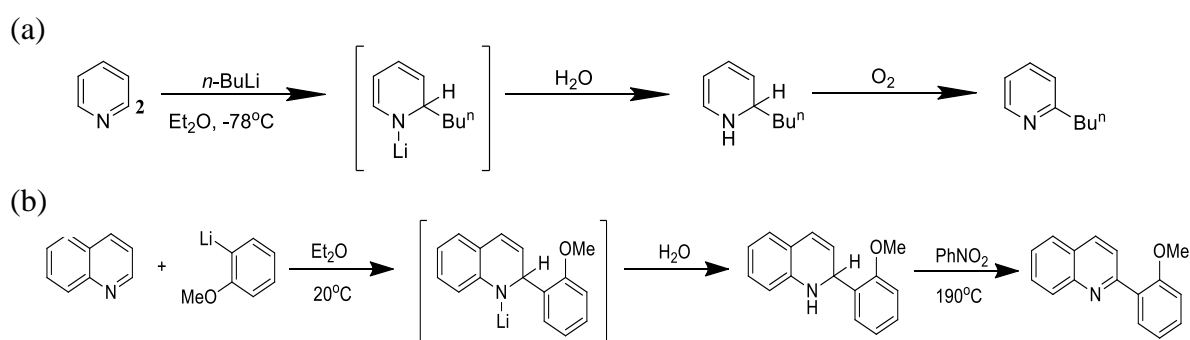
Scheme 1.4. (a) Oxidative Nucleophilic Substitution of Hydrogen of pyridine and (b) the oxidative Nucleophilic Substitution of Hydrogen of quinoline with 2-lithioanisole.

Introduction of Acetylene to Quinoxaline.

For many years, chemists have attempted to introduce acetylenes to many molecules including quinoxalines. It was discovered that the most convenient way of doing so is by adding them as nucleophiles following the ONSH reaction mechanism.[24] This meant that very strong nucleophiles were needed. On the top of the list of strong nucleophiles that can be used to introduce acetylenes to molecules was organolithium reagents. Organolithiums act as very strong nucleophiles due to the electropositive nature of the lithium atom which concentrates most of the electron density of the Li–C bond on the carbon atom which then in effect creates a carbanion.

Although organolithium reagents are very comparable to Grignard reagents, they are much more reactive and because of this, there are certain handling issues that come with their use. Organolithium reagents are not compatible with oxygen (O_2), water (H_2O) and carbon dioxide (CO_2). They react with O_2 in the air to form lithium alkoxides. They may also react with H_2O in the air which will result in the formation of lithium hydroxide and the corresponding

5

hydrocarbon.[25] Consequently, the reactivity of the organolithium reagents is lowered which then influences the desired reaction. Thus, to avoid these reactions from occurring, organometallic reagents such as organolithiums should be handled under inert atmosphere such as nitrogen or argon.

Organolithium reagents commonly used to add acetylenes to molecules are lithium acetylides. These are commonly prepared from the deprotonation of acetylene in a THF solution using organometallic bases such as *n*-BuLi at 195.15 K under inert atmosphere (see Scheme 1.5).[26]
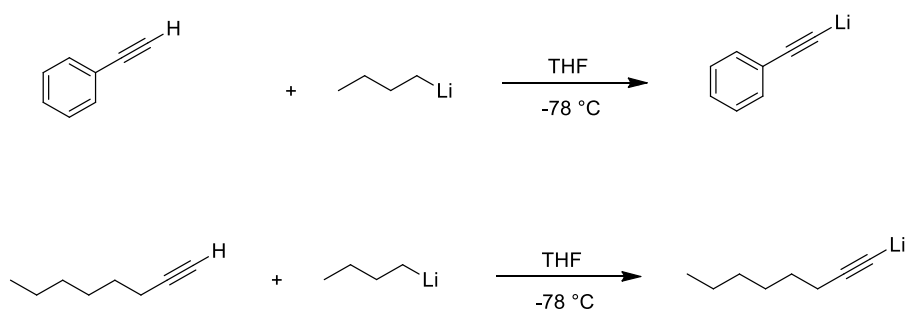
Scheme 1.5. Synthesis of lithium phenylacetylide and 1-octynyllithium.

For many years, the changes in a molecule's electronic or free energy, commonly known as potential energy surface (PES) was, in principle, used to explain the detailed processes in which chemical compounds are transformed into other chemical compounds either in the same or different phase.[27-30] Although this classical approach was successful in explaining many reaction mechanisms in chemistry, it failed to provide a deeper understanding of the processes taking place. Information including (i) the primary forces driving or preventing the reaction to proceed to completion, (ii) which atoms play a significant role in the reaction, (iii) energy changes of molecular fragments along the reaction path and (iv) the interaction energies between atoms or fragments involved in bond formation/breaking was not provided by this approach.

Thus, in view of the challenges that exist in explaining and understanding reaction mechanisms, a major step forward would be the establishment of a protocol that can be used for the understanding of reaction mechanisms from a fundamental atomic/molecular fragment level. To date, the most effective way to gain a fundamental understanding of reaction mechanisms is by making use of computational methods. Theoretical modelling of reaction mechanisms has attracted a lot of attention over the past decades and research work around it

is very active.[31-37] The use of orbitals and the topology of electron density have been the most general approaches used to gain chemical insight from quantum chemical calculations.[38-48]

Recently, a reaction energy profile and fragment attributed molecular system energy change (REP-FAMSEC) protocol was developed to elucidate consecutive energy changes along the proline-catalysed aldol reaction pathway.[49] This general purpose protocol is focused mainly on the interactions between molecular fragments that play an important role in the reaction by quantifying their energetic contributions towards a chemical change. In this work, this approach is expanded to investigate the nucleophilic substitution of a monosubstituted quinoxaline by carbon-based nucleophiles.

The reaction of quinoxaline derivatives with aryl and alkyl nucleophiles has been investigated extensively and mechanisms have been proposed.[24,50-55] However, to the best of our knowledge, no theoretical investigations have been conducted to provide a fundamental understanding of these reaction mechanisms at an atomic, molecular fragment and molecular level. Ndlovu et al., reported on the nucleophilic substitution of variously substituted 2-quinoxalines with different carbon-based nucleophiles.[55] Yields of varying degrees were observed and, not entirely surprisingly, steric hindrance and the high electron density found in the aryl and alkynyl nucleophiles were proposed as the contributing factors affecting the yields of these reactions. However, no other additional study, either experimental or theoretical, was conducted to substantiate these claims. In an attempt to explain the variation in the yields obtained in this experimental study, a theoretical investigation was conducted on the reaction of 2-phenylquinoxaline (**1**) with two different organolithium nucleophiles, namely lithium phenylacetylide (**2**) and 1-octynlithium (**10**), to give 2-phenyl-3-(2-phenylethynyl)quinoxaline and 3-(Oct-1-ynyl)-2-phenylqunoxaline in 47% and 14% yield, respectively. These reactions are assumed to follow the ONSH reaction mechanism as shown in Scheme 1.6.

R = Phenylacetylide
R = Octynyl
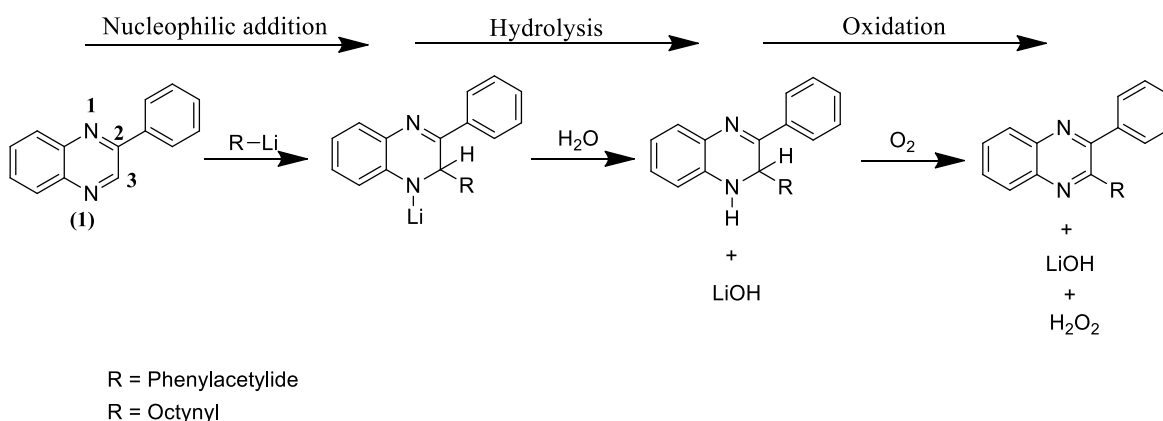
Scheme 1.6. Oxidative Nucleophilic Substitution of Hydrogen of 2-phenylquinoxaline (**1**).

AIM OF THIS PROJECT

In this project, the recently developed and implemented REP-FAMSEC[49] method by the computational chemistry research group at the university of Pretoria is set to be used together with other powerful methods such as Bader's Quantum Theory of Atoms in Molecules (QTAIM)[56] and Interacting Quantum Atoms (IQA)[57] to investigate changes in fundamental properties of selected molecular fragments along the ONSH reaction mechanism. The nature of this investigation is purely theoretical, but the modelling and validation of its findings will be guided by the availability of experimental data generated by many research groups all over the world.

As far as computational modelling is concerned, the objectives are:

1. To predict lowest energy conformer of reactants and products.
2. To generate transitional states using the functionalities in the Gaussian software.[58,59]
3. To compute the structures of the molecular systems along the reaction coordinates in small steps. Here we should be able to observe where bonds are broken and where new ones are formed. The wavefunction files generated can then be used to perform QTAIM and IQA analysis.
4. To make use of the data generated from QTAIM and IQA calculations as inputs for further and advanced analysis performed by the use of REP-FAMSEC which provides us with fundamental descriptors on molecular and atomic levels.
5. To use the obtained fundamental descriptors to interpret the molecules most reactive site.
6. To analyse and explain both successful and unsuccessful reaction mechanisms from the origin of the processes taking place.
7. Explore competing reaction pathways that might be responsible for the relatively low yields and suggest possible modifications to the reported synthetic protocols.
8. Explore possibilities of new synthetic routes.

The proceeding Chapter provides a brief discussion of widely used methods in theoretical studies. Here we also highlight those which are used extensively to achieve the above-mentioned objectives of this project.

REFERENCES

(1)   Gupta, A. K.; Sharma, M. Synthesis, Characterization And Biological Evaluation Of Novel Substituted-1-(4-Substituted Benzyl)-1h-Indolo (2, 3-B) Quinoxaline N-Benzyl Indole-2, 3-Dione Moieties. *Int. J. Pharm. Biol. Sci. Arc.* **2016**, *4*.

(2)   Pereira, J. A.; Pessoa, A. M.; Cordeiro, M. N. D.; Fernandes, R.; Prudêncio, C.; Noronha, J. P.; Vieira, M. Quinoxaline, its derivatives and applications: a state of the art review. *Eur. J. Med. Chem.* **2015**, *97*, 664-672.

(3)   Lahue, B. R.; Snyder, J. K. In *Prog. Heterocycl. Chem.* **2000**; Vol. 12, 263-293.

(4)   Jaung, J.-Y. Synthesis and halochromism of new quinoxaline fluorescent dyes. *Dyes Pigm.* **2006**, *71*, 245-250.

(5)   Zhang, Q.-Y.; Liu, B.-K.; Chen, W.-Q.; Wu, Q.; Lin, X.-F. A green protocol for synthesis of benzo-fused N, S-, N, O-and N, N-heterocycles in water. *Green Chem.* **2008**, *10*, 972-977.

(6)   Justin Thomas, K.; Velusamy, M.; Lin, J. T.; Chuen, C.-H.; Tao, Y.-T. Chromophore-labeled quinoxaline derivatives as efficient electroluminescent materials. *Chem. Mater.* **2005**, *17*, 1860-1866.

(7)   Crossley, M. J.; Johnston, L. A. Laterally-extended porphyrin systems incorporating a switchable unit. *Chem. Commun.* **2002**, 1122-1123.

(8)   Dailey, S.; Feast, W. J.; Peace, R. J.; Sage, I. C.; Till, S.; Wood, E. L. Synthesis and device characterisation of side-chain polymer electron transport materials for organic semiconductor applications. *J. Mater. Chem.* **2001**, *11*, 2238-2243.

(9)   Katoh, A.; Yoshida, T.; Ohkanda, J. Synthesis of quinoxaline derivatives bearing the styryl and phenylethynyl groups and application to a fluorescence derivatization reagent. *Heterocycles.* **2000**, *52*, 911-920.

(10)   Cheeseman, G.; Cookson, R. F. *Chem. Heterocycl. Compd.* **1979**; Vol. 35.

(11)   Watanabe, K.; Oguri, H.; Oikawa, H. Diversification of echinomycin molecular structure by way of chemoenzymatic synthesis and heterologous expression of the engineered echinomycin biosynthetic pathway. *Curr. Opin. Chem. Biol.* **2009**, *13*, 189-196.

(12)   Wang, W.; Shen, Y.; Meng, X.; Zhao, M.; Chen, Y.; Chen, B. Copper-catalyzed synthesis of quinoxalines with o-phenylenediamine and terminal alkyne in the presence of bases. *Org. Lett.* **2011**, *13*, 4514-4517.

(13)   Song, J.; Li, X.; Chen, Y.; Zhao, M.; Dou, Y.; Chen, B. Transition-Metal-Free Synthesis of Quinoxalines from o-Phenylenediamines and Arylacetaldehydes under Basic Conditions. *Synlett.* **2012**, *23*, 2416-2420.

(14)   Lima, R. N.; Porto, A. L. Facile synthesis of new quinoxalines from ethyl gallate by green chemistry protocol. *Tetrahedron Lett.* **2017**, *58*, 825-828.

(15)   Söderberg, B. C.; Wallace, J. M.; Tamariz, J. A novel palladium-catalyzed synthesis of 1, 2-dihydroquinoxalines and 3, 4-dihydroquinoxalinones. *Org. Lett.* **2002**, *4*, 1339-1342.

(16)   Issidorides, C. H.; Haddadin, M. J. Benzofurazan oxide. II. Reactions with enolate anions. *J. Org. Chem.* **1966**, *31*, 4067-4068.

(17)   Abu-Hashem, A. A. Synthesis, reactions and biological activity of quinoxaline derivatives. *ChemInform.* **2015**, *46*, no-no.

(18)   Mąkosza, M. Nucleophilic substitution of hydrogen in electron-deficient arenes, a general process of great practical value. *Chem. Soc. Rev.* **2010**, *39*, 2855-2868.

(19)   Mąkosza, M.; Wojciechowski, K. In *Metal Free CH Functionalization of Aromatics*; Springer: **2013**, 51-105.

(20)   Potts, K. T.; Cipullo, M.; Ralli, P.; Theodoridis, G. Ketene dithio acetals as synthetic intermediates. Synthesis of unsaturated 1, 5-diketones. *J. Am. Chem. Soc.* **1981**, *103*, 3584-3585.

(21)   Ziegler, K.; Sauermilch, W. Synthetische Versuche in der Gruppe arylierter Allen-Derivate. *Berichte der deutschen chemischen Gesellschaft (A and B Series).* **1930**, *63*, 1851-1864.

(22)   Kovalev, I. S.; Kopchuk, D. S.; Zyryanov, G. V. e.; Rusinov, V. L.; Chupakhin, O. N.; Charushin, V. N. Organolithium compounds in the nucleophilic substitution of hydrogen in arenes and hetarenes. *Russ. Chem. Rev.* **2015**, *84*, 1191.

(23)   Geissman, T.; Schlatter, M. J.; Webb, I. D.; Roberts, J. D. The Synthesis Of Some Intermediates For Use In The Preparation Of Analogs Of Salicylaldehyde Ethylenediimine Cobalt ("Salcomine"). *J. Org. Chem.* **1946**, *11*, 741-750.

(24)   Prokhorov, A. M.; Mąkosza, M.; Chupakhin, O. N. Direct introduction of acetylene moieties into azines by SNH methodology. *Tetrahedron Lett.* **2009**, *50*, 1444-1446.

(25)   Schlosser, M.; Hegedus, L. S. *Organometallics in synthesis: a manual*; Wiley Online Library, **2002**; Vol. 3.

(26)   Smith, A. B.; Chen, S. S.-Y.; Nelson, F. C.; Reichert, J. M.; Salvatore, B. A. Total syntheses of (+)-acutiphycin and (+)-trans-20, 21-didehydroacutiphycin. *J. Am. Chem. Soc.* **1997**, *119*, 10935-10946.

(27)   Ma, Y.-T.; Ma, X.; Li, A.; Guo, H.; Yang, L.; Zhang, J.; Hase, W. L. Potential energy surface stationary points and dynamics of the F^- + CH_3I double inversion mechanism. *Phys. Chem. Chem. Phys.* **2017**, *19*, 20127-20136.

(28)   Porter, R.; Karplus, M. Potential energy surface for H_3. *J. Chem. Phys.* **1964**, *40*, 1105-1115.

(29)   Morokuma, K.; Kato, S.; Kitaura, K.; Obara, S.; Ohta, K.; Hanamura, M. In *New Horizons of Quantum Chemistry*; Springer: **1983**, 221-241.

(30)   Balint-Kurti, G. Potential energy surfaces for chemical reactions. *Molecular Scattering: Physical and Chemical Applications.* **2009**, *60*, 137.

(31)   Liu, Y.; Hou, H.; Wang, B. Theoretical study on cycloaddition reaction of epoxides with CO2 catalyzed by metal-porphrin complexes: Reaction mechanisms and structure impacts on catalytic activity. *J. Organomet. Chem.* **2020**, *911*, 121123.

(32)   Mitani, R.; Yamamoto, H.; Sumimoto, M. Theoretical study on the reaction mechanism of imidazole-catalyzed phenol-epoxy ring-opening reaction and the evaluation of catalyst performance. *Chem. Phys. Lett.* **2020**, *742*, 137143.

(33)   Wei, B.; Sun, J.; Mei, Q.; An, Z.; Wang, X.; He, M. Theoretical study on gas-phase reactions of nitrate radicals with methoxyphenols: Mechanism, kinetic and toxicity assessment. *Environ. Pollut.* **2018**, *243*, 1772-1780.

(34)   Amiri, A.; Noorbala, M. R.; Saheb, V. Kinetics and Mechanisms of the Hydrogen Abstraction Reactions of $CF_3CF_2CH_2CH_2F$ and $CF_3CH_2CH_2CF_3$ with Hydroxyl Radicals: Theoretical Studies. *J. Fluorine Chem.* **2019**, *218*, 116-121.

(35)   Du, B.; Zhang, W. Theoretical study of the reaction mechanism and kinetics of the OH + trimethyl orthoformate $((CH_3O)_3CH) + O_2$ reaction. *Comput. Theor. Chem.* **2019**, *1159*, 38-45.

(36)   Tarumi, M.; Matsuzaki, Y.; Suzuki, K. Theoretical study on the redox reaction mechanism of quinone compounds in industrial processes. *Chem. Eng. Sci.* **2019**, *199*, 381-387.

(37)   Litvin, V. A.; Minaev, B. F.; Baryshnikov, G. V. Experimental and theoretical study of the mechanism formation of silver nanoclusters in the reduction reaction of Ag+ ions by alizarin solution. *Colloid interface Sci. Commun.* **2019**, *29*, 47-54.

(38)   Woodward, R. B.; Hoffmann, R. Selection rules for sigmatropic reactions. *J. Am. Chem. Soc.* **1965**, *87*, 2511-2513.

(39)   Fukui, K. Recognition of stereochemical paths by orbital interaction. *Acc. Chem. Res.* **1971**, *4*, 57-64.

(40)   Harcourt, R. D. Increased-valence structures and some valence bond representations for reaction mechanisms. *J. Mol. Struct: Theochem.* **1997**, *398*, 93-100.

(41)   Pavao, A. C.; Taft, C. A.; Guimaraes, T. C.; Leao, M. B.; Mohallem, J. R.; Lester, W. A. Interdisciplinary applications of Pauling's metallic orbital and unsynchronized resonance to problems of modern physical chemistry: conductivity, magnetism, molecular stability, superconductivity, catalysis, photoconductivity, and chemical reactions. *J. Phys. Chem. A.* **2001**, *105*, 5-11.

(42)   Shaik, S.; Hiberty, P. C. Valence bond theory, its history, fundamentals, and applications: a primer. *Rev. Comput. Chem.* **2004**, *20*, 1.

(43)   Hiberty, P. C.; Shaik, S. A survey of recent developments in ab initio valence bond theory. *J. Comput. Chem.* **2007**, *28*, 137-151.

(44)   Li, X.; Zeng, Y.; Meng, L.; Zheng, S. Topological characterization of HXO_2 (X= Cl, Br, I) isomerization. *J. Phys. Chem. A.* **2007**, *111*, 1530-1535.

(45)   Li, X.; Fan, H.; Meng, L.; Zeng, Y.; Zheng, S. Theoretical investigation on stability and isomerizations of CH_3SO isomers. *J. Phys. Chem. A.* **2007**, *111*, 2343-2350.

(46)   Macchi, P.; Sironi, A. Chemical bonding in transition metal carbonyl clusters: complementary analysis of theoretical and experimental electron densities. *Coord. Chem. Rev.* **2003**, *238*, 383-412.

(47)   Tognetti, V.; Bouzbouz, S.; Joubert, L. A theoretical study of the diastereoselective allylation of aldehydes with new chiral allylsilanes. *J. Mol. Model.* **2017**, *23*, 5.

(48)   Inostroza-Rivera, R.; Yahia-Ouahmed, M.; Tognetti, V.; Joubert, L.; Herrera, B.; Toro-Labbé, A. Atomic decomposition of conceptual DFT descriptors: application to proton transfer reactions. *Phys. Chem. Chem. Phys.* **2015**, *17*, 17797-17808.

(49)   Cukrowski, I.; Dhimba, G.; Riley, D. L. A reaction energy profile and fragment attributed molecular system energy change (FAMSEC)-based protocol designed to uncover reaction mechanisms: a case study of the proline-catalysed aldol reaction. *Phys. Chem. Chem. Phys.* **2019**, *21*, 16694-16705.

(50)   Hui, X.; Schmidt, F.; Fakhfakh, M. A. Novel highly regioselective syntheses of unsymmetrical 2, 3-disubstituted quinoxalines. *Heterocycles.* **2007**, *72*, 353-361.

(51)   Azev, Y. A.; Oparina, E.; Golomolzin, B.; Ermakova, O.; Bakulev, V. A simple means of preparing quinoxaline derivatives: Direct introduction of C-nucleophiles into the quinoxaline nucleus by substituting a hydrogen atom. *Pharma. Chem. J.* **2013**, *47*, 172-175.

(52)   Badr, M. Z. A.; El-Naggar, G. M.; El-Sherief, H. A. H.; Abdel-Rahman, A. E.-S.; Aly, M. F. Reaction of quinoxaline derivatives with nucleophilic reagents. *Bull. Chem. Soc. Jpn.* **1983**, *56*, 326-330.

(53)   Zhuo, F.-F.; Xie, W.-W.; Yang, Y.-X.; Zhang, L.; Wang, P.; Yuan, R.; Da, C.-S. TMEDA-assisted effective direct ortho arylation of electron-deficient N-heteroarenes with aromatic Grignard reagents. *J. Org. Chem.* **2013**, *78*, 3243-3249.

(54)   Epifani, E.; Florio, S.; Ingrosso, G.; Sgarra, R.; Stasi, F. Reaction of quimoxalines with β, γ-unsaturated grignard reagents: Synthesis of allyl-, allenyl-, propargyl-quinoxaline derivatives. *Tetrahedron.* **1987**, *43*, 2769-2778.

13

(55)   Ndlovu, N.; Nxumalo, W. Nucleophilic Substitution on 2-Monosubstituted Quinoxalines Giving 2, 3-Disubstituted Quinoxalines: Investigating the Effect of the 2-Substituent. *Molecules.* **2016**, *21*, 1304.

(56)   Bader, R. F. Atoms in molecules. *Acc. Chem. Res.* **1985**, *18*, 9-15.

(57)   Blanco, M.; Martín Pendás, A.; Francisco, E. Interacting quantum atoms: a correlated energy decomposition scheme based on the quantum theory of atoms in molecules. *J. Chem. Theor. Comput.* **2005**, *1*, 1096-1109.

(58)   Frisch, M.; Trucks, G.; Schlegel, H.; Scuseria, G.; Robb, M.; Cheeseman, J.; Scalmani, G.; Barone, V.; Petersson, G.; Nakatsuji, H. Gaussian 09. 2009: Wallingford. *Conn, USA Gaussian.*

(59)   Frisch, M.; Trucks, G.; Schlegel, H.; Scuseria, G.; Robb, M.; Cheeseman, J.; Scalmani, G.; Barone, V.; Petersson, G.; Nakatsuji, H. Gaussian 16 Revision B. 01. 2016; Gaussian Inc. *Wallingford CT.*

CHAPTER 2: COMPUTATIONAL METHODS

INTRODUCTION

Computational chemistry is a branch of chemistry that explores and resolves chemical questions using computer simulations.[1,2] This field allows the modern researcher to investigate various aspects of chemistry numerically. That is, one can study chemical phenomena by computerized calculations based on fundamental laws of physics instead of carrying out experiments in the laboratory.[3] Computational chemistry, as a tool, is unique in the sense that any researcher who makes use of it is not bound by the margins of reality. However, as much as this allows the creativity of the researcher to be unbounded as to how to resolve chemical problems, it demands a full understanding of all assumptions that are made in the calculations and analysis of molecular geometries, reactivities, spectra and other properties.

Due to the abundance of theoretical methods developed over the years as well as the improved design of quantum chemical algorithms, computational chemistry has become essential for chemical research. Improved design of quantum chemical algorithms results in faster computing speeds. This means that molecular properties of the system under study can be obtained much quicker than they would via experimental routes. Apart from this, computational chemistry is also a more cost efficient and environmentally friendly approach for chemical studies in the sense that one does not require expensive reagents that may generate large amounts of waste. Despite all these advances and advantages, computational chemistry cannot substitute experimental studies.

Computational methods devoted to the study of chemical systems belong to two broad areas within computational chemistry, namely *molecular mechanics* and *electronic structure theory*. These perform, in essence, similar basic type of calculations but are different in terms of the physics laws they use to perform these calculations.[4]

Molecular mechanics

Using classical laws of physics, molecular mechanics predicts the structures and the properties of molecules. Many molecular mechanics methods exist with each characterized by a particular force field containing three components; (i) mathematical expressions establishing how the potential energy of a molecule varies with reference to its constituent atoms (ii) a set of atom types that define the characteristics of an element within a specific chemical context and (iii) a single, if not more, parameter set that incorporates the mathematical expressions and atom types to experimental data. These parameter sets describe force constants which are the values

fitted in the mathematical expressions to relate atomic attributes to energy components and to structural data such as bond lengths and angles. Molecular mechanic computations are computationally inexpensive because this theory does not consider the electrons in a molecular system. Instead, molecular mechanic computations are based on nuclei interactions and implicitly includes electronic effects in force fields through parameterization. This allows molecular mechanics methods to be used for large systems made of many atoms such as amino acids. However, like many other approximations, it does have its own drawbacks. One of these drawbacks is that no single force field can generally be used for all molecular mechanics calculations. The second drawback is that not considering electrons in molecular mechanics calculations means that chemical problems in which electronic effects predominate cannot be treated by molecular mechanics methods.

Electronic structure methods

Unlike molecular mechanics, which uses classical laws of physics (Newtonian mechanics) to predict structures and properties of molecules, electronic structure methods use laws of quantum mechanics (QM) which state that the energy and other molecular properties may be obtained by solving the time-independent Schrödinger equation.

$$\hat{H}\Psi = E\Psi \qquad (1)$$

In equation 1, $\hat{H}$ is the Hamiltonian operator which is the sum of the momentum operator yielding kinetic energy and the position operator yielding potential energy. In simple terms, the Hamiltonian operator corresponds to the sum of the kinetic energies plus the potential energies of all particles in the system. However, even with improved computational resources, exact solutions of the time-independent Schrödinger equation are impractical due to the movement of each particle with reference to all other particles in the system. Fortunately, approximations such as the Born-Oppenheimer approximation can be made. In this approximation, one assumes that all nuclei are fixed since the movement of electrons in a molecule is much faster than that of the nuclei. This approximation allows for effective mathematical derivation of the time-independent Schrödinger equation.

Electronic structure methods can be classified into three major classes.

(i) Semi-empirical methods such as Austin Model 1 (AM1),[5] Parametric Model number 3 (PM3),[6] Modified Neglect of Differential Overlap (MNDO)[7] etc., which are implemented in various computational programs such as Gaussian.[8,9] These are abridged versions of the Hartree-Fork (HF) theory that makes use of

17

empirical corrections derived from experimental data to simplify and improve computations.

(ii)   Ab initio methods, which make no use of experimental data in their computations, are used to forecast molecular interactions and the properties of molecular systems that vary in size. Computations from the ab initio methods are based only on the laws of quantum mechanics Although the calculations of this method are computationally expensive, various methods have been developed to address this issue.

The first and most elementary method was the HF method which originates from the Hartree method, introduced by D. R. Hartree in 1927, to provide approximations to solve the Schrödinger equation.[10] However, after pointing out the lack of anti-symmetry in Hartree method, V. A. Fock used a mathematical approach to introduce anti-symmetry wave functions to the Hartree method in order for it to conform to the Pauli exclusion principle.[11,12] This gave rise to the HF method. Although this method provides accurate geometrical predictions and parameters for many molecular systems, it does not account for the energy contributions originating from electron-electron interactions. To account for this, *Møller-Plesset* (MP)[13] developed a perturbation theory by modifying the HF method such that it included electron correlation. Since then, MP methods have been used in the study of reactions involving weak interactions and to elucidate the stability of isomers.[14,15]

(iii)   Density functional theory (DFT)[16] methods. These methods have come into wide use because they include effects induced by electron correlation in their model. DFT functionals can be classified in many categories. However, we will focus only on the B3LYP[17] functional which is set to be used to fulfil the aims of this project. This is a hybrid approach, introduced by Becke, that combines HF and the DFT. The B3LYP functional integrates Becke's treatment of exact-exchange energies and Lee, Yang and Parr's method of establishing correlation energy for the predominant use of modelling geometric structures, chemical properties and chemical reactions. From its establishment, B3LYP has been a highly favoured functional of the DFT by many researchers, predominantly by organic chemists, due to its ability to provide accurate enough results at relatively low computational cost.

BASIS SET

Most methods used to carry out theoretical calculations are coupled with a mathematical descriptor of the orbitals within the system called a basis set. The main function of a basis set is to assign a group of basis functions, composed of a linear combination of gaussian functions, to every atom in a molecular system to approximate its orbitals. This imposes certain restrictions on each electron in the molecular system to a region of space. Larger basis sets are able to approximate the orbitals of a molecular system more accurately as they impose fewer restrictions on the location of electrons in space. The Gaussian program used to execute all computational calculations in this work offers a wide range of predefined basis sets. The choice of basis set is generally influenced by the nature of the molecules and reactions being investigated.

The most prevalent basis sets used in real-world quantum chemical calculations are Pople's basis sets,[18] more especially the 6-31G basis set and those adapted from it. In these basis sets, the internal orbital (core electrons) is treated with a single basis function summing up six Gaussian functions whereas the valance orbitals (valance electrons), which are more affected by the chemical environment, are treated with two autonomous basis functions, one made up of three Gaussian functions and the other made up of one Gaussian function. This type of basis set is formally known as a split valance double zeta basis set because two independent basis functions are used to describe each valance orbital. Larger split valance basis sets (triple and quadruple zeta) which approximate the orbital of molecular systems more accurately have also been defined. However, these are more computationally expensive.

There are two ways in which the accuracy of these minimal set of functions can be increased. The first way is to add polarization basis functions. These functions have a higher angular momentum than the valance orbitals. Therefore, their addition to the basis set introduces additional freedom (flexibility) to better represent the electron density of the molecule when a chemical bond is formed. In Pople's basis sets, the inclusion of polarization basis functions is indicated by a terminal * or (d) for heavy (non-hydrogen atoms) atoms and a terminal ** or (d,p) for all atoms (including H). The second way is to introduce diffuse basis functions which typically provide a more realistic representation of the electron density much further away from the nucleus. The use of diffuse basis functions in Pople's basis sets is indicated by + or ++ between the split valance basis set and the polarization basis function. The + notation indicates that one set of sp-type diffuse basis functions are added to each non-hydrogen atom. The ++

© University of Pretoria

notation indicates that one set of sp-type diffuse basis function is added to each non-hydrogen atom and one s-type diffuse function is added to each hydrogen atom.

Apart from Pople's basis sets, other basis sets used by most researchers includes Dunning correlation-consistent basis sets[19] which are used in post-HF methods and DFT. These basis sets are denoted as cc-pVNZ where N = D (double), T (triple), Q (quadruple), 5, 6 and so forth. Unlike Pople's basis sets, these include the polarization basis function by default but requires the addition of "aug" in the prefix for the inclusion of diffuse basis functions.

In this work, Pople's 6-311G split valance triple zeta basis set including both polarization and diffuse basis functions on both heavy and hydrogen atoms will be used for all quantum chemical calculations, i.e., 6-311++G(d,p).

CHARACTERIZATION OF STATIONARY POINTS

In computational chemistry, the nature of any stationary points found from energy optimization calculations is characterized by analysing the vibrational frequencies obtained from frequency calculations.

In the energy optimization calculations, the geometry of the molecular system is rearranged along the potential energy surface (PES) in such a way that the total energy of the molecular system is minimized to a point where the forces acting on the molecular system are essentially zero. A good estimate of the initial input structure makes these calculations less computationally expensive. The converged structure may correspond to either a global/local minimum on the PES or a saddle point.

All stationary points identified on the PES are submitted for frequency calculations which computes force constants and the resulting vibrational frequencies. The vibrational frequencies are determined by the establishment of the second derivative of the energy with respect to the Cartesian nuclear coordinates and the transforming to mass-weighted coordinates. It is important to note that the transformation to mass-weighted coordinates is only valid at a stationary point. It is therefore highly recommended that frequency calculation be computed using the same method as the one used to obtain the energy-optimized geometry of a molecular system. To avoid errors such as performing frequency calculations at points that are not stationary points, it is advisable that both energy-optimization and frequency calculations be computed within a single job submission by specifying both the *opt* and *freq* keywords in the route section of the particular job.

From the output of the frequency calculations, one has to analyse the vibrational frequencies to characterize the nature of the stationary points. The presence of a single imaginary frequency characterizes a transition state (TS) while the absence thereof characterizes reactants, intermediates and products. However, finding a single imaginary frequency does not guarantee that one has found the TS that connects the desired minima. Thus, one needs to analyse the normal mode of the corresponding imaginary frequency and establish whether the displacement that formulates it leads into the directions of the desired minima.

A more accurate way to confirm whether or not the identified TS connects the reactants with the expected products is to perform intrinsic reaction coordinate (IRC)[20,21] calculations. In this type of calculations, the initial input structure is that of the TS, and the reaction path is followed in both directions by integrating the intrinsic reaction coordinate. Important to note for IRC calculations is that they require initial force constants to proceed. These can be computed at the beginning of the IRC calculations by specifying *CalcFC* in the route section of the job.

SOLVATION

It is known that most chemistry in nature occurs in a gaseous medium. Even though this is true and common on Earth as well, a significant amount of chemistry also occurs in a condensed phase. That is, most chemical and biological reactions in our surroundings take place in the presence of a solvent. For this reason, it is imperative that computational chemistry, which aims to provide solutions to chemical questions, to be equipped with methods that allow a description of the solvation environment.[22]

Solvent effects are simulated using two methods, namely *continuum methods* and the *discrete* and *pseudo-discrete methods*. The continuum methods simulate the effects of the solvent by planting the solute molecules in a cavity that behaves as a continuum medium that can be outlined using macroscopic properties such as density, dielectric constant and surface tension etc. However, this approach fails to accurately simulate solvent effect in chemical problems which the solvent is capable of establishing hydrogen bonds. This is most common for polar solvents. In such situations, one has to turn to the discrete and pseudo-discrete methods to model solvent effects. In this approach, one has to manually add individual solvent molecules around the solute to represent the first solvation shell. Although this approach is efficient in the sense that it records accurately the effects of the solvent provided that a sufficient number of solvent molecules are added and placed correctly around the solute molecules, it can be computationally expensive, even for medium-sized systems.

In this work, the polarizable continuum model (PCM),[23] which is part of the continuum methods for simulating solvent effects, was employed. This model was originally formulated in 1981 by Miertus et al., and has since then been the most common model used in computational chemistry due to its ability to describe any solute without considering its shape or charge distribution.[24]

DISPERSION EFFECTS IN COMPUTATIONS

Weak, long-range dynamic correlations in electronic structures, generally termed as dispersion, are not well accounted for by standard DFT functionals such as B3LYP. These weak interactions are very common in organic systems. As such, they impact molecular conformations and their stability as well as the result of stereoselective organic reactions. For this reason, these noncovalent interactions have posed a problem in quantum chemical calculations for many years.

As mentioned above, standard DFT functionals, including the greatly favoured B3LYP functional, fail to model dispersion effects. For example, these functionals are said to predict repulsive interactions for a benzene sandwich dimer while the more reliable ab initio methods predicted a binding energy. Thus, for many years, in order to account for dispersion effects, researchers had to employ the computationally expensive ab initio methods. Fortunately, recent developments in DFT methods, aiming at improving computational performance and efficiency, have enabled many DFT functionals to treat non-covalent interactions in many organic systems. The most common way of doing so is by employing Grimme's semi-empirical dispersion correction (–D functionals)[25,26] and M05 and M06 suites of functionals from Zhao et al.[27-31] These methods have showed, beyond any reasonable doubt, reliable and accurate results for organic systems where non-covalent interactions are predominant. The Grimme-D3 semi-empirical dispersion correction is employed in this work.

THERMODYNAMIC PROPERTIES

In order to computationally determine the thermodynamic properties of any molecule, software programs such as Gaussian make use of the calculated vibrational frequencies of optimized structures. However, like many other quantum chemical programs, Gaussian makes the approximation that these frequencies are those of a quantum harmonic oscillator (QHO). By default, frequency calculations are carried out at 298.15 K and 1 atm, unless otherwise specified. An important approximation to make note of for the calculations of thermodynamic properties is that they are usually calculated for an ideal gas. This means that the equations

© University of Pretoria

used to calculate these thermodynamic properties assume that all interactions of the system are completely elastic. Therefore, in order to model any reaction in a solution, additional corrections such as the zero-point energy correction must be considered. This is because the frequencies used to calculate thermodynamic properties are approximated to be frequencies of QHOs which, due to Heisenberg's uncertainty principle, can never have exactly zero energy. Therefore, the total zero-point energy correction is obtained by summing up lowest possible energy, called the zero-point energy, of each QHO over the molecule.

The starting point in quantifying the thermodynamic properties of any molecule is the partition function q(V,T), which regulates how the energy of the system is partitioned between transitional, vibrational, rotational and electronic states at constant volume and temperature. For a detailed description on how the partition function is employed to obtain thermodynamic quantities such as entropy, enthalpy and free energy, interested readers are directed to the well documented white paper on thermochemistry by Joseph W. Ochterski.[32]

WAVEFUNCTION ANALYSIS

The preceding discussions in this Chapter provided a brief discussion of the theory behind the quantum chemical calculations associated with electronic structure methods. Over the years, the need to extract chemically relevant information from the outputs of these type of calculations for additional interpretation has grown exponentially. To address these needs, many methods based on either the wavefunction or the electron density have been developed. A large number of these developed methods were based on the electron density and were therefore grouped as Quantum Chemical Topology methods (QCT).[33,34] QCT methods are popular in computational research due to the nature of the electron density which can be perceived directly by intuition and be measured experimentally. In addition, these methods are independent of the level of theory that is used. However, these methods carry with them a major disadvantage. That is, their use leads to the loss of much needed information about the phase of the wavefunction and excited states, which then limits their use for studying molecular reactivity.

Quantum Theory of Atoms in Molecules

QCT methods include Bader's Quantum Theory of Atoms in Molecules[35] (QTAIM) which has been used extensively in this work and popular in computational research. In general, this theory is an extension of the physics describing individual atoms in a molecule partitioned by the use of a topological analysis of the gradient vector field of the electron density. Moreover, this theory describes each atom in a molecule as an open system (Ω) bounded by a surface $S(\Omega;\mathbf{r})$ of zero-flux in the gradient vector field of the electron density $\rho(\mathrm{r})$ for all $\mathbf{r}$ on the surface. That is;

$$\nabla\boldsymbol{\rho}(\boldsymbol{r}) \cdot \boldsymbol{n}(\boldsymbol{r}) = \boldsymbol{0} \qquad (2)$$

This definition results in an extensive but physically sound partitioning of a molecule into real-space atomic contributions. It also makes it possible for the properties of an atom to be calculated in the same manner as a molecule. This is done by evaluating Heisenberg's equation of motion for a given operator on the atom and its boundaries. Apart from this, the gradient vector of the electron density can also be used to find lines of maximum density between atom pairs to define molecular structures. These lines are commonly known as atomic interaction lines (AIL) or bond paths.

Interacting Quantum Atoms

Pendás, Blanco and Francisco's Interaction Quantum Atoms (IQA)[36,37] approach is a correlated energy decomposition scheme that is based on Bader's QTAIM. This method can be used to partition the electronic energy of a molecular system into self-atomic energies ($E_{\text{self}}^{\text{A}}$) and the interaction energies of all atomic pairs of the systems ($E_{\text{int}}^{\text{A,B}}$).

A molecular system is considered to constitute of atoms that leave no voids in the entire space occupied by the system. Therefore, each atom has distinct interatomic boundaries. As a result, each atom has its own energy that is mostly dependent on the kind of atom it is than the environment that it occupies within the system. This means that one can simply recover the computed electronic energy (E) of the molecular system within the IQA scheme by summing up the additive (total) atomic energies ($E_{\text{add}}^{\text{A}}$) of each atom A such that

$$E = \sum_{\text{A}} E_{\text{add}}^{\text{A}} \qquad (3)$$

However, because all atoms in a molecule are involved in some kind of interactions, the additive atomic energy of an atom A has to be a sum of the energy of A itself and the sum of all diatomic interaction energies that A encounters with every other atom B in a molecule as

24

shown in equation 4. The sum of all diatomic interaction energies is halved so that the E can be recovered.

$$E_{\text{add}}^{\text{A}} = E_{\text{self}}^{A} + 0.5 \sum_{A \neq B} E_{\text{int}}^{A,B} \tag{4}$$

From the above, it follows that the E can be recovered in the IQA scheme by summing up all self-atomic energies and all unique diatomic interaction energies between atoms A and B.

$$E = \sum_{\text{A}} E_{\text{self}}^{\text{A}} + 0.5 \sum_{\text{A}} \sum_{\text{A} \neq \text{B}} E_{\text{int}}^{\text{A,B}} \tag{5}$$

The power of IQA is not limited to the above mentioned. An understanding of the nature and strength of chemical bonding can be obtained from this energy partitioning scheme. To do so, $E_{\text{int}}^{\text{A,B}}$ is partitioned into the exchange correlation ($V_{\text{XC}}^{\text{A,B}}$) and the classical ($V_{\text{cl}}^{\text{A,B}}$) components to allow chemists to quantitively describe bonds by their covalent or electrostatic contributions.

REP-FAMSEC

The reaction energy profile–fragment attributed molecular system energy change (REP-FAMSEC) method is a general-purpose protocol recently developed and implemented by the computational chemistry research group at the University of Pretoria.[38] This protocol was designed to explain consecutive steps along reaction pathways by making use of the energy terms computed within the IQA framework and a general concept of the fragment attributed molecular system energy change (FAMSEC)[39-41] method. For a detailed description of the FAMSEC method, interested readers are directed to the referenced articles by Ignacy Cukrowski and co-workers.[39-41]

The main focus of the REP-FAMSEC protocol is on the changes of the interaction energies along the reaction pathway. The 'beauty' behind this protocol is the amount of freedom it allows chemists to explore various strategies to explain chemical processes. That is, one can select molecular fragments constituting of 2 to n-atoms in order to identify the effect that different parts of a molecule have towards chemical change. Therefore, it is clear that this protocol is not governed by any specific rules for the selection of fragments; however, it is recommended that one selects molecular fragments for which the most significant change in the intra- and intermolecular interaction energies were observed between consecutive steps in a reaction pathway. This protocol is used extensively in the scope of this project to explain the reaction mechanism under investigation.

25

COMPUTATIONAL PROTOCOLS USED

To fulfil the aims and objectives of this theoretical study, the electronic structures of all stationary points including reactants, transition states (TS), intermediates and products were fully optimized at the density functional theory (DFT) level by employing the restricted hybrid B3LYP functional coupled with Pople's 6-311++G(d,p) basis set. To account for all the weak, long-range dynamic interactions in the electronic structures, Grimme's D3 empirical dispersion correction (GD3) was included in all quantum calculations for this project. The PCM, with tetrahydrofuran (THF) as the selected solvent, was used to simulate the solvent effects in the reactions under investigation. The nature of all stationary points in this study was verified by means of vibrational frequency analysis. The presence of a single negative (imaginary) frequency was expected for the TSs and none for the fully energy-optimised reactants, intermediates and products. Identified TSs were confirmed as true TSs by means of IRC calculations. All these quantum chemical calculations were computed using the Gaussian 09 and 16 program packages[8,9] while conformational searches were performed in Spartan where molecular mechanic force field (MMFF) and the Monte Carlo algorithm are implemented.[42] The confirmation search was done by varying the torsion angle of every rotatable bond in the molecular system by 30º. Lastly, molecular graphs and QTAIM/IQA data required for computing energy terms implemented in the REP-FAMSEC method were generated using Keith's AIMAll[43] software.

REFERENCES

(1)   Lewars, E. Computational chemistry. *Introduction to the theory and applications of molecular and quantum mechanics.* Springer: **2003**, 318.

(2)   Jensen, F. *Introduction to computational chemistry*; John wiley & sons, **2017**.

(3)   Leach, A. R.; Leach, A. R. *Molecular modelling: principles and applications*; Pearson education, **2001**.

(4)   Foresman, J.; Frish, E. Exploring chemistry with electronic structure methods. *Gaussian Inc., Pittsburg, USA.* **1996**.

(5)   Dewar, M. J.; Zoebisch, E. G.; Healy, E. F.; Stewart, J. J. Development and use of quantum mechanical molecular models. 76. AM1: a new general purpose quantum mechanical molecular model. *J. Am. Chem. Soc.* **1985**, *107*, 3902-3909.

(6)   Stewart, J. J. Optimization of parameters for semiempirical methods IV: extension of MNDO, AM1, and PM3 to more main group elements. *J. Mol. Model.* **2004**, *10*, 155-164.

(7)   Dewar, M. J.; Thiel, W. Ground states of molecules. 38. The MNDO method. Approximations and parameters. *J. Am. Chem. Soc.* **1977**, *99*, 4899-4907.

(8)   Frisch, M.; Trucks, G.; Schlegel, H.; Scuseria, G.; Robb, M.; Cheeseman, J.; Scalmani, G.; Barone, V.; Petersson, G.; Nakatsuji, H. Gaussian 09. 2009: Wallingford. *Conn, USA Gaussian.*

(9)   Frisch, M.; Trucks, G.; Schlegel, H.; Scuseria, G.; Robb, M.; Cheeseman, J.; Scalmani, G.; Barone, V.; Petersson, G.; Nakatsuji, H. Gaussian 16 Revision B. 01. 2016; Gaussian Inc. *Wallingford CT.*

(10)   Hartree, D. R. The wave mechanics of an atom with a non-Coulomb central field. Part I. Theory and methods. *Сборник статей к мультимедийному электронному учебно-методическому комплексу по дисциплине «физика атома и атомных явлений»/отв. ред. Шундалов МБ; БГУ, Физический факультет.* **1928**.

(11)   Fock, V. Näherungsmethode zur Lösung des quantenmechanischen Mehrkörperproblems. *Zeitschrift für Physik.* **1930**, *61*, 126-148.

(12)   Slater, J. C. Note on Hartree's method. *Phys. Rev.* **1930**, *35*, 210.

(13)   Møller, C.; Plesset, M. S. Note on an approximation treatment for many-electron systems. *Phys. Rev.* **1934**, *46*, 618.

(14)   Bowling, N. P.; McMahon, R. J. Enediyne isomers of tetraethynylethene. *J. Org. Chem.* **2006**, *71*, 5841-5847.

(15)   Esselman, B. J.; Emmert III, F. L.; Wiederhold, A. J.; Thompson, S. J.; Slipchenko, L. V.; McMahon, R. J. Thermal Isomerizations of Diethynyl Cyclobutadienes and Implications for Fullerene Formation. *J. Org. Chem.* **2015**, *80*, 11863-11868.

(16)   Jain, R.; Ahuja, B.; Sharma, B. Density-Functional Thermochemistry. III. The Role of Exact Exchange. *Indian J. Pure Appl. Phys.* **2004**, *42*, 43-48.

(17)   Lee, C.; Yang, W.; Parr, R. Density-functional exchange-energy approximation with correct asymptotic behaviour. *Phys. Rev. B.* **1988**, *37*, 785-789.

(18)   Rassolov, V. A.; Ratner, M. A.; Pople, J. A.; Redfern, P. C.; Curtiss, L. A. 6-31G* basis set for third-row atoms. *J. Comput. Chem.* **2001**, *22*, 976-984.

(19)   Dunning Jr, T. H. Gaussian basis sets for use in correlated molecular calculations. I. The atoms boron through neon and hydrogen. *J. Chem. Phys.* **1989**, *90*, 1007-1023.

(20)   Hratchian, H. P.; Schlegel, H. B. Accurate reaction paths using a Hessian based predictor–corrector integrator. *J. Chem. Phys.* **2004**, *120*, 9918-9924.

(21)   Fukui, K. The path of chemical reactions-the IRC approach. *Acc. Chem. Res.* **1981**, *14*, 363-368.

(22)   Tantillo, D. J. *Applied Theoretical Organic Chemistry*; World Scientific, **2018**.

(23)   Tomasi, J.; Mennucci, B.; Cammi, R. Quantum mechanical continuum solvation models. *Chem. Rev.* **2005**, *105*, 2999-3094.

(24)   Bernales, V. S.; Marenich, A. V.; Contreras, R.; Cramer, C. J.; Truhlar, D. G. Quantum mechanical continuum solvation models for ionic liquids. *J. Chem. Phys. B.* **2012**, *116*, 9122-9129.

(25)   Grimme, S. Semiempirical GGA-type density functional constructed with a long-range dispersion correction. *J. Comput. Chem.* **2006**, *27*, 1787-1799.

(26)   Grimme, S.; Antony, J.; Ehrlich, S.; Krieg, H. A consistent and accurate ab initio parametrization of density functional dispersion correction (DFT-D) for the 94 elements H-Pu. *J. Chem. Phys.* **2010**, *132*, 154104.

(27)   Zhao, Y.; Schultz, N. E.; Truhlar, D. G. Design of density functionals by combining the method of constraint satisfaction with parametrization for thermochemistry, thermochemical kinetics, and noncovalent interactions. *J. Chem. Theor. Comput.* **2006**, *2*, 364-382.

(28)   Zhao, Y.; Truhlar, D. G. Density functional for spectroscopy: no long-range self-interaction error, good performance for Rydberg and charge-transfer states, and better performance on average than B3LYP for ground states. *J. Phys. Chem. A.* **2006**, *110*, 13126-13130.

(29)   Zhao, Y.; Truhlar, D. G. A new local density functional for main-group thermochemistry, transition metal bonding, thermochemical kinetics, and noncovalent interactions. *J. Chem. Phys.* **2006**, *125*, 194101.

(30)   Zhao, Y.; Truhlar, D. G. Density functionals for noncovalent interaction energies of biological importance. *J. Chem. Theor. Comput.* **2007**, *3*, 289-300.

(31)   Zhao, Y.; Truhlar, D. G. Density functionals with broad applicability in chemistry. *Acc. Chem. Res.* **2008**, *41*, 157-167.

(32)   Ochterski, J. W. Thermochemistry in gaussian. *Gaussian Inc.* **2000**, *1*, 1-19.

(33)   Popelier, P. L.; Brémond, É. A. Geometrically faithful homeomorphisms between the electron density and the bare nuclear potential. *Int. J. Quantum Chem.* **2009**, *109*, 2542-2553.

(34)   Popelier, P. L. A. The QTAIM perspective of chemical bonding. *The Chemical Bond.* **2014**, *1*, 271-308.

(35)   Bader, R. F. Atoms in molecules. *Acc. Chem. Res.* **1985**, *18*, 9-15.

(36)   Pendás, A. M.; Blanco, M. A.; Francisco, E. Chemical fragments in real space: definitions, properties, and energetic decompositions. *J. Comput. Chem.* **2007**, *28*, 161-184.

(37)   Blanco, M.; Martín Pendás, A.; Francisco, E. Interacting quantum atoms: a correlated energy decomposition scheme based on the quantum theory of atoms in molecules. *J. Chem. Theor. Comput.* **2005**, *1*, 1096-1109.

(38)   Cukrowski, I.; Dhimba, G.; Riley, D. L. A reaction energy profile and fragment attributed molecular system energy change (FAMSEC)-based protocol designed to uncover reaction mechanisms: a case study of the proline-catalysed aldol reaction. *Phys. Chem. Chem. Phys.* **2019**, *21*, 16694-16705.

(39)   Cukrowski, I. IQA-embedded fragment attributed molecular system energy change in exploring intramolecular interactions. *Comput. Theor. Chem.* **2015**, *1066*, 62-75.

(40)   Cukrowski, I.; Sagan, F.; Mitoraj, M. P. On the Stability of Cis-and Trans-2-Butene Isomers. An Insight Based on the FAMSEC, IQA, and ETS-NOCV Schemes. *J. Comput. Chem.* **2016**, *37*, 2783-2798.

(41)   Cukrowski, I.; van Niekerk, D. M.; de Lange, J. H. Exploring fundamental differences between red-and blue-shifted intramolecular hydrogen bonds using FAMSEC, FALDI, IQA and QTAIM. *Struct. Chem.* **2017**, *28*, 1429-1444.

(42)   Deppmeier, B.; Driessen, A.; Hehre, T.; Johnson, J.; Klunzinger, P.; Watanabe, M. Spartan'10. *Wavefunction Inc.* **2011**.

(43)   AIMAll (Version 19.10.12), Keith, T. A. TK Gristmill software. *Overland Park KS, USA*. **2019** (aim.tkgristmill.com).

CHAPTER 3: A DFT study of the preferred electrophilic site for nucleophilic substitution of 2-phenylquinoxaline

INTRODUCTION

The recent research study by Ndlovu et al. shows that the nucleophilic substitution of 2-phenylquinoxaline (**1**) proceeds smoothly with various organolithium nucleophiles at position 3 to afford 2,3-disubstituted quinoxaline derivatives.[1] According to classical organic chemistry, position 3 is the preferred site for nucleophilic substitution because it gives one the option of retaining the aromaticity of the molecule post the oxidation step of the assumed ONSH[2] reaction mechanism. As mentioned in Chapter 1, these reactions afforded the final product at vastly different yields. To rationalize this, steric hindrance and the high electron density in the aryl and alkynyl nucleophiles were proposed as the contributing factors affecting the yields of these reactions.

In this Chapter, we report on the comprehensive DFT[3] study performed on the nucleophilic substitution of **1** when treated with lithium phenylacetylide (**2**). Not only will this investigation help address the variations in obtained yields in the experimental work by Ndlovu and co-workers, but it will also be a steppingstone towards completely understanding the ONSH reaction mechanism at an atomic, molecular fragment and molecular level. This mechanism is said to be controlled by the fast and reversible formation of the σ^H-adduct generated by the transfer of an R-group from the nucleophile to an electrophilic site.[2] However, from our computational modelling, multiple electrophilic sites were identified in **1**. This pointed out towards a possible competition for nucleophilic addition, which in turn could lead to multiple reaction pathways yielding different outputs (products).

Therefore, the investigation in this Chapter focuses mainly on addressing how the presence of multiple electrophilic sites in **1** could influence the yield of the desired product by modelling all possible reaction paths. To provide a fundamental understanding of every consecutive step along each reaction path, the REP-FAMSEC[4] method will be employed in addition to the standard analysis of using energy profiles to investigate reaction mechanisms and preferred reaction pathways. This method allows us to monitor the bond breaking and bond forming processes through the interaction energies computed for the atoms involved. From this, fragments leading or opposing chemical changes in the chemical system will be identified. The results of this study will also be beneficial as they will allow total control over equivalent commercially important reactions.

The XYZ coordinates of all energy-optimized electronic structures considered (Tables A1-A24) and a full set of their energies (Tables A25-A34) are included in Part 1 of the Supplementary Information (SI) for Chapter 3 – see Appendix A.

RESULTS AND DISCUSSION

Nucleophilic Addition

Figure 3.1 shows the molecular graphs of **1** and **2** showing also the QTAIM-defined net atomic charges. The Li-atom is nearly $+1e$ ($+0.9463e$) and thus must be strongly attracted to N-atoms which carry charges that are more negative than $-1e$ (N1 = $-1.1164e$ and N4 = $-1.1211e$); notably, these atoms carry largest atomic charges. Therefore, it is reasonable to assume that the interaction between Li and N atoms must be seen as the driving force which brings **1** and **2** together.
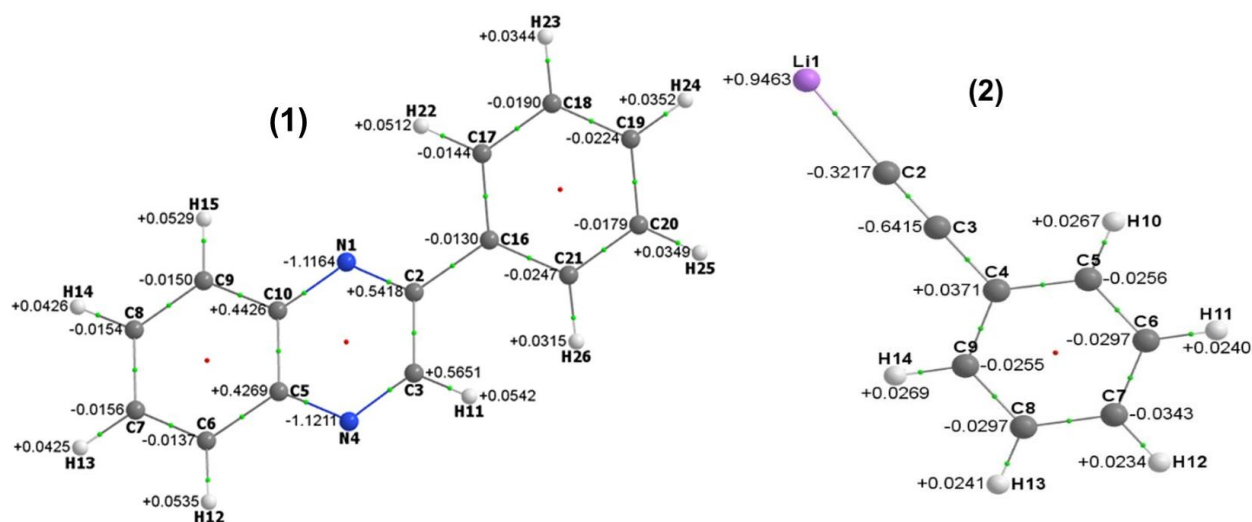
Figure 3.1. Molecular graph of 2-phenylquinoxaline (**1**) and lithium phenylacetylide (**2**) showing QTAIM-defined net atomic charges in *e.*

The molecular graph of **1** also reveals that there are four positively charged C-atoms, namely C2, C3, C5 and C10. Importantly, they are the only C-atoms in **1** with positive net charges: $+0.553 \pm 0.013e^-$ for C2 and C3, $+0.435 \pm 0.013e^-$ for C5 and C10. All remaining C-atoms carry negative and an order of magnitude smaller charges. C-atoms of this nature (positively charged) are called electrophilic sites, and this means that, in principle, there are four C-atoms where a C–C bond formation can take place. Despite this, there are only two possible approaches that **2** can make towards **1**. That is, **2** must swing either towards C2 or C10 when Li interacts with N1 or swing towards C3 or C5 when Li interacts with N4.

From a visual inspection of **1**, one might argue that steric hindrance (if playing any role at all) should be more significant for the C2 and C3 substitution sites due to the presence of the phenyl substituent at C2. However, from a charge perspective, C2 and C3 carry charges that are more positive than C5 and C10 thus making them more susceptible for nucleophilic addition. It is clear that it is difficult to make any conclusive finding based on atomic charges and assumed steric hindrance. Therefore, to gain further insight, we look at the reaction energy profiles (REPs) for the nucleophilic addition step of the four potential reaction pathways (RPs) shown in Figure 3.2.
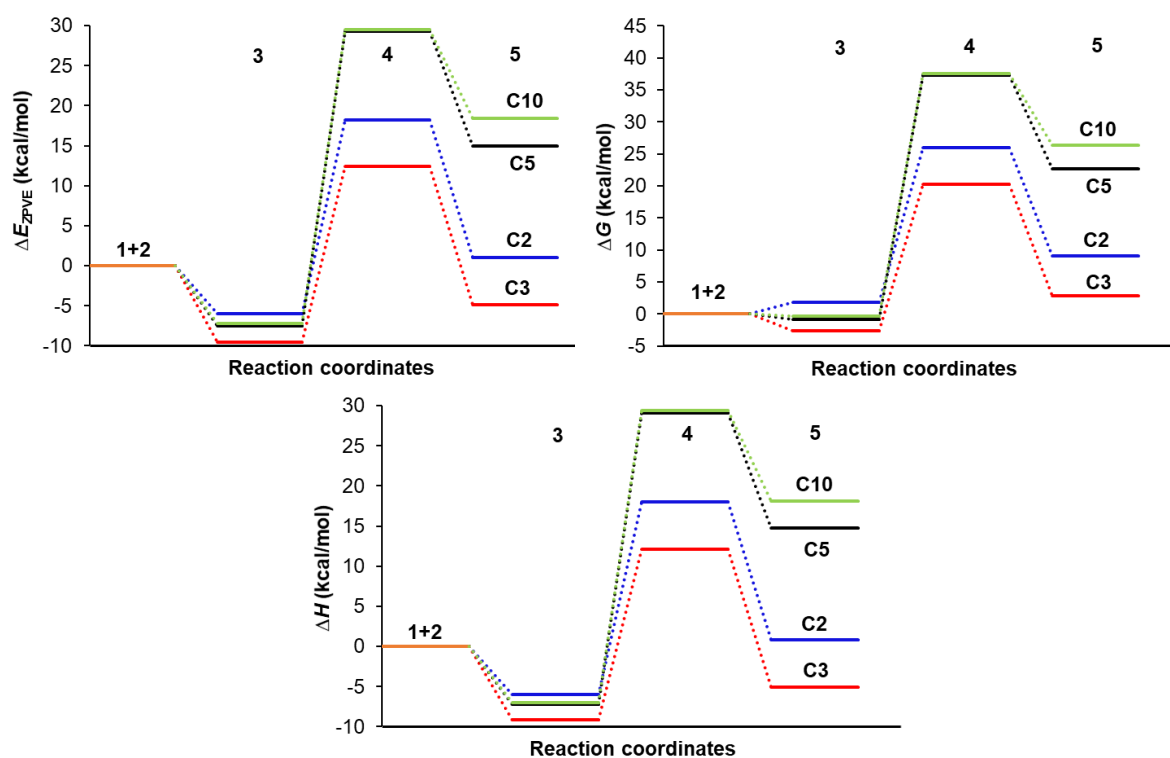
Figure 3.2. Reaction energy profiles for the nucleophilic addition step computed for the C2, C3, C5 and C10 substitution sites. Changes in the energy for adducts (**3**), TS (**4**) and intermediates (**5**) were computed relative to the energy of reactants (**1**+**2**).

From a standard analysis of the REPs, it can be seen that the energy of adducts (**3**) for all possible sites of substitution are highly comparable. This suggests that there is no hindrance at this stage of the reaction. From the energy barriers observed for each RP, possible substitution at C5 and C10 can be effectively eliminated at the transition state stage. Furthermore, the RP-C2 and RP-C3 appear to be highly comparable in terms of their REPs. This suggests possible competition for nucleophilic addition at C2 and C3.

34

2-Phenylquinoxaline – Lithium Phenylacetylide Adduct Formation

Many (if not most) reactions involving two (or more) distinct molecules, should proceed with an adduct (or an active complex) formation due to attractive intermolecular interactions driving the molecules towards each other. Upon the adduct formation, no bonds are broken or formed within the separate molecules. However, changes in their molecular geometries are expected - structural features of the energy-optimized electronic structures from **1** to **5** along all four reaction pathways can be found in Tables A35-A40, Part 2 of Appendix A. As mentioned already, the organolithium nucleophile **2** can approach **1** in two different ways forming adducts **3a**, **3b, 3c** and **3d** that are, in principle, well prepared for the subsequent formation of a C–C bond at the C2, C3, C5 and C10 electrophilic sites, respectively. The energy-optimized electronic structures of respective adducts are shown in Figure 3.3.

As expected, when the two reactants approach each other, various geometrical changes are observed. The most significant geometrical change observed upon the formation of the adducts is the change in the dihedral angle (DA) between N1,C2,C16 and C17 in **1**. This DA was observed to be 28.37º out of the plane of the quinoxaline moiety. As **2** approaches **1**, the phenyl substituent at C2 rotates to accommodate the incoming nucleophile. This results in either an increase or decrease in the DA. Another important and rather unexpected geometrical change observed is the loss of linearity in the incoming nucleophile (**2**) upon the formation of the adducts. However, this change is only significant upon the formation of **3a** and **3b** where the angle between atoms Li27, C28 and C29 changed from 177.94º to 137.54º and 155.49º, respectively. This result is explained in detail in the sections discussing the inter- and intramolecular diatomic interactions of the systems.

The energetic information, including the electronic energy (E), zero-point vibrational corrected E (E_{ZPVE}), enthalpy (H) and the Gibbs free energy (G) of the reactants (**1** and **2**) as well as the four adducts, is summarized in Table 3.1. E_{ZPVE} is the lowest possible electronic energy that a quantum mechanical system can have.[5,6] One can also define E_{ZPVE} as the corrected electronic energy of a molecule to account for the effects of molecular vibrations which persist even at absolute zero (0K). The relative energies (Δ) in Table 3.1 denote the energy difference between the computed energies of adducts and the sum of the energies of the two reactants.

(3a)

N1---C2 = 1.32 Å
C2---C3 = 1.43 Å
C2---C16 = 1.48 Å
Li27---C28 = 2.04 Å
Li27---N1 = 2.23 Å
C28---C2 = 3.59 Å

Li27,C28,C29 = 137.54°
N1,C2,C3 = 120.51°
N1,C2,C16,C17 = 37.69°

(3b)

C2---C3 = 1.43 Å
N4---C3 = 1.31 Å
C3---H11 = 1.08 Å
Li27---N4 = 2.15 Å
C28---C3 = 3.31 Å
Li27---C28 = 2.06 Å

Li27,C28,C29 = 155.49°
C2,C3,N4 = 123.06°
N1,C2,C16,C17 = 23.08°

(3c)

N4---C5 = 1.37 Å
C5---C6 = 1.42 Å
C5---C10 = 1.43 Å
Li27---C28 = 2.04 Å
Li27---N4 = 2.11 Å
C28---C5 = 4.19 Å

N4,C5,C10 = 119.63°
C6,C5,C10 = 119.92°
Li27,C28,C29 = 172.34°
N1,C2,C16,C17 = 28.72°

(3d)

N1---C10 = 1.37 Å
C5---C10 = 1.43 Å
C9---C10 = 1.42 Å
Li27---C28 = 2.04 Å
Li27---N1 = 2.15 Å
C28---C10 = 4.21 Å

N1,C10,C9 = 120.14°
C9,C10,C5 = 119.36°
Li27,C28,C29 = 175.62
N1,C2,C16,C17 = 44.21°

Figure 3.3. Energy-optimized electronic structures of adducts **3a**, **3b**, **3c** and **3d**. Important distances, angles and dihedral angles are given in Å and °, respectively.

Table 3.1. Calculated energies (E, E_{ZPVE}, H and G in au) of adducts **3a**, **3b**, **3c** and **3d** as well as the relative energies (Δ) in kcal mol^{-1} denoting the energy difference between the computed energies of the adducts and the total sum of the energies of the reactants (**1** and **2**).

	E	E_{ZPVE}	H	G
Reactants				
1	–649.2102	–649.0067	–649.0009	–649.0288
2	–315.4706	–315.3710	–315.3667	–315.3900
Total:	–964.6808	–964.3777	–964.3676	–964.4188
Adducts				
3a	–964.6927	–964.3873	–964.3772	–964.4159
Δ	–7.5	–6.0	–6.0	1.8
3b	–964.6974	–964.3929	–964.3823	–964.4229
Δ	–10.4	–9.5	–9.2	–2.6
3c	–964.6943	–964.3896	–964.3792	–964.4201
Δ	–8.5	–7.5	–7.2	–0.8
3d	–964.6939	–964.3891	–964.3788	–964.4194
Δ	–8.2	–7.2	–7.0	–0.4

Notably, a trend **3b** < **3c** < **3d** < **3a** holds for all energy terms seen in Table 3.1. This is somewhat surprising as C2 appears to be the least likely substitution site even though net atomic charges of C5 and C10 are significantly less positive. However, very comparable changes in the E_{ZPVE} of all the adducts (**3a-d**) were observed, meaning that all adducts were likely to form.

To gain an insight on the relative stability of the adducts and what drives their formation, we analysed the diatomic molecular fragments involved in the strongest attractive intermolecular interactions along all RPs – see Table 3.2; a full set of the most attractive and repulsive diatomic interactions in **3**, **4** and **5** along four reaction pathways considered is included in Table A45-A47, Part 3 of Appendix A. From this data, it is seen that Li27 interacts strongest with the respective N-atom of **1** along all RPs. That is, the reaction between **1** and **2** is driven by the favourable interactions between Li27 and N1/N4 due to the difference in the net atomic charges between these atom-pairs ($\Delta Q_{Li27,N1/N4}$) being by far much larger than any other atom-pair (net atomic charges for the reactants **1** and **2** are shown in Table A48, Part 4 of Appendix A.

37

Table 3.2. Most significant (leading) attractive diatomic intermolecular interactions in the adducts formed between **1** and **2** along four potential RPs. All values in kcal mol^{-1}.

A	B	RP-C2	A	B	RP-C3	A	B	RP-C5	A	B	RP-C10
N1	Li27	–175.0	N4	Li27	–184.9	N4	Li27	–186.6	N1	Li27	–182.5
N4	Li27	–70.7	N1	Li27	–68.6	N1	Li27	–68.2	N4	Li27	–68.2
C2	C29	–33.9	C3	C29	–32.7	C3	C29	–22.8	C2	C29	–21.5
C3	C29	–28.1	C2	C29	–23.3	C5	C29	–19.3	C10	C29	–19.0
C10	C29	–23.6	C3	C28	–20.8	C3	C28	–18.9	C2	C28	–18.0
C5	C29	–19.6	C5	C29	–19.6	C2	C29	–16.9	C3	C29	–17.6
C2	C28	–16.3	C10	C29	–16.5	C5	C28	–15.4	C10	C28	–15.7

Considering the molecule **2** (lithium phenylacetylide), the Li1–C2 (Li27–C28 in the adducts) interaction energy was computed to be –106.9 kcal mol^{-1} which was nearly entirely (85%) of classic coulombic nature ($V_{cl}^{Li27,C28}$ = –90.9 kcal mol^{-1}). That is, only 15% of this interaction was of covalent character ($V_{XC}^{Li27,C28}$ = –16.0 kcal mol^{-1}). Importantly, we discovered (see entry 20 in Table 3.3) that the strength of this interaction had weakened across all RPs upon the formation of the adducts where the Li-atom now appeared to be involved in much stronger interactions with the respective N-atom than with C28 to which it is supposedly bonded to. Therefore, one can argue whether this is indeed an adduct formation reaction or is it a spontaneous formation of a first and stable intermediate with a definite shift of the Li-atom from **2** to **1**.

From the energy-optimized electronic structures of the adducts seen in Figure 3.3, no classical covalent bond appears to have been broken or formed at this stage. Therefore, to gain insight as to whether this is an adduct formation reaction or not, we study the effect of the Li27···N1/N4 interaction on the nature of the Li27···C28 interaction in **2**. The distances between atoms Li27 and C28 (d(Li27,C28)) as well as d(Li27,N1/N4) are shown in Figure 3.3. These are significantly less than the sum of the Van Der Waals radii of the respective atoms,[7] suggesting that the electron cloud of Li27 overlaps with the electron clouds of both C28 and N1/N4. Because the exchange correlation (XC-term) outlines the extent of a covalent contribution to an interaction, it was important to note its contribution to the Li27···N1/N4 and Li27···C28 interactions.

From our computed data, it was observed that the XC-term contributed only 5% to the leading Li27··· N1/N4 interaction and three times more (15%) to the Li27···C28 interaction along all RPs. Therefore, it is clear that the nature of the Li27···C28 interaction stays the same

and is of more covalent character than the Li27···N1/N4 interaction. Classically, this might be interpreted as there is no definite shift of the Li-atom from **2** to **1**; hence, this is indeed an adduct formation reaction. One must note, however, that the interaction between Li and N1/N4 atoms is by far more ionic due to much larger charge difference when compared with the Li27,C28 atom-pair and this explains the much smaller covalent contribution. Possibly, a definite answer is provided by interaction energies between the Li-atom and either the entire molecule **1** or the molecular fragment $\mathcal{R}$ that is made of atoms of molecule **2** but Li. On average, we found interaction energies of –39 and –160 kcal mol^{-1} for Li,**1** and Li,$\mathcal{R}$, respectively (see entries 3 and 23 in Table 3.3). This indicates that, although Li interacts with N-atoms twice as strongly than with C28 in **2**, the repulsive interactions that it is involved on approaching **1** makes its interactions with the entire molecule **1** four times weaker than with $\mathcal{R}$. In general, this is quite an interesting case where classical interpretations of bonding are failing a chemist. Therefore, in such a case, the most reasonable approach would be, in our view, to treat the 2-molecular adducts as 3-component structures **1**···Li···$\mathcal{R}$, where the interactions between Li and all other atoms of **1** and **2** could classically be seen as of intermolecular character.

Although it has been established that the strength of the Li27···C28 interaction is weakened upon the formation of the adducts across all RPs, it was observed to be much weaker (by about 9 kcal mol^{-1}) along RP-C2 and RP-C3 relative to RP-C5 and RP-C10. This observation suggests that it would be easier to break the Li27–C28 bond in **2** when the C2–C28 or C3–C28 bond is to be formed which would then substantiate the lower energy barriers observed for RP-C2 and RP-C3 in Figure 3.2.

From the data in Table 3.2 (see also Table A45, Part 3 of Appendix A), it was observed that just a few atoms in each molecule are involved in significantly strong attractive and repulsive interactions. Therefore, to gain even more insight, these atoms were grouped to form molecular fragments of special interest in this work:

1. All atoms of the quinoxaline moiety in **1**, $\mathcal{Q}$ = {N1-H15}.

2. All atoms of the phenyl substituent at C2, $\mathcal{Ph}1$ = {C16-H26}.

3. Two molecular fragments made from atoms of $\mathcal{Q}$, namely a) all atoms of the benzene ring, $\mathcal{Bn}$ = {C5-C10,H12-H15}, and b) all atoms of the pyrazine ring, $\mathcal{P}$ = {N1-C5,C10,H11}.

4. Two molecular fragments are made from atoms of $\mathcal{P}$. The first is made of highly negatively charged N-atoms, $\mathcal{N} = \{N1,N4\}$, and the second contains highly positively charged C-atoms, $\mathcal{C} = \{C2,C3,C5,C10\}$.

5. 3-atom molecular fragment of **2**, $\mathcal{L} = \{Li27,C28,C29\}$.

6. Two molecular fragments made from atoms of $\mathcal{L}$, one with a highly positively charged Li-atom and another with highly negatively charged C-atoms, $\mathcal{A} = \{C28,C29\}$.

7. All atoms of **2** except Li27, $\mathcal{R} = \{C28\text{-}H40\}$.

8. All atoms of the phenyl ring in **2** $\mathcal{Ph}2 = \{C30\text{-}H40\}$.

The following molecular fragments were also considered to account for a 3-atom and 4-atom environment for the incoming nucleophile:

a) $\mathcal{G}1 = \{C2,N1,C10\}$ and $\mathcal{G}2 = \{C3,N4,C5\}$.

b) $\mathcal{F}1 = \{N1,C2,C3,C16\}$, $\mathcal{F}2 = \{C2,C3,N4,H11\}$, $\mathcal{F}3 = \{N4,C5,C6,C10\}$, and $\mathcal{F}4 = \{C5,C10,C9,N1\}$.

The inter- and intramolecular interaction energies of these molecular fragments were studied, and the computed relevant interaction energies are summarized in Table 3.3; full set of data obtained for all reaction pathways considered on the adduct and transition state formation is included in Tables A58-A73, Part 5 of Appendix A. Notably, it was observed that the overall intermolecular interactions between molecules **1** and **2** (entry 1) were in favour of RP-C3 (–64.0 kcal mol^{-1}). This observation also holds for the interactions between molecular fragment $\mathcal{R}$ and the entire molecule **1** (entry 2). Although this is in full agreement with the experimental data, attractive intermolecular interaction energies between the two molecules are also observed in all other RPs. This indicates that regardless of the approach, **1** and **2** have a strong affinity for each other.

Table 3.3. Interaction energies of molecular fragments playing an important role in the formation of adducts along the four potential RPs. All values are in kcal mol^{-1}.

Entry	Fragments	Interaction energies			
		RP-C2	**RP-C3**	**RP-C5**	**RP-C10**
1	**1, 2**	–56.6	–64.0	–45.0	–47.4
2	**1, $\mathcal{R}$**	–19.7	–25.4	–5.5	–5.5
3	**1, Li**	–36.9	–38.6	–39.4	–41.9
4	**1, C28**	–1.1	–3.6	–3.6	–4.2
5	**1, C29**	–1.2	–8.7	–1.4	–0.8
6	**1, $\mathcal{L}$**	–39.2	–51.0	–44.5	–46.9
7	**1, $\mathcal{A}$**	–2.3	–12.3	–5.0	–5.0
8	**$\mathcal{Q}$, 2**	–43.5	–50.5	–46.6	–47.3
9	**$\mathcal{P}h$1, 2**	–13.2	–13.6	1.6	–0.1
10	**$\mathcal{B}n$, 2**	23.0	27.7	17.1	17.0
11	**$\mathcal{P}$, 2**	–46.5	–54.5	–39.9	–40.2
12	**$\mathcal{N}$, 2**	–83.0	–92.0	–103.4	–100.9
13	**$\mathcal{C}$, 2**	36.7	45.4	61.1	59.5
14	**$\mathcal{G}$1, 2**	–43.3	0.9	1.5	–43.1
15	**$\mathcal{G}$2, 2**	–3.0	–47.5	–43.9	1.8
16	**$\mathcal{F}$1, 2**	–59.8	11.3	21.9	–51.6
17	**$\mathcal{F}$2, 2**	7.6	–67.7	–48.4	20.9
18	**$\mathcal{F}$3, 2**	11.4	–57.8	–65.4	8.8
19	**$\mathcal{F}$4, 2**	–54.4	13.5	8.7	–62.6
20	**Li, C28**	–90.2	–94.3	–100.5	–101.0
21	**Li, C29**	–68.9	–65.0	–63.1	–62.9
22	**$\mathcal{A}$, Li**	–159.1	–159.3	–163.3	–163.9
23	**$\mathcal{R}$, Li**	–153.2	–153.3	–158.2	–158.4
24	**$\mathcal{P}h$1, $\mathcal{R}$**	–19.2	–19.7	–4.2	–5.2
25	**$\mathcal{P}h$1, $\mathcal{P}h$2**	–9.8	–12.3	0.1	0.2

Therefore, in search for the preferred RP, we study the interaction energies of molecular fragments identified to be playing an important role in this reaction. In order to provide a clear picture of the impact made by the Li-atom, two molecular fragments, namely $\mathcal{L}$ which is made of Li27, C28 and C29 and $\mathcal{A}$, which differs from $\mathcal{L}$ by the absence of Li27, were considered. Starting with the interactions of the individual atoms of $\mathcal{L}$ (Li27, C28 or C29) with the entire molecule **1** we found that they are attractive and very comparable, particularly for Li27 and C28, across all RPs (see entries 3-5). However, the combined interaction of Li27, C28 and C29 as the molecular fragment $\mathcal{L}$ with the entire molecule **1** is attractive and in favour of RP-C3 due the contribution made by C29 (entry 6). Tables A62-A63 in Part 5 of Appendix A show

41

more interactions between either $\mathcal{L}$ or $\mathcal{A}$ and specified molecular fragments of **1**. In most cases, these interactions are of opposite nature due to the dominance of coulomb-type (electrostatic) interactions between atoms having the same or opposite large net atomic charges. However, from the data in Table 3.3, both $\mathcal{L}$ and $\mathcal{A}$ are attracted towards **1** but more significant for $\mathcal{L}$ (see entries 6 and 7). From this discussion, it is clear that although the Li-atom interacts strongest with **1**, it only takes up the responsibility of driving **2** into the vicinity of **1**. That is, Li27 or any other single atom does not differentiate between the RPs.

The atoms of **1** can be grouped into the two distinctive parts (molecular fragments), namely $\mathcal{Q}$ and $\mathcal{Ph}$1. From analysis of the interaction energies associated with these molecular fragments, we see that whereas $\mathcal{Q}$ strongly and comparably attracts the incoming nucleophile (**2**) along all RPs (by -47.5 kcal mol^{-1} on average), the $\mathcal{Ph}$1 fragment guides **2** toward RP-C2 or RP-C3 due to more favourable interactions (relative to RP-C5 and RP-C10) of about -13.0 kcal mol^{-1}, see entries 8 and 9 in Table 3.3.

For further analysis, the molecular fragment $\mathcal{Q}$ was split further into two parts, namely the benzene ring $\mathcal{Bn}$ and the pyrazine ring $\mathcal{P}$. Analysis of the intermolecular interaction energies of these molecular fragments revealed that $\mathcal{Bn}$ was the only molecular fragment of **1** that is involved in repulsive interactions with **2** (entry 10 in Table 3.3). On the other hand, $\mathcal{P}$ was observed to be involved in overall attractive interactions with **2** in favour of RP-C3 followed by RP-C2 (entry 11 in Table 3.3). Having established that the Li-atom of **2** is attracted most strongly to **1** through its interactions with the N-atoms, it is reasonable to assume that the strong attractive interactions between $\mathcal{P}$ and **2** must be a result of the combined interactions of the highly negatively charged N-atoms (as a molecular fragment $\mathcal{N}$) with **2** which compensates over the combined repulsive interactions of the positively charged C-atoms (as a molecular fragment $\mathcal{C}$) with **2**. This is fully confirmed by entries 12 and 13 in Table 3.3.

Recalling that the N-atoms are the docking space for the Li-atom which plays the important role of guiding the two reactants toward each other, the interactions of the immediate three-atom environment (fragment) around the N-atoms, *i.e.* the C–N–C $\mathcal{G}$1 and $\mathcal{G}$2 molecular fragments, with the entire molecule **2** were analysed, see entries 14 and 15 in Table 3.3. We noted that the environment around the N-atoms attracts **2** comparably with a slight preference

42

of about –4.0 kcal mol^{-1} for RP-C3 for which we obtained a quantified attraction of –47.5 kcal mol^{-1} between $\mathcal{G}$2 and **2**.

Now, considering the four-atom fragments $\mathcal{F}$1 to $\mathcal{F}$4, which describe the immediate environment around the C-atoms of $\mathcal{P}$ where the new C–C bonds with C28 are expected to form, strong attractive interactions (–64.0 ± 4 kcal mol^{-1} on average) toward **2** were observed with a slight preference for RP-C3 again for which an attractive interaction of –67.7 kcal mol^{-1} was obtained (entries 16-19 in Table 3.3).

In the experimental work, steric hindrance was proposed as the contributing factor affecting the yield of this reaction. According to classical organic chemistry, one would expect the phenyl substituent at C2 to sterically hinder nucleophilic addition along RP-C2 and RP-C3, more especially for RP-C2. However, from the data obtained from computational modelling, this generally accepted claim is not supported. Instead, we observed that the interactions between $\mathcal{P}\hat{h}$1 and either the entire molecule **2** or fragments of it ($\mathcal{R}$ and $\mathcal{P}\hat{h}$2) actually guides the nucleophile towards these RPs (entries 9, 24 and 25 in Table 3.3). Not only does this suggest that the preferred RP cannot be attributed to steric hindrance linked with or caused by $\mathcal{P}\hat{h}$1, it also explains the loss of linearity in **2** upon the formation of adducts **3a** and **3b**.

Despite all the data discussed in this section being in favour of RP-C2 and RP-C3, the E_{ZPVE} of all four potential adducts is highly comparable. Therefore, none of the RPs can be eliminated at this stage.

Transition States and σ^H-adduct Formation (C–C Bond formation)

In this section we discuss the chemical changes observed from the adduct formation stage to the transition states. Because the addition of the nucleophile to the various identified electrophilic sites is not a spontaneous process, we had to perform inter-nuclear distance scans between C28 and the C-atom (Cn) of the four potential RPs. This was done by reducing the distance between C28 and Cn by 0.1 Å per step. In this process (adducts $\rightarrow$ transition state), the molecules continuously rearrange themselves in such a way that allows C28 to get into close proximity with Cn. Reaction energy profiles computed along the respective reaction coordinates are shown in Figure A1, Part 6 of Appendix A whereas the energy-optimized electronic structures of the TSs along all RPs are shown in Figure 3.4

43
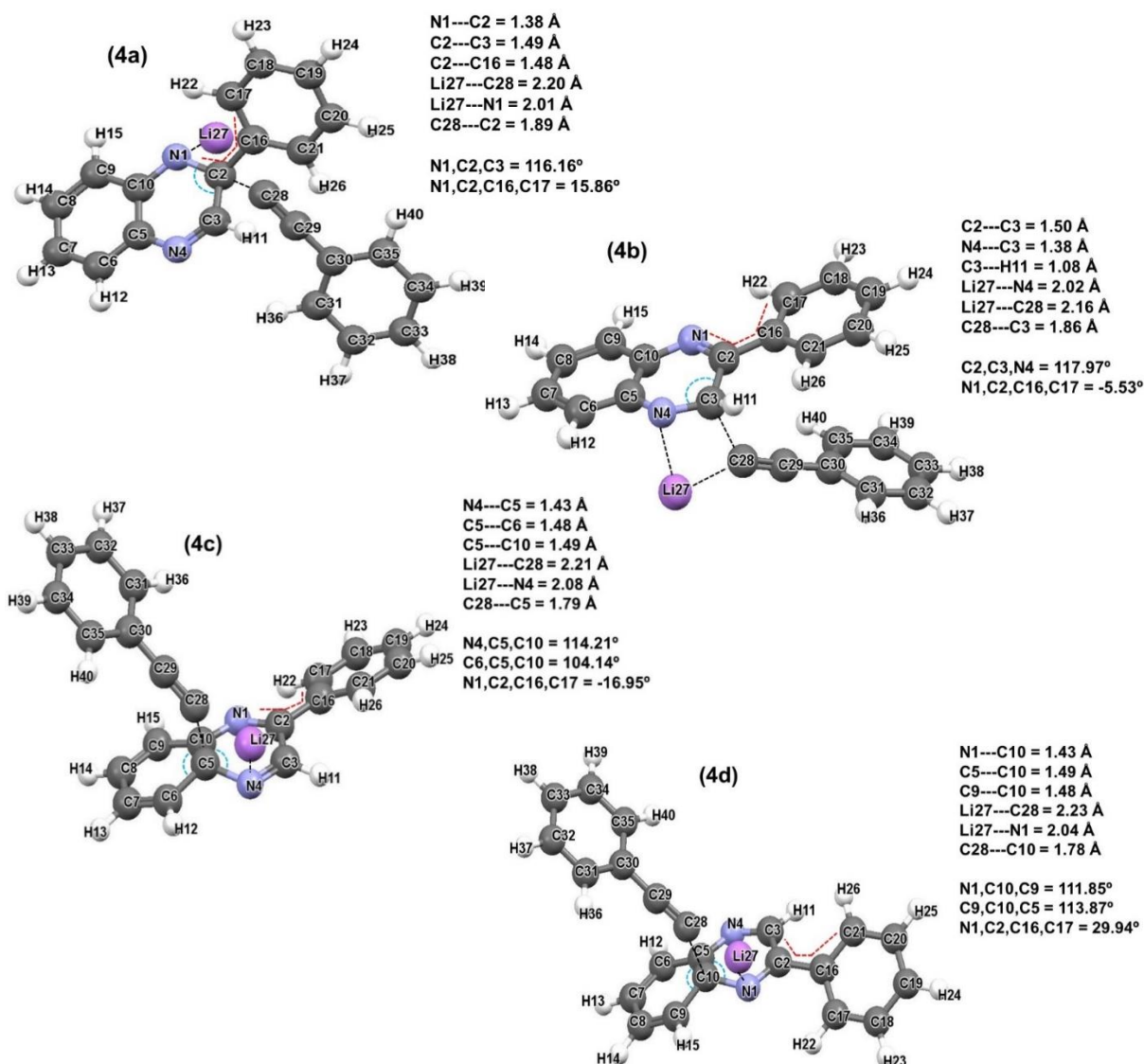
Figure 3.4. Energy-optimized electronic structures of transition states **4a**, **4b**, **4c** and **4d**. Important distances, angles and dihedral angles are given in Å and °, respectively.

As expected, from an analysis of the vibrational frequencies of these structures, a single negative frequency corresponding to the newly forming C–C bond was observed. These were verified as true TSs by means of IRC calculations where we observed that they do indeed link the adducts (**3**) and the expected intermediates (**5**). The IRC graphs for all RPs can be seen in Figure A2, Part 6 of Appendix A.

Together with the presence of a single negative frequency, certain geometrical changes such as reduced distances, elongated bond lengths and angular changes characterize these TSs. Considering **4b** as an example, the TS along RP-C3 is characterized by the reduced distance between C3 and C28 and elongated C2–C3 and C3–N4 bond lengths. The computed C2–C3 and C3–N4 bond lengths in **3b** were 1.43 Å and 1.31 Å, respectively. In **4b**, these respective values are increased to 1.50 Å and 1.38 Å. The elongation of these bonds and the reduced

distance between C3 and C28 (from 3.31 Å to 1.86 Å) is a result of an increase in the attractive intermolecular interaction energy between C3 and C28; it increased from –20.8 kcal mol⁻¹ in **3b** to –107.1 kcal mol⁻¹ in **4b**. Another important geometrical change observed is in the DA(N1,C2,C16,C17). As the distance between the C-atoms involved in the newly forming C–C bond decreases, the phenyl substituent at C2 rotates to accommodate the addition of the nucleophile at C3 thus changing the DA from 23.08º in **3b** to –5.53º in **4b**.

The success of many organic reactions depends on the structure of the TS. This structure must resemble the forming intermediate more than the reactants. This was confirmed by our computational modelling where the interaction between the diminishing Li27–C28 bond was observed to be much weaker than the interaction between developing C–C for all RPs. Although this suggests that all RPs will lead to the successful formation of the respective intermediates, a standard analysis of the REPs (Figure 3.2) showed very large energy barriers of 36.8 and 36.7 kcal mol⁻¹ for nucleophilic addition at C5 and C10, respectively. These are significantly higher than the reaction barriers observed for nucleophilic addition at C2 and C3.

Therefore, in attempt to rationalize the high energy barriers observed along RP-C5 and RP-C10, we employ our understanding of general/organic chemistry. Quinoxaline is a heterocyclic compound that contains benzene and pyrazine ring moieties. Benzene is a cyclic and planar molecule with sp²-hybridized C-atoms. This allows the π-electrons to be delocalized in the molecular orbitals which stretch around the ring. The delocalized electrons are above and below the plane of the ring making benzene very stable. Atoms C5 and C10 are part of the benzene moiety of **1**. Therefore, nucleophilic addition at any of these C-atoms would lead to the disruption of the delocalization of the π-electrons around the benzene ring with no way of reforming it.

To support this generally accepted claim, we study the impact of nucleophilic addition on the covalent interactions in $\mathcal{B}n$ and $\mathcal{P}$ rings which make up the quinoxaline moiety of **1**. The sum of the covalent interaction energies of these molecular fragments is summarized in Table 3.4. Looking first at the strength of the covalent interactions of $\mathcal{B}n$, we see that at the adduct stage, the values are very comparable along all RPs. However, the Δ1 values in Table 3.4 show that at the TS stage, these interactions strengthen by approximately 20 kcal mol⁻¹ in RP-C2 and RP-C3. The opposite trend is observed in RP-C5 and RP-C10. Here we see that at the TS stage, the covalent interactions of $\mathcal{B}n$ have weaken by approximately 40 kcal mol⁻¹. Hence, the

45

effective change is highly in favour of RP-C2 and RP-C3 (by –60 kcal mol^{-1}) and this agrees well with generally accepted interpretations.

Table 3.4. Sum of the covalent interaction energies between atoms of the molecular fragments $\mathcal{B}n$ and $\mathcal{P}$ for all stationary points along all four potential RPs. All values are in kcal mol^{-1}.

	INTERACTION ENERGIS			
Stationary point	**RP-C2**	**RP-C3**	**RP-C5**	**RP-C10**
$\mathcal{B}n$				
Adducts	–1892.6	–1892.0	–1888.4	–1890.6
Transitions states	–1916.2	–1910.9	–1848.1	–1849.4
Δ1	–23.6	–18.9	40.3	41.2
$\mathcal{P}$				
Adducts	–2211.9	–2211.2	–2221.0	–2212.4
Transitions states	–2111.6	–2104.6	–2133.1	–2128.5
Δ2	100.3	106.6	87.9	83.9
$\mathcal{Q}$				
Adducts	–3937.6	–3936.8	–3943.9	–3936.0
Transitions states	–3851.7	–3843.0	–3841.3	–3837.6
Δ3	85.9	93.8	102.6	98.4

Considering now the pyrazine ring $\mathcal{P}$, we see that at the TS stage, the covalent interactions in $\mathcal{P}$ are weakened along all RPs as Δ2 >> 0. Although this is so, it is important to note that this effect is more significant along RP-C2 and RP-C3 where the covalent interaction in $\mathcal{P}$ are weakened by 106.6 and 100.3 kcal mol^{-1}, respectively.

Therefore, it is evident that nucleophilic addition at C5 or C10 impacts both $\mathcal{B}n$ and $\mathcal{P}$ negatively while nucleophilic addition at C2 or C3 only has a negative impact on $\mathcal{P}$. However, making a conclusive statement based on this data would or might be misleading. Therefore, to gain more insight, one has to look at the combined effect since the two rings are joined. To do so, one must consider the covalent interaction of the entire molecular fragment $\mathcal{Q}$. The data thereof, also included in Table 3.4, shows that the strength of these interactions is very comparable at the adduct stage. Although these interactions weaken across all RPs at the TS stage, they appear to have weakened most along RP-C5 and RP-C10. That is, regardless of the RP followed, the aromaticity of the system is disrupted. However, this disruption is most unfavourable along RP-C5 and RP-C10 and since there is no way it can be restored, the nucleophilic addition at C5 or C10 can therefore be eliminated.

The elimination of RP-C5 and RP-C10 leaves us with two potential RPs, namely RP-C2 and RP-C3. The computed energy barriers of these RPs are very comparable. One can argue that this is a result of the very comparable net atomic charges observed for C2 and C3 in Figure 3.1. Therefore, in attempt to identify the preferred RP, we study the interaction energies between selected fragments of **2** and a set of major fragments of **1**. Prior to doing so, it is important to note that in the nucleophilic addition step of the reaction being studied, there is one bond (Li27–C28) breaking and two bonds (Li27–N4 and C3–C28) forming. That is, at the TS stage, Li27 is somewhere in the 3D space of the molecular system between N4 and C28. As such, in our analysis of interaction energies of selected molecular fragments, Li27 is treated as a separate entity and thus all its interactions at this stage are seen as intermolecular interactions either with **1** and its fragments or with $\mathcal{R}$.

From the data in Table A64, Part 5 of Appendix A, it is clear that the Li-atom does not differentiate between the two RPs as its interactions with significant fragments of **1** are mostly comparable. Further analysis of the interaction energies between larger fragments of **2**, i.e., $\mathcal{R}$ and $\mathcal{Ph}2$, and significant fragments of **1** (they are summarized in Tables A60-A61, Part 5 of Appendix A) showed comparable energies with a slight preference for RP-C3. The comparability of this data and the energy barriers suggests that the reaction has the potential to follow either RP-C2 or RP-C3 which would result in the formation of intermediates **5a** and **5b**, respectively. The formation of both **5a** and **5b** stabilizes the reaction, (see Figure 3.2). However, the energy of **5a** is 1.1 kcal mol^{-1} above the initial reactants whereas **5b** lies –4.9 kcal mol^{-1} below them. That is, **5b** is more stable, by 6.0 kcal mol^{-1}, than **5a**.

The energy-optimized intermediates **5a** and **5b** are shown in Figure 3.5 – see also Tables A26-A27 in Appendix A. Analysis of these electronic structures revealed that the elongated bonds C2–C3 and C3–N4, which characterized the **4b** TS along RP-C3, are elongated even further upon the formation of **5b**. The same phenomenon is observed for bonds N1–C2 and C2–C3 in the **4a** → **5a** process. Furthermore, upon the formation of **5a** and **5b**, the C-atom at which the nucleophile was added appears to have taken up a pseudo-tetrahedral (sp^3) geometry, losing its original trigonal planar (sp^2) geometry.
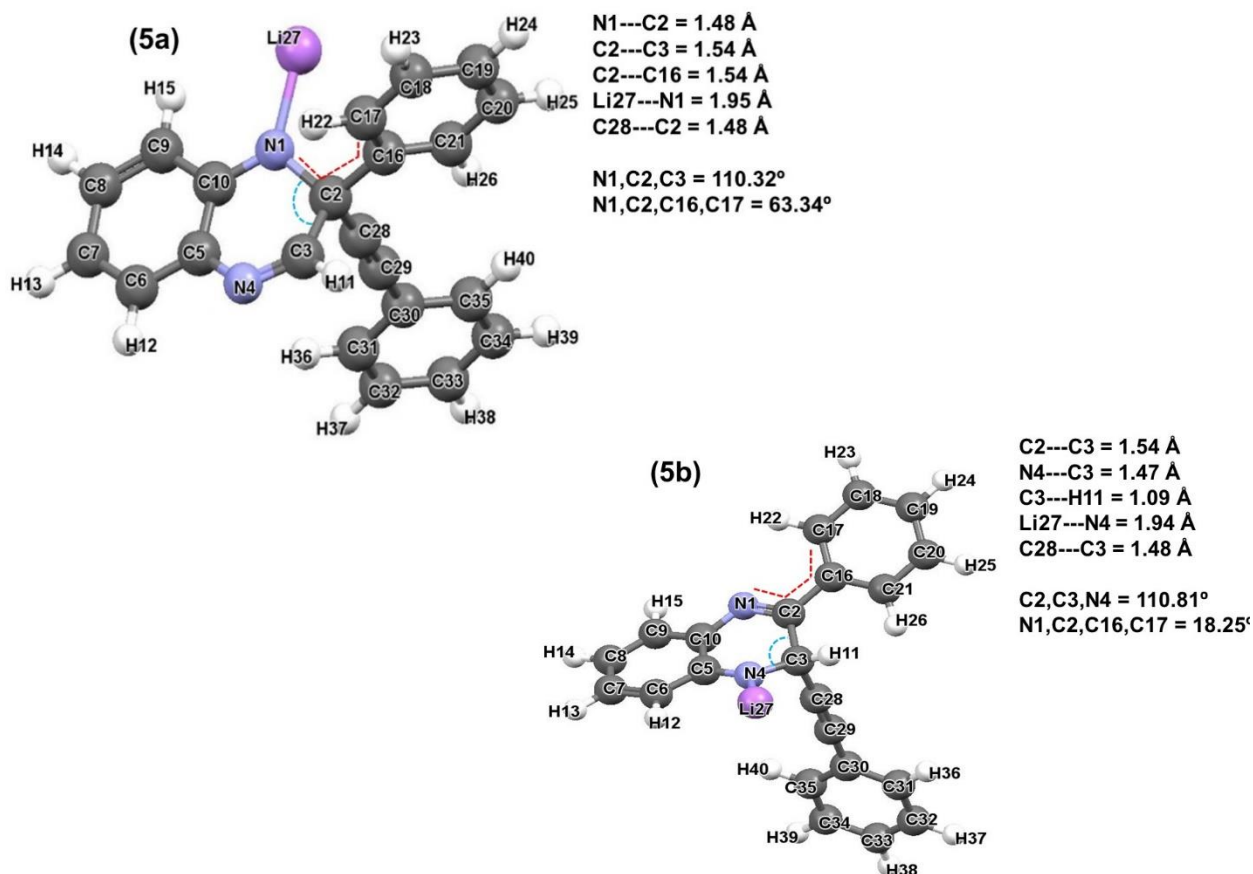
Figure 3.5. Energy-optimized electronic structures of intermediates **5a** and **5b**. Important distances, angles and dihedral angles are given in Å and °, respectively.

Thermodynamic analysis of the nucleophilic addition step

To gain a comprehensive understanding of the assumed ONSH reaction mechanism followed by the reaction between **1** and **2**, one needs to investigate the changes in the thermodynamic parameters associated with the nucleophilic step as it is said to be the rate determining step (RDS).[8] One of the most important experimental conditions associated with reactions involving organolithium reagents is to work at very low temperatures (195.15 K) as these reactions are highly exothermic. Therefore, all the changes in the thermodynamic properties were computed at 195.15 K. The data summarized in Table 3.5 reveals that upon the formation of the adducts **3a** and **3b**, the free energy (G) of the system increases slightly (by 1.8 kcal mol^{-1}) along RP-C2 and decreases (by –2.6 kcal mol^{-1}) along RP-C3. We also observe that the enthalpy (H) decreases along both RPs but in favour of RP-C3. As the reaction proceeds through the TS to the intermediates, both H and G follow the same trend. That is, from the adducts to the TSs, both parameters increase along both RPs and then decrease from the TSs to the intermediates. However, it was observed that the increase in H and G is more significant (by 6 kcal mol^{-1}) along RP-C2 relative to RP-C3. Clearly, it is evident that the decrease in H

48

and G upon the formation of the intermediates is in favour of RP-C3, but it does not exclude the RP-C2.

Table 3.5. Changes in the thermodynamic properties associated with the stationary points along RP-C2 and RP-C3. All values are given kcal mol^{-1}.

	RP-C2		RP-C3	
	ΔH	ΔG	ΔH	ΔG
Adducts	–6.0	1.8	–9.2	–2.6
Transition states	18.0	25.9	12.2	20.3
Intermediates	0.8	9.1	–5.1	2.9

From these observations, it follows that RP-C3 is both kinetically and thermodynamically more favourable than RP-C2. Although this correlates very well with the reported experimental work, from the evidence provided, one can argue that should the reaction have enough energy to overcome the energy barrier observed along RP-C2, intermediate **5a** could be formed and proceed with the subsequent hydrolysis step of the ONSH reaction mechanism. As such, the hydrolysis of both **5a** and **5b** were modelled and studied. The results thereof are discussed in the section that follows.

Hydrolysis

Hydrolysis is the second step of the ONSH reaction mechanism. Important to note here is that in the experimental work, water (H_2O) was not explicitly introduced into the system. Rather, the system was exposed to the atmosphere and the moisture from the air served the purpose of hydrolysing the intermediate formed at the nucleophilic addition step.

The hydrolysis step is initiated by the spontaneous ($\Delta G \sim -15$ kcal mol^{-1}) formation of adducts **6a**/**6b** between the intermediates **5a**/**5b** and a water molecule **H_2O** – see Figure 3.6. Importantly, all energy terms, E_{ZPVE}, G and H computed for **6a** and **6b** are lower (more negative) when compared with relevant data obtained for the initial reactants **1** and **2** – full set of data is included in Table 3.6. Such significant stabilization of **6a** and **6b** must be attributed to the huge affinity between Li and O-atom of water due to the difference between their net atomic charges (–1.1385e for O-atom and nearly +1e for Li in both **5a** and **5b**). This was well revealed by our IQA and REP-FAMSEC analysis where the strongest attractive intermolecular interaction (–191.0 kcal mol^{-1}) was observed between Li and O along both RPs. The overall interaction energies between the water molecule with either **5a** or **5b** were also computed and observed to be very comparable (–60.0 kcal mol^{-1}) along both RPs.

(6a)

N1---C2 = 1.47 Å
C2---C3 = 1.54 Å
C2---C16 = 1.54 Å
Li27---N1 = 1.98 Å
Li27---O41 = 1.96 Å
C28---C2 = 1.48 Å
H42---C16 = 3.29 Å

N1,C2,C3 = 110.52°
N1,C2,C16,C17 = 51.67°
C2,N1,Li27,O41 = 52.29°

(6b)

C2---C3 = 1.54 Å
N4---C3 = 1.47 Å
C3---H11 = 1.10 Å
Li27---N4 = 1.97 Å
Li27---O41 = 1.95 Å
C28---C3 = 1.48 Å
H43---N4 = 2.96 Å

C2,C3,N4 = 111.73°
N1,C2,C16,C17 = 16.70°
C3,N4,Li27,O41 = -45.24°
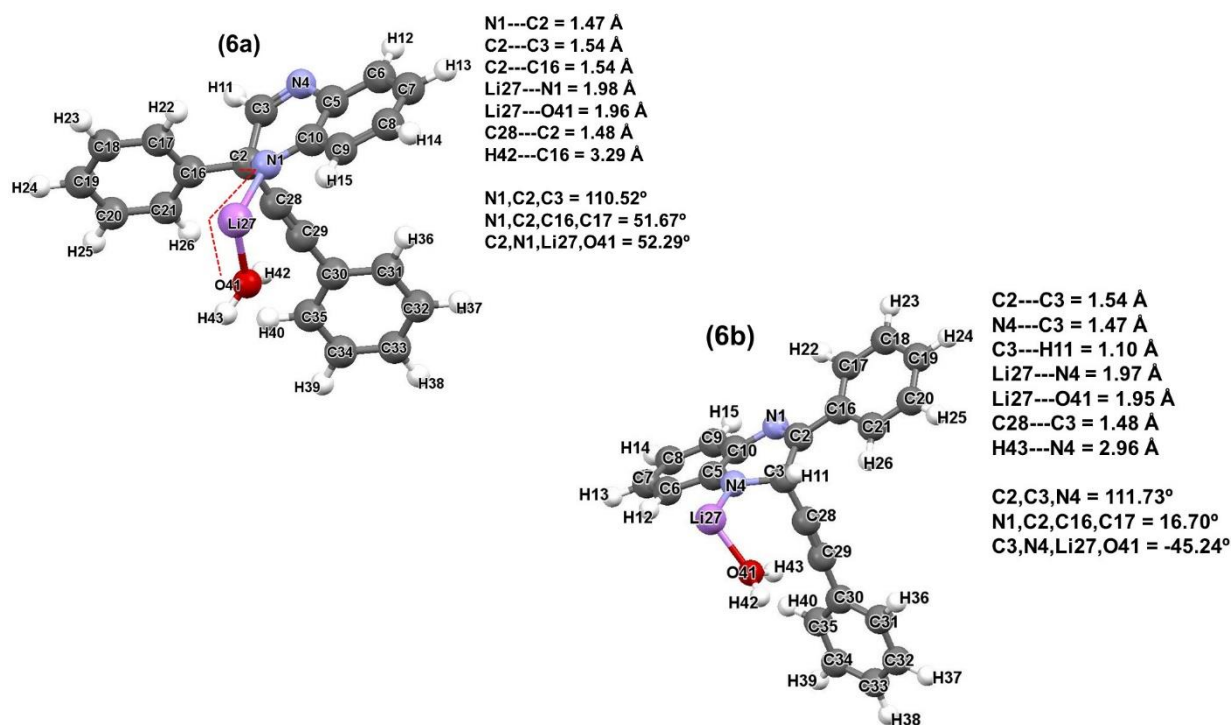
Figure 3.6. Global minimum structures of adducts **6a** and **6b** formed between a water molecule and intermediates **5a** and **5b**. Important distances, angles and dihedral angles are given in Å and °, respectively.

According to the general reaction scheme of the ONSH shown in Scheme 1.6, the hydrolysis process proceeds via a lithium-proton (Li–H) exchange reaction. That is, a proton from H_2O is transferred to the N-atom in exchange for the Li-atom. This results in the formation of an amine at the N-atom and LiOH as a by-product. To complete the modelling of this process, the inter-nuclear distance between one of the protons from H_2O and N1 (for RP-C2) or N4 (for RP-3) was scanned in –0.1 Å steps using **6a** or **6b** as the respective input structures, see Figure A3(a) and A3(b), Part 6 of Appendix A for details. The energy-optimized electronic structures of the TSs and hydrolysis products are shown in Figure 3.7. To facilitate the discussion of the hydrolysis process, consider the full set of energy profiles presented in Figure 3.8. Remarkably, the reaction energy profiles computed for the RP-C2 and RP-C3 are nearly identical when changes in the energy terms from **5** to **8** are considered. That is, upon the exposure to moisture, the reaction can proceed via two, nearly spontaneous, parallel RPs. The energy barriers of these RPs at the TSs (**7**) are about 1 kcal mol^{-1} for the free energy change and even smaller for E_{ZPVE} and H. However, only RP-C3 makes the provision for the aromaticity of the quinoxaline moiety to be recovered. That is, only **8b** can proceed with the final oxidation step of the ONSH reaction mechanism whereas **8a** is trapped leading to a possible by-product from an unwanted but very possible RP that will affect the yield of the wanted RP.

Table 3.6. Calculated energies (E, E_{ZPVE}, H and G in au) of all stationary points observed in the hydrolysis of **5a** and **5b**. The relative energies (Δ, in kcal mol^{-1}) denoting the energy difference between the computed energies of the stationary points and the total sum of the energies of the reactants is also included.

	E	E_{ZPVE}	H	G
		Reactants		
1	−649.2102	−649.0067	−649.0009	−649.0288
2	−315.4706	−315.3710	−315.3667	−315.3900
H$_2$O	−76.4650	−76.4438	−76.4400	−76.4621
Total:	−1041.1458	−1040.8215	−1040.7968	−1040.9102
		Intermediates + H$_2$O		
6a	−1041.1635	−1040.8346	−1040.8106	−1040.8897
Δ	−11.1	−8.2	−1.8	−5.5
6b	−1041.1732	−1040.8435	−1040.8194	−1040.8987
Δ	−17.2	−13.8	−7.3	−11.2
		Transition states		
7a	−1041.1582	−1040.8328	−1040.8098	−1040.8864
Δ	−7.7	−7.1	−1.3	−3.4
7b	−1041.1685	−1040.8426	−1040.8193	−1040.8973
Δ	−14.2	−13.2	−7.3	−10.3
7e	−1041.1219	−1040.7952	−1040.7717	−1040.8496
Δ	15.0	16.5	22.6	19.7
		Hydrolysis product		
8a	−1040.1704	−1040.8408	−1040.8171	−1040.8953
Δ	−15.4	−12.1	−5.9	−9.0
8b	−1041.1795	−1040.8493	−1040.8253	−1040.9054
Δ	−21.1	−17.5	−11.1	−15.4
8e	−1041.1875	−1040.8593	−1040.8342	−1040.9173
Δ	−26.1	−23.7	−16.6	−22.3

In order to rationalise relatively low yield for this reaction, we decided to investigate a possibility of another path for the RP-C2, even though this would hardly be considered by most organic synthetic chemists. We decided to test if, in principle, it is possible for H42 in **5a** to be transferred to C16. Relevant data obtained for the inter-nuclear scan along the H42···C16 reaction coordinates is shown in Figure A3(c), Part 6 of Appendix A, whereas energies computed are included in Table 3.6.
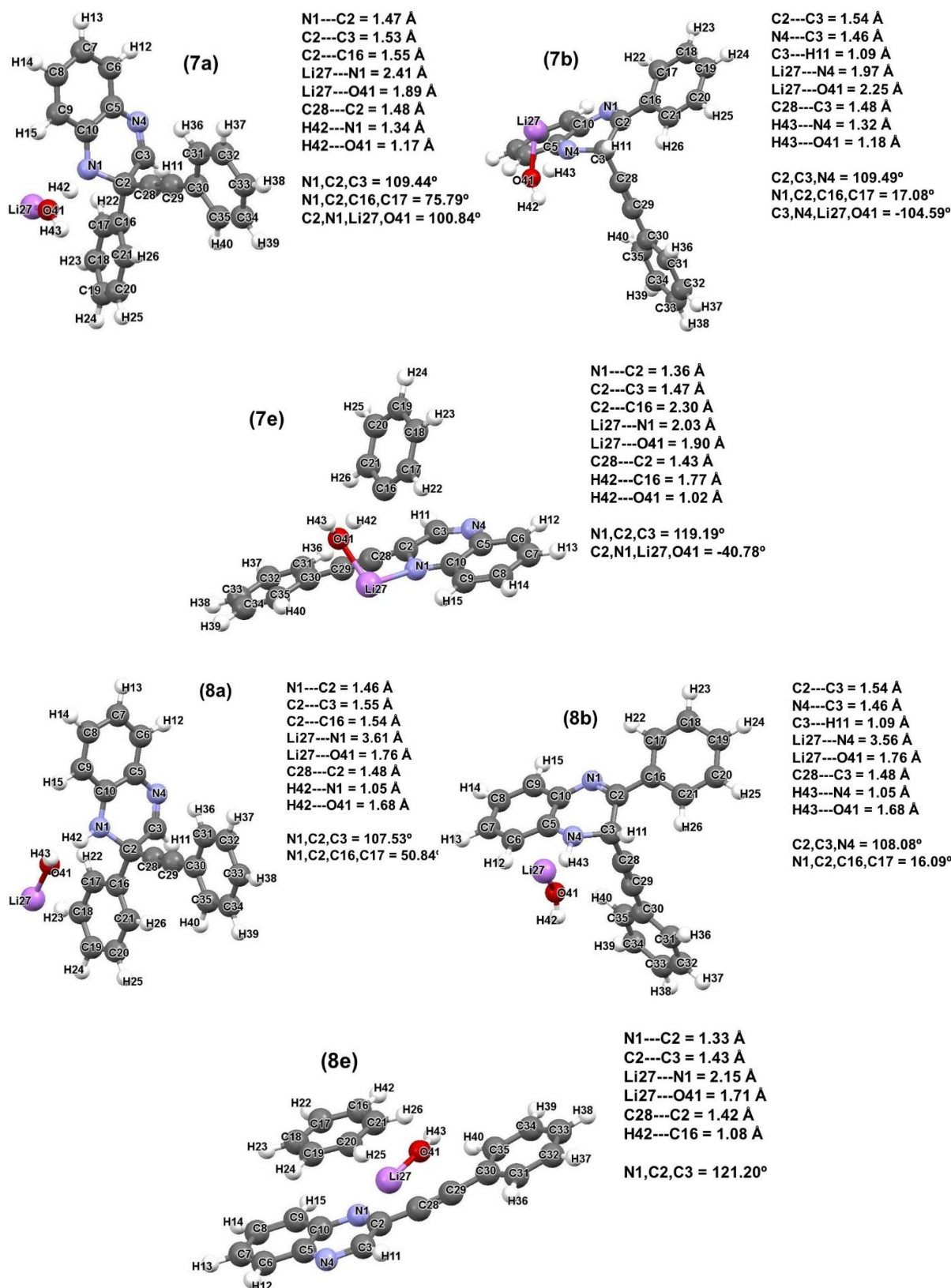
Figure 3.7. Energy-optimized electronic structures of the TSs (**7**) and products (**8**) of the hydrolysis reaction along RP-C2 and RP-C3. Important distances, angles and dihedral angles are given in Å and °, respectively.

52
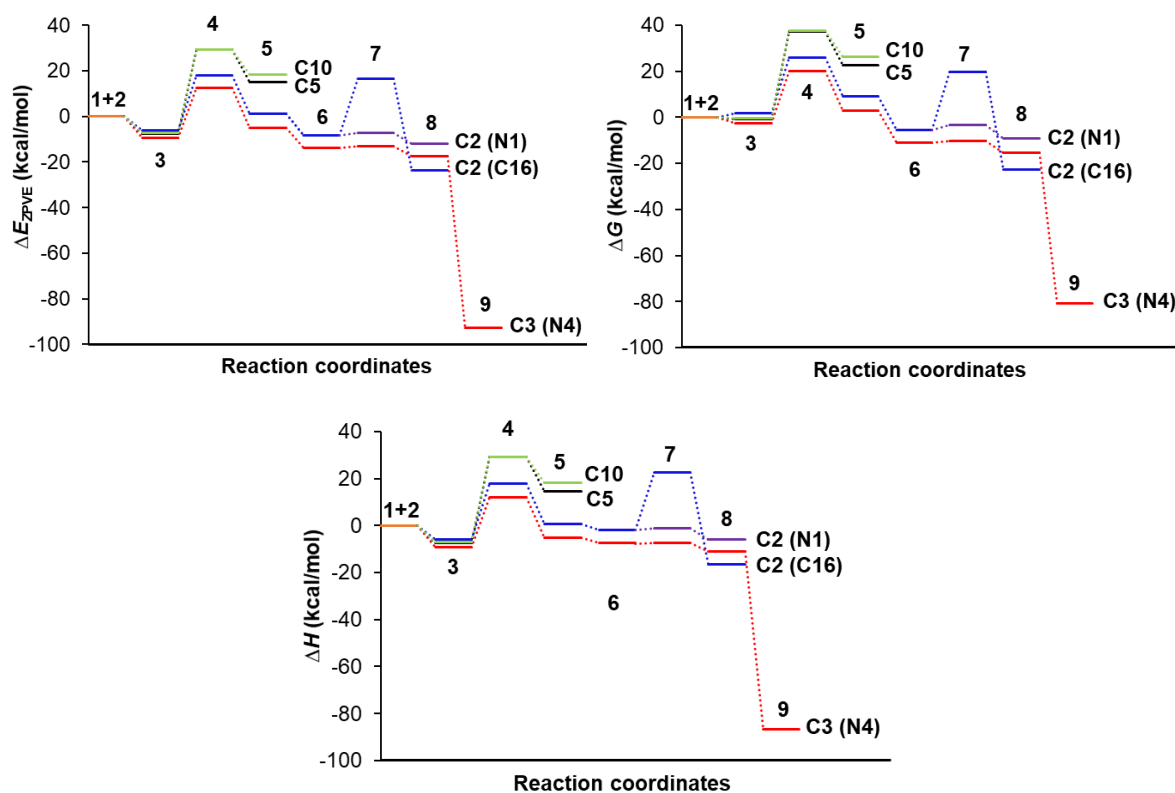
Figure 3.8. Full reaction energy profiles starting from reactants (**1**+**2**) to the ONSH product (**9**). Stage **1**+**2** to **5** represents the nucleophilic addition reaction while stage **5** to **8** represents the hydrolysis reaction. Lastly, stage **8** to **9** represents the oxidation reaction.

This new pathway produced the substitution of the phenyl at C2 to form (2-(2-phenylethynyl)quinoxaline with benzene and LiOH as by-products (**8e**) via the TS **7e**. Unexpectedly, the energy barrier (24.7 kcal mol^{-1}) at **7e** is entirely feasible for the reaction to proceed but not favourable when compared with that obtained for **7a/b**. This means that the Li-H exchange reaction leading to the formation of either **8a** or **8b** is kinetically more favourable than the transfer of H42 to C16. However, the product (**8e**) of this path is thermodynamically more stable, indicating yet another possible by-product that may contribute to the relatively low yield of the desired product.

Oxidation

Oxidation is the final step of the ONSH reaction mechanism. In this process, the formed dihydro derivative (**8b**) obtained from hydrolysis of **5b** along RP-C3 is oxidized to afford an ONSH product. Numerous experimental works report KMnO$_4$, an efficient strong oxidant, in liquid ammonia as an effective way of obtaining the ONSH product in quantitative yields.[2,9-14] However, in the work that this project stems from, oxidative elimination of H$_2$ is achieved in atmospheric oxygen (O$_2$). This guided our modelling of the oxidation step whereby O$_2$ was introduced into the system at 298.15 K to convert the amine back to an imine and to restore the

aromaticity of the system by abstracting H11 from C3. In the input structure, O_2 and **8b** were arranged in such a way that d(O44,H11) = 1.05 Å, d(O45,H42) = 1.03 Å and d(O41,H43) = 1.14 Å.

From the full set of energy profiles presented in Figure 3.8, this process is observed to proceed spontaneously and irreversibly to afford the desired 2-phenyl-3-(2-phenylethynyl)quinoxaline ONSH product (**9b**) which sits –92.8 kcal mol^{-1} below the initial reactants with LiOH and H_2O_2 as by-products.

The energy-optimized electronic structure of **9b** is shown in Figure 3.9. The energetic information associated with this electronic structure is presented in Table A34, Part 1 of Appendix A. Important geometrical changes that occur upon the formation of **9b** include the restoration of trigonal planar (sp^2) geometry at C3 which causes the nucleophile to move into the plane of the quinoxaline moiety. In order to accommodate the nucleophile within the plane of the molecule, the phenyl substituent has rotated, resulting in a change in DA(N1,C2,C16,C17) from 16.09º in **8b** to –44.50º in **9b**.
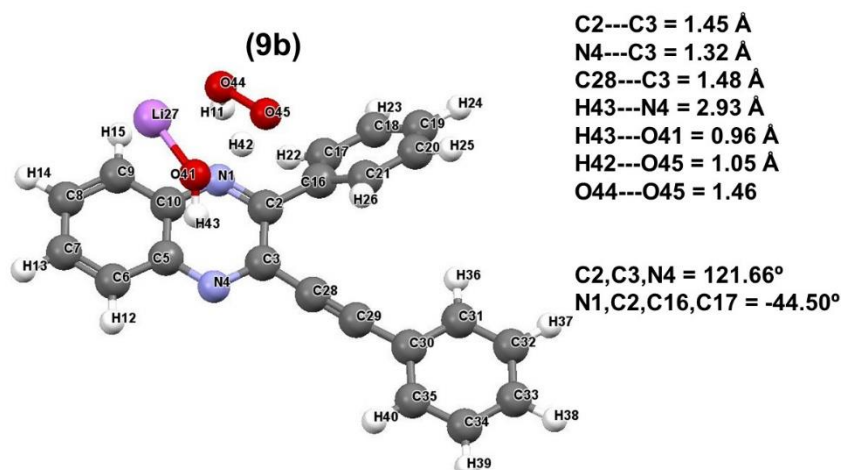
Figure 3.9. Energy-optimized electronic structures of the ONSH product (**9b**) obtained along RP-C3. Important distances, angles and dihedral angles are given in Å and º, respectively.

Simultaneous Hydrolysis and Oxidation

In order to fully elucidate the ONSH reaction mechanism, we track back to the experimental procedure followed by Ndlovu and co-workers.[1] After mixing the reactants under inert nitrogen gas (N_2) at 195.15 K, the reaction was left to warm up to the room temperature and then exposed to the atmosphere where it undergoes hydrolysis and oxidation. However, because H_2O and O_2 coexist in the air, it is not obvious as to when either of these two processes takes place. Therefore, in an attempt to gain further insight, we decided to model the reaction between **1** and **2** following the ONSH reaction mechanism with hydrolysis and oxidation

occurring simultaneously. Important to note here is that this is only practical for RP-C3 because the hydrolysis product along this RP is the only one making provision for oxidation to proceed.

In modelling this RP, which we will call RP-C3′, H_2O and O_2 were introduced into the molecular system of the formed σ^H-adduct (**5b**) along RP-C3 such that d(O44,H11) = 1.16 Å, d(O45,H43) = 1.51 Å and d(O41,Li27) = 1.78 Å. Following no-restriction-imposed energy optimization calculations, the desired aromatic 2,3-disubstituted quinoxaline product (**9b′**) with LiOH and H_2O_2 as by-products were obtained – see Figure 3.10. All energetic information of **9b′** is included in Table A34, Part 1 of Appendix A. Note that **9b** and **9b′** are exactly the same molecular systems made of three molecules and must therefore be seen as conformers. However, there is no guarantee that there is not an even lower in energy than the two.

C2---C3 = 1.45 Å
N4---C3 = 1.32 Å
C28---C3 = 1.42 Å
H43---N4 = 2.93 Å
H42---O41 = 0.96 Å
H43---O45 = 1.04 Å
H11---O44 = 1.04 Å
O44---O45 = 1.46 Å

C2,C3,N4 = 121.36°
N1,C2,C16,C17 = -45.31°
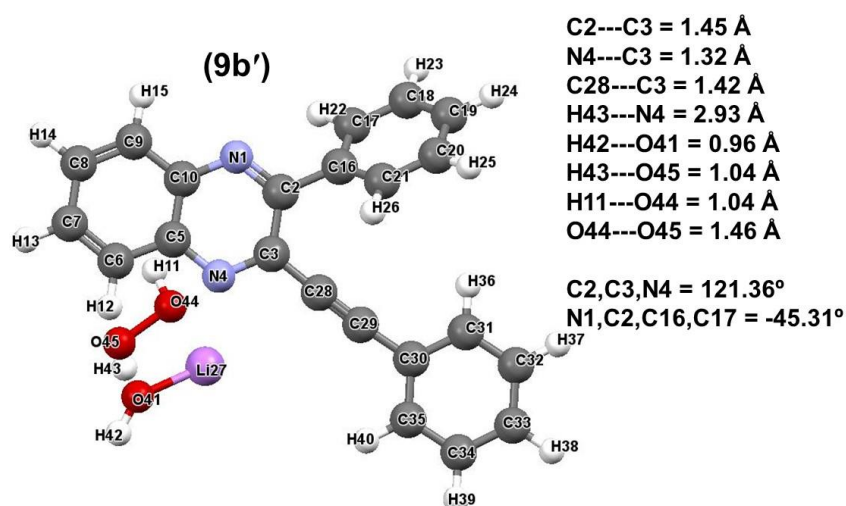
Figure 3.10. Energy-optimized electronic structures of the ONSH product (**9b′**) obtained along RP-C3′. Important distances, angles and dihedral angles are given in Å and °, respectively.

A comparative analysis of the energetic information associated with **9b** and **9b′** showed an energy difference of 4.7 kcal.mol^{-1} in favour of **9b′**. To rationalize this energy difference, we analysed the interaction energies between the three molecules. For ease of reference, the 2,3-disubstituted quinoxaline will be referred to a molecular fragment $\mathcal{DQ}$ while LiOH and H_2O_2 will be referred to as molecular fragments $\mathcal{LH}$ and $\mathcal{PO}$, respectively. The relevant computed interaction energies are summarized in Table 3.7. Here we see that the interaction between the two by-products $\mathcal{PO}$ and $\mathcal{LH}$ is stronger in **9b**. However, their combined interactions with $\mathcal{DQ}$ is more favourable in **9b′**. This indicates that the 4.7 kcal mol^{-1} energy difference between these two systems is attributed to the difference in the arrangement of the by-products relative to the 2,3-disubstituted quinoxaline.

Table 3.7. Computed interaction energies between the by-products and the 2,3-disubstituted quinoxaline in **9b** and **9b′**. All values are in kcal mol^{-1}.

	Interaction energies	
	9b	**9b′**
LH, PO	−100.8	−76.1
PO, DQ	−34.8	−9.2
LH, DQ	−12.6	−49.4

It is then absolutely clear that under the experimental conditions used (no control of O_2 or H_2O addition to the reactive system) the reaction involving C3 substitution site could follow two reaction pathways, a stepwise-one through intermediate steps **6**, **7** and **8** (Figure 3.8) or directly from the σ^H-adduct **5** to the final product **9** with three molecules involved simultaneously – see Figure 3.11. Therefore, it is reasonable to believe that the hydrolysis and oxidation reactions are concurrent. However, this observation does not, in any way eliminate RP-C2.
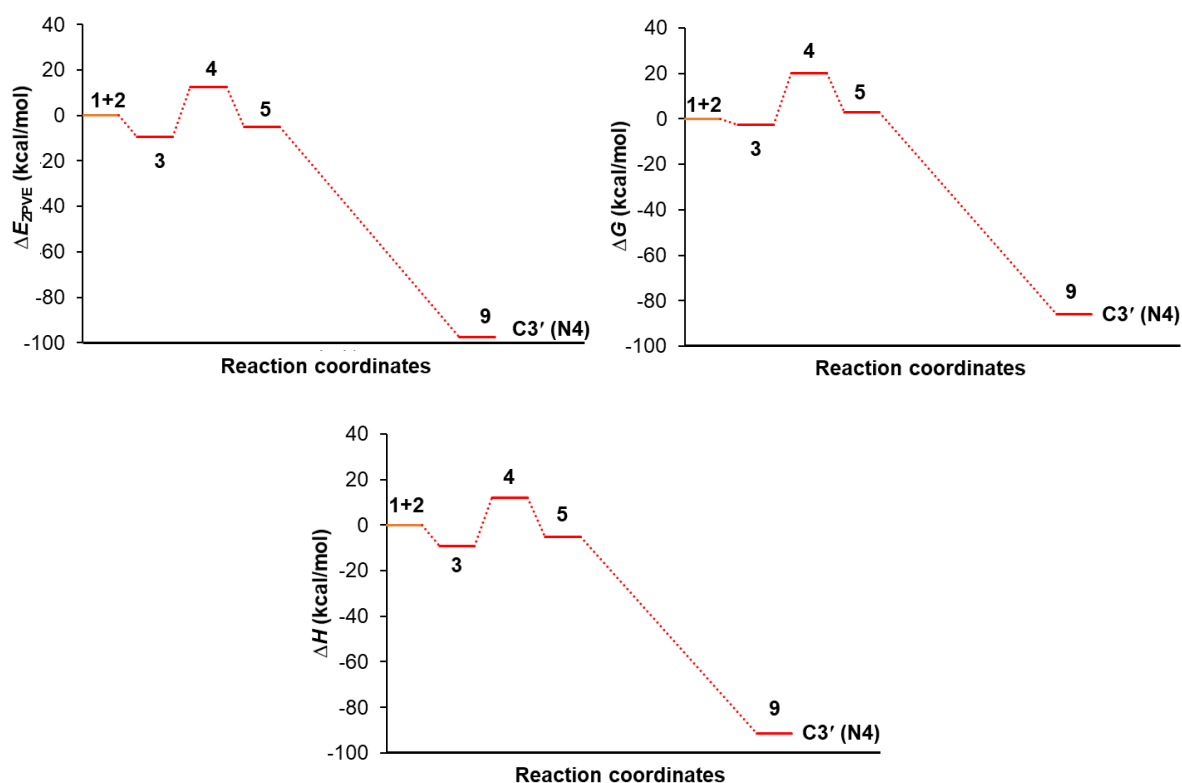
Figure 3.11. Full reaction energy profiles starting from reactants (**1**+**2**) to the ONSH product (**9**). Stage **1**+**2** to **5** represents the nucleophilic addition reaction while stage **5** to **9** represents the simultaneous hydrolysis and oxidation reaction.

CONCLUSION

Using the recently implemented REP-FAMSEC method we quantified the energy contributions of all inter- and intramolecular interactions and their changes between consecutive steps of the assumed ONSH reaction mechanism for the reaction between **1** and **2**. Energies obtained for selected molecular fragments (they varied from a single atom to an entire molecule) explained reaction energy profiles computed for four potential sites of the nucleophilic addition.

According to the experimental report by Ndlovu et al., this reaction occurs at the position occupied by a hydrogen atom in the electron deficient ring (C3 in **1**) to form the so called σ^H-adduct. However, from the generated molecular graph of **1**, three other sites, namely C2, C5 and C10, were identified as potential competing sites for the reaction being studied. This suggested that nucleophilic addition, which is said to be the key and rate determining step of the ONSH reaction mechanism, could occur at various sites, resulting in multiple RPs and, as a consequence, affect the yield of the desired product.

The REP-FAMSEC based study established that the two reactants have a strong affinity for each other driven by the strong attractive interactions between the Li-atom and either N1 or N4. From these two approaches, four different adducts (**3**), each well prepared for the subsequent formation of a C–C bond at either one of the four identified sites, were formed. These were very comparable in energy and all lead to the stabilization of the reaction. However, as the reaction proceeded through to the TS (**4**) to form the intermediates (**5**), very high energy barriers were observed for RP-C5 and RP-C10. Supported by the computed changes in the strength of covalent interactions in molecular fragments $\mathcal{B}n$, $\mathcal{P}$ and $\mathcal{Q}$ as well as our understanding of general/organic chemistry, these RPs were concluded to be impractical or impossible and therefore eliminated as possible RPs.

Following the proposal made by classical chemists that steric hindrance could be the contributing factor towards the relatively low yield (47%) obtained for this reaction, we computed the interactions between the phenyl substituent ($\mathcal{P}h1$) at C2 and either the entire molecule **2** or fragments of it. From this data, we observed that the phenyl substituent guided the nucleophile towards RP-C2 and RP-C3, indicating that the preferred RP cannot be attributed to steric hindrance caused by $\mathcal{P}h1$.

Although the data obtained at the nucleophilic addition stage indicated that RP-C3 was both kinetically and thermodynamically favoured over RP-C2, the energy barriers observed at this

stage were very comparable for both RPs. This indicates that both RPs (C2 and C3) can progress to form intermediates **5a** and **5b** which will undergo hydrolysis (second step of the ONSH reaction mechanism). Upon the introduction of H_2O to the system, we observed that both RPs were nearly spontaneous towards their respective hydrolysis products (**8a** and **8b**). However, of the two products, only **8b** can proceed to the final oxidation stage of the ONSH reaction mechanism to give the expected 2,3-disubstituted quinoxaline compound. This clearly points out that there exists an unwanted yet very possible RP (RP-C2) leading to a possible by-product (**8a**) that may justify the yield obtained for the desired product.

Furthermore, a secondary RP along RP-C2 where H42 from H_2O in **6a** is transferred to C16 instead of N1 was found. Although this path had the highest energy barrier at the hydrolysis stage, it was not high enough to be eliminated as a real possibility. This RP led to the irreversible formation of 2-(2-phenylethynyl)quinoxaline with lithium hydroxide and benzene as by-products (**8e**). This points out towards yet another very possible RP leading to an unwanted output from the hydrolysis stage that will lead to low yields for the desired product.

Clearly RP-C2 competes with RP-C3 leading to possible mixture of the respective products. In order to eliminate RP-C2 or to minimize its influence on the yield for the desired product, we strongly recommend to experimental chemists to run the first stage of the reaction at a low temperature for a longer time (2-4 hours) in a moisture-free and oxygen-free environment (glove-box). The extension of time will allow an equilibrium to be reached with **5b** as the predominant intermediate. That is, even though the reaction will follow both RP-C2 and RP-C3 initially, having sufficient time and assuming spontaneous drive of a reaction environment towards the lowest energy possible, **5a** should go back to reform adducts, particularly **3b**, and follow RP-C3 towards **5b**. In addition, the *in-situ* preparation of the Li-nucleophile should be done with precaution to ensure that sufficient amount is present during the reaction.

Upon the introduction of O_2 to the molecular system of **8b**, the only hydrolysis product that made provision for oxidation, a spontaneous reaction leading to the formation of the desired ONSH product (**9b**) with LiOH and H_2O_2 as the by-products. Moreover, the oxidation of **8b** resulted in the restoration of the aromaticity in the quinoxaline moiety. Because hydrolysis and oxidation occur once the reaction is exposed to the atmosphere, we also modelled them as concurring reactions. This led to the formation of **9b′** which is equivalent to **9b**. The slight energy difference observed between **9b** and **9b′** was concluded to be result of the arrangement

of the by-products relative to the 2,3-disubstituted quinoxaline. As such, it is reasonable to see the hydrolysis and oxidation reactions as concurrent.

REFERENCES

(1)   Ndlovu, N.; Nxumalo, W. Nucleophilic Substitution on 2-Monosubstituted Quinoxalines Giving 2, 3-Disubstituted Quinoxalines: Investigating the Effect of the 2-Substituent. *Molecules.* **2016**, *21*, 1304.

(2)   Mąkosza, M. Nucleophilic substitution of hydrogen in electron-deficient arenes, a general process of great practical value. *Chem. Soc. Rev.* **2010**, *39*, 2855-2868.

(3)   Jain, R.; Ahuja, B.; Sharma, B. Density-Functional Thermochemistry. III. The Role of Exact Exchange. *Indian J. Pure Appl. Phys.* **2004**, *42*, 43-48.

(4)   Cukrowski, I.; Dhimba, G.; Riley, D. L. A reaction energy profile and fragment attributed molecular system energy change (FAMSEC)-based protocol designed to uncover reaction mechanisms: a case study of the proline-catalysed aldol reaction. *Phys. Chem. Chem. Phys.* **2019**, *21*, 16694-16705.

(5)   Sciama, D. W. The physical significance of the vacuum state of a quantum field. **1991**.

(6)   Tantillo, D. J. *Applied Theoretical Organic Chemistry*; World Scientific, **2018**.

(7)   Bondi, A. v. van der Waals volumes and radii. *J. Phys. Chem.* **1964**, *68*, 441-451.

(8)   Abu-Hashem, A. A. Synthesis, reactions and biological activity of quinoxaline derivatives. *ChemInform.* **2015**, *46*, no-no.

(9)   Bartoli, G. Conjugate addition of alkyl Grignard reagents to mononitroarenes. *Accounts of Chem. Res.* **1984**, *17*, 109-115.

(10)   Mąkosza, M.; Surowiec, M. Alkylation of nitroarenes with Grignard reagents via oxidative nucleophilic substitution of hydrogen. *J. Org. Chem.* **2001**, *624*, 167-171.

(11)   Bartoli, G.; Bosco, M.; Dal Pozzo, R.; Ciminale, F. Conjugate addition of RMgX to mononitroarenes. Unequivocal evidence for a single-electron transfer mechanism. *J. Org. Chem.* **1982**, *47*, 5227-5229.

(12)   Counotte-Potman, A.; Van Der Plas, H. C. A new synthesis of 6-(alkyl) amino-3-aryl (alkyl)-1, 2, 4, 5-tetrazines. *J. Heterocycl. Chem.* **1981**, *18*, 123-127.

(13)   van der Plas, H. C.; Wozniak, M. Potassium Permanganate in Liquid Ammonia. An Effective Reagent in the Chichibabin Amination of Azines. *Croat. Chem. Acta.* **1986**, *59*, 33-49.

(14)   Makosza, M.; Staliski, K. Oxidative nucleophilic substitution of hydrogen with 2-phenylpropanenitrile carbanion in heterocyclic nitroarenes. *Synthesis.* **1998**, *11*, 1631-1634.

CHAPTER 4: A DFT Study of the Oxidative Nucleophilic Substitution of Hydrogen (ONSH) reaction mechanism when 2-phenylquinoxaline reacts with 1-octynyllithium

INTRODUCTION

In the preceding Chapter, the Oxidative Nucleophilic Substitution of Hydrogen (ONSH)[1] reaction mechanism was theoretically investigated when 2-phenylquinoxaline (**1**) was treated with lithium phenylacetylide (**2**). From this study, it was established that the presence of multiple electrophilic sites in **1** led to a competition between two reaction pathways (RPs) and that the relatively low yield was not attributed to steric hindrance caused by the phenyl substituent bonded to C2.

As part of our efforts to provide a fundamental understanding of reaction mechanisms, we present in this Chapter a theoretical investigation of the assumed ONSH reaction mechanism followed by the reaction between **1** and the alkynyl organolithium nucleophile, 1-octynyllithium (**10**) – see Scheme 1.6. According to the work of Nxumalo and Ndlovu, this reaction proceeds to give the final product (3-oct-1-ynyl)-2-phenylquinoxaline) in 14% yield. This large variation in yield relative to the reaction investigated in the previous Chapter presumably indicates that the reactivity is influenced by the difference in the nature of the nucleophiles. However, because the classical approach of using the PES to explain reaction mechanisms does not provide insight on chemical changes at an atomic, molecular or molecular fragment level, one fails to elucidate whether or not variations in yields are attributed to the difference in the nature of the nucleophiles. Therefore, this study also aims to address the influence that the nature of the nucleophile has when reacting with **1**.

Understanding the influence of different nucleophiles on the reactivity of **1** will not only aid in understanding the ONSH reaction mechanism, it could lead to major developments in the method and synthesis of many other complex quinoxaline derivatives that have potential medicinal applications as a large number of them have been reported to exhibit anti-viral,[2] anti-microbial[3,4] and neuroprotective activity.[5,6]

All quantum chemical calculations towards obtaining chemical descriptors to provide a deeper understanding of the ONSH reaction mechanism at an atomic, molecular and molecular fragment level when **1** reacts with **10** were computed following the same methods and protocols used in the preceding Chapter. These methods are discussed in detail in Chapter 2. The XYZ coordinates of all energy-optimized electronic structures considered (Tables B1-B14) and a full set of their energies (Tables B15-B20) are included in Part 1 of Appendix B.

© University of Pretoria

RESULTS AND DISCUSSION

Conformational Search

Unlike lithium phenylacetylide, 1-octynyllithium (**10**) has many rotatable bonds. Therefore, due to its profound flexibility, this molecule can adopt an almost an infinite number of possible conformers. In order to identify these conformers, we make use of a computational tool called Spartan,[7] where the molecular force field (MMFF) method and the Monte Carlo algorithm are implemented. This allows us to explore the conformational space in order identify all energetically favourable conformers of a molecule.

The search for the possible conformers was executed by varying the torsion angles of every rotatable bond in **10** in steps of 30º. Important to note here is that we limited ourselves to 100 conformers to make conformational analysis less computationally demanding. After the elimination of similar structural conformers, we were left with 10 conformers. All 10 conformers were then submitted for energy-optimization calculations followed by single-point frequency calculations (SPFC) at 195.15 K to verify their nature as stationary points.

The energetic information associated with of all 10 conformers is summarized is Table B52, Part 7 of Appendix B. A comparative analysis of this data observed that conformer 1 (**C1**) was the lowest energy conformer (LEC). Whereas the energy-optimized electronic structures of the other nine conformers are shown in Figures B5, Part 7 of Appendix B, the energy-optimized electronic structure of the LEC of **10** is shown in Figure 4.1.
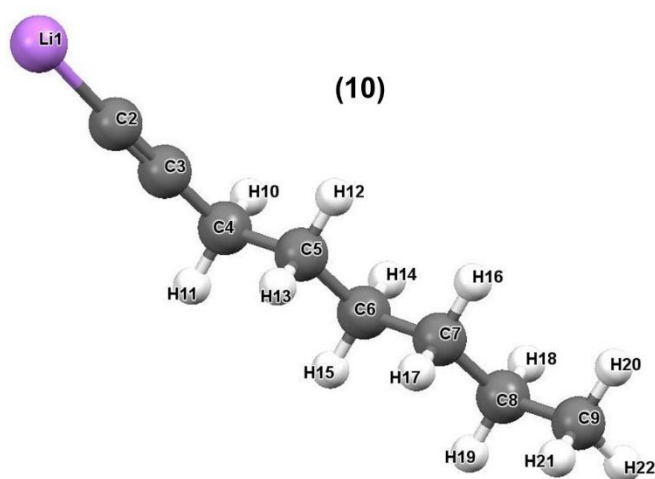
Figure 4.1. Energy-optimized electronic structures of the lowest energy conformer (LEC) of **10**.

Nucleophilic Addition

2-Phenlyquinoxaline – 1-Octynyllithium Adduct Formation

As a result of the competition for nucleophilic addition between C2 and C3 in **1**, which we have established in Chapter 3, the reaction between **1** and **10** was modelled such that the incoming nucleophile interacts with **1** to form adducts **11a** and **11b** which are, in principle, well prepared for the subsequent C–C bond formation to give the intermediates **13a** and **13b** via TSs **12a** and **12b** along RP-C2/C3, respectively. The energy-optimized electronic structures of the adducts, TSs and intermediates along both RPs at the nucleophilic addition stage are shown in in Figure 4.2.
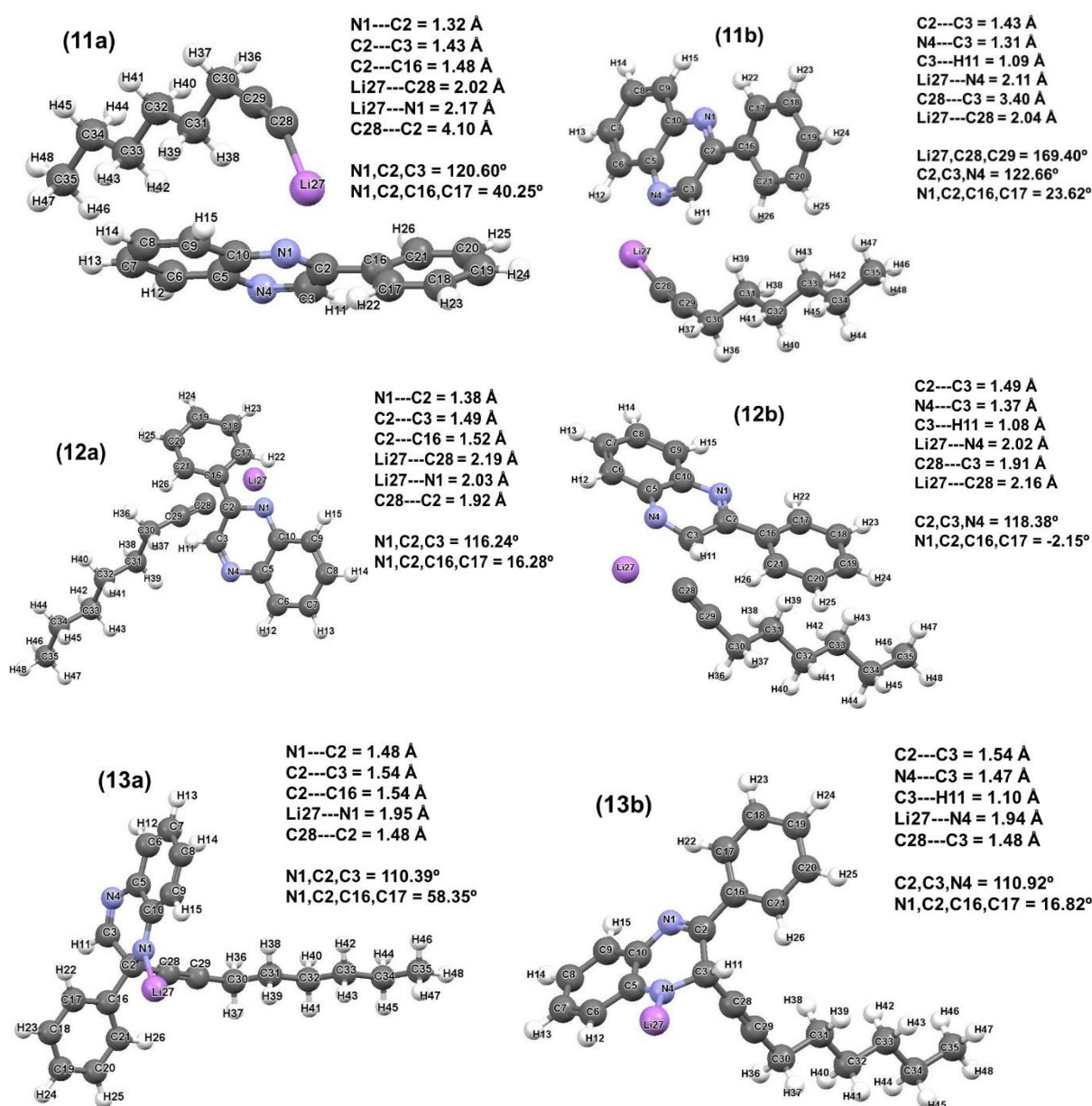
Figure 4.2. Energy-optimized electronic structures of adducts (**11**), TSs (**12**) and intermediates (**13**). Important distances, angles and dihedral angles are given in Å and º, respectively.

Upon the formation of the adducts, some geometrical changes were observed in the separate reactants. The most significant geometrical change was observed in the DA(N1,C2,C16,C17) as a result of the rotation by the phenyl substituent in order to accommodate the incoming nucleophile as well as the loss in linearity in **10** as it approaches **1**. More structural features of the energy-optimized electronic structures from the separate reactants (**1** and **10**) to the intermediates (**13**) along RP-C2 and RP-C3 can be found in Tables B21-B24, Part 2 of Appendix B.

Table 4.1 summarizes the computed energetic information of the adducts, TSs, intermediates and the respective energy changes relative to the sum of the reactants (**1**+**10**) at the nucleophilic addition stage. To simplify the discussion of this data, consider the full set of energy profiles, starting from reactants (**1**+**10**) up to the formed intermediates (**13**), presented in Figure 4.3. Interestingly, these computed reaction energy profiles are highly comparable to those observed for RP-C2 and RP-C3 in the previous Chapter – see Figure 3.2.

Table 4.1. Computed energies (E, E_{ZPVE}, H and G in au) of the adducts, TSs and intermediates as well as the relative energies (Δ) in kcal mol^{-1} denoting the energy difference between their computed energies and the total sum of the energies of the separate reactants (**1** and **10**).

	E	E_{ZPVE}	H	G
	Reactants			
1	–649.2102	–649.0067	–649.0009	–649.0288
10	–320.3090	–320.1209	–320.1143	–320.1429
Total:	–969.5192	–969.1276	–969.1152	–969.1717
	Adducts			
11a	–969.5315	–969.1378	–969.1255	–969.1694
Δ	–7.7	–6.4	–6.4	1.4
11b	–969.53608	–969.1423	–969.1300	–969.1740
Δ	–10.6	–9.3	–9.2	–1.5
	Transition states			
12a	–969.4924	–969.1001	–969.0884	–969.1310
Δ	16.8	17.2	16.9	25.6
12b	–969.5040	–969.1110	–969.0993	–969.1412
Δ	9.5	10.4	10.0	19.2
	Intermediates			
13a	–969.5230	–969.1293	–969.1175	–969.1603
Δ	–2.4	–1.1	–1.4	7.1
13b	–969.5331	–969.1385	–969.1267	–969.1698
Δ	–8.8	–6.9	–7.2	1.2
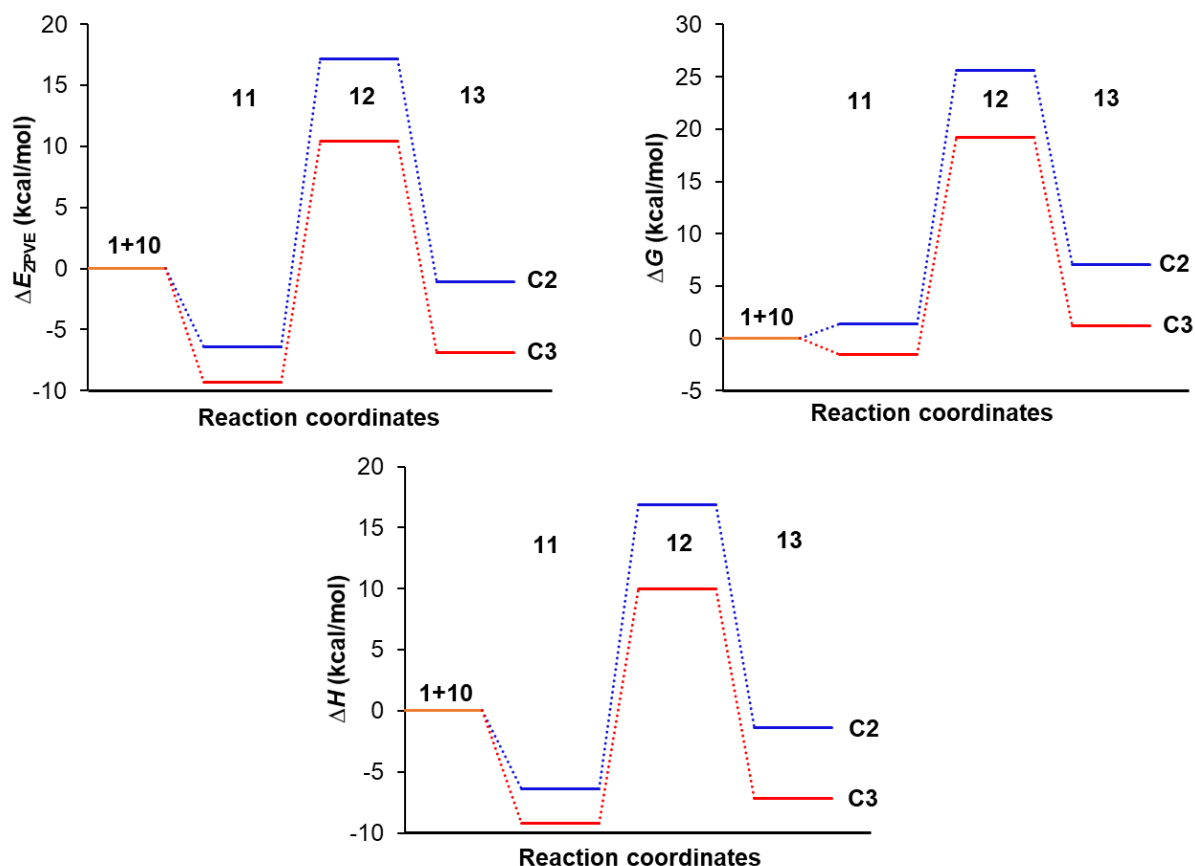
Figure 4.3. Reaction energy profiles for the nucleophilic addition step computed for the C2 and C3 substitution sites. Changes in the energy for adducts (**11**), TS (**12**) and intermediates (**13**) were computed relative to the energy of reactants (**1**+**10**).

From the data in Figure 4.3, it is evident that the reaction is initiated by the formation of the adducts **11a** and **11b** which stabilize the reaction by –6.4 and –9.3 kcal mol^{-1}, respectively. As the reaction proceeds, it has to overcome energy barriers (ΔE_{ZPVE}) of 23.6 and 19.7 kcal mol^{-1} along RP-C2 and RP-C3 before forming the respective intermediates (**13**). Moreover, this data shows that RP-C3 is both kinetically and thermodynamically more favourable at the nucleophilic addition step of the ONSH reaction mechanism. However, the energy differences between the two RPs is minimal; hence RP-C2 cannot be excluded as a real possibility at this stage.

In an attempt to rationalize the stabilization of the reaction caused by the formation of the adducts, we analyse the diatomic molecular fragments associated with the strongest attractive intermolecular interactions along both RPs – see Table 4.2 and Table B28, Part 2 of Appendix B. Notably, like in the reaction presented in the preceding Chapter, the reaction between **1** and **10** is predominantly driven by the favourable interactions between Li27 and N1/N4 due to the larger difference in the net atomic charges between these atoms when compared to any other atom-pair.

Table 4.2. Most significant (leading) attractive diatomic intermolecular interactions in the adducts formed between **1** and **10** along RP-C2 and RP-C3. All values in kcal mol^{-1}.

Atom A	Atom B	RP-C2	Atom A	Atom B	RP-C3
N1	Li27	−179.1	N4	Li27	−187.1
N4	Li27	−70.5	N1	Li27	−68.7
C2	C29	−29.1	C3	C29	−31.5
C3	C29	−25.8	C3	C28	−26.2
C10	C29	−25.7	C2	C29	−22.8
C2	C28	−20.5	C5	C29	−19.7
C5	C29	−20.4	C10	C29	−16.6
C10	C28	−17.5	C5	C28	−16.1
C3	C28	−13.7	C2	C28	−14.0
C5	C28	−10.2	C10	C28	−10.9

Moreover, following the same analysis and reasoning as in Chapter 3, these 2-molecular adducts (**11a** and **11b**) will be treated as 3-component structures made up of all atoms of **1**, Li and the molecular fragment $\mathcal{R}^*$ made up of all atoms of **10** but Li. That is, all interactions between the Li-atom and all other atoms of **1** and **10** will be seen as of intermolecular character.

In addition to the above-mentioned observations, more insight was gained by grouping atoms involved in significantly strong attractive and repulsive interactions to form molecular fragments $\mathcal{Q}, \mathcal{Ph}1, \mathcal{Bn}, \mathcal{P}, \mathcal{N}, \mathcal{C}, \mathcal{G}1$-$\mathcal{G}2$ and $\mathcal{F}1$-$\mathcal{F}4$ as defined in the Chapter 3.

Atoms of **10** were grouped in the same way as we did with **2**, however, we have included the symbol "*" in the superscript of the molecular fragment names for the purpose of clarity.

1. 3-atom molecular fragment of **10**, $\mathcal{L}^* = \{\text{Li27,C28,C29}\}$.

2. Two molecular fragments made from atoms of $\mathcal{L}^*$, one with a highly positively charged Li-atom and another with highly negatively charged C-atoms, $\mathcal{A}^* = \{\text{C28,C29}\}$.

3. All atoms of **10** except Li27, $\mathcal{R}^* = \{\text{C28-H48}\}$.

Table 4.3 summarizes the interaction energies between molecular fragments playing an important role in the formation of the adducts. Notably, the two reactants (**1** and **10**) have a great affinity for each other along both RPs (entry 1 in Table 4.3). Although this interaction shows a slight preference of about −6.6 kcal mol^{-1} for RP-C3 (formation of **11b**), it is not enough to exclude the formation of **11a** along RP-C2.

Having established the crucial role played by the Li-atom, it was of paramount importance to investigate its impact on the relative stability of the formed adducts and on the preferred RP.

However, from our analysis of the significant interactions that the Li-atom is involved in (entries 2-6 in Table 4.3 and Table B43, Part 5 of Appendix B), it was clear that it does not differentiate between the two RPs as very comparable energies were observed. Moreover, this indicates that even with the crucial role played by Li, one cannot establish, from its interactions with various atoms or molecular fragments, the origins of relative stability between **11a** and **11b**.

Therefore, in an attempt to provide a clearer picture of the origins of relative stability between **11a** and **11b**, we consider first the interaction energies between the entire molecule **1** and selected larger molecular fragments of **10**, namely $\mathcal{L}^*$, $\mathcal{A}^*$ and $\mathcal{R}^*$ - see entries 7-9 in Table 4.3. Significantly more attractive interaction energies between these molecular fragments were observed in favour of RP-C3.

Table 4.3. Interaction energies of molecular fragments playing an important role in the formation of adducts along RP-C2 and RP-C3. All values are in kcal mol^{-1}.

Entry	Fragments	Interaction energies	
		RP-C2	RP-C3
1	**1, 10**	–52.3	–58.9
2	**1, Li**	–38.4	–39.4
3	**Li, C28**	–104.5	–106.8
4	**Li, C29**	–69.7	–67.0
5	**$\mathcal{A}^*$, Li**	–174.2	–173.8
6	**$\mathcal{R}^*$, Li**	–163.7	–163.5
7	**1, $\mathcal{L}^*$**	–38.0	–47.8
8	**1, $\mathcal{A}^*$**	0.4	–8.4
9	**1, $\mathcal{R}^*$**	–13.9	–19.6
10	**$\mathcal{Q}$, 10**	–52.1	–47.8
11	**$\mathcal{P}$, 10**	–41.5	–51.7
12	**$\mathcal{Bn}$, 10**	3.2	26.6
13	**$\mathcal{N}$, 10**	–80.5	–88.3
14	**$\mathcal{C}$, 10**	38.4	42.8
15	**$\mathcal{G}1$, 10**	–42.1	0.9
16	**$\mathcal{G}2$, 10**	0.0	–46.4
17	**$\mathcal{F}1$, 10**	–50.4	10.3
18	**$\mathcal{F}2$, 10**	17.9	–64.5

Secondly, we consider the interaction energies between the entire molecule **10** and the indicated significant molecular fragments of **1**. In this analysis, the molecular fragment $\mathcal{Q}$ was split into two molecular fragments, namely $\mathcal{P}$ and $\mathcal{Bn}$. Analysis of the intermolecular

interactions of these molecular fragments revealed that $\mathcal{P}$ was involved in stronger attractive interactions with **10** (entry 11) which overcompensate for the overall repulsive interactions observed between $\mathcal{B}n$ and **10** (entry 12), hence the comparable attractive interactions observed between $\mathcal{Q}$ and **10** (entry 10). Important to note in this analysis is that the interaction energies of molecular fragments $\mathcal{P}$ and $\mathcal{B}n$ with **10** are not additive as atoms C5 and C10 form part of both fragments. As stated in the preceding Chapter, it is reasonable to assume that the strong attractive interactions observed between $\mathcal{P}$ and **10** which are in favour of the formation of **11b** (RP-C3) must be a result of the combined attractive interactions of N1 and N4 (as molecular fragment $\mathcal{N}$) with **10** which overcompensates the combined repulsive interactions of C2, C3, C5 and C10 (as molecular fragment C) with **2** – see entries 13 and 14 in Table 4.3.

Lastly, we consider the immediate 3-atom ($\mathcal{G}1$ and $\mathcal{G}2$) and 4-atom ($\mathcal{F}1$ and $\mathcal{F}2$) environments around the N and C-atoms of P, respectively. Notably, the environment around the N-atoms attracts **10** comparably with a slight preference of about -4.3 kcal mol^{-1} for RP-C3 (formation of **11b**) for which we obtained a quantified attraction of -46.4 kcal mol^{-1} between $\mathcal{G}2$ and **10** (entries 15 and 16 in Table 4.3). For the environment around the C-atom where the new C–C bond with C28 is expected to form, strong attractive interactions showing yet again preference for the formation of **11b** were observed – see entries 17 and 18.

From this data, a clear picture emerges pin-pointing the origins of the more stable adduct (**11b**) along RP-C3; this is in a full agreement with trends seen in Figure 4.3.

Transition State and σ^H-adduct Formation (C–C bond formation)

As the reaction progresses from **11** to **12**, the energy barrier is lower (by about 4.0 kcal mol^{-1}) for RP-C3 than RP-C2 – see Figure 4.3. The computed reaction energy profiles along the Cn–C28 (Cn being the C-atom of a respective RP) reaction coordinates as well as the computed IRC graphs to confirm that **12a** and **12b** connect the desired minima on either side are shown in Figure B2(a) and (b), Part 6 of Appendix B.

In an attempt to provide a more in-depth mechanistic insight into how the reaction progresses from **11** to **12**, we present in this section a discussion on the changes in interaction energies between selected molecular fragments ranging from a single atom to *n*-atoms when moving from adducts (**11**) to TSs (**12**).

From a classical organic chemist's perspective, one would expect that at the TSs stage of the nucleophilic addition reaction, C28, which is destined to form a new covalent C–C bond with Cn, would be involved in the strongest attractive intermolecular diatomic interactions. However, from the computed data in Table B29, Part 3 of Appendix B, which shows the leading attractive diatomic intermolecular interactions in the TSs (**12**) along RP-C2 and RP-C3, it is evident that the Li atom is still involved in the strongest interactions with the N-atom of the respective pathway and still dominated almost entirely by the classical electrostatic component ($V_{cl}^{Li27,Nn}$ = –190.1 kcal mol^{-1} for **12a** and –186.6 kcal mol^{-1} for **12b**) as we observed in the adducts.

However, even though the Cn⋯C28 interaction was not the strongest diatomic interaction at the TS stage as expected, a significant increase of ~78 kcal mol^{-1} in its strength as the reaction progressed from **11** to **12** along both RPs placed it as the second leading diatomic interaction with comparable interaction energies of –101.3 and –102.6 kcal mol^{-1} in **12a** and **12b**, respectively. These interactions are characterised by the largely increased covalent character shown by the XC-term ($V_{XC}^{Cn,C28}$ = –87.0 and –87.7 kcal mol^{-1} in **12a** and **12b**, respectively) which in turn indicates the partial formation of the new C–C covalent bond. Interestingly, as indicated by interaction energies of –186.7 ± 1.1 kcal mol^{-1}, the strength of the newly formed Cn–C28 bond is comparable in **13a** and **13b**.

From the data showing the leading diatomic intermolecular interactions (Table B28 of Appendix B), it follows that Li27, C28 and C29 play an important role in the **11** → **12** process. Therefore, for additional insight towards elucidating the mechanism along both RPs, we consider the interaction energies of these single atoms with the entire molecule **1**. From this analysis, we observed that C28 was involved in the strongest yet comparable interactions with **1** along both RPs – see Table B46, Part 5 of Appendix B. That is, even though Li27 is involved in the strongest diatomic intermolecular interaction at the TS, its overall interactions with all atoms of **1** are by far much less than C28; –74.9 and –70.5 kcal mol^{-1} along RP-C2 and RP-C3, respectively. Therefore, it is clear that the process from **11** to **12** is driven by C28 which interacts with **1** by –115.5 and –107.7 kcal mol^{-1} along RP-C2 and RP-C3, respectively.

As stated in the first paragraph of this section, there is an energy difference of about 4.0 kcal mol^{-1} between the observed energy barriers along RP-C2 and RP-C3. This can be explained as a result of **11b** being more stable, hence a better prepared adduct for the progression of the reaction than **11a**.

In an attempt to explain this observed energy difference at an atomic, molecular and molecular fragment level, we considered the interaction energies summarized in Table 4.4 between selected molecular fragments in the molecular systems of the TSs along both RPs. From this data, it was observed that the molecular fragment $\mathcal{R}^*$ interacts favourably with the entire molecule **1** with a slight preference of about –7.6 kcal mol⁻¹ for RP-C3 (entry 1 in Table 4.4). For additional insight on this observation, we considered the interactions of $\mathcal{R}^*$ and some significant molecular fragments of **1**. Notably, $\mathcal{R}^*$ interacts comparably with most molecular fragments of **1** except for $\mathcal{P}h$1 where a slight preference of about –7.0 kcal mol⁻¹ for RP-C3 is observed – see entries 2-9 in Table 4.4. This correlates very well with the observed difference of 6.8 kcal mol⁻¹ in the computed E_{ZPVE} values for **12a** and **12b** (see Table 4.1). Clearly, the slightly higher energy barrier observed for RP-C2 is, in this instance, a result of slightly less favourable interactions between $\mathcal{R}^*$ and $\mathcal{P}h$1 which in classical terms can be described as steric hindrance.

Table 4.4. Computed interaction energies of molecular fragments for the transition states at the nucleophilic addition step along the indicated RPs. All values are in kcal mol⁻¹.

		Interaction energies	
Entry	**Fragments**	**RP-C2**	**RP-C3**
1	**1**, $\mathcal{R}^*$	–129.2	–136.8
2	$\mathcal{R}^*$, $\mathcal{Q}$	–108.4	–108.9
3	$\mathcal{R}^*$, $\mathcal{P}$	–106.4	–106.8
4	$\mathcal{R}^*$, $\mathcal{B}n$	–43.1	–45.8
5	$\mathcal{R}^*$, $\mathcal{F}$1	–114.9	–122.0
6	$\mathcal{R}^*$, $\mathcal{F}$2	–125.1	–114.8
7	$\mathcal{R}^*$, $\mathcal{G}$1	–89.3	–8.0
8	$\mathcal{R}^*$, $\mathcal{G}$2	–13.2	–89.5
9	$\mathcal{R}^*$, $\mathcal{P}h$1	–20.8	–27.8

Lastly, from the energetic information summarized in Table 4.1, it clear that both RPs lead to the formation of stable intermediates (**13**). However, **13b** of RP-C3 is by –5.8 kcal mol⁻¹ more stable than **13a** of RP-C2. Moreover, RP-C3 appears to be more thermodynamically favourable than RP-C2. Even so, RP-C2 cannot be eliminated as a real possibility because the mechanistic insight discussed above is very comparable to what we observed for RP-C3. Moreover, the reaction can simply overcome the energy barrier along this RP and for the stable intermediate **13a** and proceed with the hydrolysis reaction discussed in the following section.

Hydrolysis and Oxidation

In the preceding Chapter, we reported that the hydrolysis and oxidation reactions concluding the ONSH reaction mechanism are concurrent. That is, as soon as the hydrolysis product forms, it is immediately oxidized to afford the final ONSH product. However, this is only possible for RP-C3 as the hydrolysis product along this RP makes provision for oxidation while RP-C2 can potentially progress only up to the formation of the hydrolysis product. To facilitate the discussion of each RP, consider the full set of energy profiles, from reactants (**1**+**10**) up to the ONSH product (**17**), presented in Figure 4.4. The energetic information associated with the stationary points **14**-**17** in Figure 4.4 is summarized in Table 4.5 and Table 4.6. For simplicity, we discuss the modelling and observations of each RP separately in following sub-sections.
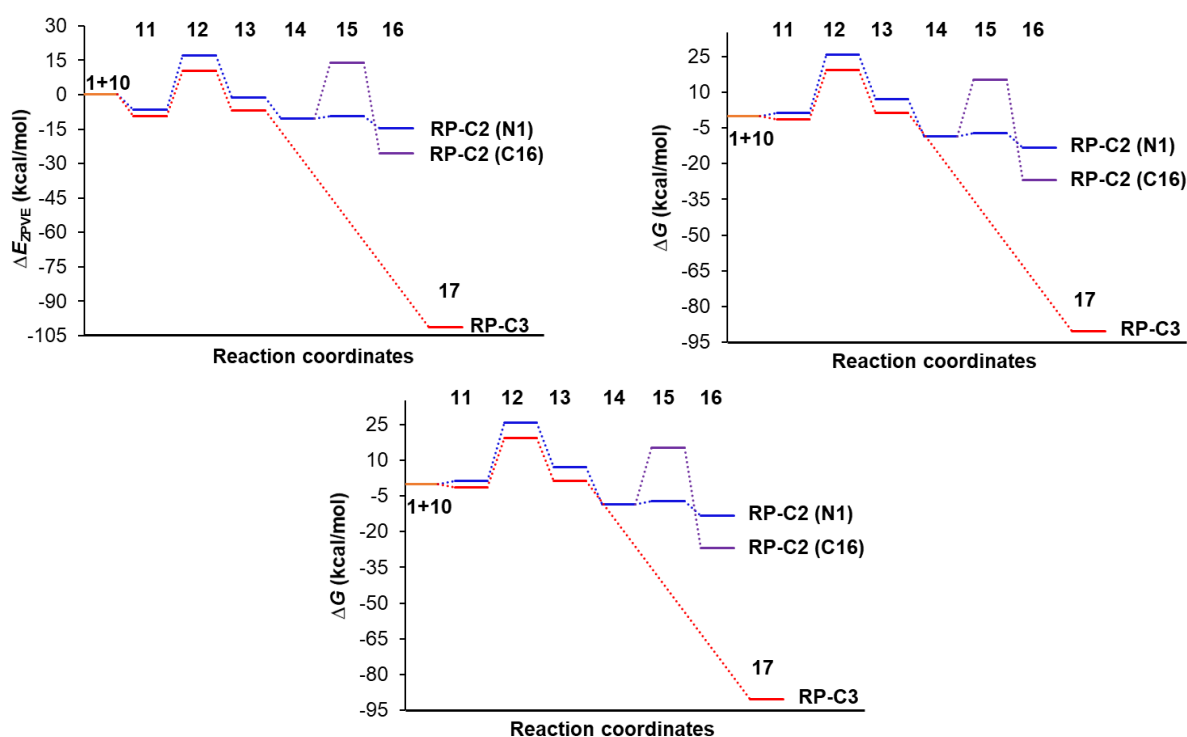
Figure 4.4. Full reaction energy profiles starting from reactants (**1**+**10**) to the ONSH product (**17**). Stage **1**+**10** to **13** represents the nucleophilic addition reaction while stage **13** to **16** represents the hydrolysis reaction. Lastly, moving straight from **13** to **17** represents simultaneous hydrolysis and oxidation reactions.

73

Table 4.5. Calculated energies (E, E_{ZPVE}, H and G in au) of all stationary points in the hydrolysis of **13a** along RP-C2 with Δ denoting energy differences of each stationary point relative to the total sum of the energies of the reactants in kcal mol^{-1}

	E	E_{ZPVE}	H	G
	Reactants			
1	–649.2102	–649.0067	–649.0009	–649.0288
2	–315.4706	–315.3710	–315.3667	–315.3900
H$_2$O	–76.4650	–76.4438	–76.4400	–76.4621
Total:	–1041.1458	–1040.8215	–1040.7968	–1040.9102
	Adduct (**13a** + H$_2$O)			
14a	–1046.0066	–1045.5880	–1045.5606	–1045.6477
Δ	–14.0	–10.4	–3.3	–8.7
	Transition states			
15a	–1046.0006	–1045.5862	–1045.5596	–1045.6454
Δ	–10.3	–9.3	–2.7	–7.3
15e	–1045.9646	–1045.5490	–1045.5217	–1045.6095
Δ	12.3	14.0	21.1	15.3
	Hydrolysis product			
16a	–1046.0133	–1045.5950	–1045.5674	–1045.6554
Δ	–18.2	–14.8	–7.6	–13.5
16e	–1046.0294	–1045.6122	–1045.5834	–104536768
Δ	–28.3	–25.6	–17.6	–27.0

RP-C2

To complete the modelling of the reaction along RP-C2, we introduced H$_2$O to the molecular system of **13a** such that d(Li27,O49) and N1–Li27···O49 were set to 1.94 Å and 104.9°, respectively and submitted this input structure for energy optimization and frequency calculations at 298.15 K. This resulted in the formation of the adduct **14a** which stabilizes the reaction by –10.4 kcal mol^{-1} due to strong attractive interactions between Li27 and O49 of –191.9 kcal mol^{-1} that are predominantly of electrostatic nature ($V_{cl}^{Li27,O49}$ = –182.3 kcal mol^{-1}). All geometrical features of the energy-optimized electronic structure of **14a** presented in Figure 4.5 can be seen in Table B25 of Appendix B.

Although the ONSH reaction mechanism indicates that the hydrolysis reaction proceeds via a Li–H exchange reaction where H50 of the water molecule is transferred to N1 in exchange for Li27 (RP-C2 (N1) in Figure 4.4), we have established in Chapter 3 that the hydrolysis reaction can also proceed with H50 of the water molecule being transferred to C16 (RP-C2 (C16) in Figure 4.4). The energy-optimized electronic structures of the TSs (**15**) and formed

hydrolysis products (**16**) formed along these RPs are shown in Figure 4.6 – see Tables B25 and B27 of Appendix B for additional geometrical features.

Notably, the transfer of H50 to C16 requires more energy than its nearly spontaneous transfer to N1. However, it remains feasible for the hydrolysis reaction to proceed with H50 being transferred to C16 as the energy (24.4 kcal mol^{-1}) required to do so is highly comparable to the energy barrier (23.6 kcal mol^{-1}) observed in the preceding nucleophilic addition reaction along RP-C2. That is, both RP-C2 (N1) and RP-C2 (C16) result in the formation of stable hydrolysis products (**16**). This clearly indicates a possible by-product that may be affecting the yield of the desired product.

N1---C2 = 1.47 Å
C2---C3 = 1.54 Å
C2---C16 = 1.54 Å
C2---C28 = 1.49 Å
Li27---N1 = 1.97 Å
Li27---O49 = 1.97 Å
O49---H50 = 0.98 Å
N1---H50 = 2.92 Å
C16---H50 = 3.20 Å

N1,C2,C3 = 111.75°
N1,C2,C16,C17 = 110.67°
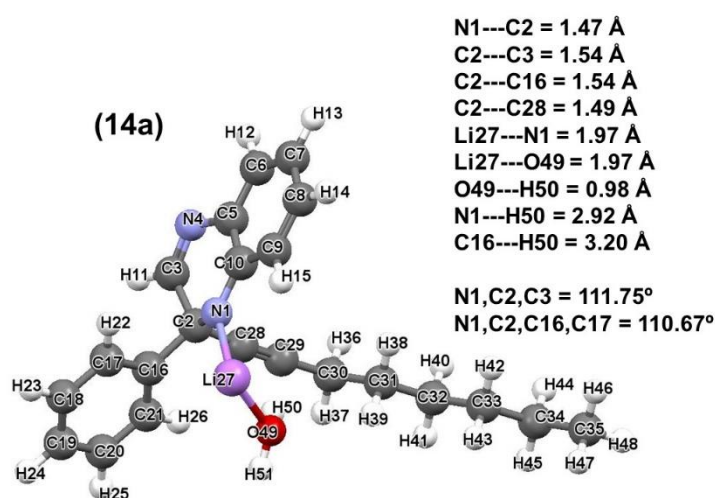
Figure 4.5. Global minimum structures of adduct **14a** formed between a water molecule and intermediate **13a**. Important distances, angles and dihedral angles are given in Å and °, respectively.

(a)

(15a)

N1---C2 = 1.48 Å
C2---C3 = 1.54 Å
C2---C16 = 1.54 Å
C2---C28 = 1.48 Å
Li27---N1 = 2.32 Å
Li27---O49 = 1.90 Å
O49---H50 = 1.17 Å
N1---H50 = 1.33 Å

N1,C2,C3 = 109.53º
N1,C2,C16,

(16a)

N1---C2 = 1.46 A
C2---C3 = 1.54 Å
C2---C16 = 1.54 Å
C2---C28 = 1.48 Å
Li27---N1 = 3.63 Å
Li27---O49 = 1.76 Å
O49---H50 = 1.68Å
N1---H50 = 1.05 Å

N1,C2,C3 = 107.42º
N1,C2,C16,C17 = 49.77º

(b)

(15e)

N1---C2 = 1.35 Å
C2---C3 = 1.47 Å
C2---C16 = 2.29 Å
C2---C28 = 1.44 Å
Li27---N1 = 2.04 Å
Li27---O49 = 1.90 Å
O49---H50 = 1.02 Å
C16---H50 = 1.76 Å

N1,C2,C3 = 118.97º

(16e)

N1---C2 = 1.32 Å
C2---C3 = 1.43 Å
C2---C16 = 4.08 Å
C2---C28 = 1.42 Å
Li27---N1 = 2.14 Å
Li27---O49 = 1.70 Å
O49---H50 = 3.55 Å
C16---H50 = 1.08 Å

N1,C2,C3 = 121.17º

Figure 4.6. Energy-optimized electronic structures of the TSs (**15**) and hydrolysis products (**16**) of the hydrolysis reaction along (a) RP-C2 (N1) and (b) RP-C2 (C16). Important distances, angles and dihedral angles are given in Å and º, respectively.

76

RP-C3

The modelled simultaneous hydrolysis and oxidation reactions at 298.15 K along RP-C3 was completed by introducing H_2O and O_2 into the molecular system of **13b** at the same time such that d(H11,O52), d(H51,O53) and d(Li27,O49) were set to 1.17, 1.27 and 1.58 Å, respectively.

Upon energy optimisation calculations, a spontaneous reaction leads to the formation of the desired 2,3-disubstituted product (**17b**) which sits –101.3 kcal mol^{-1} below the initial reactants – see Figure 4.7 and Table 4.6. In the process from **13b** to **17b**, the following transformations were noted; (i) C3–H11, Li27–N4 and O49–H51 bond cleavage, (ii) restoration of the trigonal (sp^3) geometry for C3, (iii) restoration of aromaticity in the quinoxaline moiety and lastly, (iv) formation of LiOH and H_2O_2 as by-products of the reaction.
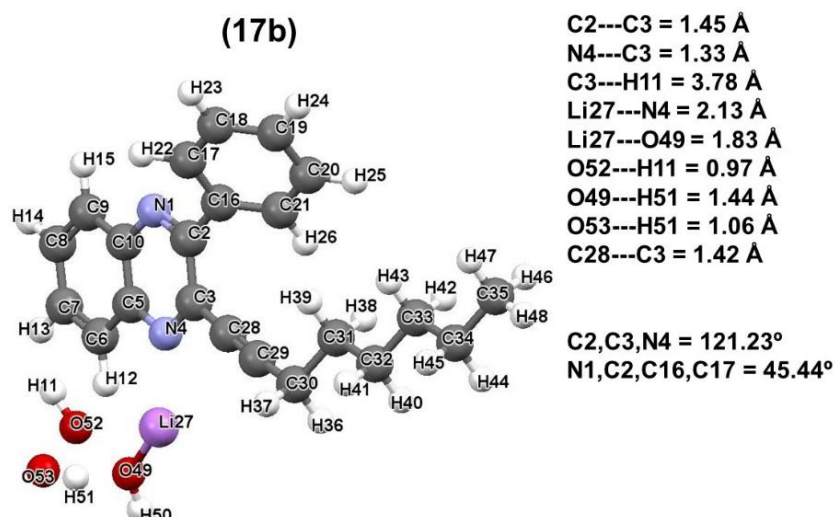
Figure 4.7. Energy-optimized electronic structures of the ONSH product (**17b**) obtained along RP-C3. Important distances, angles and dihedral angles are given in Å and °, respectively.

Table 4.6. Calculated energies (*E*, *E*$_{ZPVE}$, *H* and *G* in au) for **17b** as well as the relative energies (Δ) in kcal mol^{-1} denoting the energy difference between the computed energies of the product and the total sum of the energies of the reactants.

	E	*E*$_{ZPVE}$	*H*	*G*
Simultaneous oxidation and hydrolysis reactants				
1	–649.2102	–649.0067	–649.0009	–649.0288
11	–320.3090	–320.1209	–320.1143	–320.1429
H_2O	–76.4650	–76.4438	–76.4400	–76.4621
O_2	–150.3098	–150.3061	–150.3028	–150.3250
Total:	–1196.2940	–1195.8775	–1195.8580	–1195.9588
ONSH Product				
17b	–1196.4635	–1196.0389	–1196.0086	–1196.1030
Δ	–106.3	–101.3	–94.5	–90.5

CONCLUSION

In addition to the general approach where one uses computed reaction energy profiles to support or reject proposed reaction mechanisms, we make use of the REP-FAMSEC method to explain the origins of the processes taking place in the assumed ONSH reaction mechanism when **1** is treated with **10**. Using this approach, we were able to point atoms and molecular fragments leading to different incremental steps along two competing RPs. Moreover, being able to quantify the inter- and intramolecular interaction energies of the atoms and molecular fragments identified to be playing an important role aided us in elucidating the relative stability between the adducts (**11**) as well as the energy difference between the observed energy barriers at the TSs (**13**) stage of the reaction.

Having showed that the nucleophilic addition is also possible at C2 despite the presence of the phenyl substituent, two stable hydrolysis products (**16a** and **16e**), that may have not been considered before, along RP-C2 were identified. These can be seen as a possible by-product that may alter the yield of the desired product. Guided by the results presented in Chapter 3, the hydrolysis and oxidation reactions along RP-C3 were modelled such that they occur simultaneously. This resulted in the spontaneous and irreversible formation of the desired and 2,3-disubstituted quinoxaline (**17b**) with LiOH and H_2O_2 as by products.

Lastly, from the data presented in this study, there is no obvious indication that the variation in the yields obtained between the reactions presented in the work of Ndlovu and Nxumalo is attributed to the nature of the nucleophile. Hence, one should consider some sort of imperfect experimental conditions that could lead to highly variable yields. Consider, for instance, a possibility where a significant amount of water was present in a reaction vessel at stage **13**, or even earlier. Then H_2O would become instantly available for the RP-C2 to proceed to 16e spontaneously and irreversibly. This speculation can be supported by an additional consideration, namely much slower transport of $O_2(g)$ (coming from the air) throughout a solution in the reaction vessel.

REFERENCES

(1)   Mąkosza, M. Nucleophilic substitution of hydrogen in electron-deficient arenes, a general process of great practical value. *Chem. Soc. Rev.* **2010**, *39*, 2855-2868.

(2)   Patel, N.; Bergman, J.; Gräslund, A. 1H-NMR studies of the interaction between a self-complementary deoxyoligonucleotide duplex and indolo [2, 3-b] quinoxaline derivatives active against herpes virus. *Eur. J. Biochem.* **1991**, *197*, 597-604.

(3)   Potey, L.; Kosalge, S.; Hadke, M. Synthesis and antimicrobial activity of quinoxaline sulfonamide. *Int. J. Adv. Sci. Technol.* **2013**, *2*, 126-134.

(4)   Agboke, A.; Attama, A.; Qkoye, C.; Jackson, C. Evaluation of effectiveness of various combinations of penicillin groups commonly used in Nigeria clinics on selected microorganisms. *Innov. J. Med. Health. Sci.* **2014**, *4*, 93-98.

(5)   Le Douaron, G.; Schmidt, F.; Amar, M.; Kadar, H.; Debortoli, L.; Latini, A.; Séon-Méniel, B.; Ferrié, L.; Michel, P. P.; Touboul, D. Neuroprotective effects of a brain permeant 6-aminoquinoxaline derivative in cell culture conditions that model the loss of dopaminergic neurons in Parkinson disease. *Eur. J. Med. Chem.* **2015**, *89*, 467-479.

(6)   Le Douaron, G.; Ferrié, L.; Sepulveda-Diaz, J. E.; Amar, M.; Harfouche, A.; Séon-Méniel, B.; Raisman-Vozari, R.; Michel, P. P.; Figadère, B. New 6-aminoquinoxaline derivatives with neuroprotective effect on dopaminergic neurons in cellular and animal parkinson disease models. *J. Med. Chem.* **2016**, *59*, 6169-6186.

(7)   Deppmeier, B.; Driessen, A.; Hehre, T.; Johnson, J.; Klunzinger, P.; Watanabe, M. Spartan'10. *Wavefunction Inc.* **2011**.

CHAPTER 5: Oxidation of the σ^H-adducts of the ONSH reaction mechanism using Br_2 or Cl_2

INTRODUCTION

Due to the therapeutic usefulness of quinoxaline as a scaffold in the design for synthetic routes of compounds in medicinal chemistry,[1-9] it is important that we understand all possible ways to synthesize them. In a study of the nucleophilic addition of silyl enol ethers to aromatic nitro compounds, T. V. RanjanBadu and co-workers reported the formation of adducts leading to the synthesis of α-nitroaryl carbonyl compounds in moderate-to-high yields when oxidized with bromine (Br$_2$).[10,11] Also reported in this study was that various heterocyclic nitro compounds including nitronaphthalenes and nitroanthracene can follow the same reaction.

As part of our contribution towards expanding the existing knowledge base towards synthesizing quinoxaline derivatives, we present in this Chapter a theoretical study of the Oxidative Nucleophilic Substitution of Hydrogen (ONSH)[12,13] reaction mechanism where halogens, namely bromine (Br$_2$) and chlorine (Cl$_2$), are used for the oxidation of the σ^H-adducts (**5b** and **13b**) of the quinoxaline moiety to afford the respective final ONSH products – see Scheme 5.1.
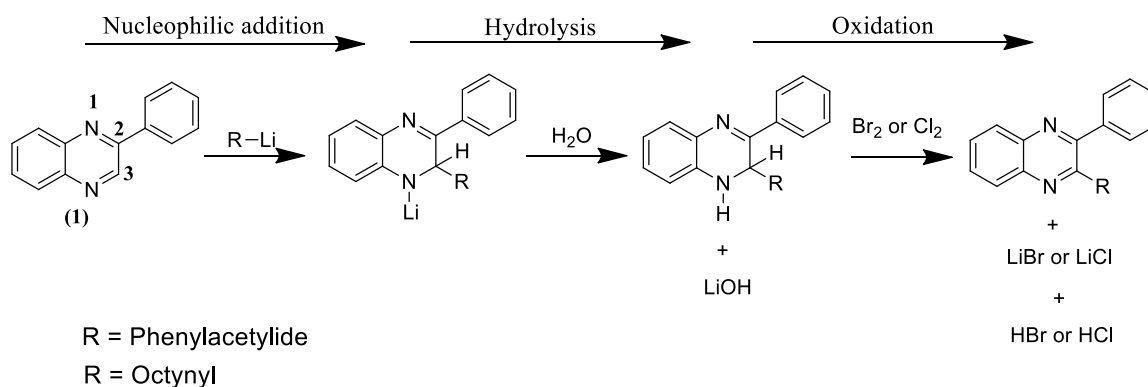
Scheme 5.1. Oxidative Nucleophilic Substitution of Hydrogen of 2-phenylquinoxaline (**1**) where oxidation is achieved by means of halogens (Br$_2$ or Cl$_2$).

Although some experimental work has been reported where Br$_2$ is used for the oxidation of the σ^H-adducts of some ONSH examples,[11,14] no theoretical investigation to this effect, particularly for quinoxalines, has been conducted. On the other hand, to the best of our knowledge, there is no literature, whether experimental or theoretical, showing Cl$_2$ as an oxidant for σ^H-adducts.

The XYZ coordinates of all energy-optimized electronic structures considered (Tables C1-C4) and a full set of their energies (Tables C5-C8) are included in Part 1 of Appendix C.

RESULTS AND DISCUSSION

The oxidation of the σ^H-adduct **5b** or **13b** entails the removal of Li27 and H11 to afford the respective aromatic 2,3-disubstituted quinoxaline product. To complete the modelling of this reaction, Br_2 or Cl_2 were introduced to the systems of **5b** and **13b** at 298.15 K. For the case where Br_2 was introduced as the oxidizing agent, the molecules were arranged such that one Br-atom was set to be ~1.13 Å from H11 while the other was set to be ~2.03 Å from Li27. Similarly, for the case where Cl_2 was introduced for the purposes of oxidation, one Cl-atom was set to be ~1.30 Å from H11 while the other was set to be ~2.33 Å from Li27.

Upon energy-optimization calculations, a spontaneous reaction between the σ^H-adducts and the halogens leading to the formation of the desired 2,3-disubstituted quinoxaline with LiX and HX (X = Br or Cl) as by-products was observed. Figure 5.1 shows the energy-optimized electronic structures of the ONSH products (**18b**, **19b**, **20b** and **21b**) obtained from the oxidation of **5b** and **13b** with Br_2 or Cl_2. The geometrical features of these energy-optimized electronic structures can be found in Tables C7-C8, Part 2 of Appendix C.

From the energetic information summarized in Table 5.1, it was observed that regardless of which halogen is used to oxidize the σ^H-adducts, the process is exothermic ($\Delta H < 0$) and spontaneous ($\Delta G < 0$). Interestingly, the ONSH products obtained from the oxidation with Cl_2 seem to be more stable (by ~21.0 kcal mol^{-1}) than those obtained via oxidation with Br_2. In an attempt to elucidate the relative stability between the outputs of the two oxidants, we decided to investigate the intermolecular interaction energies between the two by-products in each system and the 2,3-disbustituted quinoxaline ($\mathcal{DQ}$). To this effect, we discovered that in whichever case, the combined interactions of LiX and HX with $\mathcal{DQ}$ were comparable – see Table 5.2.

For additional insight, we studied the system from a single atom perspective. This analysis revealed that the Li-atom interacts stronger with Cl by approximately 10 kcal.mol^{-1} more than with Br for which, on average, interaction energies of –131.3 kcal mol^{-1} were found. Clearly, the energy difference observed between the Cl_2 and Br_2 outputs is, in this instance, a result of the stronger attractive nature of electrostatic interactions in Li$\cdots$Cl.

82
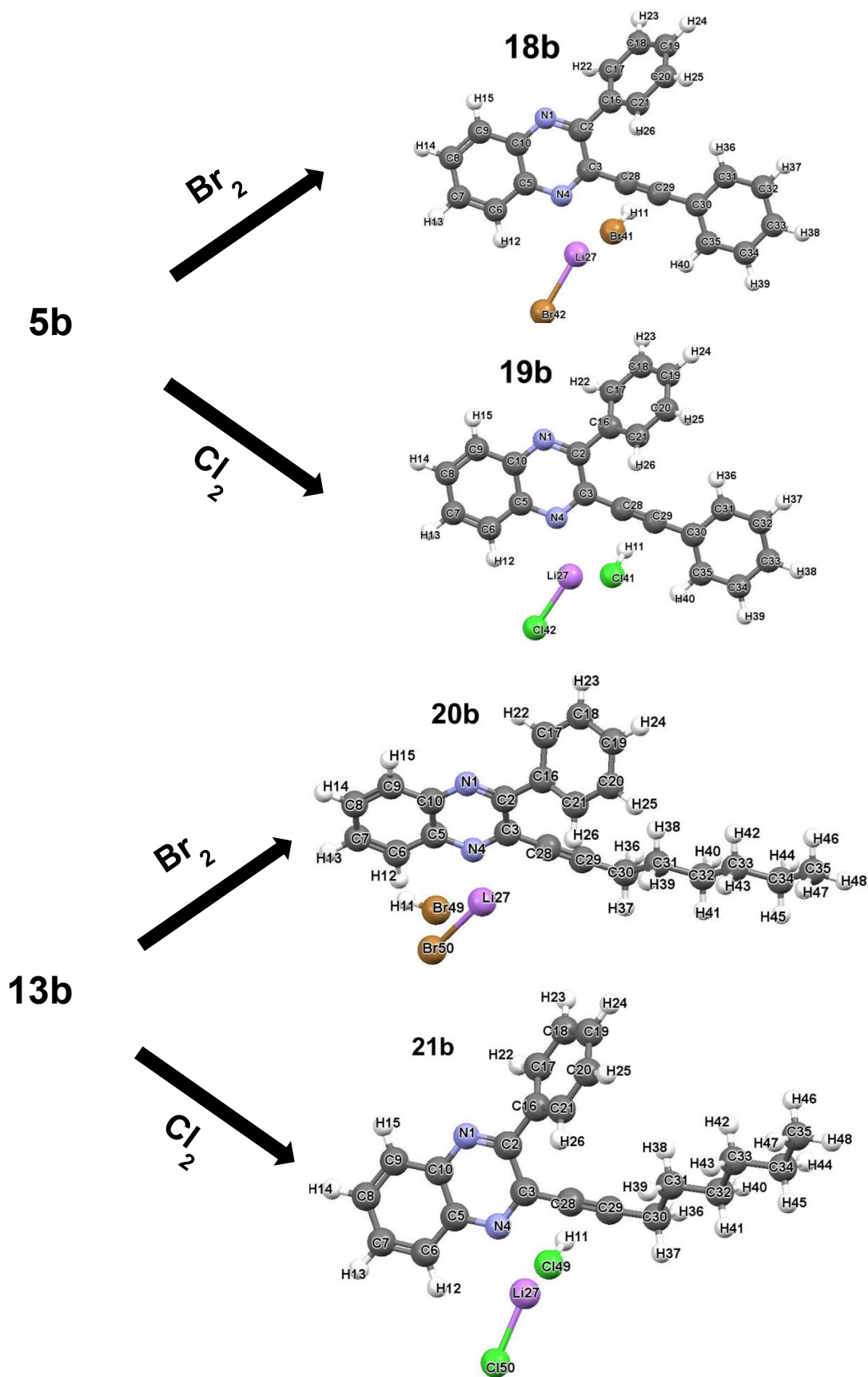
Figure 5.1. Energy-optimized electronic structures of the final ONSH products obtained from the oxidation of **5b** and **13b**

Table 5.1. Calculated energies (E, E_{ZPVE}, H and G in au) of the ONSH products (**18b**, **19b**, **20b** and **21b**) obtained via the hydrolysis of the σ^H-adducts (**5a** and **13b**) with Br_2 or Cl_2. The relative energies (Δ, in kcal mol^{-1}) denoting the energy difference between the computed energies of the stationary points and the total sum of the energies of the reactants is also included.

	E	E_{ZPVE}	*H*	*G*
OXIDATION WITH Br_2				
Reactants				
1	−649.2102	−649.0067	−649.0009	−649.0288
2	−315.4706	−315.3710	−315.3667	−315.3900
Br$_2$	−5148.2862	−5148.2855	−5148.2818	−5148.3097
Total:	−6109.9670	−6112.6632	−6112.6494	−6112.7285
ONSH products				
18b	−6113.0980	−6122.79350	−6112.7676	−6112.8545
Δ	−82.2	−81.8	−74.1	−79.1
20b	−6117.9403	−6117.5476	−6117.5174	−6117.6170
Δ	−84.7	−84.4	−75.5	−85.1
OXIDATION WITH Cl_2				
Reactants				
1	−649.2102	−649.0067	−649.0009	−649.0288
2	−315.4706	−315.3710	−315.3667	−315.3900
Cl$_2$	−920.4105	−920.4093	−920.4058	−920.4312
Total:	−1885.0913	−1884.7870	−1884.7734	−1884.800
ONSH products				
19b	−1885.2567	−1884.9512	−1884.9256	−1885.0094
Δ	−103.8	−103.0	−95.5	−100.1
21b	−1890.1001	−1889.7053	−1889.6761	−1889.7692
Δ	−107.0	−105.7	−97.3	−104.4

Table 5.2. Computed interaction energies between the by-products and the 2,3-disubstituted quinoxaline obtained when **5b** and **13b** were oxidized wit Br_2 or Cl_2. All values are in kcal mol^{-1}.

OXIDATION OF **5b**		OXIDATION OF **13b**	
HBr, $\mathcal{DQ}$	−23.0	HBr, $\mathcal{DQ}$	−17.7
LiBr, $\mathcal{DQ}$	−49.2	LiBr, $\mathcal{DQ}$	−52.7
Total:	−72.2	Total:	−70.4
HCl, $\mathcal{DQ}$	−21.8	HCl, $\mathcal{DQ}$	−25.5
LiCl, $\mathcal{DQ}$	−49.4	LiCl, $\mathcal{DQ}$	−49.2
Total:	−71.2	Total:	−74.7

CONCLUSION

Unlike in the preceding Chapters where the σ^H-adduct is exposed to the atmosphere to afford the aromatic disubstituted product, we presented in this Chapter an alternative route where oxidation of the σ^H-adduct is achieved by spiking the reaction with Br_2 or bubbling Cl_2 through it.

From our modelling, the introduction of either Br_2 or Cl_2 to the molecular systems of **5b** and **13b** resulted in a spontaneous and exothermic reaction that saw the elimination of H11 and Li27 to afford the desired 2,3-disubstituted quinoxaline. However, more stable ONSH products were observed when Cl_2 was used for the purposes of oxidation. Analysis of various interactions in the molecular systems revealed that due to the higher electronegativity of the Cl-atom, it interacts more strongly (favourably) than the Br-atom with the Li-atom. That is, LiCl is more stable than LiBr, hence the lower energy in the outputs obtained from oxidation with Cl_2. One must stress that discussion of the relative stability of molecular systems with either LiCl or LiBr is purely academic as the final products of the ONSH process are significantly lower in energy relative to initial reactants.

For the interested synthetic chemist, we strongly recommend that one follows the proposed modified experimental protocol in the conclusion of Chapter 3 in order to minimize the effect of multiple electrophilic sites in 2-phenylquinoxaline (**1**). To this effect, the reaction is expected to proceed via RP-C3, leading to the predominant formation of **5b** or **13b** depending on the organolithium reagent used. To achieve oxidation of these σ^H-adducts , the reaction can then either be spiked with Br_2 or Cl_2.

This method can also be seen as a way to eliminate nucleophilic addition at C2 as a real possibility, as the reaction is at no point exposed to moisture which is needed for this reaction path to proceed to form the hydrolysis products reported as a possible waste influencing the yield of the desired product. That is, in the absence of moisture, **5a** or **13a** are forced to go back and reform the lowest energy adducts, **3b** and **11b**, which are, in principle, well prepared for the formation of **5b** and **13b**, respectively.

Although Cl_2 appears to be a better oxidant than Br_2, we do not encourage its use as it is a highly poisonous gas that may even lead to death in high doses. Therefore, we strongly recommend that synthetic chemists make use of bromine as it also has the same benefits but is less harmful.

RFERENCES

(1)   Bharagava, D.; Garg, G. Recent trends in synthesis of quinoxaline and its derivatives. *ChemInform.* **2012**, *43*, no-no.

(2)   Richard, J. Preparation of quinoxalines, dihydropyrazines, pyrazines and piperazines using tandem oxidation processes. *Chem. Commun.* **2003**, 2286-2287.

(3)   Seitz, L. E.; Suling, W. J.; Reynolds, R. C. Synthesis and antimycobacterial activity of pyrazine and quinoxaline derivatives. *J. Med. Chem.* **2002**, *45*, 5604-5606.

(4)   Gupta, G.; Verma, P. Antimicrobial activity of quinoxaline derivatives. *Chem Sci Trans.* **2014**, *3*, 876-884.

(5)   Refaat, H. M.; Moneer, A. A.; Khalil, O. M. Synthesis and antimicrobial activity of certain novel quinoxalines. *Arc. Pharmacol. Res.* **2004**, *27*, 1093.

(6)   Blache, Y.; Gueiffier, A.; Elhakmaoui, A.; Viols, H.; Chapat, J. P.; Chavignon, O.; Teulade, J. C.; Grassy, G.; Dauphin, G.; Carpy, A. Synthesis and reactivity of pyrrolo [1, 2-α] quinoxalines. Crystal structure and AM1 calculation. *J. Heterocycl. Chem.* **1995**, *32*, 1317-1324.

(7)   Olayiwola, G.; Obafemi, C.; Taiwo, F. Synthesis and neuropharmacological activity of some quinoxalinone derivatives. *Afr. J. Biotechnol.* **2007**, *6*.

(8)   Ries, U. J.; Priepke, H. W.; Hauel, N. H.; Handschuh, S.; Mihm, G.; Stassen, J. M.; Wienen, W.; Nar, H. Heterocyclic thrombin inhibitors. Part 2: quinoxalinone derivatives as novel, potent antithrombotic agents. *Bioorg. Med. Chem. Lett.* **2003**, *13*, 2297-2302.

(9)   Zarranz, B.; Jaso, A.; Aldana, I.; Monge, A.; Maurel, S.; Deharo, E.; Jullian, V.; Sauvain, M. Synthesis and antimalarial activity of new 3-arylquinoxaline-2-carbonitrile derivatives. *Arzneimittelforschung.* **2005**, *55*, 754-761.

(10)   RajanBabu, T. V.; Reddy, G.; Fukunaga, T. Nucleophilic addition of silyl enol ethers to aromatic nitro compounds: scope and mechanism of reaction. *J. Am. Chem. Soc.* **1985**, *107*, 5473-5483.

(11)   RajanBabu, T. V.; Fukunaga, T. Nucleophilic addition of silyl enol ethers to aromatic nitro compounds: a facile synthesis of. alpha.-nitroaryl carbonyl compounds. *J. Org. Chem.* **1984**, *49*, 4571-4572.

(12)   Mąkosza, M.; Kamieńska-Trela, K.; Paszewski, M.; Bechcicka, M. Oxidative nucleophilic substitution of hydrogen in nitroarenes with phenylacetic acid derivatives. *Tetrahedron.* **2005**, *61*, 11952-11964.

(13)   Makosza, M.; Staliski, K. Oxidative nucleophilic substitution of hydrogen with 2-phenylpropanenitrile carbanion in heterocyclic nitroarenes. *Synthesis.* **1998**, *11*, 1631-1634.

(14)   Mąkosza, M. Nucleophilic substitution of hydrogen in electron-deficient arenes, a general process of great practical value. *Chem. Soc. Rev.* **2010**, *39*, 2855-2868.

CHAPTER 6: Conclusions

Conclusions

For many years, density functional theory (DFT) has spearheaded research surrounding quantum chemistry which has been very successful in theoretical studies of chemical reactions. Presented in this work was a density functional theory (DFT) study of the assumed Oxidative Nucleophilic Substitution of Hydrogen (ONSH) reaction mechanism followed when 2-phenylquinoxaline is treated with various organolithium nucleophiles such as lithium phenylacetylide and 1-octynyllithium. This study aimed at providing crucial information of the ONSH reaction mechanism at an atomic, molecular and molecular fragment level using the Reaction Energy profile-fragment attributed molecular system energy change (REP-FAMSEC) protocol so that we could expand on the existing knowledge base of understanding many reaction mechanisms in chemistry.

Guided by the experimental work of the reactions under investigation as reported by Ndlovu and Nxumalo, we modelled the nucleophilic addition reaction (first step of the ONSH reaction mechanism) at 195.15 K and the subsequent hydrolysis and oxidation reactions at 298.15 K. However, we identified three addition electrophilic sites, namely C2, C5 and C10, which may compete the reported site (C3) for nucleophilic addition. After modelling these additional reaction paths, very high energy barriers were observed for nucleophilic addition at C5 and C10 and were therefore eliminated. Interestingly, nucleophilic addition at C2 presented a reaction barrier that was very comparable to that of C3. As such, C2 was found to be a real competing site that may be involved in the reaction only up to the subsequent hydrolysis reaction leading to the formation of two possible products; hence they were seen as a possible waste influencing the yield of the desired 2,3-disubstituted quinoxaline product.

Due to the experimental work being unclear as to when hydrolysis and oxidation occurs, we modelled them as separate and concurrent reactions and studied the impact this had on the final ONSH product. It was observed that the small difference in the energies of the products was only a result of the arrangement of the LiOH and H_2O_2 by-products relative to the 2,3-disubstituted quinoxaline. Worth noting in these reactions is that H_2O_2 can break down into water and oxygen making them environmentally friendly.

The relative stability between adducts and the difference in energy barriers at the TSs at the nucleophilic addition were explained by analysing the changes in the interaction energies between atoms and molecular fragments identified to be playing an important role. From this analysis, it was established that the Li-atom was involved in the strongest attractive interactions

89

with 2-phenylquinoxaline thus driving the formation of the adducts between the two reactants. Furthermore, we observed that the phenyl substituent ($\mathcal{P}h$1) at C2 guides the nucleophile towards C2 and C3. From this, it was clear that the relatively low yields cannot be attributed to steric hindrance caused by $\mathcal{P}h$1. Moreover, it followed from the data presented in this work that the nature of the nucleophile, whether an aryl or alkynyl, does not influence the reactivity. Therefore, these reactions should proceed smoothly to give their respective products in relatively good yields after considering the recommendations made to minimize or even eliminate the possibility for nucleophilic addition at C2.

From the theoretical investigation presented in Chapter 5 where halogens are used for the purposes of oxidizing **5b** and **13b**, it was observed that the reaction proceeds smoothly to give the desired product. Moreover, the use of halogens to oxidize the σ^H-adducts eliminates the competing RP (RP-C2).

It is clear from these drawn conclusions that in addition to the standard analysis of reaction energy profiles computed using computational methods, REP-FAMSEC provides important information that many synthetic chemists can make use of in the study and development of reaction mechanisms in the future.

Future Work

For additional insight, the experimental work needs to be repeated in order to verify the competing reaction. From this, one will be able to further optimize the reaction conditions in order to eliminate the competing reaction and maximize the yield of the desired product.

From a computational modelling perspective, more insightful information can be sought by investigating the influence that the addition of various electron donating groups (EDGs) on 2-phenylquinoxaline will have on the reactivity, preferred reaction path and the reaction rates.

Appendix A

(CHAPTER 3)

Table of content

Part 1

XYZ coordinates of molecular systems (Tables A1-A24) and their energies (Tables A25-A34)

Table A1. Cartesian coordinates for 2-phenylquinoxaline (**1**). The structure was optimized at the RB3LYP-GD3/6-311++G(d,p)/THF level of theory at 195.15 K. Coordinate values are given in Å.

Centre number	Atomic number	Atom type	Coordinates		
			X	Y	Z
1	7	N	-2.561578	-5.391291	1.045448
2	6	C	-3.171860	-6.543670	0.840572
3	6	C	-2.414088	-7.727561	0.558092
4	7	N	-1.105299	-7.744966	0.509644
5	6	C	-0.459390	-6.564839	0.738712
6	6	C	0.954497	-6.514524	0.707871
7	6	C	1.603252	-5.321337	0.928172
8	6	C	0.867555	-4.137588	1.184443
9	6	C	-0.507244	-4.158598	1.220148
10	6	C	-1.202551	-5.373876	0.998761
11	1	H	-2.925606	-8.661385	0.348908
12	1	H	1.498488	-7.430306	0.508183
13	1	H	2.686007	-5.280968	0.905732
14	1	H	1.398612	-3.208124	1.354225
15	1	H	-1.085534	-3.263325	1.416276
16	6	C	-4.653299	-6.577944	0.880014
17	6	C	-5.387646	-5.432690	0.535766
18	6	C	-6.778290	-5.448719	0.564783
19	6	C	-7.460046	-6.606220	0.945821
20	6	C	-6.739983	-7.747173	1.298108
21	6	C	-5.347164	-7.735668	1.262930
22	1	H	-4.856216	-4.536676	0.240437
23	1	H	-7.332119	-4.558830	0.287779
24	1	H	-8.543756	-6.617430	0.969693
25	1	H	-7.261274	-8.646153	1.606462
26	1	H	-4.805263	-8.625147	1.561374

A2

© University of Pretoria

Table A2. Cartesian coordinates for lithium phenylacetylide (**2**). The structure was optimized at the RB3LYP-GD3/6-311++G(d,p)/THF level of theory at 195.15 K. Coordinate values are given in Å.

Centre number	Atomic number	Atom type	Coordinates		
			X	Y	Z
1	3	Li	-5.551269	6.899123	1.149833
2	6	C	-6.409846	5.503681	-0.058057
3	6	C	-6.975264	4.668254	-0.769355
4	6	C	-7.640430	3.701114	-1.585653
5	6	C	-8.981622	3.884529	-1.981672
6	6	C	-9.630771	2.939738	-2.771411
7	6	C	-8.962615	1.786883	-3.188788
8	6	C	-7.633981	1.590470	-2.807056
9	6	C	-6.980019	2.532275	-2.017420
10	1	H	-9.506335	4.776963	-1.660455
11	1	H	-10.662928	3.103583	-3.062016
12	1	H	-9.470416	1.051774	-3.802741
13	1	H	-7.104576	0.698839	-3.125411
14	1	H	-5.948772	2.372884	-1.724138

A3

Table A3. Cartesian coordinates for the adduct along RP-C2 (**3a**). The structure was optimized at the RB3LYP-GD3/6-311++G(d,p)/THF level of theory at 195.15 K. Coordinate values are given in Å.

Centre number	Atomic number	Atom type	Coordinates		
			X	Y	Z
1	7	N	-2.677838	-4.810929	-0.347156
2	6	C	-3.868354	-5.315044	-0.060273
3	6	C	-4.163881	-5.772890	1.263509
4	7	N	-3.302638	-5.726831	2.247123
5	6	C	-2.062474	-5.234618	1.964185
6	6	C	-1.084480	-5.173158	2.984877
7	6	C	0.173183	-4.692307	2.704648
8	6	C	0.499748	-4.261112	1.396425
9	6	C	-0.433836	-4.305201	0.386766
10	6	C	-1.740522	-4.786391	0.647929
11	1	H	-5.142451	-6.189645	1.476597
12	1	H	-1.356224	-5.515702	3.976246
13	1	H	0.923371	-4.644935	3.485020
14	1	H	1.498444	-3.894466	1.190200
15	1	H	-0.179657	-3.985844	-0.617376
16	6	C	-4.889064	-5.425077	-1.123854
17	6	C	-4.509917	-5.777076	-2.427651
18	6	C	-5.464234	-5.881841	-3.435373
19	6	C	-6.808573	-5.633913	-3.153697
20	6	C	-7.193576	-5.286944	-1.858364
21	6	C	-6.243216	-5.189700	-0.846490
22	1	H	-3.466861	-5.981625	-2.639707
23	1	H	-5.161144	-6.162639	-4.437570
24	1	H	-7.551566	-5.711747	-3.939206
25	1	H	-8.234064	-5.080181	-1.636459
26	1	H	-6.549952	-4.883538	0.145659
27	3	Li	-2.677762	-3.061115	-1.721302
28	6	C	-4.052338	-1.817809	-0.868748
29	6	C	-5.002988	-1.910774	-0.087462
30	6	C	-6.080786	-2.175201	0.809545
31	6	C	-5.837257	-2.785822	2.057632
32	6	C	-6.887854	-3.128875	2.903844
33	6	C	-8.208209	-2.865508	2.533526
34	6	C	-8.465350	-2.249936	1.306267
35	6	C	-7.418632	-1.908225	0.454905
36	1	H	-4.815298	-3.001095	2.345941
37	1	H	-6.675114	-3.606331	3.854334
38	1	H	-9.025784	-3.134830	3.192583
39	1	H	-9.487322	-2.039754	1.009348
40	1	H	-7.625066	-1.444327	-0.502541

A4

Table A4. Cartesian coordinates for the transition state along RP-C2 (**4a**). The structure was optimized at the RB3LYP-GD3/6-311++G(d,p)/THF level of theory at 195.15 K. Coordinate values are given in Å.

Centre number	Atomic number	Atom type	Coordinates		
			X	Y	Z
1	7	N	-2.514329	-4.745019	-0.731607
2	6	C	-3.845762	-4.972955	-0.448143
3	6	C	-4.129752	-5.747665	0.791890
4	7	N	-3.283939	-5.905038	1.747543
5	6	C	-2.020273	-5.348714	1.581820
6	6	C	-1.098321	-5.401230	2.638844
7	6	C	0.192609	-4.923554	2.475349
8	6	C	0.583361	-4.407145	1.225813
9	6	C	-0.307893	-4.355884	0.168060
10	6	C	-1.643604	-4.806219	0.318389
11	1	H	-5.118137	-6.187819	0.898672
12	1	H	-1.424832	-5.828417	3.581163
13	1	H	0.898833	-4.958513	3.296482
14	1	H	1.597093	-4.045992	1.088062
15	1	H	-0.001033	-3.966712	-0.797532
16	6	C	-4.685295	-5.400694	-1.642921
17	6	C	-4.049101	-5.851069	-2.803724
18	6	C	-4.794102	-6.306672	-3.892959
19	6	C	-6.185512	-6.333850	-3.829425
20	6	C	-6.828216	-5.897289	-2.668677
21	6	C	-6.085254	-5.430250	-1.588316
22	1	H	-2.967450	-5.848326	-2.838783
23	1	H	-4.283191	-6.648529	-4.786436
24	1	H	-6.765354	-6.692499	-4.672490
25	1	H	-7.910766	-5.913868	-2.608097
26	1	H	-6.595048	-5.066988	-0.704749
27	3	Li	-2.966423	-2.860961	-1.278682
28	6	C	-4.666444	-3.337147	0.032980
29	6	C	-5.535462	-2.914449	0.794217
30	6	C	-6.544643	-2.413824	1.662227
31	6	C	-6.249090	-2.099927	3.003952
32	6	C	-7.242848	-1.619454	3.850425
33	6	C	-8.545708	-1.444795	3.379210
34	6	C	-8.851500	-1.753918	2.051951
35	6	C	-7.863514	-2.232960	1.198462
36	1	H	-5.238366	-2.239914	3.368342
37	1	H	-7.002158	-1.382237	4.880526
38	1	H	-9.317779	-1.070591	4.041695
39	1	H	-9.861980	-1.620200	1.682543
40	1	H	-8.098357	-2.471662	0.167810

Table A5. Cartesian coordinates for the intermediate along RP-C2 (**5a**). The structure was optimized at the RB3LYP-GD3/6-311++G(d,p)/THF level of theory at 195.15 K. Coordinate values are given in Å.

Centre number	Atomic number	Atom type	Coordinates		
			X	Y	Z
1	7	N	-2.929642	-4.462909	-0.645011
2	6	C	-4.193668	-5.178884	-0.374334
3	6	C	-3.922862	-6.446356	0.458001
4	7	N	-2.988871	-6.526749	1.326356
5	6	C	-2.101556	-5.449661	1.436080
6	6	C	-1.181971	-5.430504	2.490857
7	6	C	-0.169611	-4.479871	2.547114
8	6	C	-0.055415	-3.559650	1.490838
9	6	C	-0.951262	-3.565499	0.433311
10	6	C	-2.040625	-4.479866	0.381661
11	1	H	-4.573197	-7.305040	0.297706
12	1	H	-1.273708	-6.193625	3.257701
13	1	H	0.529576	-4.462219	3.374721
14	1	H	0.743016	-2.823947	1.503067
15	1	H	-0.845740	-2.833128	-0.362022
16	6	C	-4.837731	-5.581701	-1.710369
17	6	C	-4.147885	-6.479488	-2.537387
18	6	C	-4.674489	-6.865090	-3.767597
19	6	C	-5.902744	-6.355506	-4.195550
20	6	C	-6.596641	-5.464745	-3.379802
21	6	C	-6.068402	-5.083709	-2.143329
22	1	H	-3.191410	-6.872112	-2.211492
23	1	H	-4.129404	-7.565179	-4.391178
24	1	H	-6.314216	-6.654587	-5.153063
25	1	H	-7.552623	-5.065351	-3.700337
26	1	H	-6.618211	-4.396526	-1.511411
27	3	Li	-2.834004	-3.415920	-2.286917
28	6	C	-5.096647	-4.326501	0.429792
29	6	C	-5.755500	-3.603108	1.140722
30	6	C	-6.530642	-2.751637	1.982479
31	6	C	-6.034461	-2.344356	3.234686
32	6	C	-6.791501	-1.512289	4.054021
33	6	C	-8.050871	-1.072769	3.642002
34	6	C	-8.551690	-1.471916	2.401619
35	6	C	-7.801354	-2.304169	1.576462
36	1	H	-5.057002	-2.686396	3.553360
37	1	H	-6.397773	-1.206675	5.016808
38	1	H	-8.637813	-0.425076	4.283091
39	1	H	-9.529668	-1.134964	2.076831
40	1	H	-8.191322	-2.615273	0.614399

Table A6. Cartesian coordinates for the adduct along RP-C3 (**3b**). The structure was optimized at the RB3LYP-GD3/6-311++G(d,p)/THF level of theory at 195.15 K. Coordinate values are given in Å.

Centre number	Atomic number	Atom type	Coordinates		
			X	Y	Z
1	7	N	-2.540885	-5.207869	0.754700
2	6	C	-3.165730	-6.200555	0.149768
3	6	C	-2.424778	-7.286464	-0.414816
4	7	N	-1.116636	-7.377704	-0.338431
5	6	C	-0.451149	-6.366488	0.300255
6	6	C	0.956599	-6.398878	0.423224
7	6	C	1.613215	-5.368042	1.056366
8	6	C	0.891074	-4.271301	1.586559
9	6	C	-0.479274	-4.217618	1.482119
10	6	C	-1.184210	-5.265181	0.838398
11	1	H	-2.927391	-8.089329	-0.940120
12	1	H	1.500631	-7.241876	0.012264
13	1	H	2.692373	-5.391859	1.151238
14	1	H	1.427956	-3.469414	2.079607
15	1	H	-1.048986	-3.388413	1.884290
16	6	C	-4.643143	-6.177398	0.041378
17	6	C	-5.338910	-4.960839	0.117112
18	6	C	-6.725086	-4.933126	0.002635
19	6	C	-7.440762	-6.118450	-0.183514
20	6	C	-6.760054	-7.333518	-0.251858
21	6	C	-5.372339	-7.363204	-0.141566
22	1	H	-4.782367	-4.042582	0.256862
23	1	H	-7.249272	-3.985483	0.053930
24	1	H	-8.520825	-6.092903	-0.274238
25	1	H	-7.299320	-8.263549	-0.390971
26	1	H	-4.871832	-8.321677	-0.184618
27	3	Li	-0.506003	-9.230987	-1.241854
28	6	C	-2.194178	-10.359079	-1.612780
29	6	C	-3.402037	-10.615066	-1.589208
30	6	C	-4.816343	-10.810757	-1.515669
31	6	C	-5.639583	-10.626027	-2.645283
32	6	C	-7.021966	-10.760743	-2.552664
33	6	C	-7.621789	-11.083440	-1.333890
34	6	C	-6.820700	-11.274943	-0.206474
35	6	C	-5.437630	-11.143655	-0.293887
36	1	H	-5.181059	-10.367437	-3.592691
37	1	H	-7.634470	-10.609057	-3.434885
38	1	H	-8.698959	-11.183263	-1.263261
39	1	H	-7.275449	-11.523765	0.746296
40	1	H	-4.821589	-11.285952	0.586593

Table A7. Cartesian coordinates for the transition state along RP-C3 (**4b**). The structure was optimized at the RB3LYP-GD3/6-311++G(d,p)/THF level of theory at 195.15 K. Coordinate values are given in Å.

Centre number	Atomic number	Atom type	Coordinates		
			X	Y	Z
1	7	N	-2.633552	-5.874902	0.622870
2	6	C	-3.117965	-6.350976	-0.483601
3	6	C	-2.226372	-7.015667	-1.479529
4	7	N	-0.873161	-6.745181	-1.419623
5	6	C	-0.392486	-6.324034	-0.214875
6	6	C	1.003543	-6.232361	0.017020
7	6	C	1.493062	-5.805547	1.238281
8	6	C	0.617539	-5.435493	2.278437
9	6	C	-0.749800	-5.483387	2.066320
10	6	C	-1.271571	-5.921724	0.834993
11	1	H	-2.601541	-7.011904	-2.497755
12	1	H	1.679482	-6.505142	-0.787081
13	1	H	2.565163	-5.752775	1.395746
14	1	H	1.013509	-5.102469	3.230602
15	1	H	-1.449856	-5.180574	2.837740
16	6	C	-4.583280	-6.285554	-0.705043
17	6	C	-5.423352	-5.822894	0.323840
18	6	C	-6.802914	-5.792534	0.162457
19	6	C	-7.382638	-6.223408	-1.033489
20	6	C	-6.563920	-6.678264	-2.064504
21	6	C	-5.180245	-6.709799	-1.902825
22	1	H	-4.974230	-5.499011	1.253508
23	1	H	-7.430511	-5.438586	0.972981
24	1	H	-8.459634	-6.207044	-1.156904
25	1	H	-7.000810	-7.020288	-2.995910
26	1	H	-4.575843	-7.087958	-2.716072
27	3	Li	-0.501947	-8.717651	-1.655249
28	6	C	-2.607248	-8.812688	-1.201167
29	6	C	-3.675066	-9.398424	-1.014024
30	6	C	-4.924598	-10.019480	-0.745510
31	6	C	-5.586405	-10.783153	-1.726685
32	6	C	-6.825548	-11.354420	-1.457037
33	6	C	-7.429288	-11.171054	-0.211239
34	6	C	-6.784129	-10.412675	0.768046
35	6	C	-5.541953	-9.844571	0.509318
36	1	H	-5.120630	-10.917743	-2.695807
37	1	H	-7.324102	-11.941205	-2.220313
38	1	H	-8.396749	-11.614675	-0.005538
39	1	H	-7.251418	-10.263761	1.734915
40	1	H	-5.042393	-9.248914	1.263622

Table A8. Cartesian coordinates for the intermediate along RP-C3 (**5b**). The structure was optimized at the RB3LYP-GD3/6-311++G(d,p)/THF level of theory at 195.15 K. Coordinate values are given in Å.

Centre number	Atomic number	Atom type	Coordinates		
			X	Y	Z
1	7	N	-3.113721	-5.607284	0.503028
2	6	C	-3.656034	-5.886507	-0.635509
3	6	C	-3.084776	-7.025348	-1.493826
4	7	N	-1.619324	-7.045631	-1.424380
5	6	C	-1.137041	-6.866741	-0.170954
6	6	C	0.194301	-7.224322	0.180443
7	6	C	0.666995	-7.070639	1.472930
8	6	C	-0.144562	-6.520156	2.482989
9	6	C	-1.421313	-6.087209	2.152286
10	6	C	-1.925123	-6.236087	0.850824
11	1	H	-3.366406	-6.856858	-2.537767
12	1	H	0.830808	-7.666549	-0.581312
13	1	H	1.677461	-7.389134	1.710057
14	1	H	0.230985	-6.413777	3.493972
15	1	H	-2.054770	-5.603378	2.889263
16	6	C	-4.832345	-5.121846	-1.098951
17	6	C	-5.137404	-3.872547	-0.527447
18	6	C	-6.248907	-3.149537	-0.943132
19	6	C	-7.087415	-3.655281	-1.941053
20	6	C	-6.800835	-4.893116	-2.514135
21	6	C	-5.684590	-5.618761	-2.099786
22	1	H	-4.484254	-3.481310	0.242482
23	1	H	-6.462121	-2.185742	-0.493709
24	1	H	-7.953492	-3.089769	-2.266015
25	1	H	-7.449494	-5.299764	-3.282150
26	1	H	-5.497433	-6.588988	-2.543650
27	3	Li	-0.590042	-7.415409	-3.029295
28	6	C	-3.687994	-8.311739	-1.083077
29	6	C	-4.148815	-9.372697	-0.729011
30	6	C	-4.688389	-10.616944	-0.285247
31	6	C	-5.583785	-11.343862	-1.091174
32	6	C	-6.105704	-12.555840	-0.648462
33	6	C	-5.745027	-13.064073	0.600588
34	6	C	-4.857205	-12.350435	1.407637
35	6	C	-4.331824	-11.137389	0.972759
36	1	H	-5.865284	-10.949536	-2.060529
37	1	H	-6.795989	-13.104484	-1.279348
38	1	H	-6.153500	-14.008094	0.942675
39	1	H	-4.574223	-12.739032	2.379421
40	1	H	-3.644260	-10.582073	1.599483

A9

Table A9. Cartesian coordinates for the adduct along RP-C5 (**3c**). The structure was optimized at the RB3LYP-GD3/6-311++G(d,p)/THF level of theory at 195.15 K. Coordinate values are given in Å.

Centre number	Atomic number	Atom type	X	Y	Z
			X	**Y**	**Z**
1	7	N	-2.648498	-4.774117	1.104270
2	6	C	-3.408317	-5.476974	0.285174
3	6	C	-2.815890	-6.356432	-0.674545
4	7	N	-1.517613	-6.529335	-0.778724
5	6	C	-0.713656	-5.825683	0.077856
6	6	C	0.692347	-5.973001	0.025264
7	6	C	1.482646	-5.246959	0.886410
8	6	C	0.905662	-4.353514	1.822627
9	6	C	-0.458252	-4.194558	1.892650
10	6	C	-1.301247	-4.929240	1.021789
11	1	H	-3.443608	-6.897798	-1.373696
12	1	H	1.121574	-6.658849	-0.698402
13	1	H	2.559982	-5.357564	0.849562
14	1	H	1.550154	-3.792286	2.489104
15	1	H	-0.918907	-3.518225	2.602636
16	6	C	-4.878983	-5.312091	0.356923
17	6	C	-5.423306	-4.089891	0.779553
18	6	C	-6.801794	-3.916569	0.847270
19	6	C	-7.659480	-4.962792	0.501761
20	6	C	-7.128499	-6.184446	0.089435
21	6	C	-5.748355	-6.358425	0.014016
22	1	H	-4.755535	-3.280121	1.045417
23	1	H	-7.208754	-2.963942	1.166605
24	1	H	-8.733538	-4.827067	0.556064
25	1	H	-7.787648	-7.005437	-0.168015
26	1	H	-5.354847	-7.322414	-0.286109
27	3	Li	-0.752249	-7.806490	-2.278752
28	6	C	1.169406	-8.354643	-2.685531
29	6	C	2.371729	-8.613925	-2.788932
30	6	C	3.768430	-8.901551	-2.888167
31	6	C	4.334975	-10.000764	-2.209825
32	6	C	5.696990	-10.273973	-2.300920
33	6	C	6.531961	-9.460996	-3.070068
34	6	C	5.987206	-8.369096	-3.748856
35	6	C	4.625854	-8.091327	-3.661134
36	1	H	3.692571	-10.635684	-1.610471
37	1	H	6.108772	-11.125134	-1.769220
38	1	H	7.592377	-9.675419	-3.139569
39	1	H	6.626012	-7.730640	-4.349704
40	1	H	4.209515	-7.241801	-4.190264

Table A10. Cartesian coordinates for the transition state along RP-C5 (**4c**). The structure was optimized at the RB3LYP-GD3/6-311++G(d,p)/THF level of theory at 195.15 K. Coordinate values are given in Å.

Centre number	Atomic number	Atom type	Coordinates		
			X	Y	Z
1	7	N	-1.601441	-5.546360	0.275462
2	6	C	-2.608378	-6.441369	0.213193
3	6	C	-2.528313	-7.613235	1.005340
4	7	N	-1.427132	-8.038598	1.600904
5	6	C	-0.241933	-7.325463	1.251033
6	6	C	0.839862	-7.523615	2.236865
7	6	C	1.754826	-6.553679	2.477026
8	6	C	1.661251	-5.269271	1.840471
9	6	C	0.564820	-4.950802	1.088637
10	6	C	-0.474153	-5.901767	0.870643
11	1	H	-3.437368	-8.169166	1.223035
12	1	H	0.885644	-8.487969	2.730252
13	1	H	2.559920	-6.733027	3.181702
14	1	H	2.433907	-4.530736	2.020442
15	1	H	0.432121	-3.958597	0.671326
16	6	C	-3.835126	-6.081242	-0.523779
17	6	C	-4.114556	-4.740398	-0.844791
18	6	C	-5.270411	-4.396031	-1.538917
19	6	C	-6.180774	-5.379199	-1.933126
20	6	C	-5.913233	-6.714621	-1.629993
21	6	C	-4.753393	-7.061968	-0.941109
22	1	H	-3.414166	-3.974493	-0.536906
23	1	H	-5.465124	-3.354201	-1.770141
24	1	H	-7.080795	-5.109233	-2.473833
25	1	H	-6.602990	-7.491212	-1.942457
26	1	H	-4.551995	-8.109380	-0.746944
27	3	Li	-0.879754	-9.671580	0.428887
28	6	C	0.413228	-8.025687	-0.265255
29	6	C	1.326900	-7.757774	-1.046339
30	6	C	2.359709	-7.435007	-1.964862
31	6	C	2.110345	-6.559150	-3.041994
32	6	C	3.127258	-6.227582	-3.930570
33	6	C	4.407114	-6.763345	-3.769846
34	6	C	4.665559	-7.634831	-2.709281
35	6	C	3.656083	-7.968847	-1.813181
36	1	H	1.117208	-6.143691	-3.164778
37	1	H	2.922046	-5.550018	-4.751730
38	1	H	5.196948	-6.503704	-4.465359
39	1	H	5.657822	-8.052255	-2.579859
40	1	H	3.857649	-8.640069	-0.986682

Table A11. Cartesian coordinates for the intermediate along RP-C5 (**5c**). The structure was optimized at the RB3LYP-GD3/6-311++G(d,p)/THF level of theory at 195.15 K. Coordinate values are given in Å.

Centre number	Atomic number	Atom type	Coordinates		
			X	Y	Z
1	7	N	-1.611383	-5.396214	0.812000
2	6	C	-2.299527	-6.383496	0.175461
3	6	C	-2.070066	-7.711985	0.595607
4	7	N	-1.014609	-8.116476	1.284671
5	6	C	0.080303	-7.112720	1.323383
6	6	C	1.010165	-7.458140	2.470060
7	6	C	1.472819	-6.526728	3.328854
8	6	C	1.049616	-5.147016	3.262897
9	6	C	0.065235	-4.775826	2.394324
10	6	C	-0.538891	-5.710579	1.499271
11	1	H	-2.869524	-8.441097	0.470302
12	1	H	1.345892	-8.489071	2.524541
13	1	H	2.168182	-6.819218	4.109804
14	1	H	1.475687	-4.428375	3.953078
15	1	H	-0.325779	-3.763371	2.385325
16	6	C	-3.423552	-6.023424	-0.698717
17	6	C	-3.959128	-4.719573	-0.702702
18	6	C	-5.026724	-4.381777	-1.528641
19	6	C	-5.598965	-5.331301	-2.379431
20	6	C	-5.073216	-6.624381	-2.397523
21	6	C	-3.997361	-6.962374	-1.580112
22	1	H	-3.525874	-3.979061	-0.042144
23	1	H	-5.419219	-3.370244	-1.506308
24	1	H	-6.430522	-5.065763	-3.022408
25	1	H	-5.491605	-7.370691	-3.064973
26	1	H	-3.582432	-7.962243	-1.644454
27	3	Li	-1.012352	-9.907698	2.116123
28	6	C	0.837420	-7.148174	0.046557
29	6	C	1.489060	-7.192458	-0.971661
30	6	C	2.231327	-7.232882	-2.189738
31	6	C	1.580649	-7.061104	-3.425689
32	6	C	2.303857	-7.103077	-4.613968
33	6	C	3.683521	-7.315017	-4.592337
34	6	C	4.338447	-7.484338	-3.371234
35	6	C	3.622184	-7.444820	-2.178532
36	1	H	0.510348	-6.893036	-3.441241
37	1	H	1.789790	-6.968320	-5.558972
38	1	H	4.244168	-7.345884	-5.519570
39	1	H	5.410172	-7.646707	-3.347755
40	1	H	4.131074	-7.574517	-1.230664

Table A12. Cartesian coordinates for the adduct along RP-C10 (**3d**). The structure was optimized at the RB3LYP-GD3/6-311++G(d,p)/THF level of theory at 195.15 K. Coordinate values are given in Å.

Centre number	Atomic number	Atom type	X	Y	Z
1	7	N	-2.161317	-4.919892	0.839698
2	6	C	-3.151169	-5.493258	0.172471
3	6	C	-2.881034	-6.470782	-0.835898
4	7	N	-1.670140	-6.844902	-1.162939
5	6	C	-0.635658	-6.249393	-0.503896
6	6	C	0.696028	-6.604104	-0.825465
7	6	C	1.743726	-6.003258	-0.167820
8	6	C	1.500704	-5.028722	0.830637
9	6	C	0.217151	-4.664977	1.166872
10	6	C	-0.880044	-5.270186	0.506656
11	1	H	-3.708621	-6.920963	-1.374697
12	1	H	0.856676	-7.349544	-1.595074
13	1	H	2.764237	-6.272565	-0.413361
14	1	H	2.339019	-4.562247	1.334718
15	1	H	0.023839	-3.915902	1.928293
16	6	C	-4.547747	-5.091409	0.456609
17	6	C	-4.874537	-3.734573	0.594801
18	6	C	-6.186588	-3.349997	0.858122
19	6	C	-7.186690	-4.314729	0.984631
20	6	C	-6.871007	-5.666129	0.839880
21	6	C	-5.560803	-6.054077	0.570817
22	1	H	-4.103120	-2.982975	0.470464
23	1	H	-6.429178	-2.298195	0.955266
24	1	H	-8.207710	-4.014802	1.190292
25	1	H	-7.644209	-6.418894	0.940252
26	1	H	-5.321157	-7.106837	0.473417
27	3	Li	-2.468607	-3.879250	2.693844
28	6	C	-1.301048	-2.518215	3.662500
29	6	C	-0.520284	-1.728813	4.201566
30	6	C	0.394182	-0.818267	4.816284
31	6	C	0.588067	-0.811444	6.213181
32	6	C	1.482298	0.074558	6.807669
33	6	C	2.207234	0.977994	6.027984
34	6	C	2.026853	0.984951	4.643332
35	6	C	1.134054	0.100984	4.043741
36	1	H	0.028237	-1.510078	6.824276
37	1	H	1.613872	0.060256	7.884329
38	1	H	2.902953	1.667207	6.492991
39	1	H	2.584187	1.682698	4.027495
40	1	H	0.998086	0.111605	2.968379

A13

Table A13. Cartesian coordinates for the transition state along RP-C10 (**4d**). The structure was optimized at the RB3LYP-GD3/6-311++G(d,p)/THF level of theory at 195.15 K. Coordinate values are given in Å.

Centre number	Atomic number	Atom type	Coordinates		
			X	Y	Z
1	7	N	-2.729809	-3.451478	0.573532
2	6	C	-3.116273	-4.698135	0.838287
3	6	C	-2.191347	-5.718320	1.162943
4	7	N	-0.873355	-5.546955	0.997724
5	6	C	-0.434657	-4.324187	0.719976
6	6	C	0.925667	-4.099153	0.370446
7	6	C	1.338724	-2.881094	-0.096581
8	6	C	0.385075	-1.826964	-0.301059
9	6	C	-0.903091	-1.958076	0.098049
10	6	C	-1.359190	-3.158291	0.834027
11	1	H	-2.530979	-6.723489	1.380646
12	1	H	1.608522	-4.939089	0.441017
13	1	H	2.371485	-2.727187	-0.387069
14	1	H	0.702657	-0.923074	-0.810305
15	1	H	-1.636701	-1.178076	-0.074140
16	6	C	-4.562314	-5.015090	0.689162
17	6	C	-5.341317	-4.323201	-0.251289
18	6	C	-6.697707	-4.603615	-0.395806
19	6	C	-7.304989	-5.573455	0.403605
20	6	C	-6.542184	-6.261649	1.347722
21	6	C	-5.183382	-5.987152	1.488695
22	1	H	-4.867512	-3.573251	-0.872344
23	1	H	-7.281306	-4.067544	-1.136172
24	1	H	-8.361387	-5.790197	0.292489
25	1	H	-7.006074	-7.010830	1.979540
26	1	H	-4.609459	-6.519232	2.238278
27	3	Li	-3.352115	-2.291269	2.131139
28	6	C	-1.200028	-2.697189	2.549723
29	6	C	-0.309548	-2.491082	3.373359
30	6	C	0.709345	-2.292954	4.342894
31	6	C	1.226201	-1.007150	4.601654
32	6	C	2.232541	-0.828429	5.544797
33	6	C	2.745419	-1.922726	6.245006
34	6	C	2.242455	-3.201776	5.996788
35	6	C	1.232919	-3.389327	5.058943
36	1	H	0.832275	-0.159022	4.054159
37	1	H	2.620802	0.166175	5.733377
38	1	H	3.531262	-1.779890	6.977842
39	1	H	2.638113	-4.054703	6.536708
40	1	H	0.842003	-4.380998	4.864554

Table A14. Cartesian coordinates for the intermediate along RP-C10 (**5d**). The structure was optimized at the RB3LYP-GD3/6-311++G(d,p)/THF level of theory at 195.15 K. Coordinate values are given in Å.

Centre number	Atomic number	Atom type	Coordinates		
			X	Y	Z
1	7	N	-2.336929	-3.343725	0.646652
2	6	C	-2.679257	-4.616418	0.843093
3	6	C	-1.766293	-5.686588	0.753526
4	7	N	-0.587056	-5.522462	0.115457
5	6	C	-0.178105	-4.294610	-0.133240
6	6	C	0.879214	-4.047277	-1.053973
7	6	C	1.162927	-2.788093	-1.502913
8	6	C	0.347092	-1.676793	-1.079892
9	6	C	-0.620157	-1.812172	-0.147827
10	6	C	-0.866369	-3.118154	0.585436
11	1	H	-2.092984	-6.702072	0.941529
12	1	H	1.415876	-4.912562	-1.430483
13	1	H	1.948875	-2.624955	-2.230845
14	1	H	0.504770	-0.708899	-1.546285
15	1	H	-1.213607	-0.959097	0.165237
16	6	C	-4.124534	-4.930650	1.021559
17	6	C	-5.089586	-4.400625	0.151251
18	6	C	-6.440718	-4.699402	0.319711
19	6	C	-6.851893	-5.531084	1.362408
20	6	C	-5.899648	-6.065524	2.231617
21	6	C	-4.548233	-5.768914	2.063193
22	1	H	-4.768380	-3.776526	-0.675332
23	1	H	-7.171624	-4.292315	-0.370466
24	1	H	-7.902516	-5.763872	1.493664
25	1	H	-6.209906	-6.711145	3.045865
26	1	H	-3.814364	-6.180302	2.747223
27	3	Li	-3.546399	-1.867126	1.171405
28	6	C	-0.331745	-2.995968	1.968191
29	6	C	0.082852	-2.789215	3.086538
30	6	C	0.576359	-2.539118	4.402020
31	6	C	1.598736	-1.594950	4.611897
32	6	C	2.070958	-1.341054	5.896088
33	6	C	1.534549	-2.020441	6.991277
34	6	C	0.521583	-2.960351	6.793553
35	6	C	0.044767	-3.220932	5.512108
36	1	H	2.015355	-1.067865	3.761722
37	1	H	2.859482	-0.611460	6.042465
38	1	H	1.904114	-1.820150	7.990427
39	1	H	0.102856	-3.493320	7.639763
40	1	H	-0.739332	-3.952939	5.358696

Table A15. Cartesian coordinates for **6a**. The structure was optimized at the RB3LYP-GD3/6-311++G(d,p)/THF level of theory at 298.15 K. Coordinate values are given in Å.

Centre number	Atomic number	Atom type	Coordinates		
			X	Y	Z
1	7	N	-2.884519	-4.459438	-0.648736
2	6	C	-4.162593	-5.158049	-0.419877
3	6	C	-3.937555	-6.439546	0.406271
4	7	N	-3.021978	-6.548046	1.291193
5	6	C	-2.116788	-5.491112	1.433453
6	6	C	-1.217349	-5.502515	2.505923
7	6	C	-0.191036	-4.569879	2.594678
8	6	C	-0.041013	-3.637042	1.553101
9	6	C	-0.914461	-3.613787	0.477968
10	6	C	-2.018337	-4.509183	0.392724
11	1	H	-4.600896	-7.282705	0.220062
12	1	H	-1.337102	-6.274415	3.260073
13	1	H	0.492670	-4.575618	3.435280
14	1	H	0.769307	-2.915328	1.591529
15	1	H	-0.781462	-2.874140	-0.306484
16	6	C	-4.792570	-5.546493	-1.766409
17	6	C	-4.005652	-6.245554	-2.690564
18	6	C	-4.529959	-6.636636	-3.920657
19	6	C	-5.854512	-6.337366	-4.246318
20	6	C	-6.646974	-5.650789	-3.328629
21	6	C	-6.119014	-5.260737	-2.095746
22	1	H	-2.976872	-6.473666	-2.438423
23	1	H	-3.906139	-7.177099	-4.624193
24	1	H	-6.263594	-6.639807	-5.203808
25	1	H	-7.678101	-5.415886	-3.569005
26	1	H	-6.743867	-4.727930	-1.388876
27	3	Li	-2.919670	-3.126225	-2.105139
28	6	C	-5.067160	-4.284437	0.366136
29	6	C	-5.711676	-3.524087	1.053779
30	6	C	-6.467159	-2.640623	1.881817
31	6	C	-5.955305	-2.222852	3.123707
32	6	C	-6.692738	-1.363322	3.932097
33	6	C	-7.945067	-0.906869	3.517186
34	6	C	-8.459842	-1.315792	2.285765
35	6	C	-7.729992	-2.176574	1.471688
36	1	H	-4.983119	-2.578583	3.443048
37	1	H	-6.289461	-1.049374	4.888067
38	1	H	-8.516641	-0.237650	4.149900
39	1	H	-9.432607	-0.965203	1.960218
40	1	H	-8.130639	-2.498135	0.517435
41	8	O	-4.451174	-1.988473	-1.669071
42	1	H	-4.880730	-2.380244	-0.890263
43	1	H	-5.152472	-1.595542	-2.199239

A16

Table A16. Cartesian coordinates for **7a**. The structure was optimized at the RB3LYP-GD3/6-311++G(d,p)/THF level of theory at 298.15 K. Coordinate values are given in Å.

Centre number	Atomic number	Atom type	Coordinates X	Y	Z
1	7	N	-2.994156	-4.371609	-0.63414
2	6	C	-4.260137	-5.076676	-0.36131
3	6	C	-3.972621	-6.346619	0.460134
4	7	N	-3.010810	-6.449578	1.292705
5	6	C	-2.108933	-5.378166	1.398604
6	6	C	-1.167314	-5.377457	2.432743
7	6	C	-0.185302	-4.395209	2.50337
8	6	C	-0.130901	-3.418126	1.498719
9	6	C	-1.052892	-3.406367	0.459997
10	6	C	-2.084324	-4.370379	0.394967
11	1	H	-4.656479	-7.184905	0.336866
12	1	H	-1.220396	-6.169832	3.172258
13	1	H	0.533724	-4.392776	3.313973
14	1	H	0.635970	-2.651042	1.534766
15	1	H	-1.013264	-2.634677	-0.30132
16	6	C	-4.904315	-5.438288	-1.70742
17	6	C	-4.382985	-6.506764	-2.44767
18	6	C	-4.895816	-6.820026	-3.70545
19	6	C	-5.937120	-6.063196	-4.24517
20	6	C	-6.461822	-4.998505	-3.51445
21	6	C	-5.951266	-4.691963	-2.2521
22	1	H	-3.566854	-7.094205	-2.04126
23	1	H	-4.485248	-7.655895	-4.26096
24	1	H	-6.337086	-6.304698	-5.22346
25	1	H	-7.271617	-4.404951	-3.92396
26	1	H	-6.367548	-3.865884	-1.68818
27	3	Li	-2.344608	-4.015350	-2.9261
28	6	C	-5.163949	-4.245115	0.462315
29	6	C	-5.847624	-3.555249	1.181691
30	6	C	-6.659141	-2.737837	2.02261
31	6	C	-6.106599	-2.106798	3.151965
32	6	C	-6.901745	-1.309690	3.969806
33	6	C	-8.254786	-1.129183	3.677495
34	6	C	-8.811547	-1.751961	2.55902
35	6	C	-8.023650	-2.550429	1.73569
36	1	H	-5.056411	-2.248468	3.377393
37	1	H	-6.464701	-0.828747	4.837506
38	1	H	-8.871291	-0.508131	4.317172
39	1	H	-9.861999	-1.615824	2.328073
40	1	H	-8.455213	-3.035616	0.868189
41	8	O	-3.095803	-2.446010	-2.1847
42	1	H	-3.147679	-3.246023	-1.33868
43	1	H	-3.949567	-2.018531	-2.29003

Table A17. Cartesian coordinates for **8a**. The structure was optimized at the RB3LYP-GD3/6-311++G(d,p)/THF level of theory at 298.15 K. Coordinate values are given in Å.

Centre number	Atomic number	Atom type	Coordinates		
			X	Y	Z
1	7	N	-2.972067	-4.438597	-0.57498
2	6	C	-4.274519	-5.071644	-0.36078
3	6	C	-4.040779	-6.341081	0.48739
4	7	N	-3.087787	-6.483281	1.32242
5	6	C	-2.142543	-5.449938	1.445386
6	6	C	-1.217117	-5.483109	2.491778
7	6	C	-0.225443	-4.512212	2.594118
8	6	C	-0.148481	-3.510250	1.618447
9	6	C	-1.056497	-3.463781	0.56614
10	6	C	-2.078210	-4.424929	0.470233
11	1	H	-4.769907	-7.140423	0.370625
12	1	H	-1.291509	-6.287464	3.215613
13	1	H	0.484118	-4.537735	3.412463
14	1	H	0.626136	-2.753472	1.682779
15	1	H	-0.996314	-2.686009	-0.18693
16	6	C	-4.869381	-5.471208	-1.7185
17	6	C	-4.074493	-6.211587	-2.60226
18	6	C	-4.574121	-6.609758	-3.84024
19	6	C	-5.878217	-6.273940	-4.21153
20	6	C	-6.675617	-5.543520	-3.3328
21	6	C	-6.174185	-5.146661	-2.09093
22	1	H	-3.060188	-6.464519	-2.31775
23	1	H	-3.947687	-7.184548	-4.51334
24	1	H	-6.268201	-6.583510	-5.17463
25	1	H	-7.689888	-5.278951	-3.61019
26	1	H	-6.797842	-4.574280	-1.41529
27	3	Li	-3.599379	-3.040074	-3.84593
28	6	C	-5.181552	-4.205757	0.418887
29	6	C	-5.857623	-3.498546	1.127734
30	6	C	-6.652295	-2.660226	1.963828
31	6	C	-6.112761	-2.120517	3.1456
32	6	C	-6.889603	-1.304518	3.962157
33	6	C	-8.210873	-1.015568	3.616566
34	6	C	-8.754083	-1.547297	2.445684
35	6	C	-7.984101	-2.363214	1.622559
36	1	H	-5.087393	-2.346979	3.412258
37	1	H	-6.463373	-0.894052	4.870432
38	1	H	-8.813438	-0.380404	4.255636
39	1	H	-9.779774	-1.325926	2.173419
40	1	H	-8.404551	-2.776271	0.713322
41	8	O	-3.139076	-2.336963	-2.30026
42	1	H	-3.003930	-3.592576	-1.19911
43	1	H	-3.131274	-1.481455	-1.86836

Table A18. Cartesian coordinates for **6b**. The structure was optimized at the RB3LYP-GD3/6-311++G(d,p)/THF level of theory at 298.15 K. Coordinate values are given in Å.

Centre number	Atomic number	Atom type	Coordinates		
			X	Y	Z
1	7	N	-3.083964	-5.433416	0.533188
2	6	C	-3.622491	-5.685783	-0.612348
3	6	C	-2.985946	-6.726315	-1.545726
4	7	N	-1.520507	-6.698161	-1.471600
5	6	C	-1.044177	-6.546956	-0.214181
6	6	C	0.304060	-6.858834	0.120612
7	6	C	0.776092	-6.735570	1.416279
8	6	C	-0.052142	-6.262125	2.451614
9	6	C	-1.349738	-5.878548	2.142970
10	6	C	-1.854373	-6.000715	0.839141
11	1	H	-3.273604	-6.495401	-2.576193
12	1	H	0.958859	-7.238710	-0.657921
13	1	H	1.801733	-7.016500	1.635371
14	1	H	0.324949	-6.176750	3.463951
15	1	H	-2.002724	-5.457086	2.900875
16	6	C	-4.865858	-4.994116	-1.010076
17	6	C	-5.277383	-3.829965	-0.334314
18	6	C	-6.455193	-3.180697	-0.682445
19	6	C	-7.256433	-3.676591	-1.715537
20	6	C	-6.864490	-4.830147	-2.392161
21	6	C	-5.681251	-5.481743	-2.045633
22	1	H	-4.654251	-3.446403	0.463599
23	1	H	-6.750415	-2.281897	-0.152039
24	1	H	-8.174969	-3.168705	-1.987190
25	1	H	-7.482148	-5.229232	-3.189152
26	1	H	-5.411479	-6.388677	-2.572749
27	3	Li	-0.608203	-7.460386	-3.036403
28	6	C	-3.518970	-8.076517	-1.243007
29	6	C	-3.870839	-9.209736	-0.999906
30	6	C	-4.276532	-10.541667	-0.682742
31	6	C	-5.295793	-11.177749	-1.413813
32	6	C	-5.679092	-12.478039	-1.098767
33	6	C	-5.054204	-13.162936	-0.055227
34	6	C	-4.041970	-12.538816	0.675888
35	6	C	-3.653207	-11.238703	0.368378
36	1	H	-5.782305	-10.644598	-2.222100
37	1	H	-6.467790	-12.957167	-1.667643
38	1	H	-5.355216	-14.175533	0.187589
39	1	H	-3.554950	-13.065489	1.488667
40	1	H	-2.869313	-10.751533	0.935821
41	8	O	-1.563171	-9.118956	-3.400642
42	1	H	-1.695537	-9.758612	-4.107350
43	1	H	-2.272697	-9.257492	-2.751295

Table A19. Cartesian coordinates for **7b**. The structure was optimized at the RB3LYP-GD3/6-311++G(d,p)/THF level of theory at 298.15 K. Coordinate values are given in Å.

Centre number	Atomic number	Atom type	Coordinates		
			X	Y	Z
1	7	N	-3.054269	-5.590383	0.433896
2	6	C	-3.642666	-5.854378	-0.682147
3	6	C	-3.064154	-6.924250	-1.624008
4	7	N	-1.602778	-6.856777	-1.600250
5	6	C	-1.065490	-6.775662	-0.338609
6	6	C	0.254429	-7.185903	-0.055383
7	6	C	0.767107	-7.082881	1.231437
8	6	C	-0.005430	-6.551814	2.276018
9	6	C	-1.289357	-6.095216	2.004312
10	6	C	-1.828247	-6.192825	0.713969
11	1	H	-3.384258	-6.715663	-2.648081
12	1	H	0.850633	-7.612409	-0.855175
13	1	H	1.776013	-7.429163	1.430519
14	1	H	0.400296	-6.484226	3.278610
15	1	H	-1.898108	-5.642008	2.779742
16	6	C	-4.887813	-5.145585	-1.047386
17	6	C	-5.244492	-3.955581	-0.387717
18	6	C	-6.417039	-3.284980	-0.713681
19	6	C	-7.265197	-3.788070	-1.704426
20	6	C	-6.927600	-4.969280	-2.362512
21	6	C	-5.749077	-5.640763	-2.040451
22	1	H	-4.585065	-3.568320	0.378581
23	1	H	-6.671556	-2.365436	-0.198333
24	1	H	-8.179460	-3.263721	-1.958400
25	1	H	-7.583118	-5.373310	-3.125749
26	1	H	-5.520202	-6.567542	-2.552113
27	3	Li	-0.567135	-5.841404	-3.326121
28	6	C	-3.589049	-8.254278	-1.256962
29	6	C	-3.993358	-9.348959	-0.941856
30	6	C	-4.467530	-10.638126	-0.556032
31	6	C	-5.335037	-11.364245	-1.392193
32	6	C	-5.794190	-12.620592	-1.008167
33	6	C	-5.397019	-13.173204	0.210608
34	6	C	-4.535891	-12.460299	1.046620
35	6	C	-4.073300	-11.202816	0.670835
36	1	H	-5.642971	-10.935440	-2.338504
37	1	H	-6.463019	-13.169621	-1.661314
38	1	H	-5.756104	-14.152182	0.506683
39	1	H	-4.224328	-12.884432	1.994422
40	1	H	-3.405775	-10.648003	1.319219
41	8	O	-0.350857	-7.717645	-3.529016
42	1	H	-0.658213	-8.478100	-4.027217
43	1	H	-0.986959	-7.527480	-2.557881

A20

Table A20. Cartesian coordinates for **8b**. The structure was optimized at the RB3LYP-GD3/6-311++G(d,p)/THF level of theory at 298.15 K. Coordinate values are given in Å.

Centre number	Atomic number	Atom type	Coordinates		
			X	Y	Z
1	7	N	-3.068024	-5.524598	0.452974
2	6	C	-3.671659	-5.790132	-0.652735
3	6	C	-3.095044	-6.831066	-1.632246
4	7	N	-1.640623	-6.743575	-1.580792
5	6	C	-1.078387	-6.705423	-0.325692
6	6	C	0.220286	-7.168885	-0.057220
7	6	C	0.742868	-7.072811	1.227999
8	6	C	-0.005310	-6.506585	2.269341
9	6	C	-1.279810	-6.017153	2.004810
10	6	C	-1.828516	-6.109014	0.719746
11	1	H	-3.397920	-6.581536	-2.651059
12	1	H	0.791602	-7.616261	-0.862907
13	1	H	1.740919	-7.449746	1.424712
14	1	H	0.409090	-6.441226	3.268421
15	1	H	-1.873576	-5.549398	2.782654
16	6	C	-4.952468	-5.124715	-0.972744
17	6	C	-5.344605	-3.975800	-0.262576
18	6	C	-6.549139	-3.343155	-0.543228
19	6	C	-7.394297	-3.845119	-1.536956
20	6	C	-7.020752	-4.985632	-2.245149
21	6	C	-5.809457	-5.618276	-1.969724
22	1	H	-4.687523	-3.589410	0.505988
23	1	H	-6.831228	-2.454335	0.010127
24	1	H	-8.334144	-3.350731	-1.755083
25	1	H	-7.672631	-5.387786	-3.012361
26	1	H	-5.552216	-6.513275	-2.522502
27	3	Li	0.397293	-6.707008	-4.519836
28	6	C	-3.617536	-8.171409	-1.303512
29	6	C	-4.010129	-9.272856	-0.999154
30	6	C	-4.468943	-10.570178	-0.623158
31	6	C	-5.260032	-11.335831	-1.498583
32	6	C	-5.702282	-12.600314	-1.121359
33	6	C	-5.363290	-13.121090	0.128566
34	6	C	-4.577898	-12.368410	1.003380
35	6	C	-4.132985	-11.102534	0.634972
36	1	H	-5.521506	-10.931843	-2.469416
37	1	H	-6.311845	-13.180788	-1.804565
38	1	H	-5.708863	-14.106651	0.418806
39	1	H	-4.311859	-12.767999	1.975378
40	1	H	-3.523990	-10.516553	1.312897
41	8	O	-0.286433	-8.017609	-3.570594
42	1	H	-0.339488	-8.973836	-3.541496
43	1	H	-1.135280	-7.292417	-2.320337

A21

Table A21. Cartesian coordinates for **7e**. The structure was optimized at the RB3LYP-GD3/6-311++G(d,p)/THF level of theory at 298.15 K. Coordinate values are given in Å.

Centre number	Atomic number	Atom type	Coordinates		
			X	Y	Z
1	7	N	-2.827494	-3.297539	-0.329438
2	6	C	-3.698411	-3.855217	0.546387
3	6	C	-3.203095	-4.823379	1.528126
4	7	N	-2.026157	-5.347885	1.478892
5	6	C	-1.201729	-4.950278	0.434644
6	6	C	0.054892	-5.557903	0.284301
7	6	C	0.920622	-5.151340	-0.717857
8	6	C	0.542799	-4.102652	-1.575964
9	6	C	-0.688419	-3.485544	-1.441018
10	6	C	-1.604069	-3.907128	-0.448774
11	1	H	-3.873228	-5.119900	2.330205
12	1	H	0.324208	-6.349438	0.974787
13	1	H	1.886490	-5.628465	-0.834065
14	1	H	1.224374	-3.771516	-2.351875
15	1	H	-0.965440	-2.671467	-2.103195
16	6	C	-4.896589	-5.511925	-0.505234
17	6	C	-4.083773	-6.371844	-1.258452
18	6	C	-4.340219	-7.744606	-1.323325
19	6	C	-5.418148	-8.284206	-0.615710
20	6	C	-6.235356	-7.445906	0.147204
21	6	C	-5.965046	-6.074748	0.203485
22	1	H	-3.234880	-5.967816	-1.806226
23	1	H	-3.702872	-8.394443	-1.916500
24	1	H	-5.616469	-9.350171	-0.654867
25	1	H	-7.074678	-7.862842	0.697001
26	1	H	-6.599975	-5.434474	0.814173
27	3	Li	-3.761251	-2.182751	-1.750767
28	6	C	-4.853200	-3.096109	0.921838
29	6	C	-5.824976	-2.467444	1.271983
30	6	C	-6.982744	-1.731604	1.650511
31	6	C	-7.664343	-2.032147	2.844682
32	6	C	-8.798614	-1.312115	3.205584
33	6	C	-9.271584	-0.284125	2.387810
34	6	C	-8.601954	0.020788	1.201485
35	6	C	-7.467161	-0.694021	0.831827
36	1	H	-7.297263	-2.829841	3.479365
37	1	H	-9.314904	-1.553361	4.127752
38	1	H	-10.155566	0.274669	2.672591
39	1	H	-8.965672	0.816833	0.561719
40	1	H	-6.950129	-0.459827	-0.091043
41	8	O	-5.263641	-3.278969	-2.134881
42	1	H	-5.189517	-4.067714	-1.489849
43	1	H	-5.614226	-3.640056	-2.954535

A22

Table A22. Cartesian coordinates for **8e**. The structure was optimized at the RB3LYP-GD3/6-311++G(d,p)/THF level of theory at 298.15 K. Coordinate values are given in Å.

Centre number	Atomic number	Atom type	Coordinates		
			X	Y	Z
1	7	N	-2.941655	-4.142266	0.652447
2	6	C	-3.857871	-4.766341	1.387004
3	6	C	-3.675737	-6.124264	1.803735
4	7	N	-2.623605	-6.825811	1.476055
5	6	C	-1.683129	-6.215143	0.697297
6	6	C	-0.542695	-6.940407	0.281366
7	6	C	0.405936	-6.336239	-0.510920
8	6	C	0.253215	-4.986379	-0.911786
9	6	C	-0.844068	-4.256340	-0.520450
10	6	C	-1.839549	-4.855076	0.289053
11	1	H	-4.439536	-6.596777	2.413100
12	1	H	-0.446109	-7.971207	0.600517
13	1	H	1.278026	-6.892566	-0.833332
14	1	H	1.010176	-4.527765	-1.537045
15	1	H	-0.971412	-3.227118	-0.833188
16	6	C	-5.258434	-3.999146	-2.139965
17	6	C	-4.026505	-4.419754	-2.643017
18	6	C	-3.587303	-5.724273	-2.415416
19	6	C	-4.380377	-6.607909	-1.683274
20	6	C	-5.614599	-6.188359	-1.183251
21	6	C	-6.053704	-4.884290	-1.411515
22	1	H	-3.404776	-3.728023	-3.200616
23	1	H	-2.622332	-6.045670	-2.790781
24	1	H	-4.032875	-7.617045	-1.492727
25	1	H	-6.226133	-6.873405	-0.606443
26	1	H	-7.003011	-4.552215	-1.007505
27	3	Li	-3.449957	-2.123527	0.117835
28	6	C	-5.033391	-4.052199	1.723795
29	6	C	-6.019706	-3.373254	1.900585
30	6	C	-7.144015	-2.516922	2.028819
31	6	C	-8.283019	-2.909108	2.755522
32	6	C	-9.373939	-2.052028	2.848222
33	6	C	-9.340982	-0.804251	2.221331
34	6	C	-8.210988	-0.411985	1.500030
35	6	C	-7.110516	-1.256639	1.397745
36	1	H	-8.302526	-3.878733	3.238659
37	1	H	-10.250462	-2.355902	3.408639
38	1	H	-10.194278	-0.139714	2.295843
39	1	H	-8.187601	0.557281	1.014929
40	1	H	-6.221881	-0.963181	0.841050
41	8	O	-4.133617	-0.580662	-0.188365
42	1	H	-5.591490	-2.980400	-2.303497
43	1	H	-4.289380	0.328257	-0.438824

A23

Table A23. Cartesian coordinates for **9b**. The structure was optimized at the RB3LYP-GD3/6-311++G(d,p)/THF level of theory at 298.15 K. Coordinate values are given in Å.

Centre number	Atomic number	Atom type	Coordinates		
			X	Y	Z
1	7	N	-2.371958	-5.417857	-0.196981
2	6	C	-3.162926	-6.457673	-0.361765
3	6	C	-2.702747	-7.787636	-0.001915
4	7	N	-1.479699	-7.998797	0.457625
5	6	C	-0.663947	-6.926112	0.615241
6	6	C	0.657816	-7.108606	1.091835
7	6	C	1.482976	-6.020381	1.256851
8	6	C	1.022319	-4.713668	0.960586
9	6	C	-0.257525	-4.509228	0.494532
10	6	C	-1.121340	-5.613033	0.307679
11	1	H	-2.168168	-4.582121	-1.978896
12	1	H	0.990009	-8.115154	1.316201
13	1	H	2.494434	-6.158200	1.620409
14	1	H	1.686074	-3.869358	1.106107
15	1	H	-0.627178	-3.516934	0.263004
16	6	C	-4.529578	-6.197456	-0.875991
17	6	C	-5.262619	-5.131827	-0.336914
18	6	C	-6.548436	-4.855707	-0.795546
19	6	C	-7.109312	-5.631809	-1.809757
20	6	C	-6.376637	-6.682270	-2.364866
21	6	C	-5.096509	-6.967130	-1.899735
22	1	H	-4.821964	-4.530401	0.449153
23	1	H	-7.110601	-4.036611	-0.361730
24	1	H	-8.108852	-5.416182	-2.170139
25	1	H	-6.799291	-7.275693	-3.167544
26	1	H	-4.527103	-7.768417	-2.350251
27	3	Li	0.269700	-5.258466	-2.808884
28	6	C	-3.575181	-8.904290	-0.099459
29	6	C	-4.353646	-9.825858	-0.189231
30	6	C	-5.313043	-10.862694	-0.334691
31	6	C	-6.612530	-10.549851	-0.778891
32	6	C	-7.557725	-11.557794	-0.932320
33	6	C	-7.224312	-12.883641	-0.647225
34	6	C	-5.937963	-13.200831	-0.206303
35	6	C	-4.984540	-12.200683	-0.048993
36	1	H	-6.863432	-9.518988	-0.999162
37	1	H	-8.555833	-11.310215	-1.274790
38	1	H	-7.963944	-13.666657	-0.768292
39	1	H	-5.678043	-14.229534	0.014803
40	1	H	-3.985053	-12.442455	0.291750
41	8	O	-0.187897	-7.007317	-2.813236
42	1	H	-1.519482	-6.502314	-3.158529
43	1	H	-0.187327	-7.702666	-2.153289
44	8	O	-1.787566	-4.610380	-2.881185
45	8	O	-2.326758	-5.868911	-3.394258

Table A24. Cartesian coordinates for **9b′**. The structure was optimized at the RB3LYP-GD3/6-311++G(d,p)/THF level of theory at 298.15 K. Coordinate values are given in Å.

Centre number	Atomic number	Atom type	Coordinates		
			X	Y	Z
1	7	N	-2.844280	-4.886621	-0.127169
2	6	C	-3.609764	-5.935355	-0.330433
3	6	C	-3.025622	-7.254181	-0.479942
4	7	N	-1.709124	-7.431137	-0.481221
5	6	C	-0.911923	-6.338458	-0.315849
6	6	C	0.498547	-6.477317	-0.338629
7	6	C	1.289042	-5.366004	-0.153369
8	6	C	0.713857	-4.090039	0.065839
9	6	C	-0.652897	-3.932061	0.087797
10	6	C	-1.494214	-5.052035	-0.110756
11	1	H	-0.126738	-6.837419	-3.037036
12	1	H	0.925414	-7.460899	-0.511296
13	1	H	2.367882	-5.466061	-0.174827
14	1	H	1.359909	-3.232387	0.212024
15	1	H	-1.113592	-2.964149	0.244797
16	6	C	-5.078375	-5.716102	-0.368435
17	6	C	-5.675657	-4.910468	0.610030
18	6	C	-7.048211	-4.677328	0.589383
19	6	C	-7.837507	-5.231375	-0.419198
20	6	C	-7.246649	-6.018493	-1.408064
21	6	C	-5.876208	-6.264875	-1.381117
22	1	H	-5.058425	-4.476549	1.387478
23	1	H	-7.501153	-4.062712	1.358891
24	1	H	-8.905528	-5.046466	-0.437612
25	1	H	-7.851289	-6.438305	-2.203809
26	1	H	-5.426091	-6.870974	-2.157111
27	3	Li	-0.835068	-9.347343	-0.918768
28	6	C	-3.850571	-8.403456	-0.585257
29	6	C	-4.580579	-9.365302	-0.667310
30	6	C	-5.503435	-10.438076	-0.779630
31	6	C	-6.884838	-10.162704	-0.791685
32	6	C	-7.800033	-11.202357	-0.908105
33	6	C	-7.355125	-12.521998	-1.012289
34	6	C	-5.987181	-12.801774	-1.000514
35	6	C	-5.062290	-11.769886	-0.885265
36	1	H	-7.221934	-9.136142	-0.710547
37	1	H	-8.861668	-10.984599	-0.917250
38	1	H	-8.072035	-13.329848	-1.102387
39	1	H	-5.641502	-13.825654	-1.081672
40	1	H	-4.000264	-11.983494	-0.877208
41	8	O	0.883868	-9.604319	-1.333405
42	1	H	1.524008	-10.309373	-1.223571
43	1	H	1.093099	-8.838512	-2.581291
44	8	O	-0.246766	-7.715229	-3.426211
45	8	O	1.117621	-8.229917	-3.429524

A25

Table A25. Energetic information for the reactants (**1** and **2**). The structures were optimized at the RB3LYP-GD3/6-311++G(d,p)/THF level of theory at 195.15 K and 1 atm. Energy values are given in Hartree (a.u.) units.

	REACTANTS	
	1	**2**
Electronic Energy (EE)	-649.2102	-315.4706
Zero-point Energy Correction	0.2036	0.0995
Thermal Correction to Energy	0.2087	0.1032
Thermal Correction to Enthalpy	0.2093	0.1039
Thermal Correction to Free Energy	0.1814	0.0806
EE + Zero-point Energy	-649.0067	-315.3710
EE + Thermal Energy Correction	-649.0016	-315.3673
EE + Thermal Enthalpy Correction	-649.0010	-315.3667
EE + Thermal Free Energy Correction	-649.0288	-315.3900

Table A26. Energetic information for all the stationary points involved in the nucleophilic addition step along RP-C2. The structures were optimized at the RB3LYP-GD3/6-311++G(d,p)/THF level of theory at 195.15 K and 1 atm. Energy values are given in Hartree (a.u.) units.

	RP-C2		
	3a	**4a**	**5a**
Electronic Energy (EE)	-964.6927	-964.6518	-964.6811
Zero-point Energy Correction	0.3054	0.3031	0.3050
Thermal Correction to Energy	0.3149	0.3122	0.3141
Thermal Correction to Enthalpy	0.3155	0.3129	0.3147
Thermal Correction to Free Energy	0.2768	0.2744	0.2767
EE + Zero-point Energy	-964.3873	-964.3488	-964.3760
EE + Thermal Energy Correction	-964.3778	-964.3396	-964.3670
EE + Thermal Enthalpy Correction	-964.3772	-964.3390	-964.3663
EE + Thermal Free Energy Correction	-964.4159	-964.3775	-964.4044

Table A27. Energetic information for all the stationary points involved in the nucleophilic addition step along RP-C3. The structures were optimized at the RB3LYP-GD3/6-311++G(d,p)/THF level of theory at 195.15 K and 1 atm. Energy values are given in Hartree (a.u.) units.

	RP-C3		
	3b	**4b**	**5b**
Electronic Energy (EE)	-964.6974	-964.6620	-964.6911
Zero-point Energy Correction	0.3045	0.3040	0.3056
Thermal Correction to Energy	0.3145	0.3130	0.3148
Thermal Correction to Enthalpy	0.3151	0.3137	0.3154
Thermal Correction to Free Energy	0.2745	0.2754	0.2769
EE + Zero-point Energy	-964.3929	-964.3580	-964.3855
EE + Thermal Energy Correction	-964.3829	-964.3489	-964.3763
EE + Thermal Enthalpy Correction	-964.3823	-964.3483	-964.3757
EE + Thermal Free Energy Correction	-964.4229	-964.3865	-964.4142

Table A28. Energetic information for all the stationary points involved in the nucleophilic addition step along RP-C5. The structures were optimized at the RB3LYP-GD3/6-311++G(d,p)/THF level of theory at 195.15 K and 1 atm. Energy values are given in Hartree (a.u.) units.

	RP-C5		
	3c	**4c**	**5c**
Electronic Energy (EE)	-964.6943	-964.6337	-964.6585
Zero-point Energy Correction	0.3047	0.3027	0.3046
Thermal Correction to Energy	0.3145	0.3117	0.3137
Thermal Correction to Enthalpy	0.3151	0.3123	0.3144
Thermal Correction to Free Energy	0.2742	0.2742	0.2758
EE + Zero-point Energy	-964.3896	-964.3310	-964.3539
EE + Thermal Energy Correction	-964.3798	-964.3220	-964.3448
EE + Thermal Enthalpy Correction	-964.3792	-964.3214	-964.3441
EE + Thermal Free Energy Correction	-964.4201	-964.3595	-964.3827

Table A29. Energetic information for all the stationary points involved in the nucleophilic addition step along RP-C10. The structures were optimized at the RB3LYP-GD3/6-311++G(d,p)/THF level of theory at 195.15 K and 1 atm. Energy values are given in Hartree (a.u.) units.

	RP-C10		
	3d	**4d**	**5d**
Electronic Energy (EE)	-964.6939	-964.6331	-964.6531
Zero-point Energy Correction	0.3048	0.3025	0.3047
Thermal Correction to Energy	0.3146	0.3116	0.3138
Thermal Correction to Enthalpy	0.3152	0.3123	0.3144
Thermal Correction to Free Energy	0.2745	0.2741	0.2763
EE + Zero-point Energy	-964.3891	-964.3307	-964.3484
EE + Thermal Energy Correction	-964.3794	-964.3215	-964.3394
EE + Thermal Enthalpy Correction	-964.3788	-964.3209	-964.3387
EE + Thermal Free Energy Correction	-964.4194	-964.3590	-964.3769

Table A30. Energetic information for H_2O and O_2. This structure was optimized at the RB3LYP-GD3/6-311++G(d,p)/THF level of theory at 298.15 K and 1 atm. Energy values are given in Hartree (a.u.) units.

	REACTANT	
	H_2O	**O_2**
Electronic Energy (EE)	-76.4650	-150.3098
Zero-point Energy Correction	0.0212	0.0037
Thermal Correction to Energy	0.0241	0.0061
Thermal Correction to Enthalpy	0.0250	0.0070
Thermal Correction to Free Energy	0.0029	-0.0152
EE + Zero-point Energy	-76.4438	-150.3061
EE + Thermal Energy Correction	-76.4410	-150.3037
EE + Thermal Enthalpy Correction	-76.4400	-150.3028
EE + Thermal Free Energy Correction	-76.4621	-150.3250

Table A31. Energetic information for all the stationary points involved in the hydrolysis step along RP-C2. The structures were optimized at the RB3LYP-GD3/6-311++G(d,p)/THF level of theory at 298.15 K and 1 atm. Energy values are given in Hartree (a.u.) units.

	RP-C2		
	6a	**7a**	**8a**
Electronic Energy (EE)	-1041.1635	-1041.1582	-1041.1704
Zero-point Energy Correction	0.3289	0.3254	0.3296
Thermal Correction to Energy	0.3520	0.4744	0.3524
Thermal Correction to Enthalpy	0.3530	0.3484	0.3534
Thermal Correction to Free Energy	0.2738	0.2718	0.2751
EE + Zero-point Energy	-1040.8346	-1040.8328	-1040.8408
EE + Thermal Energy Correction	-1040.8115	-1040.8108	-1040.8180
EE + Thermal Enthalpy Correction	-1040.8106	-1040.8098	-1040.8171
EE + Thermal Free Energy Correction	-1040.8897	-1040.8864	-1040.8953

Table A32. Energetic information for all the stationary points involved in the hydrolysis step along RP-C3. These structures were optimized at the RB3LYP-GD3/6-311++G(d,p)/THF level of theory at 298.15 K and 1 atm. Energy values are given in Hartree (a.u.) units.

	RP-C3		
	6b	**7b**	**8b**
Electronic Energy (EE)	-1041.1732	-1041.1685	-1041.1795
Zero-point Energy Correction	0.3297	0.3258	0.3302
Thermal Correction to Energy	0.3529	0.3482	0.3533
Thermal Correction to Enthalpy	0.3538	0.3491	0.3542
Thermal Correction to Free Energy	0.2745	0.2712	0.2741
EE + Zero-point Energy	-1040.8435	-1040.8426	-1040.8493
EE + Thermal Energy Correction	-1040.8203	-1040.8203	-1040.8263
EE + Thermal Enthalpy Correction	-1040.8194	-1040.8193	-1040.8253
EE + Thermal Free Energy Correction	-1040.8987	-1040.8973	-1040.9054

Table A33. Energetic information for all the stationary points involved in the hydrolysis step along RP-C2. The structures were optimized at the RB3LYP-GD3/6-311++G(d,p)/THF level of theory at 298.15 K and 1 atm. Energy values are given in Hartree (a.u.) units.

	RP-C2		
	6a	**7e**	**8e**
Electronic Energy (EE)	-1041.1635	-1041.1219	-1041.1875
Zero-point Energy Correction	0.3289	0.3267	0.3282
Thermal Correction to Energy	0.3520	0.3492	0.3524
Thermal Correction to Enthalpy	0.3530	0.3502	0.3534
Thermal Correction to Free Energy	0.2738	0.2723	0.2702
EE + Zero-point Energy	-1040.8346	-1040.7952	-1040.8593
EE + Thermal Energy Correction	-1040.8115	-1040.7727	-1040.8351
EE + Thermal Enthalpy Correction	-1040.8106	-1040.7717	-1040.8342
EE + Thermal Free Energy Correction	-1040.8897	-1040.8496	-1040.9173

Table A34. Energetic information for the ONSH products **9b** and **9b′** obtained along RP-C3 and RP-C3′, respectively. The structures were optimized at the RB3LYP-GD3/6-311++G(d,p)/THF level of theory at 298.15 K and 1 atm. Energy values are given in Hartree (a.u.) units.

	RP-C3	RP-C3′
	9b	**9b′**
Electronic Energy (EE)	-1191.6175	-1191.6188
Zero-point Energy Correction	0.3355	0.3357
Thermal Correction to Energy	0.3614	0.3619
Thermal Correction to Enthalpy	0.3623	0.3628
Thermal Correction to Free Energy	0.2759	0.275
EE + Zero-point Energy	-1191.2755	-1191.2831
EE + Thermal Energy Correction	-1191.2496	-1191.2569
EE + Thermal Enthalpy Correction	-1191.2487	-1191.2560
EE + Thermal Free Energy Correction	-1191.3351	-1191.3430

A29

Part 2 – Selected geometric data

Table A35. Computed dihedral angles (DA) in °, angles in ° and bond lengths in Å for energy optimised 2-phenylquinoxaline (**1**).

Energy optimized 2-phenylquinoxaline (**1**)					

Dihedral angle (º)		Angle (º)		Distance (Å)	
C6,C5,C10,C9	0.10	N1,C2,C3	120.47	C3–H11	1.09
C6,C7,C8,C9	0.11	N1,C2,C16	118.56	C2–C16	1.48
N1,C2,C3,N4	1.19	C3,C2,C16	120.96	N1–C2	1.32
N4,C5,C10,N1	1.06	C2,C3,N4	123.12	C2–C3	1.43
N1,C2,C16,C17	28.37	N4,C3,C2	116.90	C3–N4	1.31
		H11,C3,C2	119.96	N4–C5	1.37
		N4,C5,C10	120.37	C5–C6	1.42
		N4,C5,C6	120.00	C5–C10	1.43
		C6,C5,C10	119.63	N1–C10	1.36
		C5,C10,N1	121.05	C10C9	1.42
		C5,C10,C9	119.22		
		C9,C10,N1	119.73		

Table A36. Computed dihedral angles (DA) in °, angles in ° and bond lengths in Å for energy optimised lithium phenylacetylide (**2**).
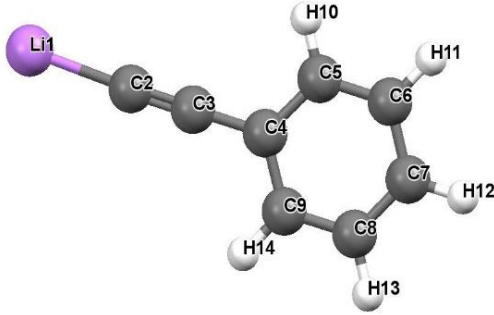
Energy optimised lithium phenylacetylide (**2**)					

Dihedral angle (º)		Angle (º)		Distance (Å)	
		Li1,C2,C3	177.94	Li1–C2	2.04

A30

Table A37. Computed dihedral angles (DA) in °, angles in ° and bond lengths in Å for the energy optimised adduct **3a**, transition state **4a** and intermediate **5a** along RP-C2.

		RP-C2		
		3a	**4a**	**5a**
Dihedral angle (º)	C6,C5,C10,C9	0.92	1.37	3.79
	C6,C7,C8,C9	0.49	0.80	1.95
	N1,C2,C3,N4	–0.10	18.44	32.70
	N4,C5,C10,N1	1.61	3.68	8.72
	N1,C2,C16,C17	37.69	15.86	63.34
	N1,Li27,C28,C2		–17.21	
Angle (º)	Li27,C28,C29	137.54		
	N1,C2,C3	120.51	116.16	110.32
	N1,C2,C16	119.55	114.67	109.04
	C3,C2,C16	119.93	113.72	109.13
Distance (Å)	N1–C2	1.32	1.38	1.48
	C2–C3	1.43	1.49	1.54
	C2–C16	1.48	1.52	1.54
	Li27–C28	2.04	2.20	
	Li27–N1	2.23	2.01	1.95
	C28–C2	3.59	1.89	1.48

Energy optimized structures
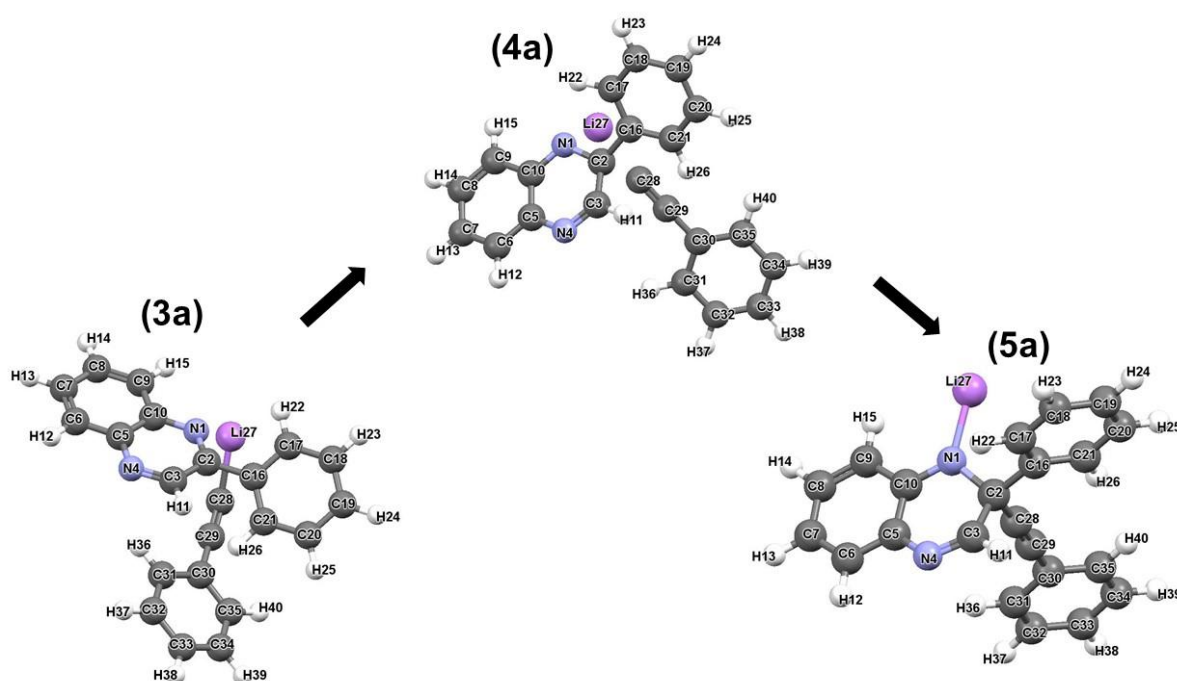
Table A38. Computed dihedral angles (DA) in °, angles in ° and bond lengths in Å for the energy optimised adduct **3b**, transition state **4b** and intermediate **5b** along RP-C3.

		RP-C3		
		3b	**4b**	**5b**
Dihedral angle (º)	C6,C5,C10,C9	0.34	–1.59	–4.84
	C6,C7,C8,C9	0.18	–0.89	–2.21
	N1,C2,C3,N4	1.76	–20.31	–38.56
	N4,C5,C10,N1	1.32	–3.91	–10.42
	N1,C2,C16,C17	23.08	–5.53	18.25
	N4,Li27,C28,C3		10.53	
Angle (º)	Li27,C28,C29	155.49		
	C2,C3,N4	123.06	117.97	110.81
	C2,C3,H11	120.91	114.71	
	N4,C3,H11	116.03	112.25	
Distance (Å)	N4–C3	1.31	1.38	1.47
	C2–C3	1.43	1.50	1.54
	C3–H11	1.08	1.08	1.09
	Li27–C28	2.06	2.16	
	Li27–N4	2.15	2.02	1.94
	C28–C3	3.31	1.86	1.48

Energy optimized structures
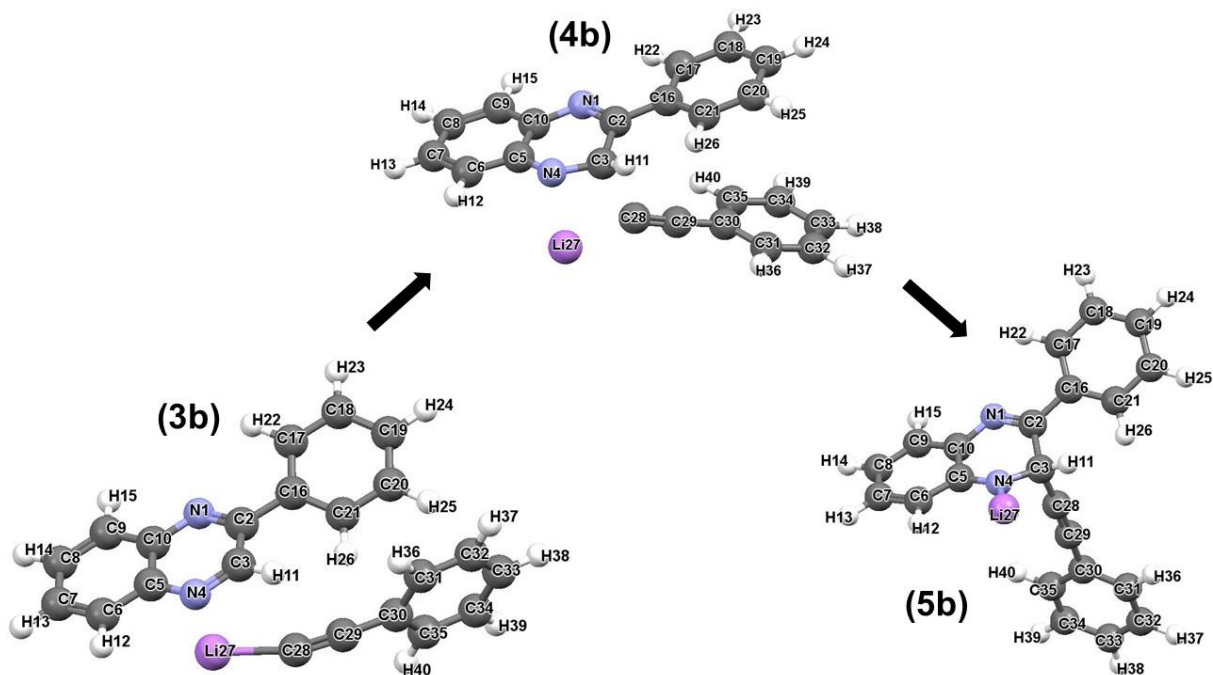
Table A39. Computed dihedral angles (DA) in °, angles in ° and bond lengths in Å for the energy optimised adduct **3c**, transition state **4c** and intermediate **5c** along RP-C5.

		RP-C5		
		3c	**4c**	**5c**
Dihedral angle (º)	C6,C5,C10,C9	0.20	20.60	18.35
	C6,C7,C8,C9	0.13	7.06	6.08
	N1,C2,C3,N4	1.20	−14.34	−18.97
	N4,C5,C10,N1	1.09	−31.80	−42.50
	N1,C2,C16,C17	28.72	−16.95	−11.82
	N4,Li27,C28,C5		13.04	
Angle (º)	Li27,C28,C29	172.34		
	N4,C5,C10	119.63	114.21	108.73
	N4,C5,C6	120.45	112.19	108.53
	C6,C5,C10	119.92	104.14	111.53
Distance (Å)	N4–C5	1.37	1.43	1.49
	C5–C6	1.42	1.48	1.52
	C5–C10	1.43	1.49	1.54
	Li27–C28	2.04	2.21	
	Li27–N4	2.11	2.08	1.98
	C28–C5	4.19	1.79	1.49

Energy optimized structures

A33
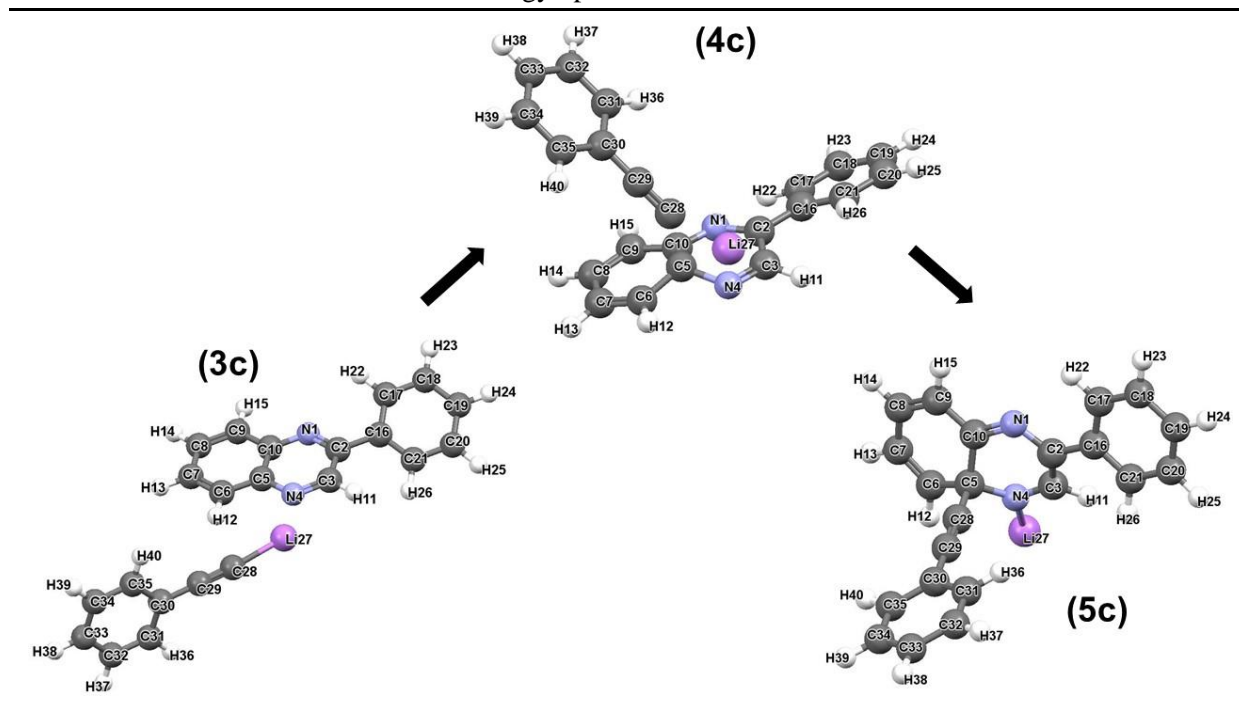
Table A40. Computed dihedral angles (DA) in °, angles in ° and bond lengths in Å for the energy optimised adduct **3d**, transition state **4d** and intermediate **5d** along RP-C10.

		RP-C10		
		3d	**4d**	**5d**
Dihedral angle (º)	C6,C5,C10,C9	0.29	21.55	19.34
	C6,C7,C8,C9	0.20	7.43	6.46
	N1,C2,C3,N4	−0.51	-11.69	−18.08
	N4,C5,C10,N1	0.55	−30.36	−40.70
	N1,C2,C16,C17	44.21	29.94	47.14
	N1,Li27,C28,C10	15.20		
Angle (º)	Li27,C28,C29	175.62		
	N1,C10,C5	120.50	114.90	110.17
	N1,C10,C9	120.14	111.85	108.08
	C9,C10,C5	119.36	113.87	111.05
Distance (Å)	N1–C10	1.37	1.43	1.49
	C5–C10	1.43	1.49	1.54
	C9–C10	1.42	1.48	1.52
	Li27–C28	2.04	2.23	
	Li27–N1	2.15	2.04	1.98
	C28–C10	4.21	1.78	1.49

Energy optimized structures
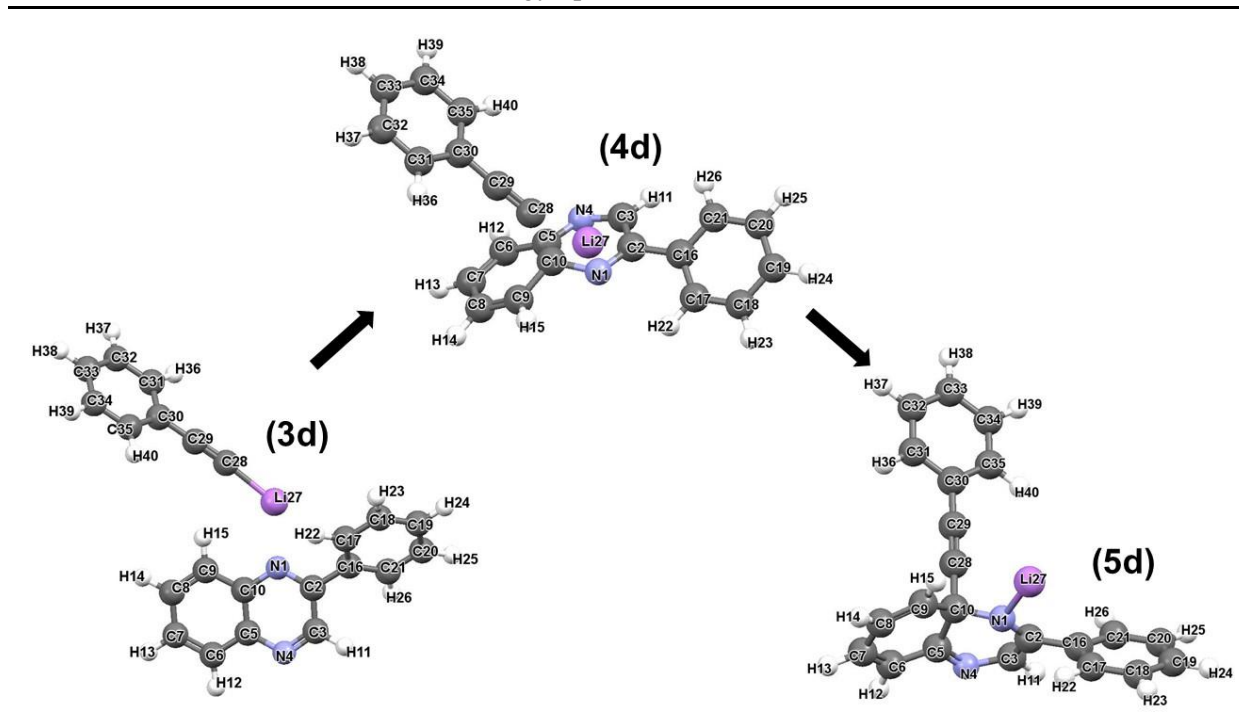
Table A41. Computed dihedral angles in °, angles in ° and bond lengths in Å for the energy optimised stationary points **6a**, **7a** and **8a** along RP-C2.

		RP-C2		
		6a	**7a**	**8a**
Dihedral angle (°)	C6,C5,C10,C9	3.68	2.10	1.08
	C6,C7,C8,C9	1.89	1.24	0.89
	N1,C2,C3,N4	32.04	30.95	28.63
	N4,C5,C10,N1	8.75	4.68	1.59
	N1,C2,C16,C17	51.67	75.79	50.84
	N1,Li27,O41,H42	-4.64		
Angle (°)	N1,Li27,O41	104.01		
	N1,C2,C3	110.52	109.44	107.53
	N1,C2,C16	109.83	108.10	109.29
	C3,C2,C16	108.63	110.60	109.14
Distance (Å)	N1–C2	1.47	1.47	1.46
	C2–C3	1.54	1.54	1.54
	C2–C16	1.53	1.53	1.54
	Li27–O41	1.96	1.89	1.76
	Li27–N1	1.96	2.41	3.61
	O41–H42	0.97	1.16	1.66
	N1–H42	2.89	1.34	1.05

Energy optimized structures
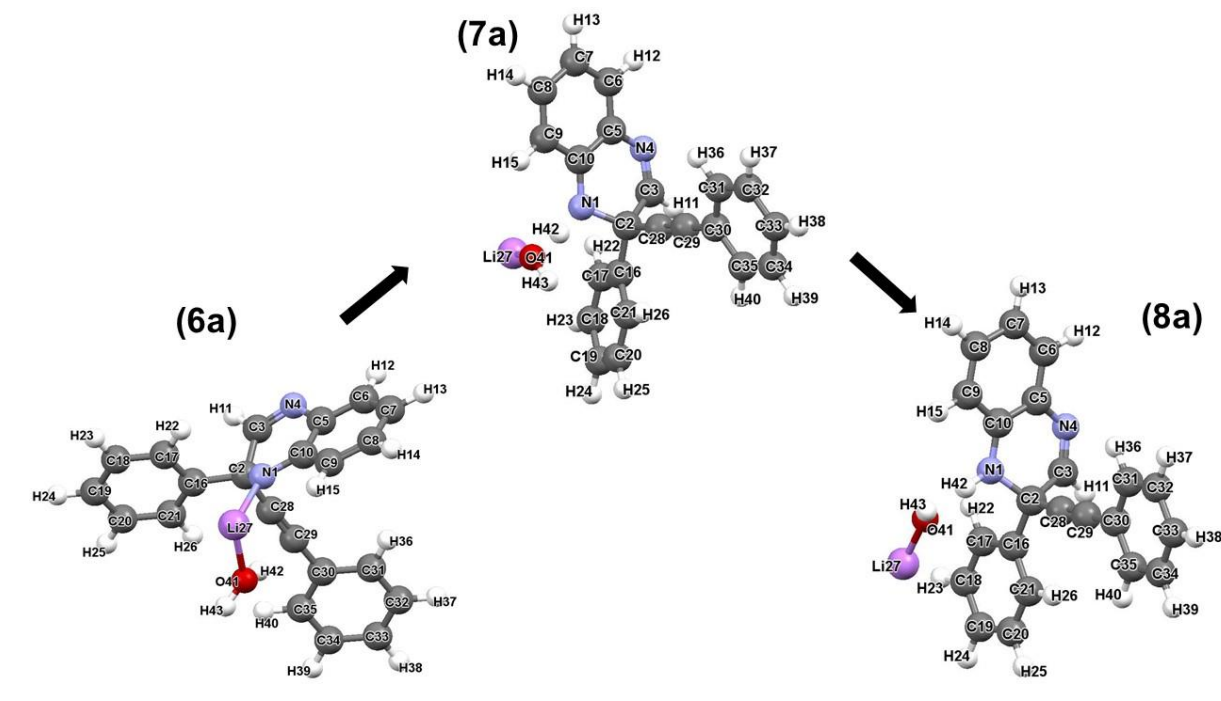
Table A42. Computed dihedral angles (DA) in º, angles in º and bond lengths in Å for the energy optimised stationary points **6b**, **7b** and **8b** along RP-C3.

		RP-C3		
		6b	**7b**	**8b**
Dihedral angle (º)	C6,C5,C10,C9	-4.32	-2.96	-1.40
	C6,C7,C8,C9	-1.95	-1.54	-0.97
	N1,C2,C3,N4	-36.18	-37.59	-35.18
	N4,C5,C10,N1	-9.53	-6.37	-3.10
	N1,C2,C16,C17	16.70	17.08	16.09
	N4,Li27,O41,H43	-1.08		
Angle (º)	N4,Li27,O41	104.57		
	N4,C3,C2	111.73	109.49	108.08
	N4,C3,H11	107.82	107.39	107.21
	C2,C3,H11	108.68	109.32	109.56
Distance (Å)	N4–C3	1.47	1.46	1.46
	C2–C3	1.54	1.54	1.54
	C3–H11	1.10	1.09	1.09
	Li27–O41	1.95	1.90	1.76
	Li27–N4	1.94	2.25	3.58
	O41–H43	0.97	1.17	1.68
	N4–H43	2.96	1.32	1.05

Energy optimized structures
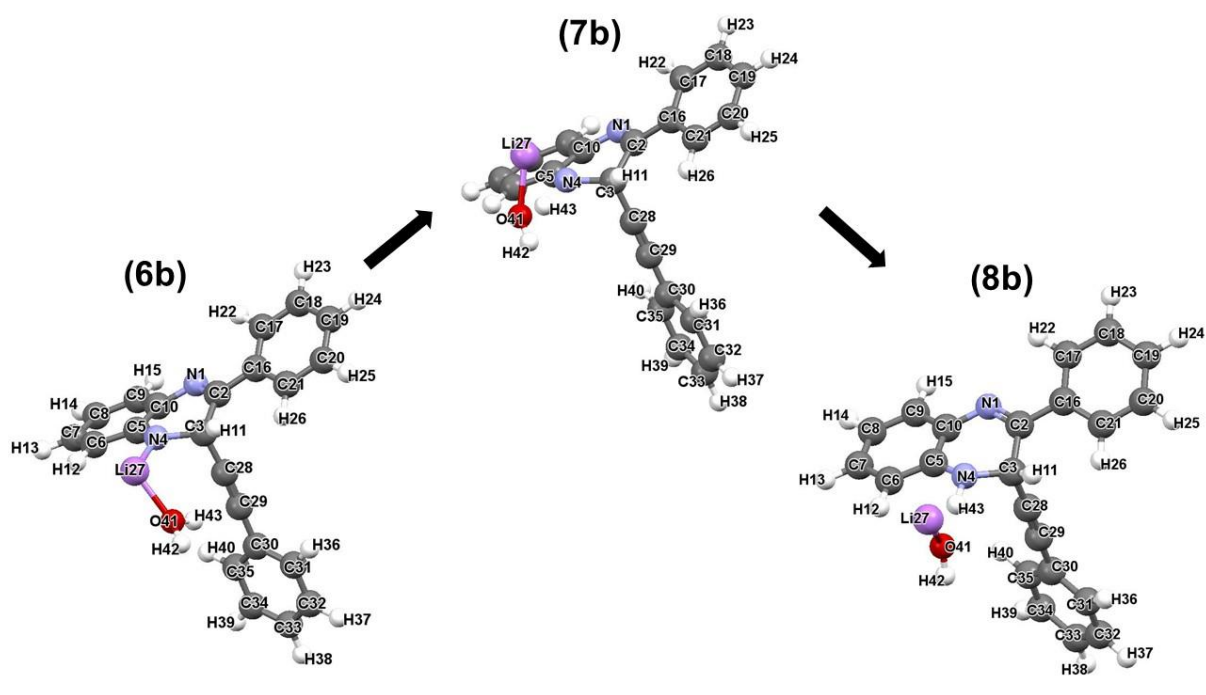
Table A43. Computed dihedral angles (DA) in °, angles in ° and bond lengths in Å for the energy optimised stationary points **6a**, **7e** and **8e** along RP-C2.

		RP-C2		
		6a	**7e**	**8e**
Dihedral angle (º)	C6,C5,C10,C9	3.68	-1.87	-0.31
	C6,C7,C8,C9	1.89	-0.82	-0.13
	N1,C2,C3,N4	32.04	-11.68	-0.98
	N4,C5,C10,N1	8.75	-2.33	-0.96
	N1,C2,C16,C17	51.67		
	N1,Li27,O41,H42	-4.64		
Angle (º)	N1,Li27,O41	104.01	100.85	
	N1,C2,C3	110.52	119.19	121.20
	N1,C2,C16	109.83		
	C3,C2,C16	108.63		
Distance (Å)	N1–C2	1.47	1.36	1.33
	C2–C3	1.54	1.47	1.43
	C2–C16	1.54	2.30	3.87
	Li27–O41	1.96	1.90	1.72
	Li27–N1	1.98	2.03	2.15
	O41–H42	0.97	1.02	3.52
	C16–H42	3.29	1.77	1.08

Energy optimized structures
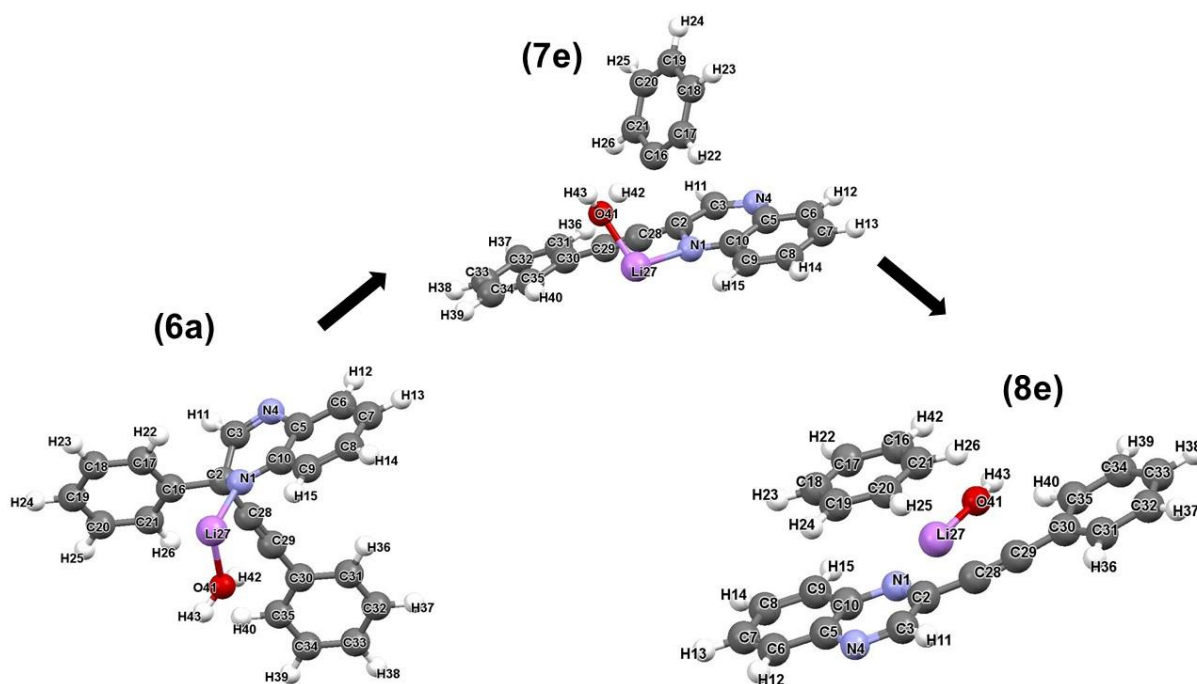
Table A44. Computed dihedral angles (DA) in °, angles in ° and bond lengths in Å for the energy optimised ONSH products **9b** and **9b′** along RP-C3 and RP C3′.

		RP-C3	RP-C3′
		9b	**9b′**
Dihedral angle (º)	C6,C5,C10,C9	-0.65	-0.96
	C6,C7,C8,C9	-0.37	-0.52
	N1,C2,C3,N4	-2.05	-3.30
	N4,C5,C10,N1	-2.41	-2.49
	N1,C2,C16,C17	51.67	-45.31
Angle (º)	N4,C3,C2	121.66	121.36
	N4,C3,C28	117.78	117.93
	C2,C3,C28	120.54	120.67
Distance (Å)	N4–C3	1.32	1.32
	C2–C3	1.45	1.45
	C3–C28	1.48	1.24
	Li27–O41	1.80	1.79
	Li27–N4	4.60	2.15
	O41–H43	0.96	1.48
	O44–H11	0.98	0.97
	Energy optimized structures		
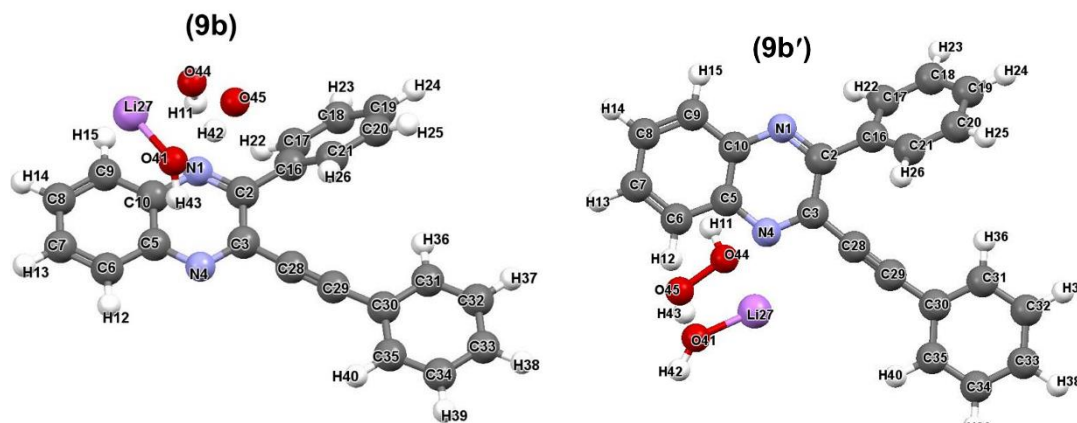
A38

Most attractive and repulsive diatomic interactions in 3, 4 and 5 along four reaction pathways considered

Table A45. Most significant (leading) attractive and repulsive diatomic inter-molecular interactions in adducts **3** formed between **1** and **2** along four potential reaction pathways (RP). All values in kcal/mol.

Atom A	Atom B	RP-C2	Atom A	Atom B	RP-C3	Atom A	Atom B	RP-C5	Atom A	Atom B	RP-C10
					Attractive interactions with $\left|E_{int}(A,B)\right| > \sim 10$ kcal/mol						
N1	Li27	-175.0	N4	Li27	-184.9	N4	Li27	-186.6	N1	Li27	-182.5
N4	Li27	-70.7	N1	Li27	-68.6	N1	Li27	-68.2	N4	Li27	-68.2
C2	C29	-33.9	C3	C29	-32.7	C3	C29	-22.8	C2	C29	-21.5
C3	C29	-28.1	C2	C29	-23.3	C5	C29	-19.3	C10	C29	-19.0
C10	C29	-23.6	C3	C28	-20.8	C3	C28	-18.9	C2	C28	-18.0
C5	C29	-19.6	C5	C29	-19.6	C2	C29	-16.9	C3	C29	-17.6
C2	C28	-16.3	C10	C29	-16.5	C5	C28	-15.4	C10	C28	-15.7
C10	C28	-12.9	C5	C28	-12.8	C10	C29	-14.9	C5	C29	-14.2
C3	C28	-9.7	H11	C29	-11.2	C2	C28	-11.7	C3	C28	-12.4
			C2	C28	-10.6				C5	C28	-9.6
									H15	C28	-9.2
					Repulsive interactions with $\left|E_{int}(A,B)\right| > \sim 10$ kcal/mol						
N4	C28	17.0	H11	Li27	11.1	N1	C28	21.6	N4	C28	21.8
C5	Li27	30.5	N1	C28	19.0	C10	Li27	30.9	C5	Li27	29.9
N1	C28	35.9	C10	Li27	30.3	N1	C29	32.9	N4	C29	32.6
C3	Li27	40.8	C2	Li27	38.1	C2	Li27	37.7	C3	Li27	39.5
N1	C29	49.6	N1	C29	40.9	N4	C28	47.1	N1	C28	47.1
C10	Li27	50.6	N4	C28	43.1	C5	Li27	50.3	C10	Li27	50.6
C2	Li27	63.9	C5	Li27	48.5	N4	C29	55.3	N1	C29	54.1
N1	C27	70.6	N4	C29	65.4	C3	Li27	67.4	C2	Li27	63.0
			C3	Li27	67.8						

Table A46. Most significant (leading) attractive and repulsive diatomic inter-molecular interactions in transition states **4** formed along four potential reaction pathways (RP). All values in kcal/mol.

Atom A	Atom B	RP-C2	Atom A	Atom B	RP-C3	Atom A	Atom B	RP-C5	Atom A	Atom B	RP-C10
Attractive interactions with $|E_{int}(A,B)| > \sim 10$ kcal/mol											
N1	Li27	-201.8	N4	Li27	-199.6	N4	Li27	-189.4	N1	Li27	-195.7
C2	C28	-102.1	C3	C28	-107.1	C5	C28	-115.7	C10	C28	-118.4
N4	Li27	-82.9	N1	Li27	-84.4	N1	Li27	-85.0	N4	Li27	-84.4
C3	C29	-36.7	C2	C29	-33.4	C10	C29	-28.4	C10	C29	-27.4
C2	C29	-30.2	C3	C29	-32.2	C5	C29	-27.0	C5	C29	-27.2
C10	C29	-18.5	C5	C29	-17.7	C3	C29	-21.1	C2	C29	-20.1
C5	C29	-16.0	C10	C29	-16.2	C2	C29	-18.9	C3	C29	-19.3
C3	C28	-14.2	C2	C28	-13.3	C10	C28	-14.0	C5	C28	-13.5
C10	C28	-9.5	C5	C28	-9.8	C3	C28	-13.4	C2	C28	-12.2
Repulsive interactions with $|E_{int}(A,B)| > \sim 10$ kcal/mol											
N1	C28	19.4	N1	C28	11.4	N1	C28	12.3	N4	C28	11.5
C5	Li27	27.7	N4	C28	21.2	N4	C28	21.0	N1	C28	20.0
N1	C29	51.9	C10	Li27	30.3	C2	Li27	35.3	C3	Li27	36.1
C3	Li27	52.8	C2	Li27	50.0	C10	Li27	43.9	C5	Li27	42.2
C10	Li27	53.7	N1	C29	50.7	N4	C29	48.6	N1	C29	48.6
N4	C29	53.9	N4	C29	50.9	N1	C29	49.8	N4	C29	49.6
C2	Li27	65.8	C5	Li27	53.5	C5	Li27	55.4	C10	Li27	57.9
			C3	Li27	66.5	C3	Li27	64.9	C2	Li27	63.0

A40

Table A47. Most significant (leading) attractive and repulsive diatomic intra-molecular interactions in intermediates **5** formed along four potential reaction pathways (RP). All values in kcal/mol.

Atom A	Atom B	RP-C2	Atom A	Atom B	RP-C3	Atom A	Atom B	RP-C5	Atom A	Atom B	RP-C10
Attractive interactions with $	E_{int}(A,B)	> {\sim}10$ kcal/mol
N1	Li27	-220.8	N4	Li27	-223.7	N4	Li27	-215.8	N1	Li27	-214.4
N4	Li27	-77.3	N1	Li27	-77.9	N1	Li27	-77.4	N4	Li27	-76.3
C29	Li27	-13.6	C28	Li27	-13.5	C29	Li27	-13.1	C29	Li27	-16.5
C28	Li27	-12.9	C29	Li27	-13.2	C28	Li27	-12.3	C28	Li27	-14.2
Repulsive interactions with $	E_{int}(A,B)	> {\sim}10$ kcal/mol
C5	Li27	23.3	C10	Li27	25.3	C2	Li27	29.4	C3	Li27	29.5
C3	Li27	46.0	C2	Li27	44.0	C10	Li27	38.5	C5	Li27	36.5
C2	Li27	47.7	C3	Li27	48.4	C5	Li27	44.8	C10	Li27	46.7
C10	Li27	56.4	C5	Li27	57.5	C3	Li27	67.2	C2	Li27	64.6

A41

Part 4
Net atomic charges

Table A48. Net atomic charges for the reactants **1** and **2**. *Q* is in *e*.

1		2	
Atom A	**Q(A)**	**Atom A**	**Q(A)**
N1	-1.1164	Li1	0.9463
C2	0.5418	C2	-0.3217
C3	0.5651	C3	-0.6415
N4	-1.1211	C4	0.0371
C5	0.4269	C5	-0.0256
C6	-0.0137	C6	-0.0297
C7	-0.0156	C7	-0.0343
C8	-0.0154	C8	-0.0297
C9	-0.0150	C9	-0.0255
C10	0.4426	H10	0.0267
H11	0.0542	H11	0.0240
H12	0.0535	H12	0.0234
H13	0.0425	H13	0.0241
H14	0.0426	H14	0.0269
H15	0.0529		
C16	-0.0130		
C17	-0.0144		
C18	-0.0190		
C19	-0.0224		
C20	-0.0179		
C21	-0.0247		
H22	0.0512		
H23	0.0344		
H24	0.0352		
H25	0.0349		
H26	0.0315		

Table A49. Net atomic charges for **H_2O**. *Q* is in *e*.

H₂O	
Atom A	**Q(A)**
O1	-1.1385
H2	0.5693
H3	0.5693

Table A50. Net atomic charges for all the stationary points involved in the nucleophilic addition step along RP-C2. Q is in e.

Atom A	Q(A)		
	3a	4a	5a
N1	-1.1725	-1.1849	-1.1814
C2	0.5430	0.4651	0.4036
C3	0.5764	0.6455	0.6338
N4	-1.1166	-1.1589	-1.1803
C5	0.4336	0.3524	0.3175
C6	-0.0090	-0.0256	-0.0322
C7	-0.0113	-0.0390	-0.0565
C8	-0.0090	-0.0306	-0.0391
C9	-0.0153	-0.0483	-0.0640
C10	0.4276	0.4191	0.4363
H11	0.0618	0.0429	0.0332
H12	0.0578	0.0337	0.0203
H13	0.0463	0.0196	0.0044
H14	0.0464	0.0214	0.0077
H15	0.0420	0.0168	-0.0111
C16	-0.0100	-0.0190	-0.0312
C17	-0.0243	-0.0292	-0.0356
C18	-0.0187	-0.0279	-0.0283
C19	-0.0200	-0.0291	-0.0300
C20	-0.0138	-0.0255	-0.0289
C21	-0.0114	-0.0251	-0.0375
H22	0.0378	0.0536	0.0353
H23	0.0343	0.0268	0.0292
H24	0.0361	0.0281	0.0289
H25	0.0367	0.0276	0.0281
H26	0.0450	0.0366	0.0381
Li27	0.9272	0.9360	0.9503
C28	-0.2885	-0.1028	-0.1431
C29	-0.6494	-0.5181	-0.2079
C30	0.0384	0.0492	0.0542
C31	-0.0281	-0.0144	-0.0128
C32	-0.0309	-0.0201	-0.0202
C33	-0.0361	-0.0240	-0.0247
C34	-0.0310	-0.0205	-0.0209
C35	-0.0236	-0.0163	-0.0154
H36	0.0291	0.0423	0.0444
H37	0.0249	0.0351	0.0346
H38	0.0228	0.0345	0.0329
H39	0.0236	0.0342	0.0330
H40	0.0284	0.0386	0.0359

A43

Table A51. Net atomic charges for all the stationary points involved in the nucleophilic addition step along RP-C3. Q is in e.

Atom A	Q(A) 3b	4b	5b
N1	-1.1100	-1.1566	-1.1710
C2	0.5471	0.6115	0.6058
C3	0.5421	0.4690	0.4139
N4	-1.1921	-1.1896	-1.1984
C5	0.4189	0.4160	0.4415
C6	-0.0127	-0.0492	-0.0641
C7	-0.0111	-0.0309	-0.0397
C8	-0.0121	-0.0388	-0.0555
C9	-0.0112	-0.0275	-0.0342
C10	0.4472	0.3795	0.3411
H11	0.0975	0.0425	0.0130
H12	0.0451	0.0182	-0.0097
H13	0.0460	0.0217	0.0080
H14	0.0460	0.0196	0.0046
H15	0.0570	0.0326	0.0199
C16	-0.0159	-0.0119	-0.0140
C17	-0.0160	-0.0194	-0.0212
C18	-0.0198	-0.0237	-0.0255
C19	-0.0238	-0.0268	-0.0303
C20	-0.0181	-0.0191	-0.0250
C21	-0.0246	-0.0196	-0.0350
H22	0.0505	0.0537	0.0496
H23	0.0330	0.0263	0.0270
H24	0.0340	0.0286	0.0276
H25	0.0426	0.0270	0.0263
H26	0.0416	0.0240	0.0235
Li27	0.9249	0.9338	0.9518
C28	-0.2816	-0.1180	-0.1559
C29	-0.6516	-0.5158	-0.2095
C30	0.0353	0.0530	0.0547
C31	-0.0234	-0.0152	-0.0158
C32	-0.0278	-0.0209	-0.0215
C33	-0.0340	-0.0242	-0.0252
C34	-0.0282	-0.0191	-0.0208
C35	-0.0256	-0.0088	-0.0131
H36	0.0288	0.0358	0.0355
H37	0.0253	0.0326	0.0324
H38	0.0237	0.0331	0.0322
H39	0.0253	0.0339	0.0339
H40	0.0280	0.0429	0.0433

Table A52. Net atomic charges for all the stationary points involved in the nucleophilic addition step along RP-C5. *Q* is in *e*.

Atom A	Q(A)		
	3c	4c	5c
N1	-1.1083	-1.1529	-1.1685
C2	0.5498	0.4370	0.3937
C3	0.5563	0.5009	0.4994
N4	-1.1868	-1.1733	-1.1848
C5	0.4159	0.3979	0.3928
C6	-0.0204	-0.0235	-0.0615
C7	-0.0115	-0.0209	-0.0264
C8	-0.0117	-0.0367	-0.0511
C9	-0.0112	-0.0231	-0.0311
C10	0.4507	0.5346	0.5320
H11	0.0602	0.0300	0.0120
H12	0.0818	0.0238	0.0046
H13	0.0489	0.0232	0.0167
H14	0.0467	0.0238	0.0151
H15	0.0569	0.0356	0.0307
C16	-0.0127	-0.0119	-0.0122
C17	-0.0129	-0.0276	-0.0364
C18	-0.0173	-0.0280	-0.0335
C19	-0.0205	-0.0346	-0.0433
C20	-0.0160	-0.0277	-0.0337
C21	-0.0243	-0.0369	-0.0448
H22	0.0526	0.0447	0.0379
H23	0.0366	0.0237	0.0168
H24	0.0374	0.0234	0.0157
H25	0.0367	0.0229	0.0159
H26	0.0304	0.0138	0.0095
Li27	0.9190	0.9401	0.9555
C28	-0.2954	-0.1135	-0.1450
C29	-0.6456	-0.4937	-0.2108
C30	0.0374	0.0504	0.0539
C31	-0.0262	-0.0149	-0.0140
C32	-0.0301	-0.0207	-0.0211
C33	-0.0349	-0.0258	-0.0253
C34	-0.0301	-0.0214	-0.0216
C35	-0.0263	-0.0167	-0.0153
H36	0.0268	0.0423	0.0424
H37	0.0238	0.0337	0.0335
H38	0.0230	0.0327	0.0320
H39	0.0238	0.0325	0.0325
H40	0.0269	0.0364	0.0377

Table A53. Net atomic charges for all the stationary points involved in the nucleophilic addition step along RP-C10. Q is in e.

Atom A	$Q(A)$		
	3d	4d	5d
N1	-1.1768	-1.1720	-1.1755
C2	0.5334	0.4860	0.4878
C3	0.5733	0.4421	0.3913
N4	-1.1123	-1.1630	-1.1798
C5	0.4350	0.5160	0.5112
C6	-0.0097	-0.0238	-0.0317
C7	-0.0115	-0.0398	-0.0542
C8	-0.0105	-0.0215	-0.0272
C9	-0.0231	-0.0278	-0.0605
C10	0.4182	0.4086	0.3954
H11	0.0633	0.0224	0.0083
H12	0.0580	0.0346	0.0287
H13	0.0470	0.0220	0.0125
H14	0.0494	0.0221	0.0147
H15	0.0791	0.0206	-0.0027
C16	-0.0191	-0.0250	-0.0266
C17	-0.0262	-0.0267	-0.0424
C18	-0.0142	-0.0260	-0.0281
C19	-0.0175	-0.0284	-0.0299
C20	-0.0142	-0.0240	-0.0258
C21	-0.0215	-0.0298	-0.0298
H22	0.0447	0.0455	0.0295
H23	0.0423	0.0291	0.0279
H24	0.0409	0.0300	0.0283
H25	0.0408	0.0303	0.0297
H26	0.0384	0.0296	0.0315
Li27	0.9183	0.9395	0.9532
C28	-0.2962	-0.1073	-0.1434
C29	-0.6440	-0.4919	-0.2244
C30	0.0371	0.0504	0.0536
C31	-0.0260	-0.0165	-0.0151
C32	-0.0300	-0.0212	-0.0213
C33	-0.0347	-0.0255	-0.0251
C34	-0.0301	-0.0211	-0.0215
C35	-0.0261	-0.0149	-0.0155
H36	0.0269	0.0365	0.0397
H37	0.0239	0.0325	0.0334
H38	0.0231	0.0327	0.0325
H39	0.0238	0.0336	0.0330
H40	0.0268	0.0416	0.0382

Table A54. Net atomic charges for all the stationary points involved in the hydrolysis step along RP-C2. Q is in e.

Atom A	Q(A)		
	6a	**7a**	**8a**
N1	-1.1636	-1.1453	-1.1136
C2	0.4041	0.4062	0.4188
C3	0.6331	0.6484	0.6621
N4	-1.1798	-1.1691	-1.1609
C5	0.3177	0.3227	0.3339
C6	-0.0323	-0.0270	-0.0214
C7	-0.0571	-0.0459	-0.0386
C8	-0.0393	-0.0330	-0.0266
C9	-0.0637	-0.0521	-0.0348
C10	0.4426	0.3991	0.3995
H11	0.0343	0.0422	0.0511
H12	0.0199	0.0278	0.0339
H13	0.0039	0.0124	0.0178
H14	0.0076	0.0158	0.0219
H15	-0.0094	0.0218	0.0323
C16	-0.0277	-0.0220	-0.0202
C17	-0.0332	-0.0412	-0.0299
C18	-0.0282	-0.0283	-0.0303
C19	-0.0299	-0.0282	-0.0312
C20	-0.0281	-0.0255	-0.0273
C21	-0.0339	-0.0262	-0.0285
H22	0.0405	0.0308	0.0446
H23	0.0282	0.0310	0.0315
H24	0.0281	0.0311	0.0311
H25	0.0270	0.0310	0.0315
H26	0.0337	0.0404	0.0431
Li27	0.9324	0.9496	0.9471
C28	-0.1473	-0.1415	-0.1364
C29	-0.2232	-0.1989	-0.1937
C30	0.0553	0.0556	0.0562
C31	-0.0097	-0.0111	-0.0103
C32	-0.0177	-0.0193	-0.0183
C33	-0.0221	-0.0235	-0.0227
C34	-0.0188	-0.0200	-0.0188
C35	-0.0146	-0.0135	-0.0118
H36	0.0479	0.0448	0.0455
H37	0.0373	0.0353	0.0362
H38	0.0355	0.0337	0.0347
H39	0.0353	0.0341	0.0349
H40	0.0366	0.0386	0.0390
O41	-1.2050	-1.2891	-1.3796
H42	0.5919	0.5620	0.4965
H43	0.5924	0.5462	0.5117

Table A55. Net atomic charges for all the stationary points involved in the hydrolysis step along RP-C3. Q is in e.

Atom A	Q(A)		
	6b	7b	8b
N1	-1.1716	-1.1625	-1.1566
C2	0.6092	0.6235	0.6375
C3	0.4108	0.4163	0.4238
N4	-1.1789	-1.1696	-1.1236
C5	0.4468	0.3973	0.3946
C6	-0.0635	-0.0504	-0.0372
C7	-0.0394	-0.0328	-0.0282
C8	-0.0563	-0.0439	-0.0387
C9	-0.0341	-0.0285	-0.0239
C10	0.3418	0.3456	0.3546
H11	0.0193	0.0279	0.0479
H12	-0.0086	0.0233	0.0345
H13	0.0077	0.0171	0.0208
H14	0.0042	0.0134	0.0174
H15	0.0196	0.0278	0.0326
C16	-0.0141	-0.0151	-0.0131
C17	-0.0206	-0.0189	-0.0163
C18	-0.0253	-0.0228	-0.0214
C19	-0.0302	-0.0270	-0.0255
C20	-0.0246	-0.0218	-0.0201
C21	-0.0352	-0.0324	-0.0299
H22	0.0504	0.0521	0.0544
H23	0.0271	0.0302	0.0312
H24	0.0276	0.0314	0.0323
H25	0.0260	0.0304	0.0315
H26	0.0222	0.0278	0.0296
Li27	0.9328	0.9477	0.9486
C28	-0.1562	-0.1526	-0.1492
C29	-0.2267	-0.1991	-0.1946
C30	0.0535	0.0558	0.0564
C31	-0.0143	-0.0135	-0.0125
C32	-0.0194	-0.0203	-0.0196
C33	-0.0227	-0.0240	-0.0232
C34	-0.0186	-0.0195	-0.0190
C35	-0.0111	-0.0117	-0.0109
H36	0.0385	0.0375	0.0394
H37	0.0351	0.0336	0.0343
H38	0.0350	0.0333	0.0339
H39	0.0366	0.0348	0.0353
H40	0.0462	0.0441	0.0445
O41	-1.2105	-1.2955	-1.3812
H42	0.5962	0.5488	0.5144
H43	0.5951	0.5632	0.4957

Table A56. Net atomic charges for all the stationary points involved in the hydrolysis step along RP-C2. Q is in e.

Atom A	$Q(A)$		
	6a	7e	8e
N1	-1.1636	-1.1725	-1.1495
C2	0.4041	0.5561	0.5939
C3	0.6331	0.6512	0.5974
N4	-1.1798	-1.1453	-1.1144
C5	0.3177	0.3684	0.4336
C6	-0.0323	-0.0204	-0.0080
C7	-0.0571	-0.0320	-0.0114
C8	-0.0393	-0.0248	-0.0083
C9	-0.0637	-0.0365	-0.0072
C10	0.4426	0.4130	0.4444
H11	0.0343	0.0525	0.0699
H12	0.0199	0.0399	0.0587
H13	0.0039	0.0259	0.0478
H14	0.0076	0.0269	0.0486
H15	-0.0094	0.0158	0.0492
C16	-0.0277	-0.2200	-0.0282
C17	-0.0332	-0.0465	-0.0259
C18	-0.0282	-0.0456	-0.0238
C19	-0.0299	-0.0434	-0.0268
C20	-0.0281	-0.0469	-0.0279
C21	-0.0339	-0.0491	-0.0201
H22	0.0405	-0.0019	0.0247
H23	0.0282	0.0109	0.0266
H24	0.0281	0.0141	0.0277
H25	0.0270	0.0102	0.0251
H26	0.0337	0.0015	0.0294
Li27	0.9324	0.9344	0.9156
C28	-0.1473	-0.1370	-0.1193
C29	-0.2232	-0.1592	-0.1665
C30	0.0553	0.0579	0.0561
C31	-0.0097	-0.0115	-0.0101
C32	-0.0177	-0.0178	-0.0160
C33	-0.0221	-0.0229	-0.0208
C34	-0.0188	-0.0185	-0.0188
C35	-0.0146	-0.0118	-0.0284
H36	0.0479	0.0418	0.0438
H37	0.0373	0.0360	0.0378
H38	0.0355	0.0348	0.0378
H39	0.0353	0.0347	0.0376
H40	0.0366	0.0363	0.1137
O41	-1.2050	-1.2387	-1.4254
H42	0.5919	0.5653	0.0314
H43	0.5924	0.5761	0.5069

A49

Table A57. Net atomic charges for ONSH products along RP-C3 (**9b**) and RP-C3′ (**9b′**). Q is in e.

Atom A	Q(A)	
	9b	**9b′**
N1	-1.1410	-1.1124
C2	0.5714	0.5728
C3	0.6086	0.5943
N4	-1.0898	-1.1505
C5	0.4551	0.4268
C6	-0.0107	-0.0329
C7	-0.0142	-0.0121
C8	-0.0177	-0.0121
C9	-0.0217	-0.0099
C10	0.4365	0.4445
H11	0.5856	0.5568
H12	0.0581	0.1106
H13	0.0454	0.0485
H14	0.0449	0.0474
H15	0.0525	0.0582
C16	-0.0022	-0.0092
C17	-0.0148	-0.0116
C18	-0.0206	-0.0183
C19	-0.0228	-0.0214
C20	-0.0189	-0.0187
C21	0.0025	-0.0157
H22	0.0420	0.0456
H23	0.0323	0.0355
H24	0.0330	0.0356
H25	0.0330	0.0351
H26	0.0461	0.0398
Li27	0.9380	0.9260
C28	-0.1153	-0.1251
C29	-0.1552	-0.1554
C30	0.0610	0.0614
C31	-0.0090	-0.0070
C32	-0.0148	-0.0124
C33	-0.0189	-0.0165
C34	-0.0145	-0.0121
C35	-0.0073	-0.0065
H36	0.0491	0.0510
H37	0.0393	0.0421
H38	0.0393	0.0423
H39	0.0397	0.0425
H40	0.0480	0.0453
O41	-1.3433	-1.3453
H42	0.6093	0.5207
H43	0.5196	0.6171
O44	-0.6975	-0.6371
O45	-0.6398	-0.6574

Part 5
Inter-fragment interaction energies

Interaction energies computed for adducts 3

Table A58. Interaction energies between molecule **1** and specified major fragments of molecule **2**, computed for the indicated reaction pathways on adducts **3** formation between **1** and **2**. All values in kcal/mol.

	Fragment	Reaction pathway			
		C2	C3	C5	C10
1	**2**	-56.6	-64.0	-45.0	-47.4
	$\mathcal{R}$	-19.7	-25.4	-5.5	-5.5
	$\mathcal{Ph}$2	-17.4	-13.0	-0.5	-0.5
	$\mathcal{L}$	-39.2	-51.0	-44.5	-46.9
	$\mathcal{A}$	-2.3	-12.3	-5.0	-5.0
	Li	-36.9	-38.6	-39.4	-41.9
	C28	-1.1	-3.6	-3.6	-4.2
	C29	-1.2	-8.7	-1.4	-0.8

Table A59. Interaction energies between molecule **2** and specified major fragments of molecule **1**, computed for the indicated reaction pathways on adducts **3** formation between **1** and **2**. All values in kcal/mol.

	Fragment	Reaction pathway			
		C2	C3	C5	C10
2	$\mathcal{Q}$	-43.5	-50.5	-46.6	-47.3
	$\mathcal{P}$	-46.5	-54.5	-39.9	-40.2
	$\mathcal{Bn}$	23.0	27.7	17.1	17.0
	$\mathcal{Ph}$1	-13.2	-13.6	1.6	-0.1
	$\mathcal{N}$	-83.0	-92.0	-103.4	-100.9
	$\mathcal{C}$	36.7	45.4	61.1	59.5
	$\mathcal{G}$1	-43.3	0.9	1.5	-43.1
	$\mathcal{G}$2	-3.0	-47.5	-43.9	1.8
	$\mathcal{F}$1	-59.8	11.3	21.9	-51.6
	$\mathcal{F}$2	7.6	-67.7	-48.4	20.9
	$\mathcal{F}$3	11.4	-57.8	-65.4	8.8
	$\mathcal{F}$4	-54.4	13.5	8.7	-62.6
	N1	-74.1	-10.5	-15.4	-85.2
	N4	-8.9	-81.5	-88.1	-15.6
	C2	15.0	5.2	10.0	24.9
	C3	1.6	16.6	27.2	10.5
	C5	4.2	17.4	16.9	6.9
	C10	15.7	6.2	7.0	17.2

A51

Table A60. Interaction energies, between the molecular fragment $\mathcal{R}$[a] of **2** and the indicated significant fragments of **1**, computed for the indicated reaction pathways on adducts **3** formation between **1** and **2**. All values in kcal/mol.

		Reaction pathway			
Fragment		**C2**	**C3**	**C5**	**C10**
$\mathcal{R}$	$\mathcal{Q}$	-0.5	-5.7	-1.3	-0.3
	$\mathcal{P}$	9.1	3.1	22.1	23.3
	$\mathcal{Bn}$	-70.7	-63.9	-80.8	-80.0
	$\mathcal{Ph}$1	-19.2	-19.7	-4.2	-5.2
	$\mathcal{N}$	162.7	161.5	151.3	149.9
	$\mathcal{C}$	-149.1	-139.3	-125.2	-123.4
	$\mathcal{G}$1	17.3	1.1	1.2	25.9
	$\mathcal{G}$2	-3.6	21.1	24.9	0.6
	$\mathcal{F}$1	12.7	-25.6	-14.8	31.5
	$\mathcal{F}$2	-30.8	0.2	26.7	-17.6
	$\mathcal{F}$3	0.5	48.6	41.5	-4.0
	$\mathcal{F}$4	41.0	2.8	-4.8	41.5
	N1	100.9	58.1	52.8	97.3
	N4	61.8	103.4	98.5	52.6
	C2	-48.8	-32.9	-27.7	-38.1
	C3	-39.1	-51.3	-40.2	-29.0
	C5	-26.3	-31.0	-33.4	-23.0
	C10	-34.8	-24.1	-23.9	-33.3

[a] $\mathcal{R}$ = {C28,C29,C30,C31,C32,C33,C34,C35,H36,H37,H38.H39.H40}

Table A61. Interaction energies, between the molecular fragment $\mathcal{P}h2$[a] of **2** and the indicated significant fragments of **1**, computed for the indicated reaction pathways on adducts **3** formation between **1** and **2**. All values in kcal/mol.

Fragment		Reaction pathway			
		C2	**C3**	**C5**	**C10**
$\mathcal{P}h2$	$\mathcal{Q}$	-7.6	-0.8	-0.6	-0.7
	$\mathcal{P}$	-8.0	-1.1	-1.0	-1.0
	$\mathcal{B}n$	3.1	2.6	2.4	2.5
	$\mathcal{P}h1$	-9.8	-12.3	0.1	0.2
	$\mathcal{N}$	-10.3	-7.0	-5.6	-5.8
	C	2.7	5.6	4.5	4.6
	$\mathcal{G}1$	-2.6	0.0	0.0	-1.2
	$\mathcal{G}2$	-5.0	-1.5	-1.1	0.0
	$\mathcal{F}1$	-6.1	1.2	0.7	-1.5
	$\mathcal{F}2$	-5.2	-1.5	-1.3	0.8
	$\mathcal{F}3$	-2.0	-2.9	-2.0	0.3
	$\mathcal{F}4$	-2.9	0.4	0.3	-2.0
	N1	-5.6	-1.9	-1.7	-4.0
	N4	-4.7	-5.1	-3.9	-1.8
	C2	1.3	1.0	0.9	1.5
	C3	-1.4	2.2	1.5	1.0
	C5	1.1	1.4	1.3	0.8
	C10	1.6	0.9	0.8	1.3

[a] $\mathcal{P}h2$ = {C30,C31,C32,C33,C34,C35,H36,H37,H38.H39.H40}

Table A62. Interaction energies, between the molecular fragment $\mathcal{L}^a$ of **2** and the indicated significant fragments of **1**, computed for the indicated reaction pathways on adducts **3** formation between **1** and **2**. All values in kcal/mol.

| | Fragment | Reaction pathway | | | |
		C2	C3	C5	C10
$\mathcal{L}$	$\mathcal{Q}$	-35.9	-49.7	-46.0	-46.6
	$\mathcal{P}$	-38.5	-53.4	-38.9	-39.1
	$\mathcal{Bn}$	19.9	25.1	14.7	14.5
	$\mathcal{Ph}$1	-3.3	-1.3	1.5	-0.3
	$\mathcal{N}$	-72.7	-85.0	-97.8	-95.1
	$\mathcal{C}$	34.0	39.9	56.6	54.9
	$\mathcal{G}$1	-40.7	0.9	1.5	-42.0
	$\mathcal{G}$2	2.0	-46.0	-42.8	1.7
	$\mathcal{F}$1	-53.7	10	21.1	-50.1
	$\mathcal{F}$2	12.8	-66.2	-47.1	20.1
	$\mathcal{F}$3	13.5	-55.0	-63.4	8.5
	$\mathcal{F}$4	-51.5	13.1	8.4	-60.6
	N1	-68.6	-8.6	-13.7	-81.3
	N4	-4.1	-76.4	-84.2	-13.8
	C2	13.7	4.1	9.0	23.4
	C3	3.0	14.3	25.7	9.5
	C5	3.2	16.0	15.6	6.1
	C10	14.1	5.4	6.2	15.9

[a)]$\mathcal{L}$ = {Li28,C28,C29}

Table A63. Interaction energies, between the molecular fragment $\mathcal{A}$[a] of **2** and the indicated significant fragments of **1**, computed for the indicated reaction pathways on adducts **3** formation between **1** and **2**. All values in kcal/mol.

		Reaction pathway			
	Fragment	C2	C3	C5	C10
$\mathcal{A}$	$\mathcal{Q}$	7.0	-4.9	-0.7	0.3
	$\mathcal{P}$	17.1	4.3	23.1	24.3
	$\mathcal{Bn}$	-73.8	-66.5	-83.2	-82.5
	$\mathcal{Ph}$1	-9.3	-7.5	-4.3	-5.3
	$\mathcal{N}$	173.0	168.5	156.9	155.6
	$\mathcal{C}$	-151.8	-144.8	-129.7	-128.0
	$\mathcal{G}$1	19.9	1.1	1.2	27.0
	$\mathcal{G}$2	1.4	22.6	26.0	0.6
	$\mathcal{F}$1	18.9	-26.9	-15.5	33.0
	$\mathcal{F}$2	-25.6	1.7	28.0	-18.4
	$\mathcal{F}$3	2.6	51.5	43.5	-4.4
	$\mathcal{F}$4	43.9	2.4	-5.1	43.5
	N1	106.5	60.0	54.5	101.2
	N4	66.5	108.5	102.4	54.4
	C2	-50.2	-33.9	-28.6	-39.6
	C3	-37.8	-53.5	-41.7	-30.0
	C5	-27.4	-32.4	-34.7	-23.8
	C10	-36.5	-25.0	-24.7	-34.7

[a] $\mathcal{A}$ = {C28,C29}

Table A64. Interaction energies, between Li27 of **2** and the indicated significant fragments of **1**, computed for the indicated reaction pathways on adducts **3** formation between **1** and **2**. All values in kcal/mol.

		Reaction pathway			
Fragment		**C2**	**C3**	**C5**	**C10**
Li27	$\mathcal{Q}$	-42.9	-44.8	-45.5	-47.0
	$\mathcal{P}$	-55.6	-57.6	-62.0	-63.5
	$\mathcal{Bn}$	93.7	91.6	97.9	97.0
	$\mathcal{Ph}$1	6.0	6.2	5.8	5.1
	$\mathcal{N}$	-245.7	-253.4	-254.7	-250.7
	C	185.7	184.7	186.3	182.9
	$\mathcal{G}$1	-60.6	-0.2	0.4	-69.0
	$\mathcal{G}$2	0.6	-68.6	-68.8	1.1
	$\mathcal{F}$1	-72.5	36.9	36.6	-83.1
	$\mathcal{F}$2	38.4	-67.8	-75.1	38.5
	$\mathcal{F}$3	10.9	-106.4	-106.9	12.8
	$\mathcal{F}$4	-95.3	10.8	13.5	-104.1
	N1	-175.0	-68.6	-68.2	-182.5
	N4	-70.7	-184.9	-186.6	-68.2
	C2	63.9	38.1	37.7	63.0
	C3	40.8	67.8	67.4	39.5
	C5	30.5	48.5	50.3	29.9
	C10	50.6	30.3	30.9	50.6

Table A65. Interaction energies, between C28 of **2** and the indicated significant fragments of **1**, computed for the indicated reaction pathways on adducts **3** formation between **1** and **2**. All values in kcal/mol.

Fragment		Reaction pathway			
		C2	C3	C5	C10
C28	$\mathcal{Q}$	1.9	-2.2	-1.8	-1.9
	$\mathcal{P}$	5.2	1.3	11.0	11.9
	$\mathcal{Bn}$	-24.0	-24.7	-38.1	-39.0
	$\mathcal{Ph}$1	-2.9	-1.5	-1.8	-2.4
	$\mathcal{N}$	52.8	62.1	68.7	68.9
	$\mathcal{C}$	-46.7	-52.6	-55.8	-55.7
	$\mathcal{G}$1	6.7	0.0	0.0	13.4
	$\mathcal{G}$2	-0.5	9.5	12.8	-0.2
	$\mathcal{F}$1	9.5	-12.2	-8.9	17.3
	$\mathcal{F}$2	-10.0	3.5	14.7	-10.0
	$\mathcal{F}$3	-3.8	22.0	21.2	-3.7
	$\mathcal{F}$4	15.8	-2.3	-3.8	21.2
	N1	35.9	19.0	21.6	47.1
	N4	17.0	43.1	47.1	21.8
	C2	-16.3	-10.6	-11.7	-18.0
	C3	-9.7	-20.8	-18.9	-12.4
	C5	-7.7	-12.8	-15.4	-9.6
	C10	-12.9	-8.4	-9.8	-15.7

Table A66. Interaction energies, between C29 of **2** and the indicated significant fragments of **1**, computed for the indicated reaction pathways on adducts **3** formation between **1** and **2**. All values in kcal/mol.

Fragment		Reaction pathway			
		C2	C3	C5	C10
C29	$\mathcal{Q}$	5.2	-2.7	1.1	2.2
	$\mathcal{P}$	11.9	3.0	12.1	12.5
	$\mathcal{B}n$	-49.9	-41.8	-45.1	-43.5
	$\mathcal{P}h\mathbf{1}$	-6.4	-6.0	-2.6	-3.0
	$\mathcal{N}$	120.2	106.4	88.2	86.7
	$\mathcal{C}$	-105.1	-92.2	-73.9	-72.3
	$\mathcal{G}\mathbf{1}$	13.1	1.1	1.1	13.6
	$\mathcal{G}\mathbf{2}$	1.9	13.1	13.2	0.8
	$\mathcal{F}\mathbf{1}$	9.4	-14.7	-6.6	15.7
	$\mathcal{F}\mathbf{2}$	-15.5	-1.8	13.3	-8.5
	$\mathcal{F}\mathbf{3}$	6.4	29.5	22.3	-0.7
	$\mathcal{F}\mathbf{4}$	28.0	4.7	-1.3	22.3
	N1	70.6	40.9	32.9	54.1
	N4	49.6	65.4	55.3	32.6
	C2	-33.9	-23.3	-16.9	-21.5
	C3	-28.1	-32.7	-22.8	-17.6
	C5	-19.6	-19.6	-19.3	-14.2
	C10	-23.6	-16.5	-14.9	-19.0

Table A67. Interaction energies between molecule **1** and specified major fragments of molecule **2**, computed for the indicated reaction pathways on transition states **4** formation between **1** and **2**. All values in kcal/mol.

	Fragment	Reaction pathway			
		C2	C3	C5	C10
1	**2**	-206.8	-209.7	-207.5	-216.6
	$\mathcal{R}$	-130.7	-137.0	-144.1	-144.6
	$\mathcal{P}h\mathbf{2}$	-5.2	-11.2	-6.3	-6.2
	$\mathcal{L}$	-201.6	-198.4	-201.2	-210.4
	$\mathcal{A}$	-125.5	-125.8	-137.7	-13.4
	Li	-76.1	-72.6	-63.5	-72.0
	C28	-118.1	-114.7	-133	-135.5
	C29	-7.3	-11.1	-4.7	-3.0

Table A68. Interaction energies, between Li27 of **2** and the indicated significant fragments of **1**, computed for the indicated reaction pathways on transition states **4** formation between **1** and **2**. All values in kcal/mol.

	Fragment	Reaction pathway			
		C2	C3	C5	C10
Li27	$\mathcal{Q}$	-80.6	-77.5	-64.1	-73.0
	$\mathcal{P}$	-80.8	-77.5	-70.8	-78.5
	$\mathcal{B}n$	81.6	83.7	106.0	105.5
	$\mathcal{P}h\mathbf{1}$	4.5	4.9	0.7	1.0
	$\mathcal{N}$	-284.7	-284.0	-274.4	-280.1
	$\mathcal{C}$	200.0	200.3	199.4	199.1
	$\mathcal{G}\mathbf{1}$	-82.2	-4.1	-5.8	-74.8
	$\mathcal{G}\mathbf{2}$	-2.4	-79.6	-69.2	-6.1
	$\mathcal{F}\mathbf{1}$	-86.0	31.9	14.9	-100.4
	$\mathcal{F}\mathbf{2}$	39.6	-76.9	-85.1	17.2
	$\mathcal{F}\mathbf{3}$	-1.9	-120.4	-90.4	15.3
	$\mathcal{F}\mathbf{4}$	-124.6	-1.3	14.0	-96.5
	N1	-201.8	-84.4	-85.0	-195.7
	N4	-82.9	-199.6	-189.4	-84.4
	C2	65.8	50.0	35.3	63.0
	C3	52.8	66.5	64.9	36.1
	C5	27.7	53.5	55.4	42.2
	C10	53.7	30.3	43.9	57.9

Table A69. Interaction energies, between the molecular fragment $\mathcal{A}$[a] of **2** and the indicated significant fragments of **1**, computed for the indicated reaction pathways on transition states **4** formation between **1** and **2**. All values in kcal/mol.

		Reaction pathway			
Fragment		**C2**	**C3**	**C5**	**C10**
$\mathcal{A}$	$\mathcal{Q}$	-104.6	-113.0	-136.7	-136.7
	$\mathcal{P}$	-102.7	-111.2	-117.7	-118.6
	$\mathcal{Bn}$	-50.8	-51.3	-204.0	-204.6
	$\mathcal{Ph}$**1**	-20.9	-12.8	-1.0	-1.7
	$\mathcal{N}$	133.5	134.2	131.6	129.7
	$\mathcal{C}$	-232.2	-235.7	-247.0	-246.5
	$\mathcal{G}$**1**	-89.1	-6.7	-7.8	-109.5
	$\mathcal{G}$**2**	-9.7	-94.8	-107.7	-7.3
	$\mathcal{F}$**1**	-117.5	-126.0	0.2	9.5
	$\mathcal{F}$**2**	-125.1	-123.8	5.2	-0.7
	$\mathcal{F}$**3**	13.5	23.9	-123.6	-126.3
	$\mathcal{F}$**4**	23.7	12.9	-123.9	-125.9
	N1	71.3	62.1	62.1	68.6
	N4	62.2	72.1	69.5	61.1
	C2	-132.3	-46.7	-27.5	-32.3
	C3	-51.0	-139.4	-34.5	-27.7
	C5	-20.9	-27.5	-142.7	-40.7
	C10	-28.0	-22.0	-42.3	-145.8

[a] $\mathcal{A}$ = {C28,C29}

Table A70. Interaction energies, between the molecular fragment $\mathcal{R}^a$ of **2** and the indicated significant fragments of **1**, computed for the indicated reaction pathways on transition states **4** formation between **1** and **2**. All values in kcal/mol.

		Reaction pathway			
	Fragment	**C2**	**C3**	**C5**	**C10**
$\mathcal{R}$	$\mathcal{Q}$	-109.7	-118.2	-142.8	-143.2
	$\mathcal{P}$	-107.5	-116.2	-122.9	-124.0
	$\mathcal{Bn}$	-43.1	-43.0	-194.0	-194.7
	$\mathcal{Ph}$1	-21.0	-18.8	-1.2	-1.5
	$\mathcal{N}$	106.6	106.1	105.9	103.9
	$\mathcal{C}$	-210.8	-213.2	-226.8	-226.4
	$\mathcal{G}$1	-92.4	-8.9	-10.6	-112.3
	$\mathcal{G}$2	-11.8	-98.2	-110.4	-10.2
	$\mathcal{F}$1	-117.7	-127.9	-3.8	5.9
	$\mathcal{F}$2	-124.4	-123.1	2.2	-4.4
	$\mathcal{F}$3	7.9	18.1	-126.0	-129.1
	$\mathcal{F}$4	17.8	7.1	-126.6	-128.3
	N1	57.9	47.9	49.0	55.9
	N4	48.7	58.2	56.9	48.0
	C2	-126.6	-38.9	-23.3	-27.5
	C3	-43.3	-133.3	-29.5	-23.3
	C5	-17.3	-23.1	-137.8	-34.9
	C10	-23.7	-18.0	-36.2	-140.7

a) $\mathcal{R}$ = {C28,C29,C30,C31,C32,C33,C34,C35,H36,H37,H38.H39.H40}

Table A71. Interaction energies, between the molecular fragment $\mathcal{P\hat{h}}2^{a}$ of **2** and the indicated significant fragments of **1**, computed for the indicated reaction pathways on transition states **4** formation between **1** and **2**. All values in kcal/mol.

Fragment		Reaction pathway			
		C2	**C3**	**C5**	**C10**
$\mathcal{P\hat{h}}2$	$\mathcal{Q}$	-5.0	-5.2	-6.1	-6.4
	$\mathcal{P}$	-4.8	-5.0	-5.2	-5.5
	$\mathcal{Bn}$	7.8	8.3	10.0	9.9
	$\mathcal{P\hat{h}}1$	-0.2	-6.0	-0.2	0.2
	$\mathcal{N}$	-26.8	-28.1	-25.7	-25.
	$\mathcal{C}$	21.4	22.5	20.2	20.0
	$\mathcal{G}1$	-3.3	-2.2	-2.8	-2.8
	$\mathcal{G}2$	-2.1	-3.4	-2.7	-3.0
	$\mathcal{F}1$	-0.2	-1.8	-4.0	-3.7
	$\mathcal{F}2$	0.6	0.7	-3.0	-3.7
	$\mathcal{F}3$	-5.7	-5.3	-2.3	-2.8
	$\mathcal{F}4$	-5.8	-5.9	-2.7	-2.4
	N1	-13.4	-14.9	-13.1	-12.6
	N4	-13.4	-13.9	-12.6	-13.1
	C2	5.7	7.9	4.2	4.8
	C3	7.7	6.1	5.0	4.4
	C5	3.6	4.4	4.9	5.8
	C10	4.4	4.1	6.1	5.1

[a]) $\mathcal{P\hat{h}}2$ = {C30,C31,C32,C33,C34,C35,H36,H37,H38.H39.H40}

Table A72. Interaction energies, between C28 of **2** and the indicated significant fragments of **1**, computed for the indicated reaction pathways on transition states **4** formation between **1** and **2**. All values in kcal/mol.

Fragment		Reaction pathway			
		C2	C3	C5	C10
C28	$\mathcal{Q}$	-105.3	-110.4	-132.2	-134.8
	$\mathcal{P}$	-104.0	-109.3	-119.3	-121.6
	$\mathcal{Bn}$	-15.7	-16.8	-142.6	-145.0
	$\mathcal{Ph}$1	-12.8	-4.2	-0.8	-0.7
	$\mathcal{N}$	27.6	32.6	33.3	31.5
	C	-130.7	-136.1	-151.7	-152.5
	$\mathcal{G}$1	-92.2	-7.7	-10.3	-110.6
	$\mathcal{G}$2	-10.9	-95.8	-108.2	-10.4
	$\mathcal{F}$1	-102.2	-110.6	-9.9	-0.3
	$\mathcal{F}$2	-109.0	-105.1	-2.0	-9.8
	$\mathcal{F}$3	-6.3	5.8	-116.0	-121.8
	$\mathcal{F}$4	5.1	-4.3	-118.7	-119.3
	N1	19.4	11.4	12.3	20.0
	N4	8.2	21.2	21.0	11.5
	C2	-102.1	-13.3	-8.7	-12.2
	C3	-14.2	-107.1	-13.4	-8.4
	C5	-4.9	-9.8	-115.7	-13.5
	C10	-9.5	-5.8	-14.0	-118.4

Table A73. Interaction energies, between C29 of **2** and the indicated significant fragments of **1**, computed for the indicated reaction pathways on transition states **4** formation between **1** and **2**. All values in kcal/mol.

Fragment		Reaction pathway			
		C2	C3	C5	C10
C29	$\mathcal{Q}$	0.7	-2.6	-4.5	-2.0
	$\mathcal{P}$	1.3	-1.9	1.6	3.1
	$\mathcal{Bn}$	-35.2	-34.6	-61.4	-59.6
	$\mathcal{Ph}$1	-8.0	-8.6	-0.2	-1.0
	$\mathcal{N}$	105.8	101.6	98.4	98.2
	$\mathcal{C}$	-101.5	-99.6	-95.3	-93.9
	$\mathcal{G}$1	3.2	1.1	2.5	1.1
	$\mathcal{G}$2	1.2	1.0	0.5	3.2
	$\mathcal{F}$1	-15.3	-15.4	10.1	9.9
	$\mathcal{F}$2	-16.1	-18.7	7.2	9.1
	$\mathcal{F}$3	19.9	18.1	-2.3	-4.5
	$\mathcal{F}$4	18.5	17.2	-2.7	-6.6
	N1	51.9	50.7	49.8	48.6
	N4	53.9	50.9	48.6	49.6
	C2	-30.2	-33.4	-18.9	-20.1
	C3	-36.7	-32.2	-21.1	-19.3
	C5	-16.0	-17.7	-27.0	-27.2
	C10	-18.5	-16.2	-28.4	-27.4

PART 6

Energy profiles along reaction coordinates
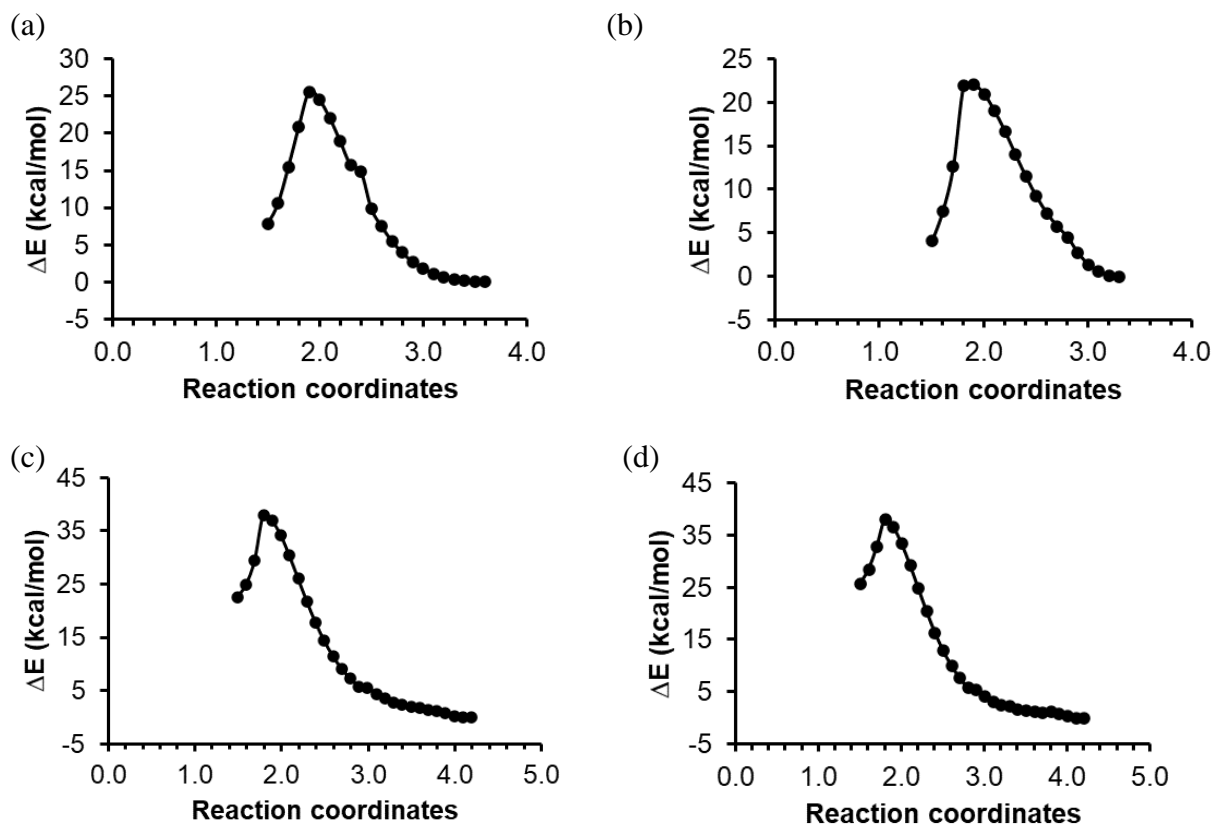
Figure A1. Computed reaction energy profiles along the C28---Cn reaction coordinates for (a) RP-C2, (b) RP-C3, (c) RP-C5 and (d) RP-C10.

(a)

(b)

(c)

(d)
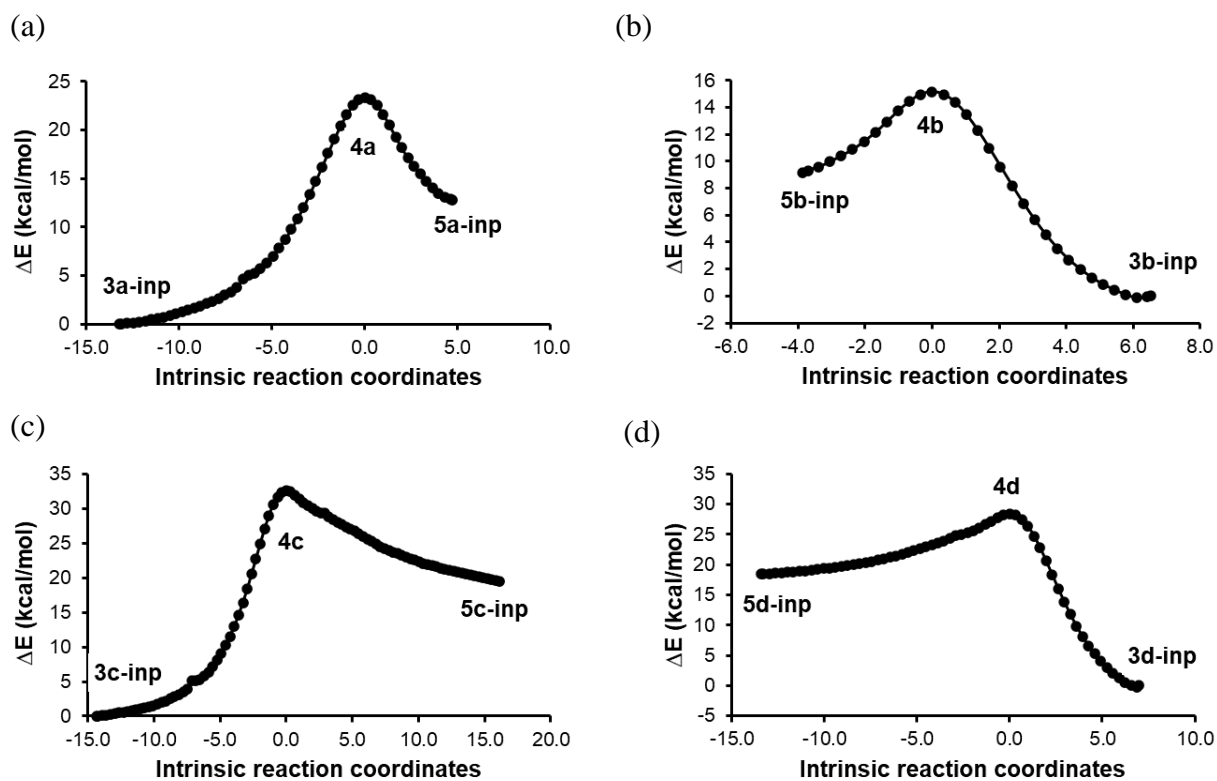
Figure A2. Computed IRC paths for the nucleophilic addition step along (a) RP-C2, (b) RP-C3, (c) RP-C5 and (d) RP-C10, confirming that **4a**, **4b**, **4c** and **4d** connect the desired minima of the respective pathways.

(a)

(b)

(c)
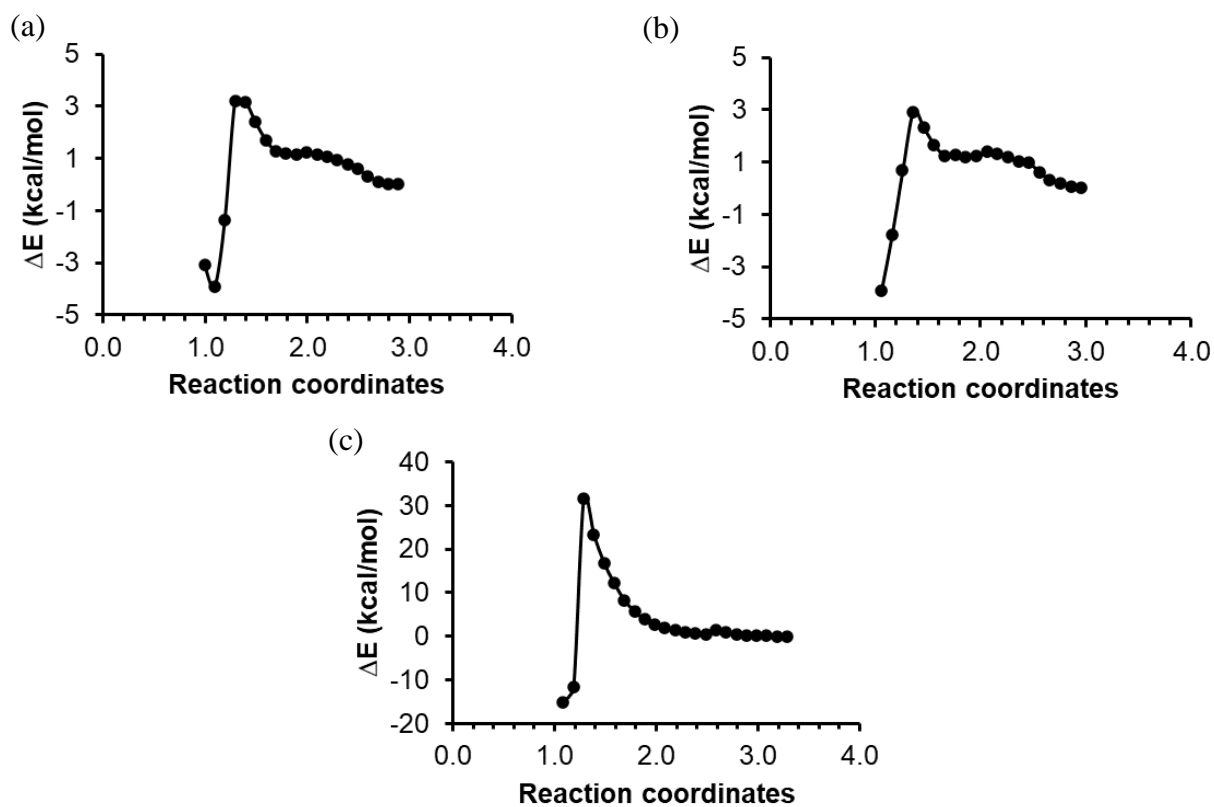
Figure A3. Computed reaction energy profiles slong (a) RP-C2, when H42 is transferred to N1 (b) RP-C3, when H43 is transferred to N4 and (c) RP-C2, when H42 is transferred to C16.
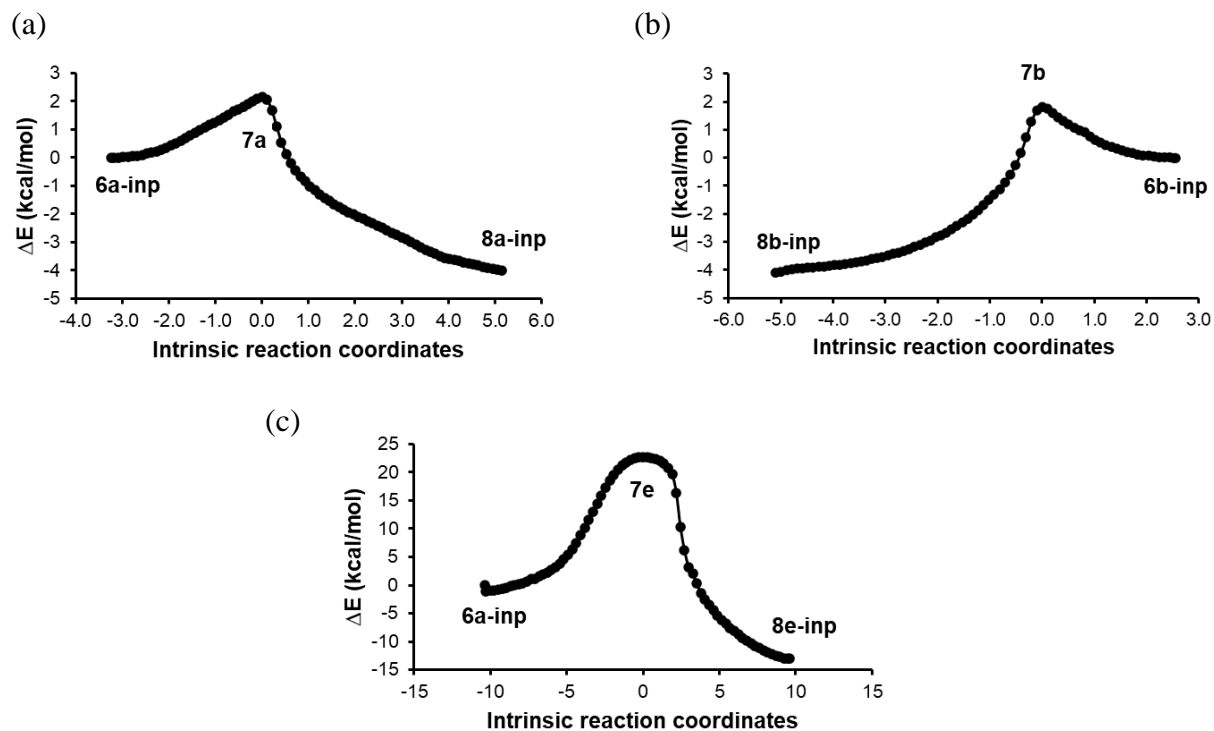
Figure A4. Computed IRC paths for the hydrolysis step along (a) RP-C2, when H42 is transferred to N1 (b) RP-C3, when H43 is transferred to N4 and (c) RP-C2, when H42 is transferred to C16.

Appendix B

(CHAPTER 4)

Table of content

Part 1

XYZ coordinates of molecular systems (Tables B1-B14) and their energies (Tables B15-B20)

Table B1. Cartesian coordinates for 2-phenylquinoxaline (**1**). The structure was optimized at the RB3LYP-GD3/6-311++G(d,p)/THF level of theory at 195.15 K. Coordinate values are given in Å.

Centre number	Atomic number	Atom type	Coordinates		
			X	Y	Z
1	7	N	-2.561578	-5.391291	1.045448
2	6	C	-3.171860	-6.543670	0.840572
3	6	C	-2.414088	-7.727561	0.558092
4	7	N	-1.105299	-7.744966	0.509644
5	6	C	-0.459390	-6.564839	0.738712
6	6	C	0.954497	-6.514524	0.707871
7	6	C	1.603252	-5.321337	0.928172
8	6	C	0.867555	-4.137588	1.184443
9	6	C	-0.507244	-4.158598	1.220148
10	6	C	-1.202551	-5.373876	0.998761
11	1	H	-2.925606	-8.661385	0.348908
12	1	H	1.498488	-7.430306	0.508183
13	1	H	2.686007	-5.280968	0.905732
14	1	H	1.398612	-3.208124	1.354225
15	1	H	-1.085534	-3.263325	1.416276
16	6	C	-4.653299	-6.577944	0.880014
17	6	C	-5.387646	-5.432690	0.535766
18	6	C	-6.778290	-5.448719	0.564783
19	6	C	-7.460046	-6.606220	0.945821
20	6	C	-6.739983	-7.747173	1.298108
21	6	C	-5.347164	-7.735668	1.262930
22	1	H	-4.856216	-4.536676	0.240437
23	1	H	-7.332119	-4.558830	0.287779
24	1	H	-8.543756	-6.617430	0.969693
25	1	H	-7.261274	-8.646153	1.606462
26	1	H	-4.805263	-8.625147	1.561374

Table B2. Cartesian coordinates for 1-octynyllithium (**10**). The structure was optimized at the RB3LYP-GD3/6-311++G(d,p)/THF level of theory at 195.15 K. Coordinate values are given in Å.

Centre number	Atomic number	Atom type	Coordinates		
			X	Y	Z
1	3	Li	-12.768014	-9.649302	7.563487
2	6	C	-12.017959	-8.714676	5.931433
3	6	C	-11.602828	-8.117601	4.936729
4	6	C	-11.130751	-7.377636	3.758942
5	6	C	-11.624406	-5.917407	3.706810
6	6	C	-11.137681	-5.164303	2.465895
7	6	C	-11.619230	-3.711133	2.413497
8	6	C	-11.146306	-2.952407	1.169357
9	6	C	-11.631489	-1.500147	1.132670
10	1	H	-11.452587	-7.890051	2.842368
11	1	H	-10.032916	-7.378707	3.729692
12	1	H	-12.720049	-5.912006	3.735141
13	1	H	-11.288269	-5.396375	4.610511
14	1	H	-11.478078	-5.691290	1.564878
15	1	H	-10.040337	-5.183004	2.435314
16	1	H	-12.716325	-3.691834	2.452149
17	1	H	-11.273167	-3.182263	3.311243
18	1	H	-11.495554	-3.478968	0.272751
19	1	H	-10.050313	-2.973934	1.129438
20	1	H	-12.725296	-1.451511	1.142482
21	1	H	-11.268244	-0.943216	2.002582
22	1	H	-11.282132	-0.982062	0.234961

B3

Table B3. Cartesian coordinates for the adduct along RP-C2 (**11a**). The structure was optimized at the RB3LYP-GD3/6-311++G(d,p)/THF level of theory at 195.15 K. Coordinate values are given in Å.

Centre number	Atomic number	Atom type	Coordinates		
			X	Y	Z
1	7	N	-3.141527	-6.103335	1.210924
2	6	C	-3.841144	-7.059249	0.620624
3	6	C	-3.519795	-8.436220	0.837172
4	7	N	-2.532590	-8.826607	1.603027
5	6	C	-1.777978	-7.854489	2.191318
6	6	C	-0.686375	-8.217424	3.014886
7	6	C	0.083907	-7.241792	3.601355
8	6	C	-0.207058	-5.872545	3.388791
9	6	C	-1.268434	-5.492198	2.601570
10	6	C	-2.078830	-6.474962	1.985420
11	1	H	-4.103185	-9.205566	0.341614
12	1	H	-0.485686	-9.270958	3.166966
13	1	H	0.917882	-7.517345	4.235697
14	1	H	0.411003	-5.117554	3.860196
15	1	H	-1.501740	-4.446256	2.443391
16	6	C	-4.949369	-6.679227	-0.284668
17	6	C	-4.796135	-5.592493	-1.159831
18	6	C	-5.830920	-5.227851	-2.016637
19	6	C	-7.030911	-5.940451	-2.008387
20	6	C	-7.190423	-7.022492	-1.142316
21	6	C	-6.155229	-7.394756	-0.288486
22	1	H	-3.857235	-5.051048	-1.175485
23	1	H	-5.698792	-4.393504	-2.695839
24	1	H	-7.836806	-5.655100	-2.674663
25	1	H	-8.123644	-7.573316	-1.126456
26	1	H	-6.295977	-8.224088	0.394878
27	3	Li	-4.310885	-4.382686	1.842975
28	6	C	-4.787653	-4.643227	3.789448
29	6	C	-4.636953	-5.278357	4.834307
30	6	C	-4.336253	-6.104312	6.010557
31	6	C	-3.203349	-7.115452	5.737735
32	6	C	-2.846677	-7.972810	6.953822
33	6	C	-1.704077	-8.955095	6.677924
34	6	C	-1.332892	-9.822246	7.884443
35	6	C	-0.183522	-10.791398	7.591864
36	1	H	-5.231318	-6.650211	6.337630
37	1	H	-4.047773	-5.469570	6.859246
38	1	H	-3.498505	-7.761539	4.903247
39	1	H	-2.317388	-6.569205	5.398533
40	1	H	-3.733752	-8.529609	7.283461
41	1	H	-2.567043	-7.319225	7.790782
42	1	H	-1.979251	-9.603454	5.835849
43	1	H	-0.819729	-8.395216	6.348524
44	1	H	-2.215765	-10.386553	8.209008
45	1	H	-1.059756	-9.172132	8.724823
46	1	H	-0.443669	-11.472695	6.775141
47	1	H	0.720046	-10.248932	7.294540
48	1	H	0.064542	-11.398619	8.467177

Table B4. Cartesian coordinates for the transition state along RP-C2 (**12a**). The structure was optimized at the RB3LYP-GD3/6-311++G(d,p)/THF level of theory at 195.15 K. Coordinate values are given in Å.

Centre number	Atomic number	Atom type	Coordinates		
			X	Y	Z
1	7	N	-2.598617	-5.269659	0.605368
2	6	C	-3.326456	-6.233135	1.267282
3	6	C	-2.569014	-7.429356	1.728931
4	7	N	-1.289603	-7.466346	1.848817
5	6	C	-0.580959	-6.324881	1.487350
6	6	C	0.804796	-6.274269	1.703059
7	6	C	1.546106	-5.179312	1.285997
8	6	C	0.899522	-4.124338	0.616415
9	6	C	-0.465284	-4.160144	0.386059
10	6	C	-1.250953	-5.251583	0.832313
11	1	H	-3.137819	-8.316726	1.995306
12	1	H	1.275541	-7.115156	2.201296
13	1	H	2.614603	-5.140540	1.462357
14	1	H	1.476783	-3.271762	0.274359
15	1	H	-0.959762	-3.349336	-0.139375
16	6	C	-4.668080	-6.564978	0.635263
17	6	C	-4.922583	-6.174608	-0.682986
18	6	C	-6.120583	-6.522245	-1.310238
19	6	C	-7.073205	-7.280238	-0.633036
20	6	C	-6.821662	-7.683863	0.680464
21	6	C	-5.633479	-7.324319	1.309854
22	1	H	-4.169334	-5.605062	-1.211667
23	1	H	-6.302001	-6.206749	-2.331913
24	1	H	-8.001549	-7.556036	-1.120678
25	1	H	-7.556907	-8.272626	1.217855
26	1	H	-5.461330	-7.613168	2.339224
27	3	Li	-3.587528	-3.842528	1.649777
28	6	C	-3.858612	-5.558432	2.978176
29	6	C	-3.968203	-5.938279	4.139863
30	6	C	-4.056119	-6.462651	5.500427
31	6	C	-3.451254	-7.880574	5.606462
32	6	C	-3.515751	-8.442488	7.028638
33	6	C	-2.917318	-9.847764	7.143141
34	6	C	-2.972019	-10.420728	8.563080
35	6	C	-2.366993	-11.823970	8.664849
36	1	H	-5.101667	-6.488505	5.830331
37	1	H	-3.528423	-5.794335	6.191420
38	1	H	-3.985111	-8.547194	4.920226
39	1	H	-2.411594	-7.850741	5.264302
40	1	H	-4.560195	-8.463364	7.365522
41	1	H	-2.985555	-7.765536	7.710702
42	1	H	-3.447260	-10.524277	6.460063
43	1	H	-1.874117	-9.825566	6.802481
44	1	H	-4.015055	-10.444862	8.901796
45	1	H	-2.444100	-9.742984	9.245047
46	1	H	-2.896488	-12.527601	8.014301
47	1	H	-1.315194	-11.820265	8.361018
48	1	H	-2.418229	-12.210293	9.686800

B5

Table B5. Cartesian coordinates for the intermediate along RP-C2 (**13a**). The structure was optimized at the RB3LYP-GD3/6-311++G(d,p)/THF level of theory at 195.15 K. Coordinate values are given in Å.

Centre number	Atomic number	Atom type	Coordinates		
			X	Y	Z
1	7	N	-2.704843	-5.636688	1.300258
2	6	C	-3.578302	-6.768405	0.925658
3	6	C	-2.927907	-7.600129	-0.194501
4	7	N	-1.664199	-7.745812	-0.319327
5	6	C	-0.832578	-7.014272	0.536965
6	6	C	0.541440	-7.278630	0.539558
7	6	C	1.430639	-6.469446	1.237487
8	6	C	0.925065	-5.340424	1.905223
9	6	C	-0.431188	-5.055469	1.909378
10	6	C	-1.376445	-5.905921	1.267178
11	1	H	-3.589536	-8.097517	-0.902630
12	1	H	0.894695	-8.128617	-0.036474
13	1	H	2.491604	-6.689474	1.246677
14	1	H	1.605589	-4.679637	2.433754
15	1	H	-0.792061	-4.178939	2.441244
16	6	C	-4.919153	-6.214135	0.414412
17	6	C	-4.901875	-5.343461	-0.684473
18	6	C	-6.083903	-4.803434	-1.185569
19	6	C	-7.307896	-5.123791	-0.593233
20	6	C	-7.335237	-5.990958	0.496700
21	6	C	-6.147897	-6.534941	0.994458
22	1	H	-3.952411	-5.089119	-1.141217
23	1	H	-6.051603	-4.135246	-2.039255
24	1	H	-8.228993	-4.703497	-0.981332
25	1	H	-8.280049	-6.248635	0.962774
26	1	H	-6.176467	-7.212247	1.839673
27	3	Li	-3.581179	-4.085629	2.093676
28	6	C	-3.766494	-7.675699	2.081154
29	6	C	-3.833831	-8.410200	3.037163
30	6	C	-3.890142	-9.265135	4.220415
31	6	C	-3.237461	-8.620549	5.460091
32	6	C	-3.290119	-9.529758	6.690253
33	6	C	-2.639306	-8.904149	7.927497
34	6	C	-2.686395	-9.807439	9.164174
35	6	C	-2.028792	-9.173340	10.393333
36	1	H	-3.391216	-10.216935	4.002584
37	1	H	-4.934757	-9.511601	4.445487
38	1	H	-2.196835	-8.373044	5.225138
39	1	H	-3.743194	-7.673103	5.677750
40	1	H	-2.791771	-10.480118	6.460246
41	1	H	-4.335510	-9.777346	6.915687
42	1	H	-1.594161	-8.656961	7.700560
43	1	H	-3.136020	-7.952215	8.156772
44	1	H	-2.192194	-10.758960	8.933281
45	1	H	-3.731155	-10.052274	9.391619
46	1	H	-0.974742	-8.947941	10.201509
47	1	H	-2.524058	-8.234857	10.663136
48	1	H	-2.075771	-9.837266	11.261195

Table B6. Cartesian coordinates for the adduct along RP-C3 (**11b**). The structure was optimized at the RB3LYP-GD3/6-311++G(d,p)/THF level of theory at 195.15 K. Coordinate values are given in Å.

Centre number	Atomic number	Atom type	Coordinates		
			X	**Y**	**Z**
1	7	N	-2.583278	-6.349571	0.796640
2	6	C	-2.917503	-7.617904	0.646386
3	6	C	-1.919098	-8.602957	0.357502
4	7	N	-0.643250	-8.308212	0.246441
5	6	C	-0.277023	-7.000299	0.409025
6	6	C	1.078973	-6.617472	0.299589
7	6	C	1.433497	-5.297294	0.458057
8	6	C	0.449700	-4.314932	0.729111
9	6	C	-0.876597	-4.661794	0.838558
10	6	C	-1.271460	-6.014007	0.680974
11	1	H	-2.179677	-9.644709	0.202472
12	1	H	1.820977	-7.378345	0.087793
13	1	H	2.472845	-5.002533	0.374648
14	1	H	0.750256	-3.280832	0.850019
15	1	H	-1.643073	-3.924615	1.045703
16	6	C	-4.344823	-7.999025	0.759817
17	6	C	-5.344515	-7.041574	0.526015
18	6	C	-6.688772	-7.383497	0.627158
19	6	C	-7.058655	-8.685545	0.970825
20	6	C	-6.073559	-9.642454	1.210474
21	6	C	-4.726669	-9.305319	1.102325
22	1	H	-5.054878	-6.033186	0.258911
23	1	H	-7.449546	-6.635411	0.435145
24	1	H	-8.106579	-8.951509	1.050513
25	1	H	-6.350820	-10.653479	1.481604
26	1	H	-3.980229	-10.063351	1.304281
27	3	Li	0.497944	-10.039719	-0.152050
28	6	C	-0.659642	-11.712889	-0.161821
29	6	C	-1.534484	-12.580665	-0.146690
30	6	C	-2.607945	-13.582836	-0.120953
31	6	C	-3.968208	-13.020226	0.338146
32	6	C	-5.079377	-14.073574	0.341569
33	6	C	-6.435403	-13.520808	0.789273
34	6	C	-7.555378	-14.565734	0.797039
35	6	C	-8.903282	-13.991041	1.242757
36	1	H	-2.330889	-14.414760	0.540267
37	1	H	-2.731091	-14.025163	-1.118587
38	1	H	-3.857002	-12.599007	1.344230
39	1	H	-4.249697	-12.188098	-0.316850
40	1	H	-4.791366	-14.904064	0.999169
41	1	H	-5.177971	-14.499830	-0.665231
42	1	H	-6.336898	-13.093637	1.796183
43	1	H	-6.722570	-12.691404	0.130224
44	1	H	-7.271526	-15.393492	1.458292
45	1	H	-7.653182	-14.995624	-0.207282
46	1	H	-8.838863	-13.581073	2.256001
47	1	H	-9.223021	-13.181734	0.578172
48	1	H	-9.686749	-14.754197	1.240532

B7

Table B7. Cartesian coordinates for the transition state along RP-C3 (**12b**). The structure was optimized at the RB3LYP-GD3/6-311++G(d,p)/THF level of theory at 195.15 K. Coordinate values are given in Å.

Centre number	Atomic number	Atom type	Coordinates		
			X	Y	Z
1	7	N	-2.760422	-7.391366	0.570417
2	6	C	-2.904911	-8.193514	-0.440770
3	6	C	-1.733594	-8.575473	-1.274779
4	7	N	-0.620643	-7.770372	-1.245468
5	6	C	-0.460795	-7.004138	-0.126801
6	6	C	0.752175	-6.310989	0.110819
7	6	C	0.915831	-5.537806	1.246232
8	6	C	-0.125176	-5.406220	2.186728
9	6	C	-1.332394	-6.044349	1.960175
10	6	C	-1.519686	-6.842309	0.815561
11	1	H	-1.973406	-8.923158	-2.272909
12	1	H	1.551159	-6.403962	-0.617797
13	1	H	1.857131	-5.025052	1.413431
14	1	H	0.015684	-4.798238	3.072699
15	1	H	-2.161859	-5.942144	2.651889
16	6	C	-4.246604	-8.764247	-0.711625
17	6	C	-5.318437	-8.466693	0.149000
18	6	C	-6.571029	-9.036480	-0.043948
19	6	C	-6.789328	-9.917211	-1.106249
20	6	C	-5.741062	-10.212138	-1.975259
21	6	C	-4.483802	-9.642864	-1.781234
22	1	H	-5.145136	-7.795626	0.979950
23	1	H	-7.378786	-8.801223	0.640172
24	1	H	-7.764051	-10.369136	-1.251266
25	1	H	-5.895846	-10.896005	-2.802269
26	1	H	-3.685346	-9.915007	-2.457626
27	3	Li	0.524795	-9.437698	-1.172959
28	6	C	-1.363452	-10.340129	-0.637410
29	6	C	-2.068783	-11.314313	-0.385011
30	6	C	-2.954476	-12.432738	-0.070636
31	6	C	-4.051708	-12.068172	0.951029
32	6	C	-5.042750	-13.211358	1.178090
33	6	C	-6.169103	-12.837892	2.146272
34	6	C	-7.184567	-13.963919	2.364279
35	6	C	-8.310992	-13.576038	3.326624
36	1	H	-2.366368	-13.277708	0.309408
37	1	H	-3.428752	-12.783881	-0.995969
38	1	H	-3.579914	-11.784902	1.898236
39	1	H	-4.590175	-11.187995	0.593225
40	1	H	-4.511349	-14.094452	1.556209
41	1	H	-5.480146	-13.503857	0.214500
42	1	H	-5.736840	-12.547847	3.112793
43	1	H	-6.688876	-11.949523	1.764981
44	1	H	-6.663715	-14.850390	2.746605
45	1	H	-7.612293	-14.254073	1.396653
46	1	H	-7.911821	-13.310543	4.310931
47	1	H	-8.866638	-12.710627	2.950999
48	1	H	-9.022099	-14.395619	3.464455

Table B8. Cartesian coordinates for the intermediate along RP-C3 (**13b**). The structure was optimized at the RB3LYP-GD3/6-311++G(d,p)/THF level of theory at 195.15 K. Coordinate values are given in Å.

Centre number	Atomic number	Atom type	Coordinates		
			X	Y	Z
1	7	N	-2.925785	-6.915153	0.144115
2	6	C	-3.230451	-7.721276	-0.818328
3	6	C	-2.237433	-8.809389	-1.251495
4	7	N	-0.856857	-8.311440	-1.196166
5	6	C	-0.589684	-7.581728	-0.087725
6	6	C	0.742059	-7.340894	0.351294
7	6	C	1.005472	-6.616569	1.501843
8	6	C	-0.038227	-6.060956	2.265927
9	6	C	-1.344940	-6.215871	1.823238
10	6	C	-1.638459	-6.950249	0.663990
11	1	H	-2.447593	-9.080224	-2.291249
12	1	H	1.560062	-7.779064	-0.213796
13	1	H	2.034396	-6.484721	1.822429
14	1	H	0.177365	-5.503875	3.170172
15	1	H	-2.172206	-5.754984	2.354115
16	6	C	-4.548078	-7.608902	-1.478915
17	6	C	-5.322020	-6.443074	-1.328344
18	6	C	-6.569621	-6.330928	-1.929867
19	6	C	-7.080466	-7.381513	-2.698155
20	6	C	-6.328279	-8.544629	-2.852975
21	6	C	-5.075176	-8.657771	-2.251893
22	1	H	-4.923279	-5.630309	-0.734505
23	1	H	-7.146492	-5.420903	-1.805346
24	1	H	-8.053458	-7.292648	-3.168162
25	1	H	-6.718381	-9.370257	-3.437990
26	1	H	-4.521928	-9.581679	-2.367023
27	3	Li	0.350237	-8.824661	-2.618575
28	6	C	-2.445011	-10.026364	-0.433259
29	6	C	-2.600944	-11.012518	0.246175
30	6	C	-2.841772	-12.188685	1.079855
31	6	C	-4.337843	-12.427702	1.367770
32	6	C	-4.574981	-13.661565	2.241933
33	6	C	-6.056647	-13.916448	2.533919
34	6	C	-6.301871	-15.150941	3.407691
35	6	C	-7.786346	-15.397176	3.692407
36	1	H	-2.304332	-12.075631	2.028938
37	1	H	-2.420638	-13.077000	0.593695
38	1	H	-4.752763	-11.539871	1.856745
39	1	H	-4.870950	-12.538484	0.417101
40	1	H	-4.033632	-13.544569	3.189524
41	1	H	-4.145713	-14.543862	1.749580
42	1	H	-6.485960	-13.034267	3.026141
43	1	H	-6.598432	-14.031509	1.586059
44	1	H	-5.760734	-15.034559	4.354635
45	1	H	-5.871406	-16.031582	2.915277
46	1	H	-8.232796	-14.543133	4.211907
47	1	H	-8.344439	-15.547174	2.762476
48	1	H	-7.933922	-16.282692	4.317198

Table B9. Cartesian coordinates for **14a**. The structure was optimized at the RB3LYP-GD3/6-311++G(d,p)/THF level of theory at 298.15 K. Coordinate values are given in Å.

Centre number	Atomic number	Atom type	Coordinates		
			X	Y	Z
1	7	N	-2.627193	-5.630746	1.342904
2	6	C	-3.545134	-6.714912	0.947095
3	6	C	-2.938615	-7.550648	-0.195745
4	7	N	-1.682285	-7.734303	-0.342272
5	6	C	-0.813304	-7.049347	0.514081
6	6	C	0.551961	-7.356465	0.489784
7	6	C	1.475388	-6.592614	1.193767
8	6	C	1.014952	-5.464460	1.896001
9	6	C	-0.330583	-5.136686	1.925848
10	6	C	-1.311224	-5.942002	1.277690
11	1	H	-3.627715	-8.010825	-0.902510
12	1	H	0.870758	-8.203428	-0.110227
13	1	H	2.529005	-6.845295	1.181868
14	1	H	1.723567	-4.838129	2.429538
15	1	H	-0.658683	-4.261481	2.480327
16	6	C	-4.876894	-6.119829	0.456366
17	6	C	-4.839694	-5.081484	-0.482790
18	6	C	-6.017695	-4.527365	-0.979547
19	6	C	-7.255995	-5.006508	-0.547350
20	6	C	-7.302111	-6.045881	0.379812
21	6	C	-6.119588	-6.599566	0.875611
22	1	H	-3.878066	-4.708303	-0.814323
23	1	H	-5.969662	-3.723577	-1.706164
24	1	H	-8.173513	-4.575842	-0.932514
25	1	H	-8.257989	-6.428894	0.720256
26	1	H	-6.165101	-7.407730	1.596050
27	3	Li	-3.433977	-4.249908	2.486931
28	6	C	-3.754549	-7.632368	2.097228
29	6	C	-3.820487	-8.352750	3.066111
30	6	C	-3.861941	-9.202565	4.254171
31	6	C	-3.192686	-8.550879	5.481564
32	6	C	-3.225992	-9.457083	6.714384
33	6	C	-2.568499	-8.821584	7.942962
34	6	C	-2.595568	-9.722041	9.182275
35	6	C	-1.936077	-9.076788	10.404557
36	1	H	-3.363141	-10.152250	4.028862
37	1	H	-4.902948	-9.450467	4.492293
38	1	H	-2.156701	-8.300799	5.230292
39	1	H	-3.696668	-7.603953	5.705604
40	1	H	-2.722245	-10.403888	6.481975
41	1	H	-4.267103	-9.712204	6.950752
42	1	H	-1.528069	-8.565422	7.705000
43	1	H	-3.071804	-7.873683	8.174211
44	1	H	-2.092168	-10.668401	8.950117
45	1	H	-3.635654	-9.978265	9.418474
46	1	H	-0.886409	-8.839067	10.203939
47	1	H	-2.440648	-8.143741	10.675880
48	1	H	-1.968253	-9.739078	11.274320
49	8	O	-4.488460	-5.207456	3.847581
50	1	H	-4.378081	-6.149118	3.622019
51	1	H	-5.420775	-5.091548	4.060512

Table B10. Cartesian coordinates for **15a**. The structure was optimized at the RB3LYP-GD3/6-311++G(d,p)/THF level of theory at 298.15 K. Coordinate values are given in Å.

Centre number	Atomic number	Atom type	Coordinates		
			X	Y	Z
1	7	N	-2.570584	-5.697351	1.358401
2	6	C	-3.487733	-6.791610	0.977167
3	6	C	-2.945089	-7.505625	-0.272781
4	7	N	-1.705367	-7.602060	-0.559127
5	6	C	-0.782408	-6.950620	0.276778
6	6	C	0.582607	-7.202381	0.108851
7	6	C	1.534016	-6.508906	0.849917
8	6	C	1.103650	-5.529608	1.755647
9	6	C	-0.248352	-5.261132	1.930721
10	6	C	-1.230614	-5.974880	1.208680
11	1	H	-3.674407	-7.977628	-0.929579
12	1	H	0.877543	-7.949501	-0.620731
13	1	H	2.589813	-6.716789	0.722809
14	1	H	1.833011	-4.977706	2.339770
15	1	H	-0.569640	-4.518302	2.653132
16	6	C	-4.866223	-6.182787	0.676942
17	6	C	-5.052778	-5.472705	-0.516597
18	6	C	-6.273013	-4.862319	-0.800111
19	6	C	-7.326902	-4.947267	0.111601
20	6	C	-7.149068	-5.650075	1.301907
21	6	C	-5.927752	-6.266845	1.579577
22	1	H	-4.236931	-5.394002	-1.227030
23	1	H	-6.402190	-4.324792	-1.733030
24	1	H	-8.277374	-4.473828	-0.107271
25	1	H	-7.961543	-5.723242	2.016387
26	1	H	-5.797731	-6.817751	2.503252
27	3	Li	-3.285773	-3.493680	1.508282
28	6	C	-3.557870	-7.802815	2.055275
29	6	C	-3.525735	-8.599466	2.960895
30	6	C	-3.480666	-9.501502	4.108318
31	6	C	-3.321742	-8.746914	5.444574
32	6	C	-3.261056	-9.688223	6.649698
33	6	C	-3.108645	-8.944729	7.980177
34	6	C	-3.042455	-9.874391	9.196147
35	6	C	-2.892242	-9.117440	10.519043
36	1	H	-2.648983	-10.205056	3.985464
37	1	H	-4.394512	-10.106548	4.136205
38	1	H	-2.412274	-8.138303	5.402449
39	1	H	-4.158945	-8.049770	5.560621
40	1	H	-2.422321	-10.384904	6.524787
41	1	H	-4.170166	-10.302612	6.678745
42	1	H	-2.201525	-8.327464	7.947907
43	1	H	-3.948074	-8.248051	8.103887
44	1	H	-2.202391	-10.568709	9.072862
45	1	H	-3.948421	-10.491989	9.227092
46	1	H	-1.977872	-8.515319	10.524516
47	1	H	-3.736091	-8.438755	10.680590
48	1	H	-2.846472	-9.802157	11.370675
49	8	O	-3.274734	-4.268764	3.247240
50	1	H	-2.939494	-5.091233	2.480529
51	1	H	-3.973144	-4.608604	3.812635

Table B11. Cartesian coordinates for **16a**. The structure was optimized at the RB3LYP-GD3/6-311++G(d,p)/THF level of theory at 298.15 K. Coordinate values are given in Å.

Centre number	Atomic number	Atom type	Coordinates		
			X	Y	Z
1	7	N	-2.592490	-5.720796	1.293425
2	6	C	-3.537897	-6.801803	1.006560
3	6	C	-2.951800	-7.632080	-0.154661
4	7	N	-1.705768	-7.756416	-0.396796
5	6	C	-0.792975	-7.043636	0.400652
6	6	C	0.573461	-7.316264	0.297138
7	6	C	1.503210	-6.575620	1.021079
8	6	C	1.054559	-5.532208	1.840979
9	6	C	-0.300620	-5.241455	1.952980
10	6	C	-1.248611	-6.001117	1.244355
11	1	H	-3.668410	-8.165940	-0.776074
12	1	H	0.887149	-8.115471	-0.365700
13	1	H	2.560905	-6.797134	0.943158
14	1	H	1.770693	-4.942381	2.403339
15	1	H	-0.646656	-4.434665	2.589515
16	6	C	-4.874937	-6.186521	0.565475
17	6	C	-4.862430	-5.205432	-0.433771
18	6	C	-6.050280	-4.621170	-0.868642
19	6	C	-7.269352	-5.008874	-0.307425
20	6	C	-7.288479	-5.990776	0.681347
21	6	C	-6.097408	-6.580278	1.111835
22	1	H	-3.915780	-4.894707	-0.859060
23	1	H	-6.024701	-3.863910	-1.644384
24	1	H	-8.194101	-4.553056	-0.643023
25	1	H	-8.229689	-6.301768	1.120982
26	1	H	-6.117318	-7.338706	1.884830
27	3	Li	-5.113695	-3.382233	2.445125
28	6	C	-3.691237	-7.720003	2.154532
29	6	C	-3.734988	-8.484007	3.086895
30	6	C	-3.776063	-9.367422	4.248222
31	6	C	-3.266864	-8.689575	5.536718
32	6	C	-3.309034	-9.629261	6.744139
33	6	C	-2.809786	-8.971734	8.034082
34	6	C	-2.846529	-9.906370	9.247613
35	6	C	-2.346412	-9.238845	10.531986
36	1	H	-3.173727	-10.260374	4.043966
37	1	H	-4.803678	-9.717623	4.401512
38	1	H	-2.242283	-8.339117	5.373565
39	1	H	-3.874092	-7.799991	5.735809
40	1	H	-2.702891	-10.519446	6.532726
41	1	H	-4.336793	-9.985030	6.892604
42	1	H	-1.782878	-8.614060	7.884463
43	1	H	-3.416110	-8.081296	8.245352
44	1	H	-2.239820	-10.795148	9.035478
45	1	H	-3.872829	-10.264291	9.395308
46	1	H	-1.311587	-8.899407	10.420094
47	1	H	-2.956045	-8.364660	10.782718
48	1	H	-2.382475	-9.926256	11.381917
49	8	O	-3.569842	-3.920489	3.104893
50	1	H	-2.919868	-5.036608	2.019876
51	1	H	-3.135066	-3.966198	3.957867

Table B12. Cartesian coordinates for **17b**. The structure was optimized at the RB3LYP-GD3/6-311++G(d,p)/THF level of theory at 298.15 K. Coordinate values are given in Å.

Centre number	Atomic number	Atom type	Coordinates		
			X	Y	Z
1	7	N	-2.866925	-6.402190	-0.465141
2	6	C	-3.186511	-7.651492	-0.207381
3	6	C	-2.157241	-8.664973	-0.084807
4	7	N	-0.870861	-8.355483	-0.189331
5	6	C	-0.533628	-7.053768	-0.417276
6	6	C	0.829634	-6.681129	-0.522189
7	6	C	1.150583	-5.368063	-0.781215
8	6	C	0.140550	-4.387974	-0.944240
9	6	C	-1.188800	-4.728101	-0.843046
10	6	C	-1.553099	-6.068992	-0.574687
11	1	H	0.348454	-8.962145	-2.898074
12	1	H	1.592550	-7.444498	-0.395423
13	1	H	2.191247	-5.076660	-0.863405
14	1	H	0.422141	-3.361671	-1.149070
15	1	H	-1.977146	-3.994285	-0.960763
16	6	C	-4.632633	-7.978340	-0.106397
17	6	C	-5.512051	-7.477193	-1.075815
18	6	C	-6.873461	-7.759956	-1.006603
19	6	C	-7.375267	-8.533212	0.041322
20	6	C	-6.508409	-9.020150	1.019546
21	6	C	-5.144494	-8.749314	0.944743
22	1	H	-5.119070	-6.873817	-1.885287
23	1	H	-7.541830	-7.378055	-1.769886
24	1	H	-8.435456	-8.752988	0.095841
25	1	H	-6.892706	-9.614258	1.840650
26	1	H	-4.480043	-9.130739	1.709293
27	3	Li	0.619755	-9.864627	-0.402527
28	6	C	-2.500464	-10.034570	0.098438
29	6	C	-2.824452	-11.188486	0.246170
30	6	C	-3.327797	-12.538199	0.455834
31	6	C	-4.786391	-12.537632	0.960226
32	6	C	-5.336905	-13.950232	1.164316
33	6	C	-6.787388	-13.952633	1.656625
34	6	C	-7.357749	-15.358591	1.868531
35	6	C	-8.809726	-15.346100	2.355247
36	1	H	-2.682835	-13.061217	1.171187
37	1	H	-3.259853	-13.096707	-0.485318
38	1	H	-4.836987	-11.980528	1.901579
39	1	H	-5.410066	-11.993114	0.244358
40	1	H	-4.706593	-14.487962	1.883888
41	1	H	-5.272173	-14.506487	0.220646
42	1	H	-6.851473	-13.391255	2.597863
43	1	H	-7.414668	-13.413008	0.935351
44	1	H	-6.732150	-15.895642	2.591813
45	1	H	-7.290221	-15.919725	0.928608
46	1	H	-8.899298	-14.816256	3.309158
47	1	H	-9.460659	-14.841483	1.633929
48	1	H	-9.193389	-16.360071	2.499087
49	8	O	2.415251	-9.525300	-0.334255
50	1	H	3.181195	-9.906378	0.098287
51	1	H	2.421546	-9.634280	-1.767642
52	8	O	0.666479	-9.795548	-2.524128
53	8	O	2.106242	-9.717770	-2.780079

Table B13. Cartesian coordinates for **15e**. The structure was optimized at the RB3LYP-GD3/6-311++G(d,p)/THF level of theory at 298.15 K. Coordinate values are given in Å.

Centre number	Atomic number	Atom type	Coordinates		
			X	**Y**	**Z**
1	7	N	-0.88145	-6.45296	1.36945
2	6	C	-1.93283	-7.28809	1.55464
3	6	C	-2.58368	-7.88083	0.38268
4	7	N	-2.36977	-7.48974	-0.82754
5	6	C	-1.46886	-6.44688	-1.00046
6	6	C	-1.27750	-5.91241	-2.28436
7	6	C	-0.35725	-4.89890	-2.49820
8	6	C	0.40655	-4.41883	-1.41913
9	6	C	0.23941	-4.93756	-0.14698
10	6	C	-0.71592	-5.95051	0.10299
11	1	H	-3.29170	-8.68746	0.55187
12	1	H	-1.87041	-6.31550	-3.09803
13	1	H	-0.21935	-4.48452	-3.48987
14	1	H	1.13565	-3.63304	-1.58434
15	1	H	0.83527	-4.56039	0.67786
16	6	C	-3.82333	-6.06536	1.99227
17	6	C	-4.02609	-4.99690	1.10482
18	6	C	-5.30693	-4.63702	0.67581
19	6	C	-6.41787	-5.35722	1.12399
20	6	C	-6.23887	-6.42966	2.00183
21	6	C	-4.95045	-6.77818	2.41994
22	1	H	-3.17134	-4.43011	0.74155
23	1	H	-5.44269	-3.80262	-0.00675
24	1	H	-7.41384	-5.08725	0.78872
25	1	H	-7.10079	-6.99038	2.35321
26	1	H	-4.82333	-7.62550	3.09238
27	3	Li	-0.27343	-5.56098	3.10050
28	6	C	-1.97841	-8.05706	2.76683
29	6	C	-2.03967	-8.74070	3.75948
30	6	C	-2.16691	-9.50500	4.99557
31	6	C	-3.14942	-8.86315	5.99748
32	6	C	-3.26779	-9.66815	7.29368
33	6	C	-4.24136	-9.04677	8.29944
34	6	C	-4.36511	-9.84659	9.60043
35	6	C	-5.34031	-9.21681	10.59923
36	1	H	-1.18090	-9.60621	5.46423
37	1	H	-2.49899	-10.52270	4.75918
38	1	H	-2.81689	-7.84366	6.21982
39	1	H	-4.13251	-8.77331	5.52326
40	1	H	-2.27676	-9.75925	7.75676
41	1	O	-3.59217	-10.68998	7.05850
42	1	H	-3.91765	-8.02419	8.53318
43	1	H	-5.23206	-8.95529	7.83576
44	1	H	-3.37437	-9.93801	10.06224
45	1	H	-4.68872	-10.86789	9.36534
46	1	H	-5.02210	-8.20588	10.87390
47	1	H	-6.34560	-9.14254	10.17208
48	1	H	-5.41035	-9.80623	11.51784
49	8	O	-1.96766	-5.09608	3.81377
50	1	H	-2.65577	-5.52054	3.18595
51	1	H	-2.36477	-4.27859	4.12771

Table B14. Cartesian coordinates for **16e**. The structure was optimized at the RB3LYP-GD3/6-311++G(d,p)/THF level of theory at 298.15 K. Coordinate values are given in Å.

Centre number	Atomic number	Atom type	Coordinates		
			X	Y	Z
1	7	N	-1.840337	-6.663115	1.508941
2	6	C	-2.353477	-7.877026	1.349411
3	6	C	-2.347660	-8.521758	0.071369
4	7	N	-1.857879	-7.956971	-1.000574
5	6	C	-1.344272	-6.700368	-0.864763
6	6	C	-0.832527	-6.029607	-2.000147
7	6	C	-0.319208	-4.759973	-1.874650
8	6	C	-0.292826	-4.117275	-0.612555
9	6	C	-0.783109	-4.744653	0.508151
10	6	C	-1.325823	-6.048624	0.406327
11	1	H	-2.768595	-9.518020	-0.019515
12	1	H	-0.861648	-6.541603	-2.954498
13	1	H	0.069696	-4.243367	-2.744108
14	1	H	0.116307	-3.117001	-0.533380
15	1	H	-0.773435	-4.251657	1.472620
16	6	C	-4.999224	-4.838878	2.005684
17	6	C	-4.393891	-4.201563	0.921816
18	6	C	-4.337051	-4.836996	-0.318553
19	6	C	-4.885606	-6.110338	-0.475243
20	6	C	-5.491254	-6.748018	0.608532
21	6	C	-5.546653	-6.113258	1.849377
22	1	H	-3.955105	-3.218232	1.047922
23	1	H	-3.851186	-4.349561	-1.156304
24	1	H	-4.829593	-6.609454	-1.435949
25	1	H	-5.907022	-7.742318	0.489024
26	1	H	-6.004950	-6.613949	2.694754
27	3	Li	-2.083694	-5.831515	3.468333
28	6	C	-2.922775	-8.528721	2.477651
29	6	C	-3.415289	-9.050163	3.449522
30	6	C	-3.979213	-9.624883	4.661872
31	6	C	-3.306860	-9.082694	5.941072
32	6	C	-3.917570	-9.675079	7.213039
33	6	C	-3.253355	-9.151520	8.489994
34	6	C	-3.857130	-9.732751	9.772533
35	6	C	-3.182243	-9.204954	11.041939
36	1	H	-3.885735	-10.716040	4.623032
37	1	H	-5.053903	-9.407372	4.688575
38	1	H	-2.236084	-9.308456	5.902857
39	1	H	-3.396999	-7.991722	5.957065
40	1	H	-3.834954	-10.769043	7.182076
41	1	O	-4.990658	-9.447033	7.241314
42	1	H	-2.180249	-9.380274	8.459857
43	1	H	-3.331920	-8.057252	8.516535
44	1	H	-3.780438	-10.826579	9.743405
45	1	H	-4.928816	-9.501228	9.802920
46	1	H	-2.115510	-9.451200	11.050272
47	1	H	-3.270698	-8.115847	11.109127
48	1	H	-3.631145	-9.633061	11.942707
49	8	O	-2.058387	-4.832821	4.850952
50	1	H	-5.031380	-4.349269	2.972508
51	1	H	-2.041375	-4.282928	5.631674

Table B15. Energetic information for the reactants (**1** and **10**). The structures were optimized at the RB3LYP-GD3/6-311++G(d,p)/THF level of theory at 195.15 K and 1 atm. Energy values are given in Hartree (a.u.) units.

	REACTANTS	
	1	**10**
Electronic Energy (EE)	-649.2102	-320.3090
Zero-point Energy Correction	0.2036	0.1881
Thermal Correction to Energy	0.2087	0.1940
Thermal Correction to Enthalpy	0.2093	0.1947
Thermal Correction to Free Energy	0.1814	0.1661
EE + Zero-point Energy	-649.0067	-320.1209
EE + Thermal Energy Correction	-649.0016	-320.1149
EE + Thermal Enthalpy Correction	-649.0010	-320.1143
EE + Thermal Free Energy Correction	-649.0288	-320.1429

Table B16. Energetic information for all the stationary points involved in the nucleophilic addition step along RP-C2. The structures were optimized at the RB3LYP-GD3/6-311++G(d,p)/THF level of theory at 195.15 K and 1 atm. Energy values are given in Hartree (a.u.) units.

	RP-C2		
	11a	**12a**	**13a**
Electronic Energy (EE)	-969.5315	-969.4924	-969.5230
Zero-point Energy Correction	0.3937	0.3923	0.3937
Thermal Correction to Energy	0.4054	0.4034	0.4049
Thermal Correction to Enthalpy	0.4061	0.4040	0.4055
Thermal Correction to Free Energy	0.3621	0.3614	0.3626
EE + Zero-point Energy	-969.1378	-969.1001	-969.1293
EE + Thermal Energy Correction	-969.1261	-969.0890	-969.1181
EE + Thermal Enthalpy Correction	-969.2255	-969.0884	-969.1175
EE + Thermal Free Energy Correction	-969.1694	-969.1310	-969.1603

Table B17. Energetic information for all the stationary points involved in the nucleophilic addition step along RP-C3. The structures were optimized at the RB3LYP-GD3/6-311++G(d,p)/THF level of theory at 195.15 K and 1 atm. Energy values are given in Hartree (a.u.) units.

	RP-C3		
	11b	**12b**	**13b**
Electronic Energy (EE)	-969.5361	-969.5040	-969.5331
Zero-point Energy Correction	0.3938	0.3930	0.3946
Thermal Correction to Energy	0.4055	0.4041	0.4058
Thermal Correction to Enthalpy	0.4061	0.4047	0.4065
Thermal Correction to Free Energy	0.3621	0.3628	0.3634
EE + Zero-point Energy	-969.1423	-969.1110	-969.1385
EE + Thermal Energy Correction	-969.1306	-969.0999	-969.1273
EE + Thermal Enthalpy Correction	-969.1300	-969.0993	-969.1267
EE + Thermal Free Energy Correction	-969.1740	-969.1412	-969.1698

Table B17. Energetic information for **H₂O** and **O₂**. This structure was optimized at the RB3LYP-GD3/6-311++G(d,p)/THF level of theory at 298.15 K and 1 atm. Energy values are given in Hartree (a.u.) units.

	REACTANTS	
	H₂O	**O₂**
Electronic Energy (EE)	-76.4650	-150.3098
Zero-point Energy Correction	0.0212	0.0037
Thermal Correction to Energy	0.0241	0.0061
Thermal Correction to Enthalpy	0.0250	0.0070
Thermal Correction to Free Energy	0.0029	-0.0152
EE + Zero-point Energy	-76.4438	-150.3061
EE + Thermal Energy Correction	-76.4410	-150.3037
EE + Thermal Enthalpy Correction	-76.4400	-150.3028
EE + Thermal Free Energy Correction	-76.4621	-150.3250

Table B18. Energetic information for all the stationary points involved in the hydrolysis step along RP-C2. The structures were optimized at the RB3LYP-GD3/6-311++G(d,p)/THF level of theory at 298.15 K and 1 atm. Energy values are given in Hartree (a.u.) units.

	RP-C2		
	14a	**15a**	**16a**
Electronic Energy (EE)	-1046.0066	-1046.0006	-1046.0133
Zero-point Energy Correction	0.4186	0.4144	0.4183
Thermal Correction to Energy	0.4451	0.4401	0.4450
Thermal Correction to Enthalpy	0.4460	0.4411	0.4459
Thermal Correction to Free Energy	0.3590	0.3553	0.3579
EE + Zero-point Energy	-1045.5880	-1045.5862	-1045.5950
EE + Thermal Energy Correction	-1045.5616	-1045.5605	-1045.5683
EE + Thermal Enthalpy Correction	-1045.5606	-1045.5596	-1045.5674
EE + Thermal Free Energy Correction	-1045.6477	-1045.6454	-1045.6554

Table B19. Energetic information for the ONSH products **17b** along RP-C3. This structure was optimized at the RB3LYP-GD3/6-311++G(d,p)/THF level of theory at 298.15 K and 1 atm. Energy values are given in Hartree (a.u.) units.

	RP-C3
	17b
Electronic Energy (EE)	-1196.4635
Zero-point Energy Correction	0.4246
Thermal Correction to Energy	0.4539
Thermal Correction to Enthalpy	0.4549
Thermal Correction to Free Energy	0.3605
EE + Zero-point Energy	-1196.0389
EE + Thermal Energy Correction	-1196.0096
EE + Thermal Enthalpy Correction	-1196.0086
EE + Thermal Free Energy Correction	-1196.1030

Table B20. Energetic information for all the stationary points involved in the hydrolysis step along RP-C2. The structures were optimized at the RB3LYP-GD3/6-311++G(d,p)/THF level of theory at 298.15 K and 1 atm. Energy values are given in Hartree (a.u.) units.

	RP-C2		
	14a	**15e**	**16e**
Electronic Energy (EE)	-1046.0066	-1045.9646	-1046.0294
Zero-point Energy Correction	0.4186	0.4156	0.4172
Thermal Correction to Energy	0.4451	0.4419	0.4451
Thermal Correction to Enthalpy	0.4460	0.4429	0.4460
Thermal Correction to Free Energy	0.3590	0.3551	0.3526
EE + Zero-point Energy	-1045.5880	-1045.5490	-1045.6122
EE + Thermal Energy Correction	-1045.5616	-1045.5227	-1045.5843
EE + Thermal Enthalpy Correction	-1045.5606	-1045.5217	-1045.5834
EE + Thermal Free Energy Correction	-1045.6477	-1045.6095	-1045.6768

Part 2 – Selected geometric data

Table B21. Computed dihedral angles (DA) in °, angles in ° and bond lengths in Å for energy optimised 2-phenylquinoxaline (**1**).

Energy optimized 2-phenylquinoxaline (**1**)

Dihedral angle (º)		Angle (º)		Distance (Å)	
C6,C5,C10,C9	0.10	N1,C2,C3	120.47	C3–H11	1.09
C6,C7,C8,C9	0.11	N1,C2,C16	118.56	C2–C16	1.48
N1,C2,C3,N4	1.19	C3,C2,C16	120.96	N1–C2	1.32
N4,C5,C10,N1	1.06	C2,C3,N4	123.12	C2–C3	1.43
N1,C2,C16,C17	28.37	N4,C3,C2	116.90	C3–N4	1.31
		H11,C3,C2	119.96	N4–C5	1.37
		N4,C5,C10	120.37	C5–C6	1.42
		N4,C5,C6	120.00	C5–C10	1.43
		C6,C5,C10	119.63	N1–C10	1.36
		C5,C10,N1	121.05	C10C9	1.42
		C5,C10,C9	119.22		
		C9,C10,N1	119.73		

B19

Table B22. Computed dihedral angles (DA) in °, angles in ° and bond lengths in Å for energy optimised 1-octynyllithium (**10**).

Energy optimised lithium phenylacetylide (**2**)
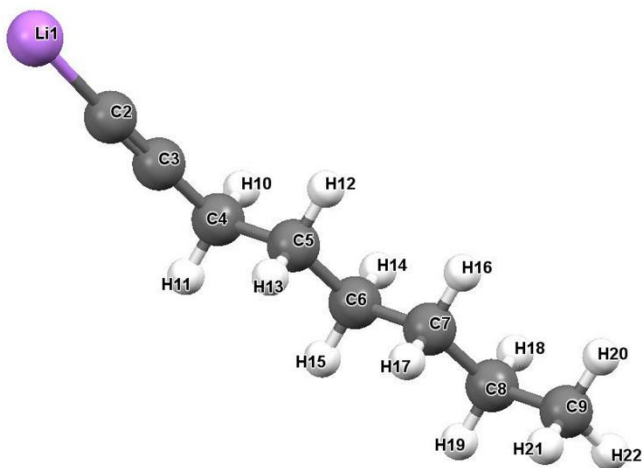
Dihedral angle (º)	Angle (º)		Distance (Å)	
	Li1,C2,C3	177.67	Li1–C2	2.02

B20

Table B23. Computed dihedral angles (DA) in °, angles in ° and bond lengths in Å for the energy optimised adduct **11a**, transition state **12a** and intermediate **13a** along RP-C2.

		RP-C2		
		11a	**12a**	**13a**
Dihedral angle (º)	C6,C5,C10,C9	0.58	1.43	4.01
	C6,C7,C8,C9	0.46	0.84	2.03
	N1,C2,C3,N4	-0.61	17.96	31.94
	N4,C5,C10,N1	1.00	3.62	8.80
	N1,C2,C16,C17	40.25	16.28	58.35
Angle (º)	Li27,C28,C29	148.70		
	N1,C2,C3	120.60	116.24	110.39
	N1,C2,C16	118.88	114.81	108.88
	C3,C2,C16	120.51	113.73	108.73
Distance (Å)	N1–C2	1.32	1.38	1.48
	C2–C3	1.43	1.49	1.54
	C2–C16	1.48	1.52	1.54
	Li27–C28	2.02	2.19	3.60
	Li27–N1	2.17	2.03	1.95
	C28–C2	4.10	1.92	1.48

Energy optimized structures

B21
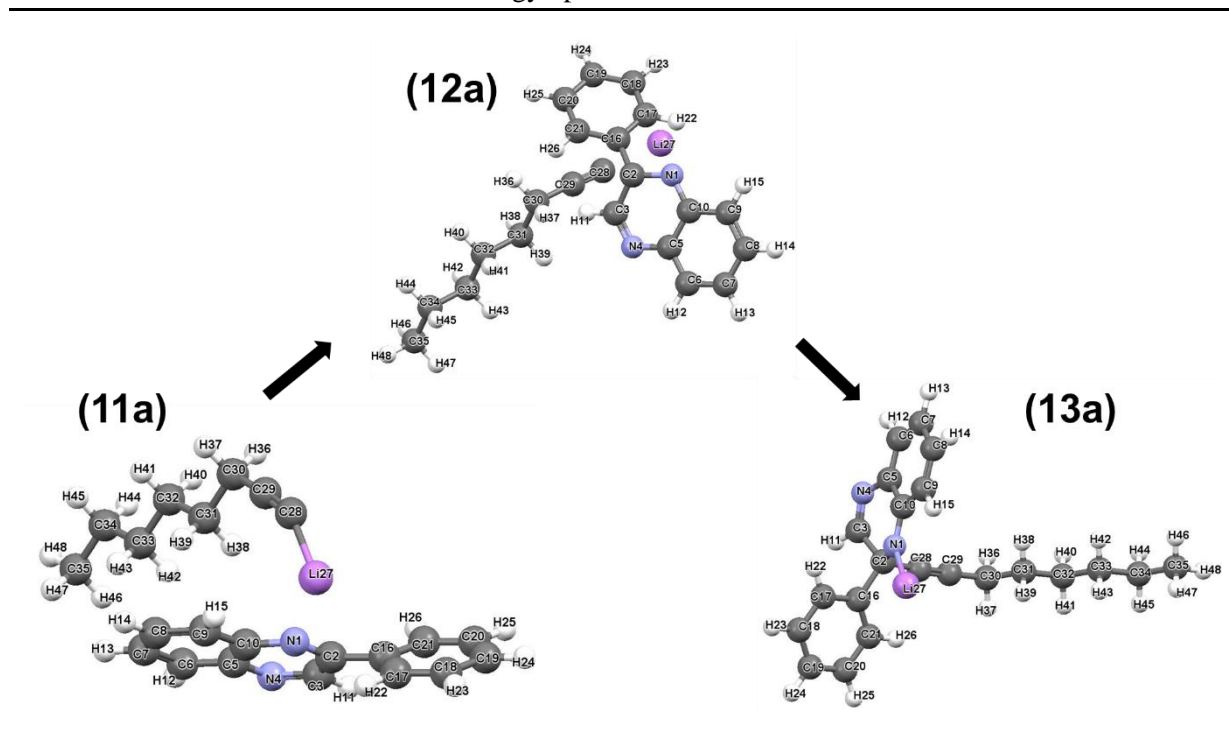
Table B24. Computed dihedral angles (DA) in º, angles in º and bond lengths in Å for the energy optimised adduct **11b**, transition state **12b** and intermediate **13b** along RP-C3.

		RP-C3		
		11b	**12b**	**13b**
Dihedral angle (º)	C6,C5,C10,C9	-0.08	-1.76	-4.32
	C6,C7,C8,C9	-0.01	-0.92	-1.98
	N1,C2,C3,N4	0.92	-20.56	-37.74
	N4,C5,C10,N1	0.68	-4.15	-9.71
	N1,C2,C16,C17	23.62	-2.15	16.82
Angle (º)	Li27,C28,C29	169.40		
	C2,C3,N4	122.66	118.38	110.92
	C2,C3,H11	121.46	115.11	108.60
	N4,C3,H11	115.88	112.76	107.47
Distance (Å)	N4–C3	1.31	1.37	1.47
	C2–C3	1.43	1.49	1.54
	C3–H11	1.09	1.08	1.10
	Li27–C28	2.04	2.16	3.75
	Li27–N4	2.11	2.02	1.94
	C28–C3	3.40	1.91	1.48

Energy optimized structures
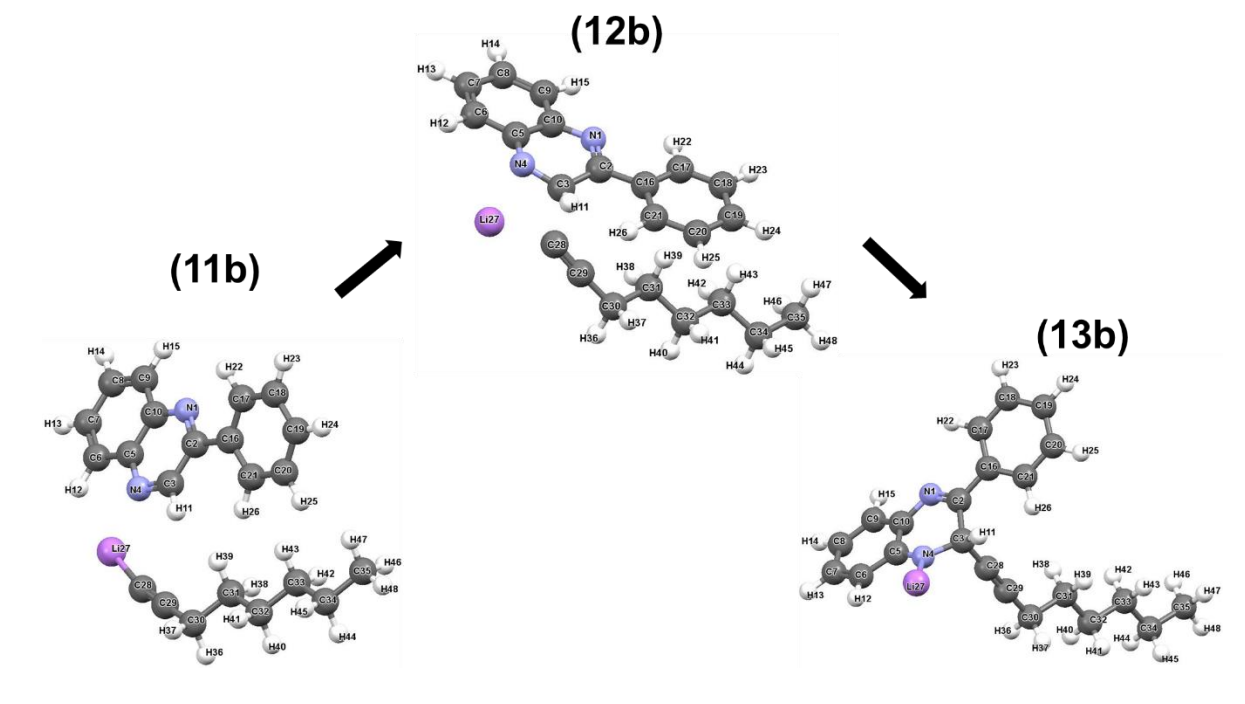
Table B25. Computed dihedral angles in °, angles in ° and bond lengths in Å for the energy optimised stationary points **14a**, **15a** and **16a** along RP-C2.

		RP-C2		
		14a	**15a**	**16a**
Dihedral angle (º)	C6,C5,C10,C9	3.99	1.17	0.93
	C6,C7,C8,C9	1.96	0.85	0.86
	N1,C2,C3,N4	31.02	29.97	28.50
	N4,C5,C10,N1	8.80	3.24	1.49
	N1,C2,C16,C17	48.84	74.22	49.77
	N1,Li27,O49,H50	-1.18		
Angle (º)	N1,Li27,O49	106.27		
	N1,C2,C3	110.67	109.53	107.42
	N1,C2,C16	109.87	108.29	108.81
	C3,C2,C16	108.30	109.97	109.26
Distance (Å)	N1–C2	1.48	1.48	1.46
	C2–C3	1.54	1.54	1.54
	C2–C16	1.53	1.54	1.54
	Li27–O49	1.97	1.90	1.76
	Li27–N1	1.96	2.32	3.63
	O49–H50	0.98	1.17	1.69
	N1–H50	2.92	1.33	1.05

Energy optimized structures

B23
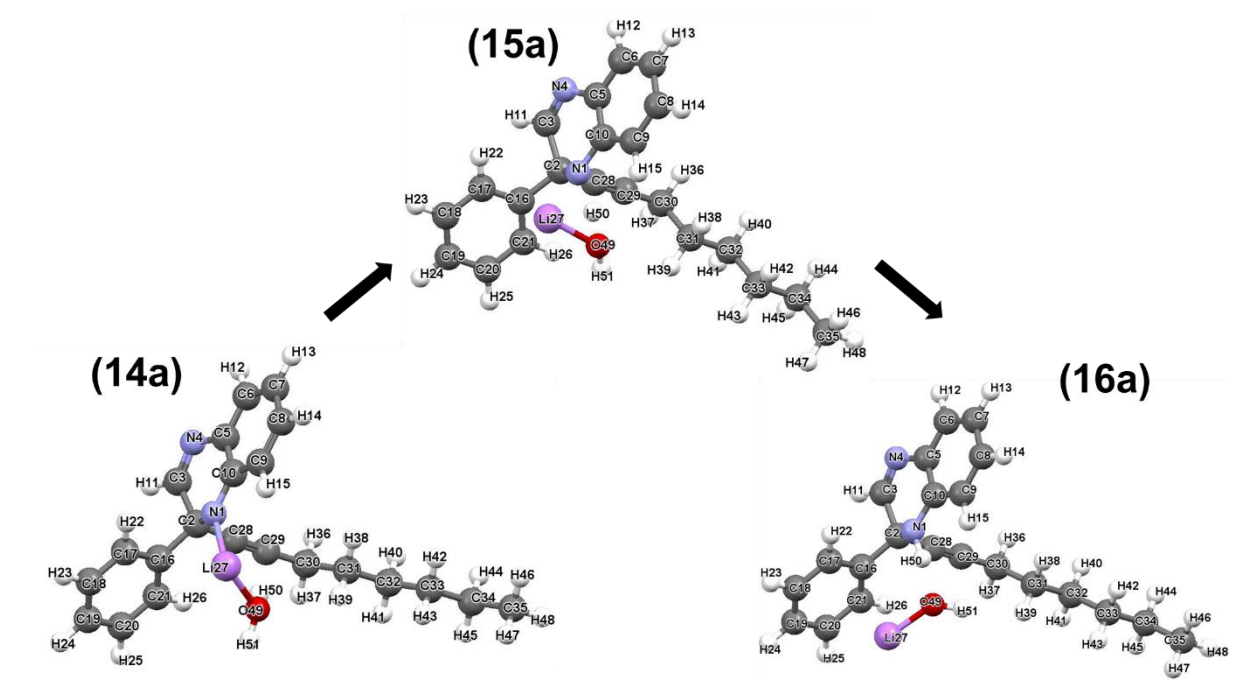
Table B26. Computed dihedral angles (DA) in °, angles in ° and bond lengths in Å for the energy optimised ONSH product **17b** along RP-C3.

		RP-C3
		17b
Dihedral angle (°)	C6,C5,C10,C9	0.39
	C6,C7,C8,C9	0.18
	N1,C2,C3,N4	2.00
	N4,C5,C10,N1	-1.78
	N1,C2,C16,C17	45.44
Angle (°)	N4,C3,C2	121.23
	N4,C3,C28	117.91
	C2,C3,C28	120.81
Distance (Å)	N4–C3	1.33
	C2–C3	1.45
	C3–C28	1.42
	Li27–O49	1.82
	Li27–N4	2.13
	O49–H51	1.44
	O52–H11	0.97
	O53–H51	1.06
Energy optimized structures		

(17b)
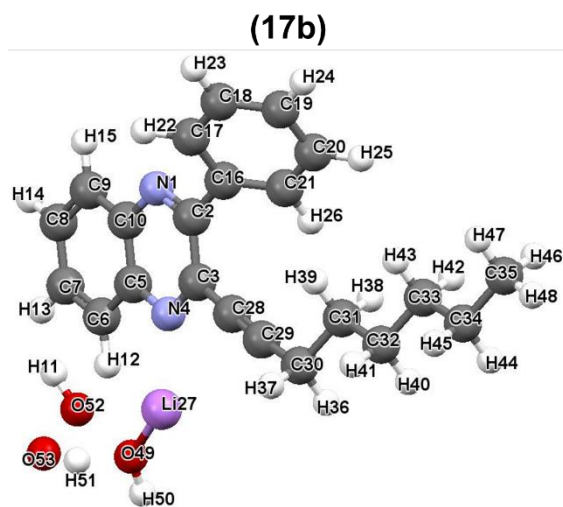
Table B27. Computed dihedral angles (DA) in º, angles in º and bond lengths in Å for the energy optimised stationary points **14a**, **15e** and **16e** along RP-C2.

		RP-C2		
		14a	**15e**	**16e**
Dihedral angle (º)	C6,C5,C10,C9	3.99	-1.49	-0.57
	C6,C7,C8,C9	1.96	-0.65	-0.27
	N1,C2,C3,N4	31.02	-12.14	-0.76
	N4,C5,C10,N1	8.80	-1.95	-0.97
	N1,C2,C16,C17	48.84		
	N1,Li27,O49,H50	-1.18		
Angle (º)	N1,Li27,O49	106.27	99.21	
	N1,C2,C3	110.67	118.97	121.17
	N1,C2,C16	109.87	109.69	
	C3,C2,C16	108.30	90.12	
Distance (Å)	N1–C2	1.48	1.36	1.33
	C2–C3	1.54	1.47	1.43
	C2–C16	1.53	2.30	4.08
	Li27–O49	1.97	1.90	1.70
	Li27–N1	1.96	2.04	2.14
	O49–H50	0.98	1.02	3.55
	C16–H50	3.21	1.76	1.09

Energy optimized structures
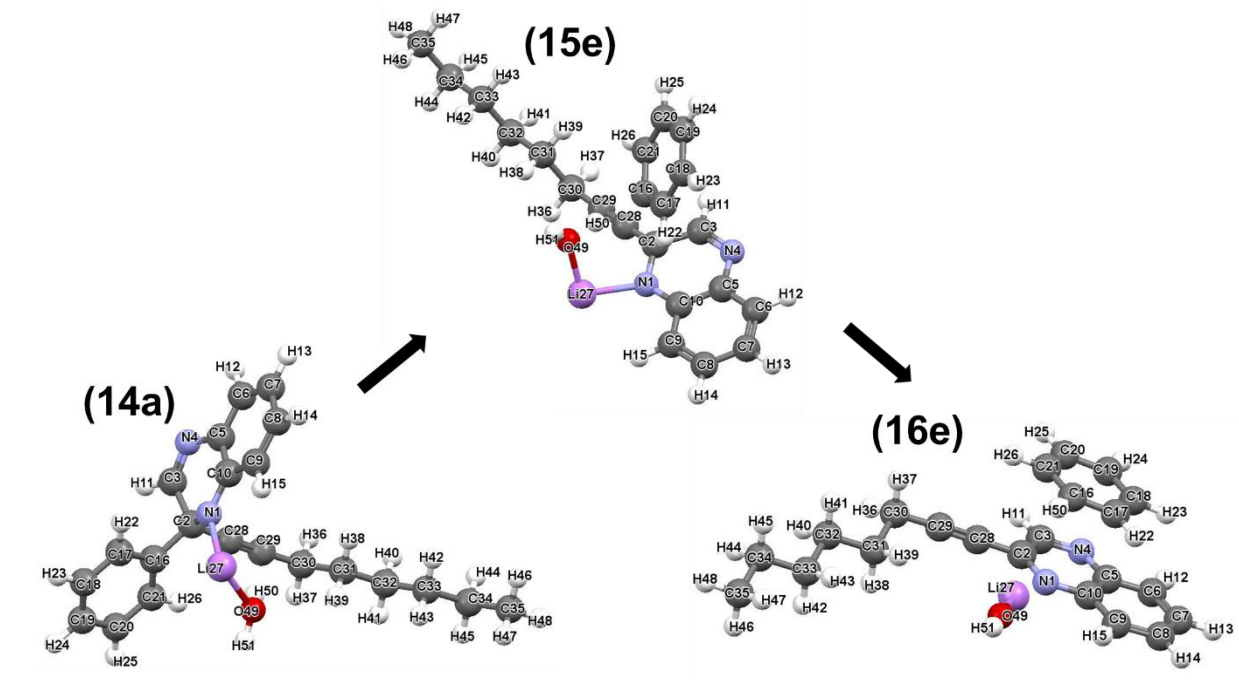
Part 3
Most attractive and repulsive diatomic interactions in 11, 12 and 13 along four reaction pathways considered

Table B28. Most significant (leading) attractive and repulsive diatomic inter-molecular interactions in adducts **11** formed between **1** and **10** along two potential reaction pathways (RP). All values in kcal/mol.

Atom A	Atom B	RP-C2	Atom A	Atom B	RP-C3
Attractive interactions with $E_{int}(A,B) > \sim 10$ kcal mol^{-1}
N1	Li27	-179.1	N4	Li27	-187.1
N4	Li27	-70.5	N1	Li27	-68.7
C2	C29	-29.1	C3	C29	-31.5
C3	C29	-25.8	C3	C28	-26.2
C10	C29	-25.7	C2	C29	-22.8
C2	C28	-20.5	C5	C29	-19.7
C5	C29	-20.4	C10	C29	-16.6
C10	C28	-17.5	C5	C28	-16.1
C3	C28	-13.7	C2	C28	-14.0
C5	C28	-10.2	C10	C28	-10.9
Repulsive interactions with $E_{int}(A,B) > \sim 10$ kcal mol^{-1}
N4	C28	23.4	H11	Li27	10.9
C5	Li27	30.7	N1	C28	24.8
C3	Li27	40.8	C10	Li27	30.7
N1	C28	47.8	C2	Li27	37.9
N4	C29	48.4	N1	C29	40.6
C10	Li27	51.9	C5	Li27	49.4
C2	Li27	64.2	N4	C28	53.9
N1	C29	69.4	N4	C29	65.1
			C3	Li27	68.1

Table B29. Most significant (leading) attractive and repulsive diatomic inter-molecular interactions in transition states **12** formed along two potential reaction pathways (RP). All values in kcal/mol.

Atom A	Atom B	RP-C2	Atom A	Atom B	RP-C3
Attractive interactions with $E_{int}(A,B) > {\sim}10$ kcal mol^{-1}					
N1	Li27	-200.3	N4	Li27	-199.7
C2	C28	-101.3	C3	C28	-102.6
N4	Li27	-83.2	N1	Li27	-83.7
C3	C29	-38.0	C2	C29	-34.2
C2	C29	-31.7	C3	C29	-33.7
C10	C29	-19.1	C5	C29	-18.4
C5	C29	-16.5	C10	C29	-17.0
C3	C28	-16.2	C2	C28	-15.9
C10	C28	-10.6	C5	C28	-11.4
Repulsive interactions with $E_{int}(A,B) > {\sim}10$ kcal mol^{-1}					
N4	C28	11.1	N1	C28	15.5
N1	C28	23.1	N4	C28	26.1
C5	Li27	27.6	C10	Li27	30.2
C10	Li27	53.1	C2	Li27	49.9
C3	Li27	53.1	N1	C29	52.6
N1	C29	53.8	C5	Li27	52.8
N4	C29	55.7	N4	C29	53.8
C2	Li27	66.7	C3	Li27	68.4

Table B30. Most significant (leading) attractive and repulsive diatomic intra-molecular interactions in intermediates **13** formed along two potential reaction pathways (RP). All values in kcal/mol.

Atom A	Atom B	RP-C2	Atom A	Atom B	RP-C3
Attractive interactions with $E_{int}(A,B) > {\sim}10$ kcal mol^{-1}					
N1	Li27	-221.7	N4	Li27	-225.3
N4	Li27	-77.1	N1	Li27	-78.3
C29	Li27	-14.9	C28	Li27	-15.1
C28	Li27	-14.8	C29	Li27	-14.4
Repulsive interactions with $E_{int}(A,B) > {\sim}10$ kcal mol^{-1}					
C5	Li27	23.2	C10	Li27	25.3
C3	Li27	45.9	C2	Li27	44.1
C2	Li27	47.7	C3	Li27	48.7
C10	Li27	57.2	C5	Li27	57.7

Part 4
Net atomic charges

Table B31. Net atomic charges for the reactants **1** and **10**. Q is in e.

	1		10
Atom A	**Q(A)**	**Atom A**	**Q(A)**
N1	-1.1164	Li1	0.9438
C2	0.5418	C2	-0.3766
C3	0.5651	C3	-0.6801
N4	-1.1211	C4	0.0915
C5	0.4269	C5	0.0615
C6	-0.0137	C6	0.0513
C7	-0.0156	C7	0.0544
C8	-0.0154	C8	0.0637
C9	-0.0150	C9	0.0271
C10	0.4426	H10	-0.0002
H11	0.0542	H11	-0.0001
H12	0.0535	H12	-0.0200
H13	0.0425	H13	-0.0200
H14	0.0426	H14	-0.0265
H15	0.0529	H15	-0.0264
C16	-0.0130	H16	-0.0262
C17	-0.0144	H17	-0.0261
C18	-0.0190	H18	-0.0244
C19	-0.0224	H19	-0.0244
C20	-0.0179	H20	-0.0150
C21	-0.0247	H21	-0.0150
H22	0.0512	H22	-0.0120
H23	0.0344		
H24	0.0352		
H25	0.0349		
H26	0.0315		

Table B32. Net atomic charges for **H_2O**. Q is in e.

H_2O	
Atom A	**Q(A)**
O1	-1.1385
H2	0.5693
H3	0.5693

B29

Table B33. Net atomic charges for all the stationary points involved in the nucleophilic addition step along RP-C2. *Q* is in *e*.

Atom A	*Q*(A) 11a	12a	13a
N1	-1.1775	-1.1861	-1.1863
C2	0.5354	0.4744	0.4017
C3	0.5735	0.6488	0.6335
N4	-1.1136	-1.1605	-1.1826
C5	0.4363	0.3511	0.3162
C6	-0.0036	-0.0262	-0.0333
C7	-0.0079	-0.0392	-0.0584
C8	-0.0080	-0.0313	-0.0402
C9	-0.0031	-0.0486	-0.0665
C10	0.4361	0.4160	0.4425
H11	0.0613	0.0403	0.0303
H12	0.0564	0.0326	0.0189
H13	0.0441	0.0187	0.0029
H14	0.0456	0.0206	0.0062
H15	0.0466	0.0162	-0.0133
C16	-0.0200	-0.0164	-0.0318
C17	-0.0259	-0.0296	-0.0367
C18	-0.0166	-0.0285	-0.0296
C19	-0.0179	-0.0297	-0.0310
C20	-0.0135	-0.0264	-0.0298
C21	-0.0189	-0.0253	-0.0387
H22	0.0429	0.0527	0.0361
H23	0.0386	0.0260	0.0277
H24	0.0398	0.0272	0.0275
H25	0.0407	0.0266	0.0268
H26	0.0407	0.0366	0.0393
Li27	0.9212	0.9357	0.9501
C28	-0.3524	-0.1302	-0.1613
C29	-0.6859	-0.5398	-0.2252
C30	0.0908	0.0931	0.1031
C31	0.0626	0.0613	0.0626
C32	0.0518	0.0539	0.0533
C33	0.0551	0.0547	0.0545
C34	0.0631	0.0634	0.0635
C35	0.0265	0.0271	0.0273
H36	-0.0034	0.0168	0.0255
H37	-0.0034	0.0214	0.0198
H38	-0.0201	-0.0129	-0.0070
H39	-0.0143	-0.0047	-0.0164
H40	-0.0281	-0.0235	-0.0207
H41	-0.0286	-0.0222	-0.0237
H42	-0.0259	-0.0242	-0.0228
H43	-0.0265	-0.0223	-0.0262
H44	-0.0245	-0.0241	-0.0224
H45	-0.0252	-0.0235	-0.0240
H46	-0.0153	-0.0143	-0.0138
H47	-0.0167	-0.0137	-0.0153
H48	-0.0121	-0.0114	-0.0109

Table B34. Net atomic charges for all the stationary points involved in the nucleophilic addition step along RP-C3. Q is in e.

Atom A	Q(A)		
	11b	**12b**	**13b**
N1	-1.1109	-1.1539	-1.1737
C2	0.5462	0.6126	0.6053
C3	0.5436	0.4842	0.4123
N4	-1.1905	-1.1943	-1.2041
C5	0.4206	0.4135	0.4449
C6	-0.0122	-0.0475	-0.0653
C7	-0.0104	-0.0305	-0.0405
C8	-0.0117	-0.0383	-0.0570
C9	-0.0111	-0.0272	-0.0350
C10	0.4507	0.3812	0.3418
H11	0.0962	0.0414	0.0066
H12	0.0449	0.0187	-0.0102
H13	0.0467	0.0218	0.0070
H14	0.0464	0.0199	0.0035
H15	0.0573	0.0332	0.0186
C16	-0.0139	-0.0121	-0.0149
C17	-0.0146	-0.0193	-0.0220
C18	-0.0187	-0.0231	-0.0263
C19	-0.0224	-0.0270	-0.0311
C20	-0.0166	-0.0216	-0.0257
C21	-0.0233	-0.0212	-0.0358
H22	0.0521	0.0558	0.0495
H23	0.0342	0.0278	0.0261
H24	0.0352	0.0288	0.0268
H25	0.0378	0.0266	0.0253
H26	0.0366	0.0271	0.0243
Li27	0.9192	0.9335	0.9512
C28	-0.3412	-0.1471	-0.1757
C29	-0.6861	-0.5471	-0.2267
C30	0.0912	0.0921	0.1029
C31	0.0614	0.0586	0.0624
C32	0.0520	0.0531	0.0529
C33	0.0539	0.0540	0.0545
C34	0.0632	0.0634	0.0635
C35	0.0268	0.0269	0.0272
H36	-0.0001	0.0202	0.0234
H37	0.0002	0.0164	0.0171
H38	-0.0229	-0.0143	-0.0074
H39	-0.0184	0.0030	-0.0130
H40	-0.0253	-0.0264	-0.0220
H41	-0.0248	-0.0257	-0.0245
H42	-0.0289	-0.0250	-0.0227
H43	-0.0255	-0.0220	-0.0249
H44	-0.0233	-0.0246	-0.0232
H45	-0.0232	-0.0249	-0.0245
H46	-0.0152	-0.0143	-0.0137
H47	-0.0151	-0.0149	-0.0148
H48	-0.0111	-0.0120	-0.0115

Table B35. Net atomic charges for all the stationary points involved in the hydrolysis step along RP-C2. Q is in e.

Atom A	Q(A) 14a	15a	16a
N1	-1.1702	-1.1484	-1.1162
C2	0.4028	0.4005	0.4178
C3	0.6335	0.6514	0.6618
N4	-1.1812	-1.1705	-1.1625
C5	0.3173	0.3224	0.3328
C6	-0.0334	-0.0270	-0.0224
C7	-0.0586	-0.0457	-0.0398
C8	-0.0395	-0.0330	-0.0270
C9	-0.0655	-0.0533	-0.0356
C10	0.4472	0.3926	0.4036
H11	0.0319	0.0407	0.0484
H12	0.0188	0.0276	0.0326
H13	0.0029	0.0125	0.0167
H14	0.0068	0.0158	0.0209
H15	-0.0116	0.0213	0.0312
C16	-0.0279	-0.0216	-0.0228
C17	-0.0333	-0.0398	-0.0299
C18	-0.0291	-0.0282	-0.0304
C19	-0.0307	-0.0290	-0.0326
C20	-0.0294	-0.0265	-0.0297
C21	-0.0361	-0.0277	-0.0316
H22	0.0411	0.0294	0.0455
H23	0.0273	0.0297	0.0315
H24	0.0272	0.0299	0.0305
H25	0.0261	0.0295	0.0306
H26	0.0340	0.0410	0.0445
Li27	0.9311	0.9480	0.9467
C28	-0.1650	-0.1575	-0.1530
C29	-0.2344	-0.2132	-0.2083
C30	0.1024	0.1031	0.1028
C31	0.0605	0.0626	0.0626
C32	0.0536	0.0531	0.0530
C33	0.0548	0.0548	0.0546
C34	0.0635	0.0633	0.0634
C35	0.0272	0.0272	0.0270
H36	0.0326	0.0270	0.0281
H37	0.0238	0.0233	0.0244
H38	-0.0033	-0.0063	-0.0061
H39	-0.0139	-0.0135	-0.0100
H40	-0.0194	-0.0210	-0.0211
H41	-0.0230	-0.0231	-0.0232
H42	-0.0219	-0.0228	-0.0227
H43	-0.0252	-0.0251	-0.0246
H44	-0.0222	-0.0229	-0.0229
H45	-0.0240	-0.0239	-0.0240
H46	-0.0135	-0.0139	-0.0138
H47	-0.0150	-0.0149	-0.0147
H48	-0.0107	-0.0112	-0.0111
O49	-1.2074	-1.2881	-1.3804
H50	0.5889	0.5577	0.4945
H51	0.5894	0.5435	0.5100

Table B36. Net atomic charges for all the stationary points involved in the hydrolysis step along RP-C3. Q is in e.

Atom A	Q(A) 17b
N1	-1.1144
C2	0.5683
C3	0.5935
N4	-1.1533
C5	0.4248
C6	-0.0328
C7	-0.0141
C8	-0.0136
C9	-0.0115
C10	0.4445
H11	0.5783
H12	0.1176
H13	0.0458
H14	0.0454
H15	0.0563
C16	-0.0089
C17	-0.0126
C18	-0.0196
C19	-0.0221
C20	-0.0163
C21	-0.0128
H22	0.0443
H23	0.0344
H24	0.0343
H25	0.0332
H26	0.0371
Li27	0.9174
C28	-0.1378
C29	-0.1593
C30	0.1000
C31	0.0628
C32	0.0538
C33	0.0546
C34	0.0634
C35	0.0274
H36	0.0384
H37	0.0415
H38	-0.0076
H39	-0.0012
H40	-0.0199
H41	-0.0190
H42	-0.0240
H43	-0.0227
H44	-0.0226
H45	-0.0223
H46	-0.0143
H47	-0.0140
H48	-0.0100
O49	-1.3337
H50	0.5216
H51	0.6113
O52	-0.6756
O53	-0.6344

Table B37. Net atomic charges for all the stationary points involved in the hydrolysis step along RP-C2. Q is in e.

Atom A	Q(A)		
	14a	15e	16e
N1	-1.1702	-1.1725	-1.1521
C2	0.4028	0.5546	0.5962
C3	0.6335	0.6496	0.5945
N4	-1.1812	-1.1477	-1.1154
C5	0.3173	0.3663	0.4362
C6	-0.0334	-0.0216	-0.0086
C7	-0.0586	-0.0333	-0.0117
C8	-0.0395	-0.0259	-0.0083
C9	-0.0655	-0.0375	-0.0059
C10	0.4472	0.4113	0.4415
H11	0.0319	0.0506	0.0690
H12	0.0188	0.0386	0.0582
H13	0.0029	0.0247	0.0474
H14	0.0068	0.0256	0.0487
H15	-0.0116	0.0143	0.0546
C16	-0.0279	-0.2192	-0.0305
C17	-0.0333	-0.0472	-0.0233
C18	-0.0291	-0.0468	-0.0241
C19	-0.0307	-0.0446	-0.0266
C20	-0.0294	-0.0483	-0.0261
C21	-0.0361	-0.0508	-0.0244
H22	0.0411	-0.0027	0.0276
H23	0.0273	0.0098	0.0272
H24	0.0272	0.0129	0.0281
H25	0.0261	0.0085	0.0253
H26	0.0340	-0.0006	0.0263
Li27	0.9311	0.9348	0.9147
C28	-0.1650	-0.1532	-0.1378
C29	-0.2344	-0.1725	-0.1682
C30	0.1024	0.1029	0.1009
C31	0.0605	0.0626	0.0612
C32	0.0536	0.0531	0.0539
C33	0.0548	0.0551	0.0550
C34	0.0635	0.0634	0.0632
C35	0.0272	0.0269	0.0270
H36	0.0326	0.0251	0.0391
H37	0.0238	0.0285	0.0408
H38	-0.0033	-0.0083	-0.0053
H39	-0.0139	-0.0083	-0.0010
H40	-0.0194	-0.0230	-0.0212
H41	-0.0230	-0.0214	-0.0199
H42	-0.0219	-0.0241	-0.0226
H43	-0.0252	-0.0228	-0.0196
H44	-0.0222	-0.0239	-0.0239
H45	-0.0240	-0.0230	-0.0231
H46	-0.0135	-0.0145	-0.0140
H47	-0.0150	-0.0138	-0.0130
H48	-0.0107	-0.0109	-0.0111
O49	-1.2074	-1.2406	-1.4406
H50	0.5889	0.5649	0.0313
H51	0.5894	0.5753	0.5093

Inter-fragment interaction energies

Interaction energies computed for adducts 11

Table B38. Interaction energies between molecule **1** and specified major fragments of molecule **10**, computed for the indicated reaction pathways on adducts **11** formation between **1** and **10**. All values in kcal/mol.

	Fragment	Reaction pathway	
		C2	**C3**
1	**10**	-52.3	-58.9
	$\mathcal{R}^*$	-13.9	-19.6
	$\mathcal{L}^*$	-38.0	-47.8
	$\mathcal{A}^*$	0.4	-8.4
	Li	-38.4	-39.4
	C28	-1.1	-4.5
	C29	1.6	-3.9

Table B39. Interaction energies between molecule **10** and specified major fragments of molecule **1**, computed for the indicated reaction pathways on adducts **11** formation between **1** and **10**. All values in kcal/mol.

	Fragment	Reaction pathway	
		C2	**C3**
10	$\mathcal{Q}$	-52.1	-47.8
	$\mathcal{P}$	-41.5	-51.7
	$\mathcal{Bn}$	3.2	26.6
	$\mathcal{Ph}1$	–0.2	-11.1
	$\mathcal{N}$	-80.5	-88.3
	$\mathcal{C}$	38.4	42.8
	$\mathcal{G}1$	-42.1	0.9
	$\mathcal{G}2$	0.0	-46.4
	$\mathcal{F}1$	-50.4	10.3
	$\mathcal{F}2$	17.9	-64.5
	$\mathcal{F}3$	3.9	-55.7
	$\mathcal{F}4$	-61.1	13.1
	N1	-73.2	-9.8
	N4	-7.3	-78.4
	C2	19.1	4.9
	C3	5.4	15.3
	C5	1.9	16.8
	C10	12.0	5.9

Table B40. Interaction energies, between the molecular fragment $\mathcal{R}^{*a}$ of **10** and the indicated significant fragments of **1**, computed for the indicated reaction pathways on adducts **11** formation between **1** and **10**. All values in kcal/mol.

| | Fragment | Reaction pathway | |
		C2	C3
$\mathcal{R}^*$	$\mathcal{Q}$	-9.3	-2.4
	$\mathcal{P}$	16.2	6.9
	$\mathcal{Bn}$	-94.2	-66.8
	$\mathcal{Ph}$1	-4.6	-17.2
	$\mathcal{N}$	169.1	167.4
	C	-149.1	-143.3
	$\mathcal{G}$1	21.0	0.9
	$\mathcal{G}$2	-1.0	23.2
	$\mathcal{F}$1	27.6	-26.7
	$\mathcal{F}$2	-21.0	5.6
	$\mathcal{F}$3	-9.0	51.5
	$\mathcal{F}$4	35.4	1.2
	N1	105.9	58.8
	N4	63.2	108.6
	C2	-45.1	-33.0
	C3	-35.4	-52.8
	C5	-28.8	-32.7
	C10	-39.9	-24.8

a) $\mathcal{R}^* = \{C28, \ldots ,H48\}$

Table B41. Interaction energies, between the molecular fragment $\mathcal{L}^{*a}$ of **10** and the indicated significant fragments of **1**, computed for the indicated reaction pathways on adducts **11** formation between **1** and **10**. All values in kcal/mol.

		Reaction pathway	
Fragment		**C2**	**C3**
$\mathcal{L}^*$	$\mathcal{Q}$	-37.2	-46.9
	$\mathcal{P}$	-36.0	-49.9
	$\mathcal{Bn}$	7.5	19.8
	$\mathcal{Ph}$**1**	-0.7	-0.9
	$\mathcal{N}$	-60.6	-71.2
	$\mathcal{C}$	24.5	28.4
	$\mathcal{G}$**1**	-38.7	1.2
	$\mathcal{G}$**2**	2.5	-44.0
	$\mathcal{F}$**1**	-47.8	8.6
	$\mathcal{F}$**2**	17.2	-63.5
	$\mathcal{F}$**3**	10.2	-51.1
	$\mathcal{F}$**4**	-53.5	13.9
	N1	-61.9	-3.2
	N4	1.3	-68.0
	C2	14.5	1.2
	C3	1.2	10.4
	C5	0.0	13.6
	C10	8.7	3.2

[a]$\mathcal{L}^* = \{Li28,C28,C29\}$

Table B42. Interaction energies, between the molecular fragment $\mathcal{A}^{*a}$ of **10** and the indicated significant fragments of **1**, computed for the indicated reaction pathways on adducts **11** formation between **1** and **10**. All values in kcal/mol.

		Reaction pathway	
Fragment		**C2**	**C3**
$\mathcal{A}^*$	$\mathcal{Q}$	5.5	-1.5
	$\mathcal{P}$	21.7	8.7
	$\mathcal{B}n$	-90.0	-73.5
	$\mathcal{P}h\mathbf{1}$	-5.1	-7.0
	$\mathcal{N}$	189	184.5
	$\mathcal{C}$	-163.1	-157.8
	$\mathcal{G}\mathbf{1}$	24.4	1.2
	$\mathcal{G}\mathbf{2}$	1.6	25.5
	$\mathcal{F}\mathbf{1}$	30.3	-26.9
	$\mathcal{F}\mathbf{2}$	-21.7	6.6
	$\mathcal{F}\mathbf{3}$	-2.7	56.1
	$\mathcal{F}\mathbf{4}$	43.0	2.0
	N1	117.2	65.5
	N4	71.8	119.0
	C2	-49.7	-36.7
	C3	-39.6	-57.7
	C5	-30.7	-35.8
	C10	-43.2	-27.5

[a] $\mathcal{A}^* = \{C28,C29\}$

Table B43. Interaction energies, between Li27 of **10** and the indicated significant fragments of **1**, computed for the indicated reaction pathways on adducts **11** formation between **1** and **10**. All values in kcal/mol.

Fragment		Reaction pathway	
		C2	C3
Li27	$\mathcal{Q}$	-42.8	-45.5
	$\mathcal{P}$	-57.7	-58.7
	$\mathcal{Bn}$	97.5	93.3
	$\mathcal{Ph}$**1**	4.4	6.1
	$\mathcal{N}$	-249.6	-255.7
	$\mathcal{C}$	187.5	186.1
	$\mathcal{G}$**1**	-63.1	0.0
	$\mathcal{G}$**2**	1.0	-69.6
	$\mathcal{F}$**1**	-78.1	37.0
	$\mathcal{F}$**2**	38.9	-70.1
	$\mathcal{F}$**3**	12.9	-107.2
	$\mathcal{F}$**4**	-96.5	11.9
	N1	-179.1	-68.7
	N4	-70.5	-187.1
	C2	64.2	37.9
	C3	40.8	68.1
	C5	30.7	49.4
	C10	51.9	30.7

Table B44. Interaction energies, between C28 of **10** and the indicated significant fragments of **1**, computed for the indicated reaction pathways on adducts **11** formation between **1** and **10**. All values in kcal/mol.

Fragment		Reaction pathway	
		C2	C3
C28	*Q*	0.6	-2.2
	P	7.7	2.2
	Bn	-34.8	-31.4
	*Ph***1**	-1.7	-2.4
	N	71.2	78.7
	C	-62.0	-67.1
	*G***1**	9.8	0.0
	*G***2**	-0.5	11.7
	*F***1**	14.7	-15.2
	*F***2**	-12.4	4.4
	*F***3**	-4.6	27.1
	*F***4**	19.0	-2.3
	N1	47.8	24.8
	N4	23.4	53.9
	C2	-20.5	-14.0
	C3	-13.7	-26.2
	C5	-10.2	-16.1
	C10	-17.5	-10.9

Table B45. Interaction energies, between C29 of **10** and the indicated significant fragments of **1**, computed for the indicated reaction pathways on adducts **11** formation between **1** and **10**. All values in kcal/mol.

	Fragment	Reaction pathway	
		C2	C3
C29	$\mathcal{Q}$	4.9	0.7
	$\mathcal{P}$	14.0	6.5
	$\mathcal{B}n$	-55.2	-42.1
	$\mathcal{P}h$1	-3.4	-4.6
	$\mathcal{N}$	117.8	105.8
	$\mathcal{C}$	-101.1	-90.6
	$\mathcal{G}$1	14.6	1.3
	$\mathcal{G}$2	2.1	13.9
	$\mathcal{F}$1	15.6	-13.2
	$\mathcal{F}$2	-9.3	2.2
	$\mathcal{F}$3	2.0	29.0
	$\mathcal{F}$4	24.0	4.2
	N1	69.4	40.6
	N4	48.4	65.1
	C2	-29.1	-22.8
	C3	-25.8	-31.5
	C5	-20.4	-19.7
	C10	-25.7	-16.6

Interaction energies computed for transition states 12 of the nucleophilic addition step

Table B46. Interaction energies between molecule **1** and specified major fragments of molecule **10**, computed for the indicated reaction pathways on transition states **12** formation between **1** and **10**. All values in kcal/mol.

		Reaction pathway	
	Fragment	**C2**	**C3**
1	**10**	-204.1	-207.3
	$\mathcal{R}^*$	-129.2	-136.8
	$\mathcal{L}^*$	-197.1	-187.9
	$\mathcal{A}^*$	-122.3	-117.3
	Li	-74.9	-70.5
	C28	-115.5	-107.7
	C29	-6.7	-9.7

Table B47. Interaction energies, between Li27 of **10** and the indicated significant fragments of **1**, computed for the indicated reaction pathways on transition states **12** formation between **1** and **10**. All values in kcal/mol.

		Reaction pathway	
	Fragment	**C2**	**C3**
Li27	$\mathcal{Q}$	-79.3	-75.6
	$\mathcal{P}$	-79.1	-75.9
	$\mathcal{Bn}$	80.6	83.4
	$\mathcal{Ph}$**1**	4.5	5.0
	$\mathcal{N}$	-283.4	-283.4
	$\mathcal{C}$	200.6	201.3
	$\mathcal{G}$**1**	-80.5	-3.6
	$\mathcal{G}$**2**	-2.4	-78.5
	$\mathcal{F}$**1**	-83.0	34.4
	$\mathcal{F}$**2**	40.4	-75.3
	$\mathcal{F}$**3**	-2.9	-120.9
	$\mathcal{F}$**4**	-123.9	-1.3
	N1	-200.3	-83.7
	N4	-83.2	-199.7
	C2	66.7	49.9
	C3	53.1	68.4
	C5	27.6	52.8
	C10	53.1	30.2

Table B48. Interaction energies, between the molecular fragment $\mathcal{A}^{*a}$ of **10** and the indicated significant fragments of **1**, computed for the indicated reaction pathways on transition states **12** formation between **1** and **10**. All values in kcal/mol.

		Reaction pathway	
Fragment		**C2**	**C3**
$\mathcal{A}^*$	$\mathcal{Q}$	-101.1	-104.5
	$\mathcal{P}$	-99.3	-102.4
	$\mathcal{Bn}$	-53.7	-55.9
	$\mathcal{Ph}$**1**	-21.2	-12.9
	$\mathcal{N}$	143.8	147.9
	$\mathcal{C}$	-239.1	-240.3
	$\mathcal{G}$**1**	-85.7	-6.2
	$\mathcal{G}$**2**	-9.6	-86.2
	$\mathcal{F}$**1**	-115.8	-119.7
	$\mathcal{F}$**2**	-124.3	-116.6
	$\mathcal{F}$**3**	15.3	27.3
	$\mathcal{F}$**4**	26.5	14.6
	N1	76.9	68.1
	N4	66.8	79.8
	C2	-133.0	-50.1
	C3	-54.2	-136.3
	C5	-22.2	-29.8
	C10	-29.7	-24.2

a) $\mathcal{A}^* = \{C28, C29\}$

Table B49. Interaction energies, between the molecular fragment $\mathcal{R}^{*a}$ of **10** and the indicated significant fragments of **1**, computed for the indicated reaction pathways on transition states **12** formation between **1** and **10**. All values in kcal/mol.

		Reaction pathway	
Fragment		**C2**	**C3**
$\mathcal{R}^*$	$\mathcal{Q}$	-108.4	-108.9
	$\mathcal{P}$	-106.4	-106.8
	$\mathcal{Bn}$	-43.1	-45.8
	$\mathcal{Ph}$1	-20.8	-27.8
	$\mathcal{N}$	107.6	115.2
	$\mathcal{C}$	-210.2	-212.7
	$\mathcal{G}$1	-89.3	-8.0
	$\mathcal{G}$2	-13.2	-89.5
	$\mathcal{F}$1	-114.9	-122.0
	$\mathcal{F}$2	-125.1	-114.8
	$\mathcal{F}$3	6.7	20.8
	$\mathcal{F}$4	19.7	8.2
	N1	59.8	51.7
	N4	47.8	63.5
	C2	-125.2	-40.4
	C3	-43.8	-128.6
	C5	-17.2	-24.5
	C10	-23.9	-19.3

[a] $\mathcal{R}^* = \{C28, \dots ,H48\}$

Table B50. Interaction energies, between C28 of **10** and the indicated significant fragments of **1**, computed for the indicated reaction pathways on transition states **12** formation between **1** and **10**. All values in kcal/mol.

	Fragment	Reaction pathway	
		C2	**C3**
C28	$\mathcal{Q}$	-102.0	-102.9
	$\mathcal{P}$	-100.7	-101.6
	$\mathcal{Bn}$	-17.6	-19.9
	$\mathcal{Ph}$1	-13.5	-4.8
	$\mathcal{N}$	34.2	41.6
	$\mathcal{C}$	-133.9	-137.1
	$\mathcal{G}$1	-88.8	-7.6
	$\mathcal{G}$2	-10.8	-87.9
	$\mathcal{F}$1	-99.7	-104.4
	$\mathcal{F}$2	-107.5	-98.5
	$\mathcal{F}$3	-5.3	7.8
	$\mathcal{F}$4	7.0	-3.1
	N1	23.1	15.5
	N4	11.1	26.1
	C2	-101.3	-15.9
	C3	-16.2	-102.6
	C5	-5.7	-11.4
	C10	-10.6	-7.2

Table B51. Interaction energies, between C29 of **10** and the indicated significant fragments of **1**, computed for the indicated reaction pathways on transition states **12** formation between **1** and **10**. All values in kcal/mol.

Fragment		Reaction pathway	
		C2	C3
C29	$\mathcal{Q}$	1.0	-1.5
	$\mathcal{P}$	1.5	-0.8
	$\mathcal{Bn}$	-36.1	-36.1
	$\mathcal{Ph}$1	-7.7	-8.1
	$\mathcal{N}$	109.5	106.4
	$\mathcal{C}$	-105.2	-103.2
	$\mathcal{G}$1	3.2	1.5
	$\mathcal{G}$2	1.2	1.7
	$\mathcal{F}$1	-16.0	-15.3
	$\mathcal{F}$2	-16.8	-18.1
	$\mathcal{F}$3	20.6	19.5
	$\mathcal{F}$4	19.5	17.7
	N1	53.8	52.6
	N4	55.7	53.8
	C2	-31.7	-34.2
	C3	-38.7	-33.7
	C5	-16.5	-18.4
	C10	-19.1	-17.0

PART 6

Energy profiles along reaction coordinates

(a)

(b)
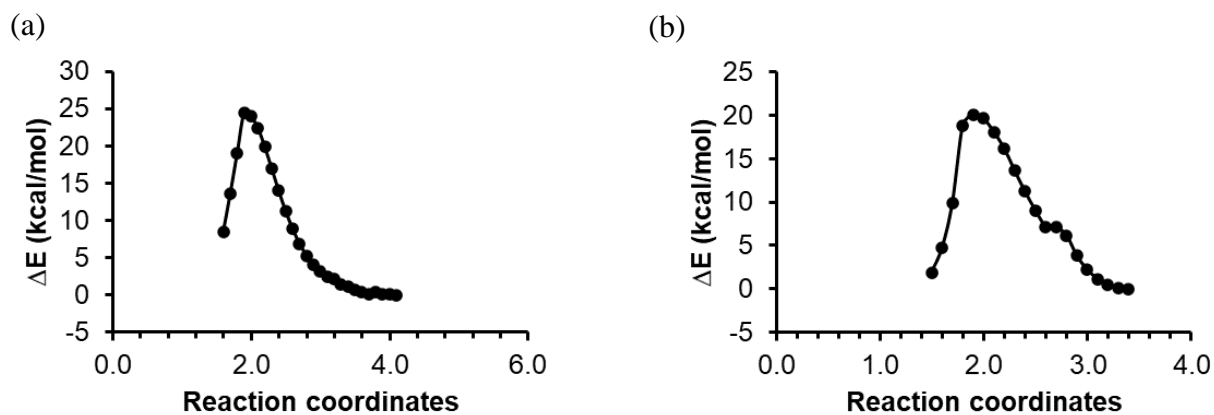
Figure B1. Computed reaction energy profiles along the C28---Cn reaction coordinates for (a) RP-C2 and (b) RP-C3.

(a)

(b)
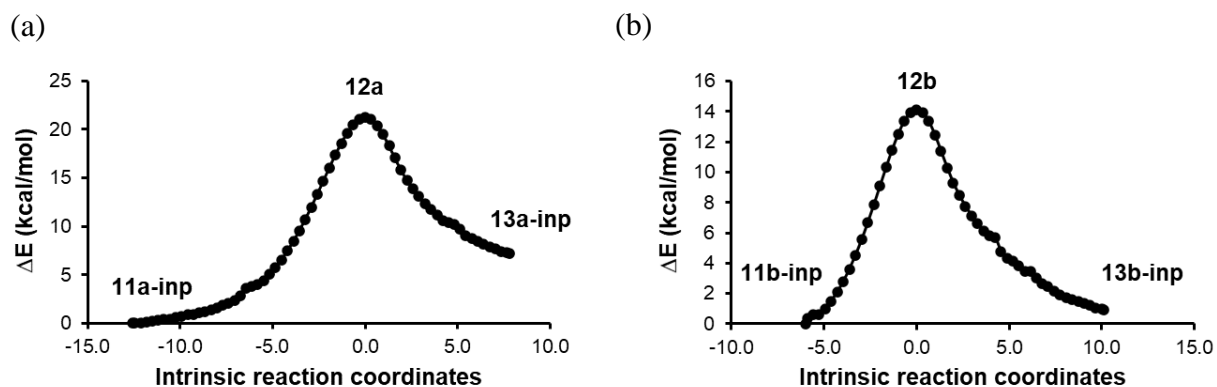
Figure B2. Computed IRC paths for the nucleophilic addition step along (a) RP-C2 and (b) RP-C3, confirming that **12a** and **12b** connect the desired minima of the respective pathways.

(a)

(b)
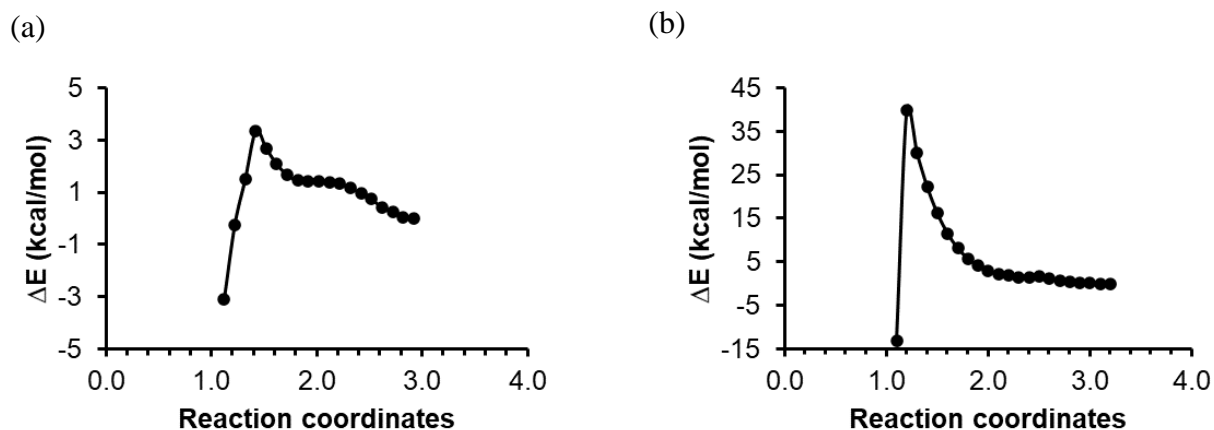
Figure B3. Computed reaction energy profiles along (a) RP-C2, when H50 is transferred to N1 and (b) RP-C2, when H50 is transferred to C16.

(a)

(b)
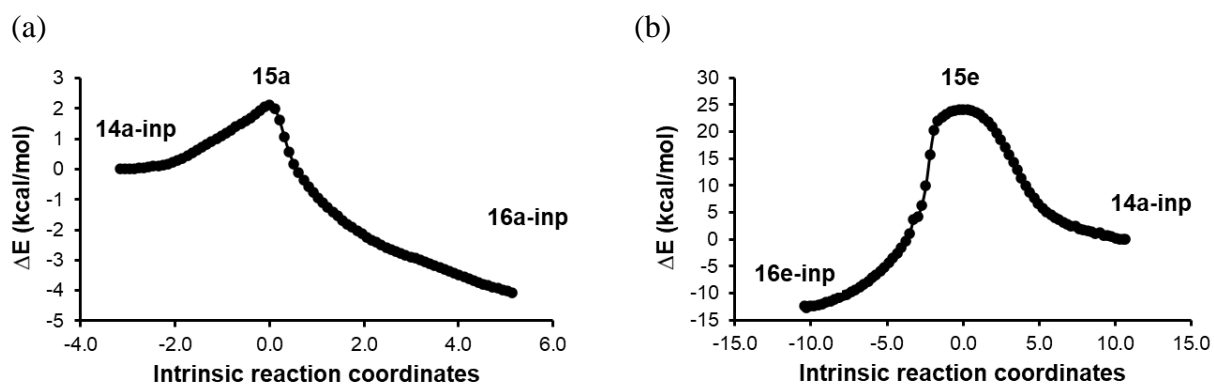
Figure B4. Computed IRC paths for the hydrolysis step along RP-C2, when (a) H50 is transferred to N1 and when (b) H50 is transferred to C16.

PART 7

Energies for 10 identified conformers of 10

Table B52. Calculated energies (E, E_{ZPVE}, H and G in au) of 10 conformers of 1-octynyllithium (**10**).

	E	E_{ZPVE}	H	G
C1	-320.3090	-320.1209	-320.1143	-320.1429
C2	-320.3087	-320.1203	-320.1139	-320.1418
C3	-320.3081	-320.1196	-320.1133	-320.1411
C4	-320.3079	-320.1194	-320.1131	-320.1412
C5	-320.3078	-320.1192	-320.1130	-320.1407
C6	-320.3077	-320.1193	-320.1129	-320.1409
C7	-320.3077	-320.1191	-320.1127	-320.1411
C8	-320.3076	-320.1189	-320.1126	-320.1404
C9	-320.3072	-320.1181	-320.1120	-320.1393
C10	-320.3053	-320.1166	-320.1104	-320.1378
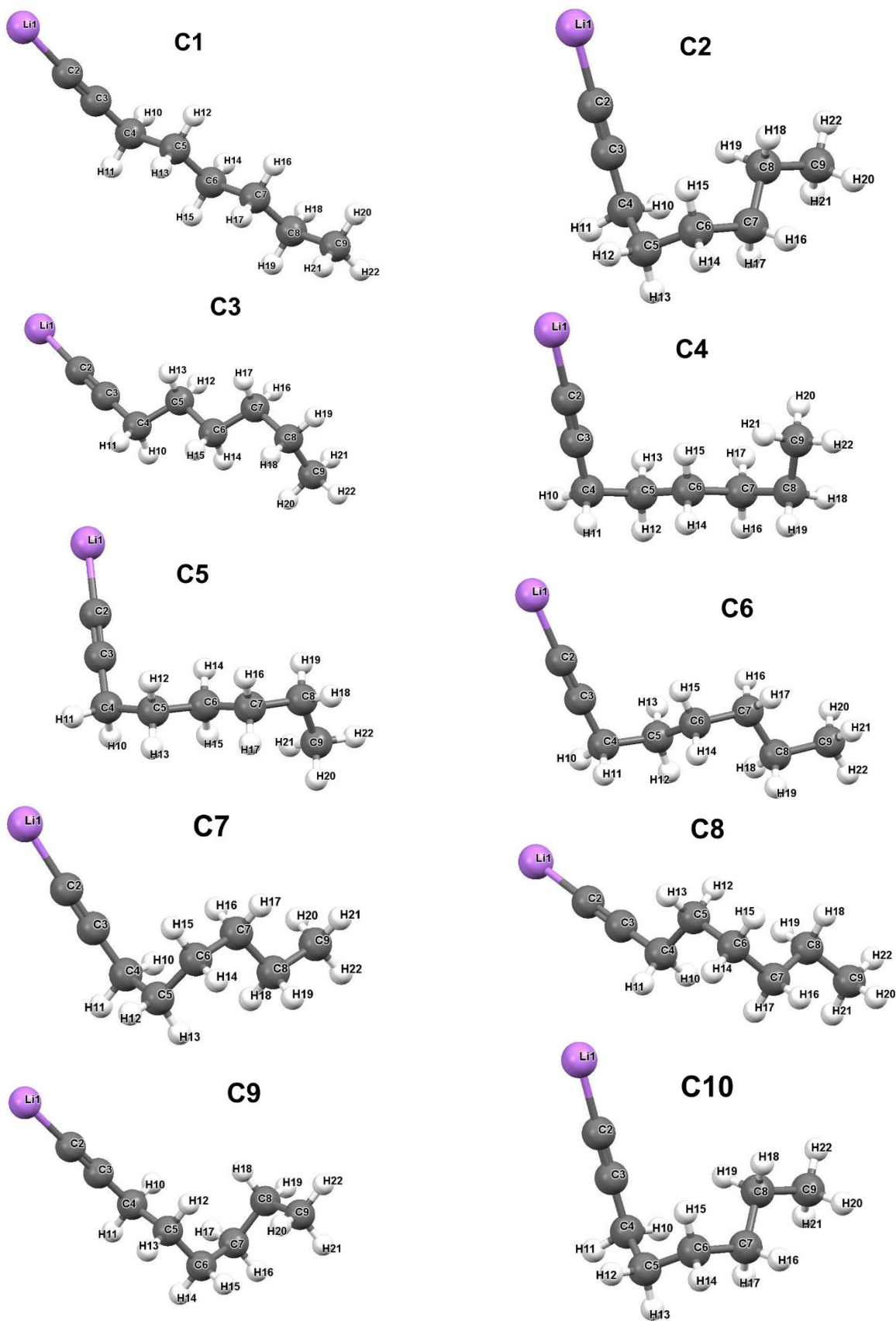
Figure B5. Energy-optimized electronic structures of the 10 conformers of **10**.

Appendix C

(CHAPTER 5)

Table of content

Part 1

XYZ coordinates of molecular systems (Tables C1-C4) and their energies (Tables C5-C8)

Table C1. Cartesian coordinates for the ONSH product **18b**. The structure was optimized at the RB3LYP-GD3/6-311++G(d,p)/THF level of theory at 298.15 K. Coordinate values are given in Å.

| Centre number	Atomic number	Atom type	Coordinates		
			X	Y	Z
1	7	N	-2.591832	-4.850008	0.464904
2	6	C	-3.345616	-5.854534	0.076531
3	6	C	-2.767208	-7.164078	-0.129298
4	7	N	-1.461413	-7.378601	-0.002571
5	6	C	-0.671879	-6.331022	0.364425
6	6	C	0.726404	-6.502974	0.516620
7	6	C	1.501527	-5.439277	0.915315
8	6	C	0.921808	-4.173244	1.177714
9	6	C	-0.432461	-3.980527	1.036128
10	6	C	-1.257400	-5.053614	0.623719
11	1	H	-2.972005	-8.745161	-2.617842
12	1	H	1.167118	-7.475580	0.327295
13	1	H	2.570492	-5.569975	1.034518
14	1	H	1.555525	-3.352414	1.491963
15	1	H	-0.896593	-3.020728	1.228019
16	6	C	-4.797446	-5.602669	-0.105344
17	6	C	-5.498759	-4.896836	0.880710
18	6	C	-6.859762	-4.643917	0.731269
19	6	C	-7.530963	-5.077266	-0.412838
20	6	C	-6.833893	-5.761801	-1.408846
21	6	C	-5.475770	-6.028215	-1.255101
22	1	H	-4.972316	-4.557951	1.764860
23	1	H	-7.395834	-4.108898	1.506708
24	1	H	-8.590003	-4.877836	-0.530173
25	1	H	-7.345671	-6.085415	-2.307867
26	1	H	-4.941473	-6.550790	-2.038646
27	3	Li	-0.697613	-9.346757	-0.405758
28	6	C	-3.589377	-8.279135	-0.439459
29	6	C	-4.303893	-9.224092	-0.694599
30	6	C	-5.184045	-10.284851	-1.030821
31	6	C	-6.562616	-10.027218	-1.158669
32	6	C	-7.429945	-11.056963	-1.503066
33	6	C	-6.938290	-12.345464	-1.723761
34	6	C	-5.572265	-12.606032	-1.598725
35	6	C	-4.694485	-11.585079	-1.253157
36	1	H	-6.934293	-9.023970	-0.987711
37	1	H	-8.490308	-10.856013	-1.600308
38	1	H	-7.618516	-13.145072	-1.992930
39	1	H	-5.191479	-13.605814	-1.770414
40	1	H	-3.634026	-11.783378	-1.155898
41	35	Br	-2.020599	-8.787285	-3.695075
42	35	Br	1.444819	-10.406435	-0.067610

Table C2. Cartesian coordinates for the ONSH product **19b**. The structure was optimized at the RB3LYP-GD3/6-311++G(d,p)/THF level of theory at 298.15 K. Coordinate values are given in Å.

Centre number	Atomic number	Atom type	Coordinates		
			X	Y	Z
1	7	N	-2.579824	-4.871706	0.154191
2	6	C	-3.355606	-5.889547	-0.148715
3	6	C	-2.808670	-7.226593	-0.216465
4	7	N	-1.511848	-7.460025	-0.041101
5	6	C	-0.699888	-6.403282	0.235903
6	6	C	0.690024	-6.599253	0.428036
7	6	C	1.489182	-5.522609	0.733403
8	6	C	0.941121	-4.221602	0.859542
9	6	C	-0.404764	-4.006225	0.675615
10	6	C	-1.254141	-5.092100	0.356608
11	1	H	-3.001027	-9.182173	-2.495125
12	1	H	1.099628	-7.599610	0.337152
13	1	H	2.552400	-5.668366	0.882567
14	1	H	1.593441	-3.391080	1.102170
15	1	H	-0.843051	-3.019481	0.763372
16	6	C	-4.797532	-5.619008	-0.376135
17	6	C	-5.484396	-4.780717	0.512034
18	6	C	-6.835766	-4.507110	0.319287
19	6	C	-7.512156	-5.053156	-0.772394
20	6	C	-6.829573	-5.871713	-1.672525
21	6	C	-5.481242	-6.157810	-1.474305
22	1	H	-4.954229	-4.354947	1.355374
23	1	H	-7.360534	-3.868149	1.020180
24	1	H	-8.563787	-4.837918	-0.923585
25	1	H	-7.344822	-6.285020	-2.531923
26	1	H	-4.959028	-6.786189	-2.184627
27	3	Li	-0.817642	-9.454433	-0.247892
28	6	C	-3.648840	-8.351269	-0.431647
29	6	C	-4.375359	-9.308866	-0.586882
30	6	C	-5.266796	-10.392181	-0.801299
31	6	C	-6.643403	-10.138054	-0.953532
32	6	C	-7.521408	-11.192678	-1.173185
33	6	C	-7.042242	-12.502566	-1.244938
34	6	C	-5.677990	-12.759678	-1.095799
35	6	C	-4.789645	-11.713861	-0.874201
36	1	H	-7.005672	-9.118530	-0.897544
37	1	H	-8.580406	-10.994487	-1.288986
38	1	H	-7.730752	-13.321638	-1.417021
39	1	H	-5.306703	-13.776026	-1.152248
40	1	H	-3.730405	-11.909632	-0.759858
41	17	Cl	-2.172086	-9.494359	-3.444616
42	17	Cl	1.177563	-10.422761	0.026816

C3

Table C3. Cartesian coordinates for the ONSH product **20b**. The structure was optimized at the RB3LYP-GD3/6-311++G(d,p)/THF level of theory at 298.15 K. Coordinate values are given in Å.

Centre number	Atomic number	Atom type	Coordinates		
			X	Y	Z
1	7	N	-2.646713	-6.437964	-0.413717
2	6	C	-3.006087	-7.636265	-0.009386
3	6	C	-2.004964	-8.638713	0.295241
4	7	N	-0.710587	-8.392865	0.132110
5	6	C	-0.337188	-7.163064	-0.321709
6	6	C	1.029244	-6.868820	-0.553115
7	6	C	1.385726	-5.626972	-1.029408
8	6	C	0.405794	-4.635634	-1.281129
9	6	C	-0.926079	-4.898301	-1.060286
10	6	C	-1.325505	-6.169955	-0.584118
11	1	H	0.342429	-7.733522	-2.955227
12	1	H	1.775983	-7.630893	-0.358090
13	1	H	2.429928	-5.403286	-1.212776
14	1	H	0.712608	-3.665902	-1.654453
15	1	H	-1.693663	-4.158901	-1.254016
16	6	C	-4.459621	-7.895812	0.151068
17	6	C	-5.257540	-6.933390	0.784769
18	6	C	-6.625416	-7.141784	0.937568
19	6	C	-7.215576	-8.306330	0.444137
20	6	C	-6.430653	-9.259827	-0.204138
21	6	C	-5.060059	-9.059422	-0.346657
22	1	H	-4.796575	-6.028178	1.161263
23	1	H	-7.230326	-6.396187	1.440763
24	1	H	-8.281155	-8.467752	0.561258
25	1	H	-6.884208	-10.161343	-0.599654
26	1	H	-4.461350	-9.802856	-0.856638
27	3	Li	0.634330	-9.989696	0.470390
28	6	C	-2.370744	-9.909024	0.819786
29	6	C	-2.701035	-10.979392	1.271682
30	6	C	-3.204505	-12.248771	1.774372
31	6	C	-4.651258	-12.524426	1.312117
32	6	C	-5.195630	-13.843501	1.863851
33	6	C	-6.629625	-14.129622	1.408175
34	6	C	-7.190623	-15.446232	1.954978
35	6	C	-8.624047	-15.722212	1.492089
36	1	H	-3.160445	-12.240454	2.870015
37	1	H	-2.544232	-13.059104	1.445415
38	1	H	-5.290789	-11.694227	1.627897
39	1	H	-4.678305	-12.540059	0.217448
40	1	H	-5.159940	-13.821110	2.960356
41	1	H	-4.542545	-14.667698	1.550314
42	1	H	-7.280306	-13.302210	1.719527
43	1	H	-6.663949	-14.150252	0.311164
44	1	H	-7.156160	-15.424316	3.050978
45	1	H	-6.538760	-16.271715	1.644243
46	1	H	-9.301224	-14.925466	1.816523
47	1	H	-8.679484	-15.779745	0.400181
48	1	H	-9.001104	-16.666054	1.895814
49	35	Br	-0.719483	-8.402402	-3.643672
50	35	Br	3.023176	-10.206087	0.102120

C4

Table C4. Cartesian coordinates for the ONSH product **21b**. The structure was optimized at the RB3LYP-GD3/6-311++G(d,p)/THF level of theory at 298.15 K. Coordinate values are given in Å.

Centre number	Atomic number	Atom type	Coordinates		
			X	**Y**	**Z**
1	7	N	-2.472154	-6.285891	-0.344978
2	6	C	-2.888298	-7.471177	0.046046
3	6	C	-1.940014	-8.537988	0.274511
4	7	N	-0.643960	-8.380100	0.035539
5	6	C	-0.214190	-7.167556	-0.413978
6	6	C	1.156947	-6.952146	-0.698494
7	6	C	1.574064	-5.711913	-1.121589
8	6	C	0.651905	-4.646804	-1.275368
9	6	C	-0.684556	-4.832839	-1.010811
10	6	C	-1.147151	-6.099092	-0.579205
11	1	H	-2.076630	-11.212397	-0.905863
12	1	H	1.859078	-7.770225	-0.577792
13	1	H	2.621970	-5.543948	-1.339896
14	1	H	1.008100	-3.679090	-1.608288
15	1	H	-1.407311	-4.034576	-1.128352
16	6	C	-4.344877	-7.650764	0.272806
17	6	C	-5.051152	-6.674970	0.988577
18	6	C	-6.419042	-6.814385	1.207003
19	6	C	-7.100114	-7.921159	0.698187
20	6	C	-6.406843	-8.886337	-0.032375
21	6	C	-5.036315	-8.755695	-0.240749
22	1	H	-4.519564	-5.814701	1.377209
23	1	H	-6.953005	-6.060003	1.773369
24	1	H	-8.165636	-8.028432	0.866423
25	1	H	-6.932121	-9.741290	-0.442201
26	1	H	-4.510390	-9.506052	-0.817213
27	3	Li	0.696514	-9.998046	0.390510
28	6	C	-2.361219	-9.793775	0.801390
29	6	C	-2.732215	-10.849043	1.261095
30	6	C	-3.274692	-12.107118	1.751448
31	6	C	-4.657072	-12.419075	1.138320
32	6	C	-5.234165	-13.738558	1.654570
33	6	C	-6.603052	-14.062021	1.048759
34	6	C	-7.192815	-15.384013	1.550622
35	6	C	-8.560284	-15.698084	0.937128
36	1	H	-3.352540	-12.056458	2.843604
37	1	H	-2.571364	-12.916835	1.527352
38	1	H	-5.341225	-11.595459	1.365053
39	1	H	-4.562576	-12.457778	0.048017
40	1	H	-5.319990	-13.695622	2.747596
41	1	H	-4.535065	-14.553984	1.430619
42	1	H	-7.301178	-13.245496	1.274210
43	1	H	-6.515660	-14.097738	-0.044818
44	1	H	-7.279629	-15.347779	2.643347
45	1	H	-6.493362	-16.198161	1.325352
46	1	H	-9.286102	-14.913369	1.173847
47	1	H	-8.493804	-15.769783	-0.153284
48	1	H	-8.958973	-16.645535	1.310438
49	17	Cl	-1.687969	-11.752276	-2.025225
50	17	Cl	2.865336	-10.357595	-0.010142

C5

Table C5. Energetic information for **18b** and **20b** obtained from the oxidation of **5a** and **13a** with Br$_2$. These structures were optimized at the RB3LYP-GD3/6-311++G(d,p)/THF level of theory at 298.15 K and 1 atm. Energy values are given in Hartree (a.u.) units.

	Oxidation with Br$_2$	
	18b	**20b**
Electronic Energy (EE)	-6113.0980	-6117.9403
Zero-point Energy Correction	0.3045	0.3927
Thermal Correction to Energy	0.3294	0.4219
Thermal Correction to Enthalpy	0.3304	0.4229
Thermal Correction to Free Energy	0.2435	0.3233
EE + Zero-point Energy	-6112.7935	-6117.5476
EE + Thermal Energy Correction	-6112.7686	-6117.5183
EE + Thermal Enthalpy Correction	-6112.7676	-6117.5174
EE + Thermal Free Energy Correction	-6112.8545	-6117.6170

Table C6. Energetic information for **19b** and **21b** obtained from the oxidation of **5a** and **13a** with Cl$_2$. These structures were optimized at the RB3LYP-GD3/6-311++G(d,p)/THF level of theory at 298.15 K and 1 atm. Energy values are given in Hartree (a.u.) units.

	Oxidation with Cl$_2$	
	19b	**21b**
Electronic Energy (EE)	-1885.2567	-1890.1001
Zero-point Energy Correction	0.3055	0.3948
Thermal Correction to Energy	0.3301	0.4230
Thermal Correction to Enthalpy	0.3311	0.4240
Thermal Correction to Free Energy	0.2473	0.3309
EE + Zero-point Energy	-1884.9512	-1889.7053
EE + Thermal Energy Correction	-1884.9265	-1889.6770
EE + Thermal Enthalpy Correction	-184.9256	-1889.6761
EE + Thermal Free Energy Correction	-1885.0094	-1889.7692

Part 2 – Selected geometric data

Table C7. Computed dihedral angles (DA) in °, angles in ° and bond lengths in Å for the energy optimised ONSH products **18b** and **19b** from oxidation with Br_2 or Cl_2.

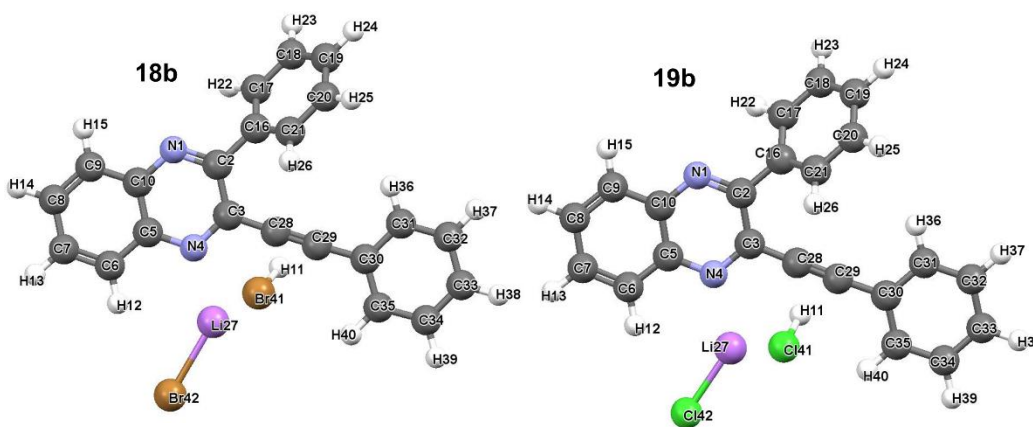|		ONHS Products	
		18b	**19b**
Dihedral angle (º)	C6,C5,C10,C9	-0.35	-0.39
	C6,C7,C8,C9	-0.13	-0.16
	N1,C2,C3,N4	-3.52	-3.24
	N4,C5,C10,N1	-2.33	-2.25
	N1,C2,C16,C17	-46.14	-44.77
Angle (º)	N4,C3,C2	121.69	121.67
	N4,C3,C28	117.58	117.26
	C2,C3,C28	120.71	121.04
Distance (Å)	N4–C3	1.33	1.33
	C2–C3	1.45	1.45
	C3–C28	1.42	1.42
	Li27–Br42/Cl42	2.41	2.24
	Li27–N4	2.15	2.12
	C3–H11	2.96	3.01
	Br41/Cl42–H11	1.44	1.30

Energy optimized structures

Table C8. Computed dihedral angles (DA) in º, angles in º and bond lengths in Å for the energy optimised ONSH products **20b** and **21b** from oxidation with Br_2 or Cl_2.

		ONHS Products	
		20b	**21b**
Dihedral angle (º)	C6,C5,C10,C9	-0.61	-0.74
	C6,C7,C8,C9	-0.35	-0.34
	N1,C2,C3,N4	-2.33	-3.45
	N4,C5,C10,N1	-1.32	-2.63
	N1,C2,C16,C17	-44.36	-45.37
Angle (º)	N4,C3,C2	121.31	121.62
	N4,C3,C28	117.48	117.38
	C2,C3,C28	121.18	120.98
Distance (Å)	N4–C3	1.33	1.33
	C2–C3	1.45	1.45
	C3–C28	1.42	1.43
	Li27–Br50/Cl50	2.43	2.24
	Li27–N4	2.16	2.13
	C3–H11	4.11	2.93
	Br49/Cl49–H11	1.43	1.30

Energy optimized structures
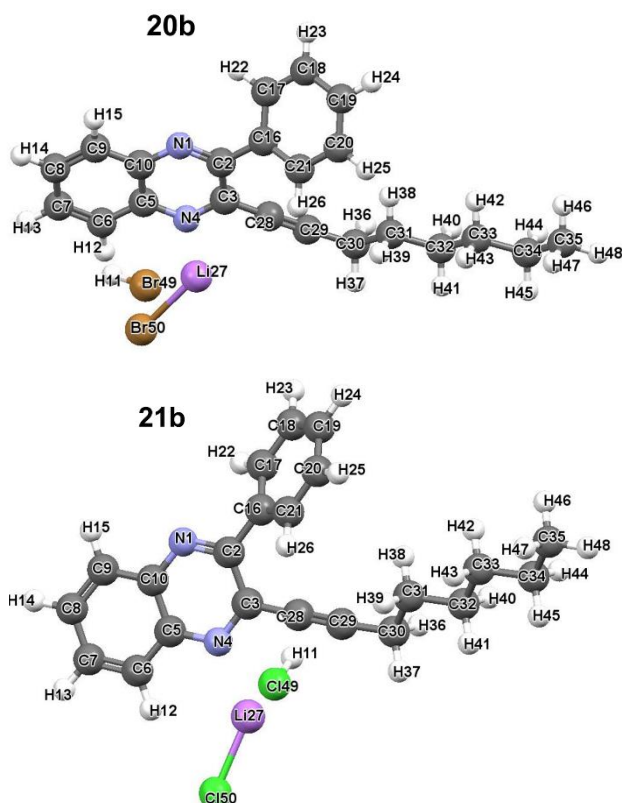
Part 3
Net atomic charges

Table C9. Net atomic charges for **18b**, **19b**, **20b** and **21b**. *Q* is in *e*.

Atom A	18b	Atom A	19b	Atom A	20b	Atom A	21b
N1	-1.1082	N1	-1.1075	N1	-1.1101	N1	-1.1078
C2	0.5748	C2	0.5738	C2	0.5722	C2	0.5719
C3	0.5917	C3	0.5920	C3	0.5944	C3	0.5948
N4	-1.1622	N4	-1.1621	N4	-1.1710	N4	-1.1626
C5	0.4375	C5	0.4392	C5	0.4288	C5	0.4354
C6	-0.0146	C6	-0.0144	C6	-0.0329	C6	-0.0153
C7	-0.0068	C7	-0.0069	C7	-0.0118	C7	-0.0070
C8	-0.0089	C8	-0.0091	C8	-0.0099	C8	-0.0089
C9	-0.0067	C9	-0.0066	C9	-0.0073	C9	-0.0071
C10	0.4502	C10	0.4508	C10	0.4495	C10	0.4522
H11	0.1177	H11	0.2880	H11	0.1078	H11	0.2914
H12	0.0704	H12	0.0757	H12	0.0748	H12	0.0744
H13	0.0525	H13	0.0525	H13	0.0538	H13	0.0524
H14	0.0503	H14	0.0504	H14	0.0506	H14	0.0502
H15	0.0607	H15	0.0608	H15	0.0617	H15	0.0607
C16	-0.0088	C16	-0.0091	C16	-0.0086	C16	-0.0090
C17	-0.0107	C17	-0.0105	C17	-0.0117	C17	-0.0112
C18	-0.0172	C18	-0.0171	C18	-0.0187	C18	-0.0179
C19	-0.0203	C19	-0.0203	C19	-0.0212	C19	-0.0207
C20	-0.0174	C20	-0.0173	C20	-0.0162	C20	-0.0163
C21	-0.0154	C21	-0.0155	C21	-0.0131	C21	-0.0135
H22	0.0466	H22	0.0472	H22	0.0455	H22	0.0459
H23	0.0370	H23	0.0370	H23	0.0353	H23	0.0362
H24	0.0369	H24	0.0370	H24	0.0354	H24	0.0363
H25	0.0363	H25	0.0364	H25	0.0343	H25	0.0358
H26	0.0358	H26	0.0365	H26	0.0384	H26	0.0358
Li27	0.9249	Li27	0.9232	Li27	0.9256	Li27	0.9245
C28	-0.1402	C28	-0.1426	C28	-0.1414	C28	-0.1558
C29	-0.1657	C29	-0.1685	C29	-0.1583	C29	-0.1652
C30	0.0624	C30	0.0623	C30	0.1003	C30	0.1002
C31	-0.0040	C31	-0.0038	C31	0.0624	C31	0.0609
C32	-0.0096	C32	-0.0095	C32	0.0538	C32	0.0543
C33	-0.0136	C33	-0.0134	C33	0.0546	C33	0.0547
C34	-0.0084	C34	-0.0081	C34	0.0633	C34	0.0635
C35	-0.0040	C35	-0.0035	C35	0.0273	C35	0.0272
H36	0.0537	H36	0.0538	H36	0.0434	H36	0.0500
H37	0.0449	H37	0.0451	H37	0.0403	H37	0.0449
H38	0.0455	H38	0.0457	H38	-0.0008	H38	0.0005
H39	0.0465	H39	0.0468	H39	-0.0065	H39	-0.0053
H40	0.0481	H40	0.0487	H40	-0.0187	H40	-0.0179
Br41	-0.1483	Cl41	-0.3213	H41	-0.0191	H41	-0.0172
Br42	-0.9339	Cl42	-0.9357	H42	-0.0228	H42	-0.0229
				H43	-0.0233	H43	-0.0219
				H44	-0.0223	H44	-0.0223
				H45	-0.0222	H45	-0.0217
				H46	-0.0141	H46	-0.0142
				H47	-0.0140	H47	-0.0135
				H48	-0.0098	H48	-0.0096
				Br49	-0.1138	Br49	-0.3335
				Br50	-0.9332	Br50	-0.9359

C9

C10